

AD-A067 242

SCIENCE APPLICATIONS INC LA JOLLA CALIF

F/G 1/5

DEVELOPMENT OF CRITERIA FOR MONITORING OF AIRPORT GROUND POLLUT--ETC(U)

NOV 78 C B LUDWIG, J R YODER

DOT-FA76WA-3725

UNCLASSIFIED

SAI-77-910-LJ-VOL-1-

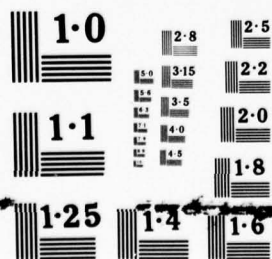
FAA/RD-77-178-1

NL

1 OF 5
AD A
067242



1 OF 5
AD A
067242



FAA-RD-77-178, I

LEVEL *III*

(12)

AD 67243

AD A0 67242

**DEVELOPMENT OF CRITERIA
FOR MONITORING OF
AIRPORT GROUND POLLUTION**

Volume I - Study

Science Applications, Inc.
1200 Prospect Street
La Jolla, California 92038



DDC
RECEIVED
APR 12 1979
C

DDC FILE COPY

November 1978

FINAL REPORT

Document is available to the U.S. public through
the National Technical Information Service,
Springfield, Virginia 22161

Prepared for

**U.S. DEPARTMENT OF TRANSPORTATION
FEDERAL AVIATION ADMINISTRATION
Systems Research & Development Service
Washington, D.C. 20590**

79 04 12 020

NOTICE

This document is disseminated under the sponsorship of the Department of Transportation in the interest of information exchange. The United States government assumes no liability for its contents or use thereof.

Technical Report Documentation Page

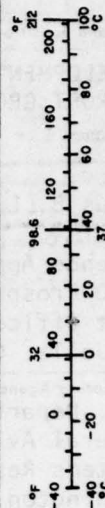
1. Report No. 18 FAA/RD-77-178-1	2. Government Accession No.	3. Recipient's Catalog No.
4. Title and Subtitle 6 DEVELOPMENT OF CRITERIA FOR MONITORING OF AIRPORT GROUND POLLUTION. Volume I, Study,	5. Report Date 11 Nov 1978	6. Performing Organization Code
7. Author(s) 10 Claus B. Ludwig J. Richard Yoder	8. Performing Organization Report No. 14 SAI-77-910-LJ-VOL-1 Volumes I and II	9. Performing Organization Name and Address Science Applications, Inc. 1200 Prospect Street Post Office Box 2351 La Jolla, CA 92038
10. Work Unit No. (TRAIS)	11. Contract or Grant No. 15 DOT-FA76 WA-3725 new	12. Sponsoring Agency Name and Address U.S. Department of Transportation Federal Aviation Administration Systems Research & Development Service Washington, D.C. 20590
13. Type of Report and Period Covered 9 FINAL REPORT, Sep 1975 - Jul 1977,	14. Sponsoring Agency Code	15. Supplementary Notes 12 438 p.
16. Abstract Criteria are developed by which the validity of pollution predictions and measurements in the airport environs can be judged. The criteria are applied to three technologies: (1) predictive mathematical models, (2) measurements by point samplers, and (3) measurements by remote monitors. For mathematical models the criterion is the agreement between predicted and measured pollution levels. Various mathematical models are described, analyzed and ranked by weighted attributes as screening models and as validation models. For point samplers, the criteria have been developed based on EPA-approved measurement principles and procedures for testing performance characteristics and for determining a consistent relationship to reference methods. Remote monitors belong to an evolving technology that has not yet been approved as to measurement principles. Thus criteria are developed to select certain remote sensing systems as potential candidates for air enforcement monitors. Data validation procedures are developed for the selected remote monitors.		
17. Key Words Pollution monitors Remote monitors Airport environment Mathematical models Point sampler		18. Distribution Statement Document is available to the U.S. public through the National Technical Information Service, Springfield, Virginia 22161.
19. Security Classif. (of this report) Unclassified	20. Security Classif. (of this page) Unclassified	21. No. of Pages 437
22. Price		

METRIC CONVERSION FACTORS

Approximate Conversions to Metric Measures

Symbol	When You Know	Multiply by	To Find	Symbol
LENGTH				
in	inches	*2.5	centimeters	cm
ft	feet	30	centimeters	cm
yd	yards	0.9	meters	m
mi	miles	1.6	kilometers	km
AREA				
m ²	square inches	6.5	square centimeters	cm ²
ft ²	square feet	0.09	square meters	m ²
yd ²	square yards	0.8	square meters	m ²
mi ²	square miles	2.6	square kilometers	km ²
	acres	0.4	hectares	ha
MASS (weight)				
oz	ounces	28	grams	g
lb	pounds	0.45	kilograms	kg
	short tons (2000 lb)	0.9	tonnes	t
VOLUME				
tap	teaspoons	5	milliliters	ml
Tabsp	tablespoons	15	milliliters	ml
fl oz	fluid ounces	30	milliliters	ml
c	cups	0.24	liters	l
pt	pints	0.47	liters	l
qt	quarts	0.95	liters	l
gal	gallons	3.8	liters	l
ft ³	cubic feet	0.03	cubic meters	m ³
yd ³	cubic yards	0.76	cubic meters	m ³
TEMPERATURE (exact)				
°F	Fahrenheit temperature	5/9 (after subtracting 32)	Celsius temperature	°C

Symbol	When You Know	Multiply by	To Find	Symbol
LENGTH				
mm	millimeters	0.04	inches	in
cm	centimeters	0.4	inches	in
m	meters	3.3	feet	ft
km	kilometers	1.1	yards	yd
		0.6	miles	mi
AREA				
cm ²	square centimeters	0.16	square inches	in ²
m ²	square meters	1.2	square yards	yd ²
km ²	square kilometers	0.4	square miles	mi ²
ha	hectares (10,000 m ²)	2.5	acres	
MASS (weight)				
g	grams	0.035	ounces	oz
kg	kilograms	2.2	pounds	lb
t	tonnes (1000 kg)	1.1	short tons	
VOLUME				
ml	milliliters	0.03	fluid ounces	fl oz
l	liters	2.1	pints	pt
l	liters	1.06	quarts	qt
m ³	liters	0.26	gallons	gal
m ³	cubic meters	35	cubic feet	ft ³
m ³	cubic meters	1.3	cubic yards	yd ³
TEMPERATURE (exact)				
°C	Celsius temperature	9/5 (then add 32)	Fahrenheit temperature	°F



*1 in. = 2.54 (exactly). For other exact conversions and more detailed tables, see NBS Mon., Publ. 286, Units of Weights and Measures, Price \$2.25, SD Catalog No. C13.10-286.

TABLE OF CONTENTS

	<u>Page</u>
EXECUTIVE SUMMARY	ix
1.0 INTRODUCTION	1-1
1.1 Objective of the Study	1-1
1.2 Study Plan	1-1
1.3 Historical Background	1-4
2.0 MEASUREMENT REQUIREMENTS OF THE TARGET POLLUTANTS	2-1
2.1 Overview	2-1
2.2 National Ambient Air Quality Standards	2-3
2.3 Classification and Emission Factors of Commercial Aircraft	2-9
2.4 Classification and Emission Factors of Military Aircraft	2-12
3.0 DESCRIPTION AND EVALUATION OF MATHEMATICAL MODELS	3-1
3.1 Basic Model Concepts	3-5
3.2 Model Descriptions	3-36
3.3 Model Assessment and Comparison	3-68
3.4 Summary and Conclusions	3-79
4.0 DESCRIPTION OF POINT SAMPLERS	4-1
4.1 Introduction	4-1
4.2 Ambient Air Monitoring Reference and Equivalent Methods and Measurements Principles	4-4
4.3 Sampling Criteria	4-30

TABLE OF CONTENTS

		<u>Page</u>
5.0	DESCRIPTION OF REMOTE MONITORS	5-1
5.1	Introduction	5-1
5.2	Description of Active Pulsed Systems	5-8
5.2.1	Active (Pulsed) System: LIDAR	5-8
5.2.2	Active (Pulsed) System: Differential Absorption	5-32
5.2.3	Active (Pulsed) System: Raman Scattering	5-64
5.2.4	Active (Pulsed) System: Resonant Raman/Fluorescence	5-85
5.3	Description of Non-Pulsed Systems	5-97
5.3.1	Active CW System: Long-Path with Laser Source	5-97
5.3.2	Active CW System: Long-Path with Broad-Band Source	5-163
5.3.3	Passive Systems	5-195
6.0	SELECTION AND RANKING OF REMOTE MONITORS	6-1
6.1	Development of Criteria	6-1
6.2	Selection and Ranking of Remote Monitors	6-24

Accession for

NTS

DOC

UNANNOUNCED

JCS/IT ICA 104

White Section

B-HI Section

BY

DATE

DISPOSITION / AVAILABILITY CODES

SPECIAL

A

TABLE OF CONTENTS

	<u>Page</u>
7.0 DATA VALIDATION PROCEDURES	7-1
7.1 Procedures Applicable to All Remote Monitors	7-1
7.2 Remote Monitors Providing Line Profile Data	7-8
7.2.1 LWIR Differential Absorption	7-10
7.2.2 MWIR-DAS	7-26
7.2.3 SWIR Differential Absorption	7-41
7.2.4 UV/Visible Differential Absorption	7-57
7.2.5 LIDAR	7-73
7.3 Remote Monitors Providing Line Average Data	7-87
7.3.1 LWIR Long-Path with Laser Source	7-87
7.3.2 MWIR Long-Path with Laser Source	7-103
7.3.3 SWIR Long-Path with Laser Source	7-117
7.3.4 UV/Visible Long-Path with Laser Source	7-130
7.3.5 IR Long-Path with Broadband Source and Dispersive Receiver	7-143
7.3.6 IR Long-Path with Broadband Source (Bi-Static) Using Fourier Transform Spectrometer Receiver	7-171
7.3.7 IR Long-Path with Broadband Source Using Gas Filter Correlation Receiver	7-197
7.3.8 IR Long-Path with Broadband Source Using Filterwheel Receiver	7-217
7.3.9 UV/Visible Long Path with Broadband Source and Matched Filter Correlation Receiver	7-236
7.3.10 Passive Downward-Looking Monitor Using Gas Filter Correlation Receiver	7-250

TABLE OF CONTENTS

	<u>Page</u>
7.4 Remote Monitors Providing Line Integral Data	7-285
7.4.1 Infrared Spectrometer (Tunable Receiver) Uplooking Monitor	7-285
7.4.2 Infrared Gas Filter Correlation Uplooking Monitor	7-296
REFERENCES	R-1
APPENDIX I National Primary and Secondary Ambient Air Quality Standards (40 CFR 50)	I-1
APPENDIX II Ambient Air Monitoring Reference and Equivalent Methods (40 CFR 53)	II-1
APPENDIX III Guideline for Public Reporting of Daily Air Quality	III-1
APPENDIX IV Control of Air Pollution from Aircraft and Aircraft Noises	IV-1
APPENDIX V Review of Calibration Span Gases	V-1
APPENDIX VI List of Commercially Available Point Samplers	VI-1
APPENDIX VII Derivation of Signal-to-Noise Ratio Equations and Error Analysis	VII-1
APPENDIX VIII Meteorological Instruments for Use in the Calibration Test Range	VIII-1
APPENDIX IX Electromagnetic Interference Characteristics Requirements for Equipment	IX-1

EXECUTIVE SUMMARY

The objective of this study is the development of criteria by which the validity of pollution predictions and measurements in the airport environs can be judged. These criteria are to be applied to three technologies: (1) predictive mathematical models, (2) measurements by point samplers, and (3) measurements by remote monitors. Different approaches apply to the criteria development for the three technologies. For the mathematical models, the only criteria of the usefulness of a given model is the agreement between predicted and measured pollution levels in the vicinity of airports. The decision as to the most useful model is still outstanding, awaiting the availability of a definitive experimental data base. For the point samplers, the criteria have already been developed. They are based upon EPA developed measurement principles and procedures for testing performance characteristics of point samplers and for determining a consistent relationship to reference methods. Remote monitors belong to an evolving technology that has not yet been designated as an acceptable measurement principle. Thus, criteria had to be developed to select certain remote systems as potential candidates for air enforcement monitors. The requirements for the prediction and measurement of pollutants are based upon the "National Ambient Air Quality Standards (NAAQS)" (40 CFR 50) that have been established for total suspended particles (TSP), sulfur dioxide (SO_2), carbon monoxide (CO), photochemical oxidants (O_3), total hydrocarbons (THC) and nitrogen oxides (NO_x).

Predictive Mathematical Models

Several mathematical models currently in use for predicting the pollution levels in the vicinity of airports are described. They are either based upon the Gaussian dispersion approach or upon the cell approach.

Several models developed for other uses are surveyed for possible modification to the airport modeling application.

The characteristics of suitable models are presented and discussed. A rating chart is developed, ranking each model according to various criteria.

Four models are selected as most suitable for airport modeling. They are the NREC, GEOMET, AVAP and AQAM Models.

Point Samplers

The many point samplers commercially available for the different pollutants are based on a variety of measurement principles. To assure the validity of pollution data obtained by the various state and local agencies, the Environmental Protection Agency has standardized one measurement principle for each of the six pollutants. Any instrument that is based on this measurement principle and fulfills stringent calibration tests and performance tests can be designated as a reference method. Instruments that are based on other measurement principles can be designated as equivalent methods after passing prescribed tests. Up to the present time (September 1977), about fifteen commercially available automated analyzers have been designated as reference or equivalent methods. (Notices of such designations are published in the Federal Register). Thus, only measurements taken by those reference or equivalent methods that have been officially designated, and that have been operated according to the approved procedures, have to be accepted as valid when leading to enforcement action directed toward pollution abatement. However, the question of how representative such a point measurement is in terms of the total airport environs is not addressed explicitly in this report. The answer to that question will depend upon the ultimate selection of a model that makes the connection between point sampled data, meteorological data, topography and the distribution of the various sources. In this

report, the important EPA procedures are discussed, together with the selected measurement principles for the six primary pollutants; i.e., the manual titration method using pararosaniline and a colorimeter for SO_2 , the manual high-volume sampling method using a weighing scale for TSP, the non-dispersive infrared method for CO, the chemiluminescence method using the reaction with ethylene for O_3 , the same method using the reaction with O_3 for NO_2 and the hydrogen flame ionization method for THC. (Some Air Quality Control Regions may still use unapproved and/or unacceptable methods. According to the regulations, these methods have to be phased out by 1980.) The presently designated reference and equivalent methods are listed in this report, together with their measurement principle, range of operation, model number, distributor and issue of the Federal Register when published. This list together with future designations forms the basis for the acceptability of data taken in the airport environs.

Since future designations may also be based upon different measurement principles, brief descriptions of twelve measurement principles are given together with a list of commercially available point samplers which are potential candidates for designation as reference or equivalent method. However, as stated above, as long as they are not designated as such by the EPA, measurements taken by them cannot be used in enforcement actions.

Remote Monitors

Instrument systems that monitor air pollution remotely have a great advantage over point samplers. They can gather information continuously in a volume of air that envelops the airport environs. Since remote monitors are an evolving technology, this report deals with their characteristics in great detail. The legal validity of measurements taken by remote monitors has not been established since none of the remote measurement principles have been designated as a reference or equivalent method. In other words, measurements taken by a remote monitor do not have to be accepted as valid

when leading to air enforcement action. It appears that there are two approaches to promote remote monitors to the status of reference or equivalent methods. One approach is to develop a new (parallel) set of National Ambient Air Quality Standards, based on the measurement methodology of remote sensing, which specify remote measurement principles that can become reference or equivalent methods. This approach has not been pursued in the present study since it would require extensive effort over several years involving various Government Agencies. The other approach, which has been pursued here, is to attempt to fit the remote measurement principle into the present procedural framework of determining a consistent relationship between a candidate remote monitor and an established reference point sampling method.

The vigorous and diverse development of remote air pollution monitors over the last decade is categorized into three measurement principles:

- Remote monitors that provide line profile data
- Remote monitors that provide line average data
- Remote monitors that provide line integral data.

These remote monitors employ beams of energy in the form of light (visible), infrared or ultraviolet radiation. Suspended particles are measured by observing the strength of the scattered radiation from a projected beam. Chemical pollutants are measured by observing their spectroscopic effect on either a probing light beam or on their self-emission radiance. Spectroscopic interpretation is accomplished variously by spectrometric receivers (dispersive, interferometric or filter-wheel), by gas-cell correlation receivers, or by instruments employing multiple wavelength probing beams.

The measurements made by remote monitors are generally assignable to a path traversed by the measured radiance. When the radiance source is pulsed, the time of traversal from source to receiver indicates the location

of the sample of atmosphere corresponding to each instantaneous measurement. A time resolved measurement thus is spatially resolved (i. e., range-resolved) along the line of sight, and a line profile data result. The spectroscopic interpretation is accomplished by the two-wavelength source technique. A line profile of pollutant concentration results.

Where the probing beam is continuous, (or, if pulsed, is not range-resolved) the line of sight is terminated by the locations of transmitter, receiver (and reflector, if used). Spectroscopic interpretation can be by any of the methods. The concentration measured is thus assignable to a path of specified length, and the data are interpreted as a line average.

In passive systems, where the radiance originates from a natural temperature difference between the pollutant and its background the effective path length may be indefinite, resulting in line integral data.

A variety of remote monitor systems have been developed employing scattering principles for particulates, or spectroscopic absorption or emission for chemical pollutants and operating in either active pulsed mode for line profile data, active non-pulsed mode for line average data or passive mode for line integral data. A number of these have been tested in the laboratory and in the field.

In the present study, the principle of operation of each system and the present state-of-art of its development, together with its identified advantages and disadvantages and operational requirements is described. In addition, a critical analysis is performed for each system. This critical analysis forms the basis for the selection and ranking of the remote monitors as potential candidates for possible future designation as "equivalent methods".

The selection criteria and ranking guidelines are developed. It is found that monitors to be used in air enforcement programs must fulfill the following requirements:

- o Monitors must have the potential of being designated as an "equivalent method"; as a consequence, it is found that only monitors that provide either line profile or line average data can be selected;
- o Monitors must have a sensitivity and a dynamic range that span the "National Ambient Air Quality Standards (NAAQS); i. e., 7-350 ppm for CO, 0.06 to .8 ppm for O_3 , 0.02-1.2 ppm for SO_2 , 0.04-0.5 ppm for NO_2 and 0.2-2.4 ppm THC;
- o Monitors should have a range capability of greater than 100 m;
- o Monitors using lasers as the transmitter must not emit more than the maximum permissible exposure (MPE) according to HEW standards for Eye Safety.
- o Monitors (transmitter and receiver stations) must not interfere with normal airport operations;
 - (a) electromagnetic emission must not interfere with any instrument landing systems (ILS) or air surveillance radar (ASR), as determined by the FAA, and
 - (b) the access to monitoring equipment for service or data retrieval must not interfere with air traffic on the ground as determined by the local airport authority.

Based on these selection criteria, the following 14 remote monitor systems providing line profile and average data are listed together with their useful applicability to the NAAQS pollutants.

Based on these selection criteria, the following 14 remote monitor systems providing line profile and average data are listed together with their useful applicability to the NAAQS pollutants.

Measurement Principle	TSP	CO	HC	O ₃	NO _X	SO ₂
LINE PROFILE DATA						
Lidar	(Yes) *					
DAS (SWIR, MWIR, LWIR)	Yes	Yes	Yes	Yes	Yes	Yes
DAS (ultraviolet)					Yes	Yes
Raman	_____	Not acceptable			_____	_____
Resonance Raman	_____	Not acceptable			_____	_____
Fluorescence	_____	Not acceptable			_____	_____
LINE AVERAGE DATA						
Long-path laser system (SWIR, MWIR, LWIR)	Yes	Yes	Yes	Yes	Yes	Yes
Long-path laser system in the UV/Visible	(Yes) *				Yes	Yes
Long-path system in the IR:						
Dispersive type	Yes			Yes		
Gas Filter Correlation	Yes	Yes			Yes	Yes
Interferometer	Yes	Yes		Yes	Yes	Yes
Filterwheel	Yes			Yes		
Long-path system in the UV/Visible:						
Matched Filter					Yes	Yes
Passing Downward Looking	_____	Not acceptable			_____	_____

* Requires establishment of relationship between scattering and mass density

A summary of the findings for the selected remote monitor systems is shown in Table ES-1.

	SYSTEM MEASUREMENT PRINCIPLE	SPECIES	WAVELENGTH REGION	RANGE (km)	SENSITIVITY	MAJOR ADVANTAGE	MAJOR DISADVANTAGE	STATUS	MARKING/REMARK
LINE PROFILE	LIDAR	PARTICLES	VISIBLE	.1-.1	NOT ESTABLISHED	MONOSTATIC PROFILE	NO STANDARDS FOR OPACITY	PROTOTYPES ROUTINELY USED IN FIELD	AFTER RELATIONSHIP BETWEEN OPACITY AND MASS LOADING ESTABLISHED, LIDAR IS THE MOST USEFUL REMOTE MONITOR FOR PARTICLES
	LMIR DAS/DIAL	O ₃ , HC	9.1-11.3 μ m	.1-.1	.01 ppm	MONOSTATIC PROFILE, CAN MEASURE MANY HC	COMPLEX, NEEDS METERODYNE DETECTION	FIELDABLE PROTOTYPE BEING TESTED	THE ONLY METHOD TO MEASURE THE PROFILE OF O ₃ AND HC TO DISTANCES UP TO 1 KM
	PMIR DAS/DIAL	CO, NO	4.8-5.2 μ m	.1-.3	.1	MONOSTATIC PROFILE	COMPLEX, ONLY TWO POLLUTANTS NEEDS METERODYNE DETECTION	THEORETICAL	THE ONLY METHOD TO MEASURE THE PROFILE OF CO AND NO TO DISTANCES UP TO 300 M
	SMIR DAS/DIAL	NO ₂ , HC, SO ₂ , CO	2.6-5.2 μ m	.1	.1-.25	MONOSTATIC PROFILE, MANY POLLUTANTS	COMPLEX, RESTRICTED RANGE	THEORETICAL	THE ONLY METHOD TO MEASURE THE PROFILE OF NO ₂ , SO ₂ TO DISTANCES UP TO 100 M
	UV/VIS DAS/DIAL	PARTICLES, NO ₂ , SO ₂	3000-5000 \AA	TBD	TBD	MONOSTATIC PROFILE	COMPLEX, SENSITIVITY LIMITED	THEORETICAL	
LINE AVERAGE	LMIR LONG-PATH WITH LASER SOURCE					ONE OF THE MOST SENSITIVE METHODS	NEEDS LINING UP OPTICALLY	FIELD TESTED BY GE AND JPL	VERY SENSITIVE METHOD TO OBTAIN LINE AVERAGE DATA FOR O ₃ AND HC
	A) BISTATIC	O ₃ , HC	9.1-11.3 μ m	.01-1	10 ⁻⁶ ppm				
	B) MONOSTATIC	O ₃ , HC	9.1-11.3 μ m	.01-1	10 ⁻¹ ppm	EASY TO SET UP	SENSITIVITY GREATLY REDUCED, NEEDS METERODYNE	FIELD TESTED BY GE AND JPL	NOT SUITABLE SINCE SENSITIVITY NOT SUFFICIENT FOR HAAGS
	PMIR LONG-PATH WITH LASER SOURCE					ONE OF THE MOST SENSITIVE METHODS	NEEDS LINING UP OPTICALLY	FIELD TESTED BY MIT AND JPL	VERY SENSITIVE METHOD TO OBTAIN LINE AVERAGE DATA FOR CO AND NO
	A) BISTATIC	CO, NO	4.8-5.2 μ m	.01-1	10 ⁻⁶ ppm				
	B) MONOSTATIC	CO, NO	4.8-5.2 μ m	.01-1	10 ⁻¹ ppm	EASY TO SET UP	SENSITIVITY GREATLY REDUCED, NEEDS METERODYNE	FIELD TESTED BY MIT AND JPL	NOT SUITABLE SINCE SENSITIVITY NOT SUFFICIENT FOR HAAGS
	SMIR LONG-PATH WITH LASER SOURCE					ONE OF THE MOST SENSITIVE METHODS	NEEDS LINING UP OPTICALLY	NOT TESTED	VERY SENSITIVE METHOD TO OBTAIN LINE AVERAGE DATA FOR MOST POLLUTANTS
	A) BISTATIC	NO ₂ , HC, SO ₂ , CO	2.6-5.0 μ m	.01-1	10 ⁻⁶ ppm				
	B) MONOSTATIC	NO ₂ , HC, SO ₂ , CO	2.6-5.0 μ m	.01-1	10 ⁻¹ ppm	EASY TO SET UP	SENSITIVITY GREATLY REDUCED, NEEDS METERODYNE	SOME FIELD TESTS	NOT SUITABLE SINCE SENSITIVITY NOT SUFFICIENT FOR HAAGS
	UV/VIS LONG-PATH WITH LASER SOURCE	PARTICLES, SO ₂ , NO ₂	3000-5000 \AA	TBD	TBD	—	SENSITIVITY LIMITED DUE TO LOW MPE	NOT TESTED	
	LONG-PATH WITH BLACKBODY SOURCE AND DISPERSIVE RECEIVER	CO, O ₃ , HC (P)	2.5-12 μ m	.01-1	.01 ppm	SIMPLE RECEIVER, DIRECT OUTPUT	RESOLUTION NOT HIGH ENOUGH TO MEASURE ALL POLLUTANTS	IN USE	SUITABLE FOR CO, O ₃ AND POSSIBLY HC &
	LONG-PATH WITH BLACKBODY SOURCE AND PPS RECEIVER	CO, O ₃ , HC, SO ₂ , NO ₂	2.5-12 μ m	.01-1	.001 ppm	ALL SPECIES	COMPLEX DATA REDUCTION	TESTED, EXTENSIVE FIELD TESTS PLANNED BY EPA	SUITABLE FOR ALL HAAGS POLLUTANTS
	LONG-PATH WITH BLACKBODY SOURCE AND SFC RECEIVER	CO, LIGHT HC, NO ₂ , SO ₂	2.5-12 μ m	.01-.3	.001 ppm	SIMPLE DEVICE	NOT SUITABLE FOR O ₃	FIELD TESTS IN PROGRESS	SUITABLE FOR ALL HAAGS POLLUTANTS
	LONG-PATH WITH BLACKBODY SOURCE AND FILTERWHEEL RADIOMETER AS RECEIVER	O ₃ , CO	4.5-10 μ m	.01-1	.01	SIMPLE DEVICE	ONLY TWO POLLUTANTS	FIELD TESTED (NOT SUCCESSFUL)	LIMITED SUITABILITY
	LONG-PATH WITH UV/VIS SOURCE AND SFC/MFC RECEIVER	NO ₂ , NO	3000-5000 \AA	TBD	TBD	SIMPLE DEVICE	ONLY TWO POLLUTANTS, SHORT RANGE	FIELD TESTED	SUITABLE ONLY FOR NO ₂ AND NO

For ranking these remote systems, guidelines are developed, viz. ,

- o Number of pollutants measurable with any given measurement principle;
- o Line profile versus line average;
- o Sensitivity and range as determined by theoretical analysis;
- o Bistatic versus monostatic;
- o Complexity in data analysis

Based on these guidelines, four remote monitors are judged to be superior, while the remainder are about equal. These four all operating in the infrared, are:

- (1) Short wavelength Long-Path Monitor with laser source,
- (2) Long-path monitor with blackbody source and Fourier-Transform Spectrometer receiver,
- (3) Short wavelength differential absorption spectrometer, and
- (4) Long-path monitor with blackbody source and gas filter correlation receiver.

In addition to the selection and ranking of remote monitors, procedures are developed that will allow the FAA to methodically interrogate remotely sensed data, taken by any Air Quality Control Region. These are phrased in the form of five questions:

1. Has the remote monitor that is collecting data in the vicinity of an airport been selected according to the selection criteria? There exist two major differences:
For R&D monitoring, the remote data do not need to be

relatable to the standards, and eye safety limits can probably be relaxed, while for air enforcement monitoring, the remote data must be relatable to the standards, and eye safety regulations must be observed.

2. What is the theoretical performance of the remote monitor? This can be answered by a step-by-step calculation of the signal-to-noise ratio, assuming a detector-noise-limited system. For R&D application, the results of the calculation will indicate whether or not the instrument is sensitive enough in the concentration and distance range for the intended measurement.
3. Has the instrument fulfilled the equivalency requirement? This question is relevant only for the future air enforcement application. If present procedures are followed, only data taken by individual instruments designated by manufacturer, model number, etc., and approved by the EPA and notice of acceptance duly published in the Federal Register need be accepted.
4. Have field calibrations been performed? For R&D application, established experimental practices of calibrating should be followed, namely as often as deemed necessary. For future air enforcement application, calibration before and after data collection is required.
5. Is the operator(s) of the remote monitor competent? The complexity of the remote monitors make it mandatory that the operator must be competent and familiar with the instrument, since it will be nearly impossible to make these complex machines "foolproof".

In addition to the interrogation procedures, a formalized validation procedure for each of the remote monitoring measurement principles selected is developed. It contains a description of the principle of operation and of the system, a definition of the system parameters, an algorithm to test the theoretical performance prediction, a description of the special performance requirements and the data analysis procedure. These validation procedures should be helpful in the selection of remote monitors for R&D work and future air enforcement action. Figure ES-1 presents the data interrogation and validation procedures in flow-chart form.

Since an airport is a (large) volume source composed of strongly-patterned, moving, changeable subsources, remote monitoring is especially necessary. The operational convenience and economy of remote monitors hold strong promise for their future adoption as standardized and accepted tools for airport pollution monitoring. The operating principles are well established. Increasing research usage provides a performance baseline upon which production designs can be developed.

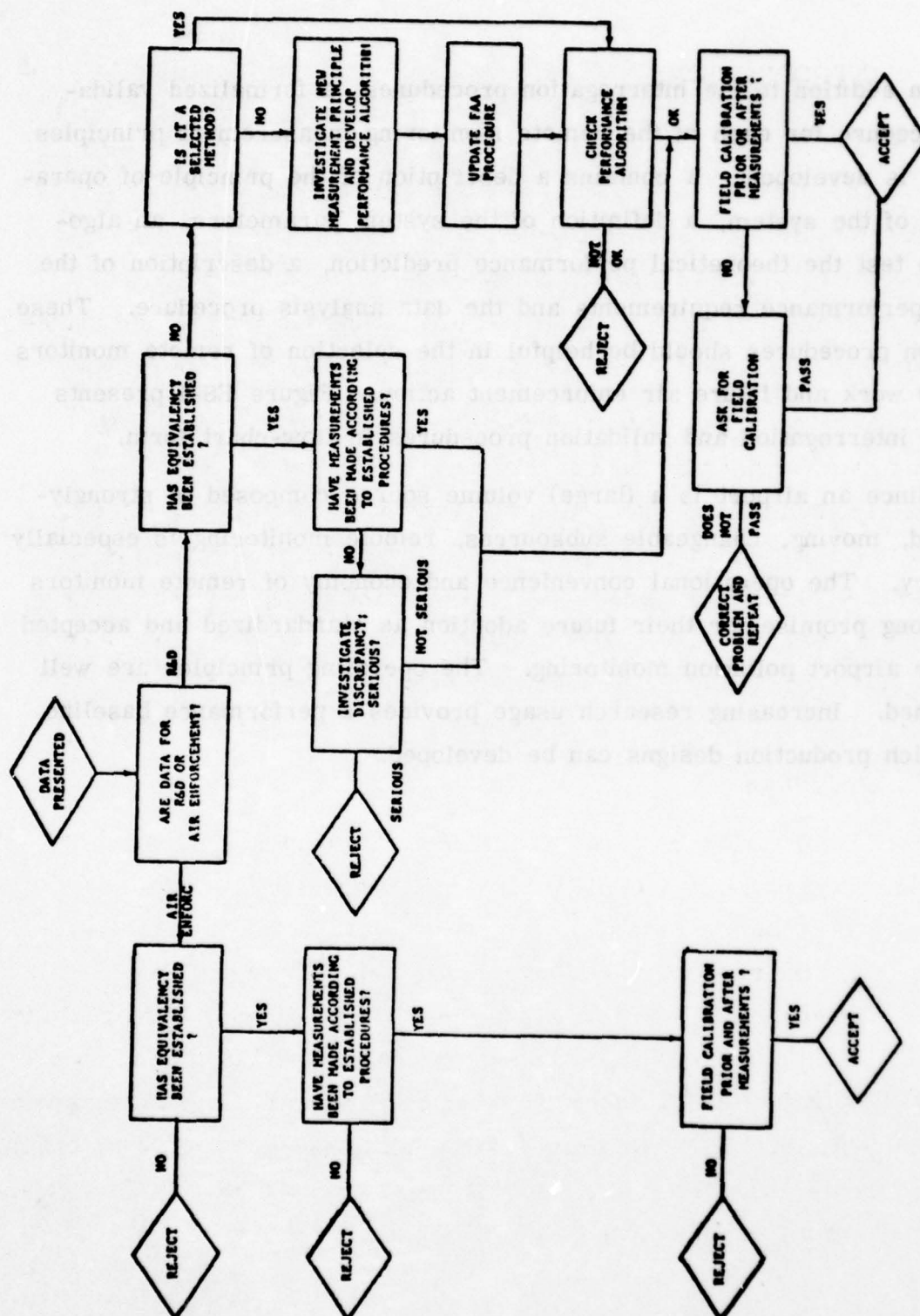


Figure ES-1. Data Interrogation and Validation Procedures.

1.0 INTRODUCTION

1.1 Objective of the Study

The objective of this study is the development of criteria by which the validity of pollution predictions and measurements in the airport environs can be judged. These criteria are to be applied to three technologies: (1) predictive mathematical models, (2) measurements by point samplers, and (3) measurements by remote monitors.

Because there are basic differences in the three technologies, the approaches in the criteria development are different. As will be shown, the criteria for the usefulness of the mathematical models is the agreement between predicted and measured pollution levels; the decision as to the most useful model is still outstanding. The criteria for the point samplers are already developed and codified by the EPA. The criteria for the remote monitors did not exist and had to be developed.

1.2 Study Plan

The first step in the present study is the consideration of the measurement requirements of the target pollutants within the constraints of the National Ambient Air Quality Standards (NAAQS). (The extension of the measurement requirements toward lower pollutant levels for the purpose of air pollution research and model validation should also be kept in mind in evaluating the point samplers and remote monitors). In addition to the NAAQS, there are other codified regulations of relevance to this study, such as measurement methodologies and control of air pollution from aircraft and aircraft engines, that need to be considered. The subject matter of this first step is discussed in Section 2.

The next step is the description and evaluation of the three technologies, i. e. ,

- o mathematical models
- o point samplers
- o remote monitors .

The description of the mathematical models are divided into "basic model concepts" and "individual models". These are then critically reviewed. Since all of them have certain advantages and disadvantages, the ultimatum criteria for their usefulness is the agreement between prediction and experimental data. No definitive experimental data set has yet been obtained and no comparison has been possible. The subject matter is discussed in Section 3.

The NAAQS are based upon the measurement methodologies of point samplers. Certain measurement principles have been designated and a mechanism for approval of reference and equivalent methods has been set up by the EPA. Details about this mechanism and a description of the different point samplers are given in Section 4. It is evident that measurements made with designated reference and equivalent methods that have been conducted according to the prescribed instructions must be accepted as valid. How these point samplings relate to the overall airport pollution is an entirely different question which can only be solved by applying a validated mathematical model(s).

The remote monitors require a more detailed treatment, since they are an evolving technology that has not been designated by the EPA acceptable measurement principle as yet. In Section 5, the principle of operation, state-of-the-art, advantages and disadvantages, operational requirements and critical analysis are described for several

remote monitoring systems. Selection criteria are then developed and some systems are selected as being potentially useful (Section 6). Formalized descriptions and requirements are then given for the selected systems, which constitute a potential procedure for validation of air pollution measurements. (Section 7)

1. 3 HISTORICAL BACKGROUND

In order to obtain the proper perspective for the purpose and needs of the present program, we have looked into the development that led to the present rules and regulations for aircraft emission standards. Much of the information contained herein was obtained from Mr. R. Evans^{(300)*} (EPA-Las Vegas). However, opinions expressed in this section are our own.

The Air Quality Act of 1967 required DHEW to investigate aircraft emissions. The report "Nature and Control of Aircraft Engine Exhaust Emissions" (Secretary DHEW, Dec. 1968) concluded that reduction of particulate emissions should be undertaken, that further research is needed for other aircraft pollution problems and, if warranted, further corrective action be implemented. At that time the important conclusion was reached that "in light of the relatively small contribution of aircraft to community air pollution in all places for which adequate data are available, and in view of the practical problems that would result from State and local regulatory action in this field, it is the Department's conclusion that adoption and enforcement of State or local emission control regulations pertaining to aircraft cannot be adequately justified at this time. The Department recommends that, if and when regulations become necessary, the rationale used to develop Federal rather than local emission standards for motor vehicles be applied to aircraft." Based on the conclusion of that study, a retrofit program was implemented to significantly abate smoke emissions.

The 1970 Clean Air Act Amendments required EPA to reassess the aircraft emission problem and its impact on the air quality. In 1972, EPA completed the report "Aircraft Emissions: Impact on Air Quality and Feasibility of Control"⁽⁹⁾. The data base for this report was provided by information developed by Northern Research and Engineering Corp.

*Superscript numbers refer to references listed at the end of this report.

(NREC), Cornell Research Laboratories and a study by EPA and the LAAPCD on the Los Angeles International Airport. The 1970 EPA report finds that emissions from aircraft are significant contributors to the regional burden of pollution. The conclusions are in toto:⁽⁹⁾

- "1. Aircraft emissions are significant contributors to the regional burden of pollution in comparison to other sources which will have to be controlled to meet National Ambient Air Quality Standards.
2. When airports are viewed as concentrated area sources of pollution emissions, either in isolation or in concert with their surrounding pollution sources, it can be demonstrated that airports will probably exert localized impact on air quality, in excess of the standards, even though relief is provided elsewhere in the region by controls relating to automobiles and stationary sources. That is, unless aircraft emissions are reduced, airports will still remain intense area emitters of pollutants when the emission densities in the surrounding region have been greatly reduced.
3. Aircraft emissions have impact on air quality in residential and business areas adjacent to major U. S. airports. The control of non-aircraft sources in and around such airports will not be adequate to insure compliance with the National Ambient Air Quality Standards indicating the need for controlling aircraft emissions.
4. There exists a variety of control techniques for effecting aircraft emissions reductions which appear both feasible and economically attractive during the next two decades. Emissions may be reduced by means of the following general approaches:

- (a) Modification of ground operational procedures.
- (b) Improvement in maintenance and quality control procedures to minimize emissions from existing families of turbine engines.
- (c) Development and demonstration of new combustion technology for major reductions in emissions from second-generation turbine and piston aircraft engines.
- (d) Retrofit of turbine engine fleets with existing technology for near-term reduction of emission. "

It is interesting to note that the major emphasis is placed upon emission from aircraft and less on non-aircraft sources. Inspection of the location of the sampling sites and the results of monitoring carbon monoxide at LAX ⁽¹⁾ does not necessarily support the above conclusions. It is found that some of the sampling sites near the automobile parking lots show the highest values while the sampling site at the end of the runway show some of the lowest values of carbon monoxide concentrations (effect of wind direction apparently included).

From 1972 on, mathematical models to calculate and predict pollution levels at airports were being developed by NREC, GEOMET and Argonne National Laboratory (see Section 3). To clarify remaining questions and to verify the models, further studies were sponsored by EPA and FAA.

Argonne National Laboratory conducted a study for the EPA of the air pollution impact methodology for airports and attendant land use. ⁽²⁾ This methodology was intended to integrate the air pollution impact of an airport and its associated ground support activities with that of the induced urban development in its vicinity. Flexibility was achieved through identifying, isolating and quantifying an array of airport-related and urban activities.

GEOMET conducted a program of air quality measurement, model development and model validation at the Washington National Airport during 1973/74 under EPA sponsorship. Data were taken over a period of six months. The sampling results indicated that the contribution from the airport-related emissions were small when compared to the total pollution burden at Washington National Airport.

In order to separate the contribution from airport-related emissions and surrounding environs, GEOMET conducted a study at the Atlanta International Airport, ⁽³⁾ especially to establish the difference in ground pollution levels between "normal" and "controlled" ground operations. The conclusions were that no significant and statistically meaningful reduction in pollution levels were measured with the limited amount of data available.

In 1971, the FAA initiated a program with Argonne National Laboratory (ANL) to study the total air quality impact of all airport operations on the airport vicinity. In the Introduction of the final report ⁽⁴⁾, it is stated "that the airport emission density is roughly equal to, or slightly exceeds, that of surrounding urban areas." The authors feel that this conjecture is supported by the LAX study ⁽¹⁾ "as well as by numerous other investigations, including the present one." On the other hand, the Heathrow Airport Study ⁽⁵⁾, as quoted in Reference 4, found that the pollution levels measured inside the airport never exceeded those found in Central London, and was not contributing "unduly" to local pollution.

From all of these results, we conclude tentatively that the contribution from inside an airport can hardly be distinguished from the pollution contributed by the environs when measured at ground level. It appears that measurements above ground will be necessary to determine

the impact of aircraft emission on the regional air quality and to validate the dispersion models above ground level.

Recently, the U. S. Air Force has started to investigate the environmental impact of its air bases. A brief intensive measurement program was conducted by EPA-Las Vegas and ANL at the Williams AFB in Arizona. Relatively low levels of THC, CH₄ and CO were measured near the runway. Higher values measured at certain times could conceivably result from the transport of polluted air from Phoenix (35 miles away)⁽⁶⁾. A much larger program is planned under a cooperative agreement between the USAF, AFCEC, Tyndall AFB and EPA, NERC-LV. The purpose is to assess the impact of aircraft emissions on ambient air quality, making possible the inclusion of one or more sites having large aircraft traffic volume, low neighboring auto traffic, simple mix of aircraft and well defined procedures and traffic patterns. This is expected to greatly simplify the modelling and model validation efforts inherent in any such study. The scope will include a determination of the impact of airport-related pollutant emissions on local air quality and the measurement of that impact over a statistically acceptable period of time. The data provided will be used to calculate air quality frequency distributions and to evaluate and to validate existing airport models.

2.0 MEASUREMENT REQUIREMENTS OF THE TARGET POLLUTANTS

2.1 Overview

The Code of Federal Regulations Number 40 (40 CFR) contains the rules and regulations for the protection of the environment. The parts relevant to the present study are listed in the following:

Part 50:

National primary and secondary ambient air quality standards. (It sets the standards for several pollutants: sulfur dioxide, particulate matter, carbon monoxide, photochemical oxidants, hydrocarbons and nitrogen dioxide. Its appendices A through F describe the reference methods for the determination of the pollutants).

Part 51:

Requirement for preparation, adoption and submittal of implementation plans for air pollution control. (It applies to the state agencies, and sets control strategies for the maintenance of the national standards. Its Appendix D contains the forms for listing the pollutant emissions inventory summaries, including the transportation area sources for motor vehicles, aircraft, railroads, etc. Its Appendix F indicates the type of information required; for aircraft it is "number of flights per year per type of aircraft".

Part 52:

Approval and promulgation of implementation plans for air pollution control. (It lists the implementation plans for all states.)

Part 53:

Ambient air monitoring reference and equivalent methods. (In Subpart B, it sets the performance specifications for automated methods for sulfur dioxide, oxidants, carbon monoxide and nitrogen dioxide, and in Subpart C, it sets the procedures for determining a consistent relationship between candidate methods and reference methods. In 53.16, the supersession of reference methods is described.)

Part 60:

Standards of performance for new stationary sources. (It sets the limits for the discharge of pollutants into the atmosphere by various manufacturing and treatment plants. The pollutants regulated so far are particulate matter, SO_2 , NO_x , H_2S , CO, total fluorides, and acid mist. In Appendix A, fourteen reference methods for determining pollutant concentrations are described. Appendix B contains performance specifications for continuous monitors for opacity, SO_2 and NO_x , and CO_2 and O_2 .)

Part 61:

National emission standards for hazardous air pollutants. (It sets the standards for asbestos, beryllium (including beryllium rocket motor firing) and mercury. In Appendix B, the test methods (101 through 105) for those pollutants are specified).

Part 81:

Air quality control regions, criteria, and control techniques.
(It specifies over 250 air quality control regions in the U. S. Guidelines for the use of pollutant standards index (PSI) for those control agencies wishing to report an air quality index on a daily basis have been published in 41FR37660, September 7, 1976).

Part 87:

Control of air pollution from aircraft and aircraft engines.
(It sets the standards for fuel venting and exhaust emissions for in-use and new aircraft and aircraft gas turbine engines, including supersonic aircraft, and aircraft piston engines. Test procedures for engine exhaust gaseous (hydrocarbons, carbon monoxide, oxides of nitrogen) emissions and smoke emissions are given.)

2. 2 National Ambient Air Quality Standards

The National Ambient Air Quality Standards (NAAQS) were promulgated in 1971. The primary standards define levels of air quality which EPA judges are necessary, with an adequate margin of safety, to protect the public health. The secondary standards define levels of air quality which EPA judges necessary to protect the public welfare from any known or anticipated adverse effects of a pollutant. Such standards are subject to revision, and additional primary and secondary standards may be promulgated as EPA deems necessary to protect the public health and welfare.

To implement these standards, the U. S. A. has been divided into more than 250 Air Quality Control Regions (40C FR81), the boundaries of which are based on considerations of urban-industrial distribution, topographical and meteorological factors, etc. In accordance with the provisions of Section 110 of the Clean Air Act, the States have submitted plans that provide for the implementation, maintenance, and enforcement of the National Air Quality Standards on a regional (air quality region) basis. The State Implementation Plan (SIP) for each region must provide for attainment of the primary standards in 3-5 years depending on whether an extension has been granted. The State plan is required to set forth the procedure for attaining the secondary standards within a reasonable amount of time. In the meantime, EPA has promulgated the requirements of emission monitoring of all point and area sources to be included in the SIP's (40CFR51). These requirements include the source categories to be affected and emission monitoring, recording, and reporting requirements for those sources. In Table 2-1, the NAAQS for six pollutants are shown. EPA has stipulated that the promulgation, or revision of national primary and secondary ambient air quality standards shall not prohibit any State from establishing ambient air quality standards for that State or any portion thereof which are more stringent than the national standards.

As an example, we show a comparison between the NAAQS and the California standards, which are generally considered to be more stringent than in other States (Table 2-2). The California standards are values that are not to be equaled or exceeded. Concentration expressed first in units in which it was promulgated. Equivalent units given in parentheses are based upon a reference temperature of 25°C and a

TABLE 2-1. National Ambient Air Quality Standards

Pollutant	Standard Description
Carbon monoxide (Primary and secondary standards are the same)	<ul style="list-style-type: none"> - 10 milligrams per cubic meter (9 ppm), maximum 8-hour concentration not to be exceeded more than once per year. - 40 milligrams per cubic meter (35 ppm), maximum 1-hour concentration not to be exceeded more than once per year.
Nitrogen dioxide (Primary and secondary standards are the same)	<ul style="list-style-type: none"> - 100 micrograms per cubic meter (0.05 ppm), annual arithmetic mean.
Hydrocarbons (non-methane) (Primary and secondary standards are the same)	<ul style="list-style-type: none"> - 160 micrograms per cubic meter (0.24 ppm), maximum 3-hour concentration (6-9 a.m.) not to be exceeded more than once per year. For use as a guide in devising implementation plans to meet the oxidant standards.
Particulate matter Primary standard	<ul style="list-style-type: none"> - 75 micrograms per cubic meter, annual geometric mean. - 260 micrograms per cubic meter, maximum 24-hour concentration not to be exceeded more than once per year.
Secondary standard	<ul style="list-style-type: none"> - 60 micrograms per cubic meter, annual geometric mean, as a guide to be used in assessing implementation plans to achieve the 24-hour standard. - 150 micrograms per cubic meter, maximum 24-hour concentration not to be exceeded more than once per year.
Sulfur dioxide Primary standard	<ul style="list-style-type: none"> - 80 micrograms per cubic meter, annual arithmetic mean. - 365 micrograms per cubic meter, maximum 24-hour concentration not to be exceeded more than once per year.
Secondary standard	<ul style="list-style-type: none"> - 1300 micrograms per cubic meter, maximum 3-hour concentration not to be exceeded more than once per year.
Oxidant (Primary and secondary standards are the same)	<ul style="list-style-type: none"> - 160 micrograms per cubic meter, maximum 1-hour concentration, not to be exceeded more than once per year.

TABLE 2-2. Comparison between NAAQS and California Ambient Air Quality Standards

Pollutant	Averaging Time	California Standards		National Standards		
		Concentration	Method	Primary	Secondary	Method
Oxidant (Ozone)	1 hour	0.10 ppm (200 ug/m ³)	Ultraviolet Photometry	160 ug/m ³ (0.08 ppm)	Same as Primary Std.	Chemiluminescent Method
Carbon Monoxide	12 hour	10 ppm (11 mg/m ³)	Non-Dispersive Infrared Spectroscopy	—	Same as Primary Standards	Non-Dispersive Infrared Spectroscopy
	8 hour	—		10 mg/m ³ (9 ppm)		
	1 hour	40 ppm (46 mg/m ³)		40 mg/m ³ (35 ppm)		
Nitrogen Dioxide	Annual Average	—	Saltzman Method	100 ug/m ³ (0.05 ppm)	Same as Primary Standards	Modified J-H Saltzman (O ₃ corr.) Chemiluminescent
	1 hour	0.25 ppm (470 ug/m ³)		—		
Sulfur Dioxide	Annual Average	—	Conductimetric Method	80 ug/m ³ (0.03 ppm)	—	Pararosaniline Method
	24 hour	0.04 ppm (105 ug/m ³)		365 ug/m ³ (0.14 ppm)	—	
	3 hour	—		—	1300 ug/m ³ (0.5 ppm)	
	1 hour	0.5 ppm (1310 ug/m ³)		—	—	
Suspended Particulate Matter	Annual Geometric Mean	60 ug/m ³	High Volume Sampling	75 ug/m ³	60 ug/m ³	High Volume Sampling
	24 hour	100 ug/m ³		260 ug/m ³	150 ug/m ³	
Sulfates	24 hour	25 ug/m ³	AIHL Method No. 61	—	—	—
Lead	30 Day Average	1.5 ug/m ³	AIHL Method No. 54	—	—	—
Hydrogen Sulfide	1 hour	0.03 ppm (42 ug/m ³)	Cadmium Hydroxide Stractan Method	—	—	—
Hydrocarbons (Corrected for Methane)	3 hour (6-9 a.m.)	—	—	160 ug/m ³ (0.24 ppm)	Same as Primary Standards	Flame Ionization Detection Using Gas Chromatography
Ethylene	8 hour	0.1 ppm	—	—	—	—
	1 hour	0.5 ppm		—	—	—
Visibility Reducing Particles	1 observation	In sufficient amount to reduce the prevailing visibility to less than 10 miles when the relative humidity is less than 70%		—	—	—

reference pressure of 760 mm of mercury. All measurements of air quality are to be corrected to a reference temperature of 25°C and a reference pressure of 760 mm of Hg (1,013.2 millibar); ppm in this table refers to ppm by volume, or micromoles of pollutant per mole of gas. The method in the California standards can be substituted by any equivalent procedure which can be shown to the satisfaction of the Air Resources Board to give equivalent results at or near the level of the air quality standard. The California standard for prevailing visibility is defined as the greatest visibility which is attained or surpassed around at least half of the horizon circle, but not necessarily in continuous sectors.

Recently⁽²⁸⁹⁾, the EPA has issued guidelines for the use of the Pollutant Standards Index (PSI) for those local and state air pollution control agencies wishing to report an air quality index on a daily basis. The document also includes appropriate monitoring and reporting guidance. The guideline is the result of an earlier study showing that of all the air quality indices in use today, no two are exactly the same. A potentially serious problem of public confusion can occur in regions where neighboring states and cities use different indices. The PSI places maximum emphasis on protecting the public health; that is, it advises the public of any possible adverse health effects due to pollution. In order to err on the side of public safety, the index stresses reporting on the basis of the stations with the highest pollutant concentrations and assumes that other unsampled portions of the community will also experience high concentrations. In addition, its emphasis is upon acute health effects occurring over very short time periods (24 hours or less) rather than chronic effects occurring over months or years.

It is not intended for, and should not be used for, ranking urban areas in terms of the severity of their air pollution problems. Such rankings require the use of many other kinds of environmental data not incorporated in this index.

Finally, the Appendix discusses the meteorological information needs of forecasting relative index changes. This was prepared by personnel from the National Oceanic and Atmospheric Administration. The complete text of the 'Guideline for Public Reporting of Daily Air Quality' is reproduced in Appendix III of this report (Volume II).

2. 3 Classification and Emission Factors of Commercial Aircraft

Because emission rates vary according to engine type, number of engines and operating mode, EPA has classified commercial aircraft by type and defined the typical operating modes for each class throughout their landing and take-off (LTO) cycles (Ref. 9). The twelve classes are listed in Table 2 -3; classes 8-11 are exclusively military aircraft and are not included here.

EPA has categorized the operating modes as follows:⁽⁹⁾

- (1) Start-up and idle
- (2) Taxi
- (3) Idle at runway
- (4) Take-off
- (5) Climb-out to 3,000 foot elevation
- (6) Fuel dumping
- (7) Approach from 3,000 foot elevation
- (8) Landing
- (9) Idle and shutdown
- (10) Maintenance

According to Ref. 9, the aircraft emission data, obtained through various research programs funded by EPA, are summarized in Ref. 10.

Some data for three classes of turbine engines were given in Ref. 9. The three classes are:

- | | |
|----|--------------------------|
| T1 | < 6000 lb. thrust |
| T2 | 6000 - 29,000 lb. thrust |
| T3 | > 29,000 lb. thrust. |

TABLE 3

AIRCRAFT CLASSIFICATION SYSTEM

Category	Class	Type	Examples	Engine Model	Type	Thrust or power	Engines per aircraft
Air							
Carrier	1	Supersonic transport	Concorde Tupolev TU-144	R-R/Snecma Olympus 593	Turbojet	39,000 lb.	4
	2	Jumbo jet transport	Boeing 747 Douglas DC-10	P&WA JT9D	Turbofan	43,000 lb.	4
	3	Long-range jet transport	Boeing 707 Douglas DC-8	P&WA JT3D	Turbofan	18,000 lb.	4
	4	Medium range jet transport	Boeing 727 Douglas DC-9	P&WA JT8D	Turbofan	13,900 lb.	2.6
	5	Turboprop transport	Lockheed Electra Fairchild Hiller FH-227	Allison 501-D13	Turbo-prop	3,750 hp.	2.5
General Aviation							
	6	Business jet	Lockheed Jetstar North American Sabreliner	P&WA JT12	Turbojet	2,900 lb.	2.1
	7	Piston-engine utility	Cessna 210 Centurion Piper 32-300 Cherokee Six	Continental 10-520-A	Opposed piston	292 hp.	1
V/Stol							
	12	Helicopters and V/Stol	Silorsky S-61 Vertol 107	General Electric CT58	Turbo-shaft	1,390 hp.	2

2. 3b

The emission levels are reported for the case in which a "minor combustion chamber redesign" was made, i. e., the assumption is made that emission rates for all engines within a given class can be reduced to common, optimum levels (on a lb/1000 lb fuel basis) by minor combustor modifications. These optimum emission rates are based on the best performance reported for each engine class, excluding extreme data points. The results are listed in Table 2-4.

TABLE 2-4. Emission Rates in lb/1000 lb. of Fuel

Engine class	Pollutant	Mode		
		Idle/taxi	Approach	Takeoff
T1	CO	25	5	2
T1	THC	10	1	0.2
T1	NO _x	3	7	11
T1	DP	0.2	0.5	0.5
T2	CO	45	6	1
T2	THC	10	1	0.1
T2	NO _x	2	6	12
T2	DP	0.2	0.5	0.5
T3	CO	50	3	0.5
T3	THC	10	1	0.1
T3	NO _x	3	10	40
T3	DP	0.1	0.1	0.1

2. 4 Classification and Emission Factors of Military Aircraft

Because of the on-going measurement program at Williams AFB, conducted by EPA, NERC-LV* and its potential implication for the present program (see Section 2), we reproduce the list of USAF aircraft engine emission factors as published in Ref. 11. According to the preface in Ref. 11, this report is one of six closely related AFWL** technical reports:

"AFWL-TR-74-303 presents aircraft pollution emission data and landing and take-off cycle times for Air Force aircraft in common use.

AFWL-TR-74-54 is the Air Quality Assessment Model (AQAM) Operator's Manual and describes how to code input data in a usable computer format.

AFWL-TR-74-304 functions as the AQAM Technical Report in discussion of modelling theory and methods used.

AFWL-TR-279 describes the techniques used to develop the take-off length equations and climbout angles for most Air Force aircraft.

A computer documentation manual with a discussion of the mechanisms of the computer code will be published as a result of the FY 1975 USAF contract with Argonne National Laboratory.

"A field data collection manual is being planned to include detailed procedures and methods by which base level personnel can collect the required raw data to perform a complete air quality analysis on an Air Force Base." Updated engine emission factors are presented in the main body of Ref. 11, and are given here in Table 2-5. "The emission factors are intended to be used as 'best estimates' for environmental impact analysis. No attempt is made to assign statistical confidence levels since many variables are as yet undetermined such as engine-to-engine

* National Environmental Research Center - Las Vegas

** Air Force Weapons Laboratory

variability, single engine degradation factors, sampling variability and precise engine thrust variability for each of the aircraft operational modes. Continuing efforts both within the Air Force and by others will improve the confidence in the emission data base in years to come. The bulk of the recent emission data added to Reference 11 has been added from U. S. Navy reports. The errors in using this data from engines using JP-5 fuel versus Air Force engines using JP-4 data cannot be ascertained at this time.

Most if not all of the emission data presented for carbon monoxide, total hydrocarbons, and oxides of nitrogen has been taken with the use of measurement procedures as described in the Society of Automotive Engineers Aerospace Recommended Practice 1256. A considerable number of "judgement" decisions had to be made in the reduction of all data to the simplified summary which is presented.

Sulfur emissions were calculated using the percent of sulfur in fuel. Since essentially all sulfur is oxidized in the engine combustion process and the fuel sulfur content is relatively easy to measure, this calculated emission factor is considered more accurate than a measured emission factor would be. The sulfur emission factors used are based on the current average of 0.05 percent sulfur by weight in JP-4 and 0.03 percent sulfur in aviation gas for non-turbine aircraft.

Special caution should be used when applying any of the particulate emission data. There is no accepted measurement technique and considerable dependence of the results on the test methods used. Data which are presented generally include both the dry carbon particulates as well as all condensable organic materials. This data, for some engines, may considerably overestimate the particulate emissions since most condensables formed during the probe sampling measurement may have remained in the vapor form in the atmosphere. Consequently, the particulate data

presented should be used only as exaggerated "worst case" data for preliminary impact analysis and as a comparative value for future particulate emission data."

TABLE 2-5. USAF Aircraft Engine Emission Factors

ENGINE MODEL	ENGINE SERIES	AIRCRAFT TYPE	MODE	FUEL FLOW (1000 LB/HR)	POLLUTANT EMISSION RATE (LB/1000 LBS OF FUEL)*			
					CARBON MONOXIDE	UNBURNED HYDROCARBONS	OXIDES OF NITROGEN	TOTAL PARTICULATES*
J-52	PW-3	Hound Dog Missile	IDLE	.83	79.7	22.2 ¹	1.8 ¹	
			75% THRUST	4.86	9.5 ¹	1.0 ¹	7.5 ¹	
			MILITARY	6.49	2.1 ¹	.4 ¹	9.5 ¹	
J-57	PW-19W	B-52 C-E	IDLE	1.104	58.5 ¹	53.4 ¹	2.5 ¹	8.3 ¹
	PW-21	F-100 A-F	APPROACH (75% RPM)	1.709	26.4 ¹	12.0 ¹	3.6 ¹	
	PW-23	F-102 A	MILITARY	8.52	2.0 ¹	.7 ¹	11.8 ¹	12.0 ¹
	PW-55	F-101	AFTERBURNER	36.10	31.7 ¹	.7 ¹	4.4 ¹	
	PW-43W	B-52 F-G	IDLE	1.214	75.3 ¹	61.8 ¹	1.9 ¹	8.3 ¹
	PW-59W	YC-135 A	APPROACH (75% RPM)	1.849	46.1 ¹	22.8 ¹	3.6 ¹	
J-69	T-25	T-37 B	MILITARY	10.612	2.3 ¹	.9 ¹	15.2 ¹	12.0 ¹
			IDLE	.453	106.5 ¹	7.9 ¹	3.4 ¹	
			APPROACH (53% THRUST)	1.052	47.5 ¹	.04 ¹	5.26 ¹	
J-75	PW-17	F-106 A-B	MILITARY	1.307	20.6 ¹	.02 ¹	6.91 ¹	
			APPROACH (-90% THRUST)	1.7	76.2 ¹	56.86 ¹	1.29 ¹	.5 ¹
			MILITARY	11.3	1.4	0.1 ¹	11.9 ¹	
			AFTERBURNER	13.2	.6	0.23 ¹	8.2 ¹	1.05 ¹
J-79	GE-3	F-104 A-B	AFTERBURNER	51.7	12.0 ¹	0.12 ¹	4.1 ¹	
			MILITARY	9.33	13.0	.03 ¹	4.6 ¹	
			APPROACH (65% RPM)	2.72	10.0 ¹	.8 ¹	5.5 ¹	4.3 ¹
			IDLE	1.121	38.8 ¹	9.6 ¹	2.4 ¹	72.4 ¹
	GE-7-7A	F-104 C-D	MILITARY	9.33	13.0	.03 ¹	4.6 ¹	
	GE-15	F-4 C-D	AFTERBURNER	34.17	13.0	.01 ¹	4.6 ¹	10.8 ¹
J-85	GE-5	T-38, F-5	MILITARY	2.65	38.0 ¹	1.3 ¹	4.4 ¹	
			APPROACH	1.8	58.0 ¹	9.4 ¹	3.6 ¹	
			IDLE	.65	150.0	42.0 ¹	5.3 ¹	
			AFTERBURNER	7.2	21.0 ¹	.04 ¹	3.0 ¹	
TF-30	PW-3,7	F-111 A	AFTERBURNER	26.4	6.39 ¹	.014 ¹	9.0 ¹	29.3 ¹
			MILITARY	7.12	3.1	.165	26.9 ¹	8.34 ¹
			APPROACH (75% THRUST)	6.65	6.3 ¹	2.0 ¹	12.0 ¹	26.5 ¹
			IDLE	1.25	46.4 ¹	12.58 ¹	6.52 ¹	24.0 ¹
	PW-9	F-111 D	APPROACH	6.65	16.0 ¹	2.0 ¹	12.0 ¹	24.0 ¹
	PW-100	F-111 F	MILITARY	7.12	3.0 ¹	1.2 ¹	19.7 ¹	8.34 ¹
TF-33	PW-3	B-52 H	AFTERBURNER	42.95	24.8 ¹	2.0	4.47 ¹	5.36 ¹
			MILITARY	9.979	.41 ¹	.11 ¹	14.13 ¹	
			APPROACH	3.797	8.33 ¹	3.79 ¹	7.30 ¹	
TF-34	GE-100	A-10	MILITARY	3.532	114.0 ¹⁰	10.3 ¹⁰	3.7 ¹⁰	
			APPROACH	1.296	15.0 ¹⁰	0.6 ¹⁰	7.7 ¹⁰	
			IDLE	.365	0.6 ¹⁰	0.21 ¹⁰	12.6 ¹⁰	

Footnotes:

¹Aircraft Engine Emissions Catalog, AESD 101-74-1, Navy Environmental Protection Data Base, North Island, CA, March 1974.

²Data from Nature and Control of Aircraft Engine Exhaust Emissions: Northern Research and Engineering Corporation, Report No. 1134-T, Eng. A - JT3C. Data does not specify whether soluble particulates are included or not.

³Exhaust Emission Measurements on Teledyne CAE Turbojet Engines, CAE TN 717-71-09-02, August 1971.

⁴Robson, F. L., Kesten, A. S., and Lessard, R. D.: Analysis of Jet Engine Test Cell Pollution Abatement Methods, AFML-TN-73-18.

⁵Blazowski, William S., Personal Correspondence using recent data collected under AFAPL Contract F33615-73-C-2047 with the General Electric Company, 20 September 1974.

⁶Sulfur emissions are 1.0 lbs/1000 lbs fuel for all turbine engines using JP-4 fuel.

⁷A Particulate measurement technique has not yet been standardized. These values include all condensable particulates and are far higher than solid particulates alone.

⁸Author's estimate based on data in references 1 and 5.

⁹Lazlier, G. R. and Gearhart, J. W.: Measurement of Pollutant Emissions From an Afterburning Turbojet Engine at Ground Level, AEDC-TN-72-70, August 1972.

¹⁰Data from Burnett, R. D.: Noise and Pollution Emissions from Noise Suppressors for Engine Test Stands and Aircraft Power Check Pads, Report 71R-19 January, 1972, USAF Environmental Health Laboratory.

¹¹Bogden, Leonard and McAdams, H. T.: Analysis of Exhaust Emission Measurements, CAE Report No. NA-6007-K-1, October 15, 1971.

¹²Personal telephone communication from Lt. Roth (ASD) to Capt Nauque (AFML) on 17 Dec 74 based on most recent A-10 System Program Office data.

TABLE 2-5. (continued)

ENGINE MODEL	ENGINE SERIES	AIRCRAFT TYPE	MODE	FUEL FLOW (1000 LB/HR)	POLLUTANT EMISSION RATE (LB/1000 LBS OF FUEL)*				
					CARBON MONOXIDE	UNBURNED HYDROCARBONS	OXIDES OF NITROGEN	TOTAL PARTICULATES*	
TF-39	GE-1	C-5	IDLE	1.13	50.0 ¹¹	15.0 ¹¹	3.5 ¹¹	0.3 ¹¹	(Dry
			APPROACH	5.74	3.0 ¹¹	0.3 ¹¹	25.0 ¹¹	1.4 ¹¹	Particles
			MILITARY	11.41	0.5 ¹¹	0.1 ¹¹	38.0 ¹¹	1.5 ¹¹	Only)
TF-41	GE-1 (low smoke)	C-5	IDLE	1.13	50.0 ¹¹	15.0 ¹¹	3.5 ¹¹	0.04 ¹¹	
			APPROACH	5.74	3.0 ¹¹	0.3 ¹¹	28.0 ¹¹	0.07 ¹¹	
			MILITARY	11.41	0.5 ¹¹	0.1 ¹¹	40.0 ¹¹	0.04 ¹¹	
F-100	A-1	A-7	IDLE	1.07	107.1 ¹¹	66.2 ¹¹	1.3 ¹¹		
			APPROACH (62% THRUST)	5.31	5.2 ¹¹	2.4 ¹¹	10.6 ¹¹		
			MILITARY	9.04	1.6 ¹¹	0.6 ¹¹	22.3 ¹¹		
F-101	PW-100	F-15	IDLE	1.06	19.3 ¹²	2.3 ¹²	4.0 ¹²	11 ¹²	(Dry
			APPROACH	3.0	3.0 ¹²	.6 ¹²	11.0 ¹²	.33 ¹²	Particles
			MILITARY	10.04	1.8 ¹²	.05 ¹²	44.0 ¹²	.83 ¹²	Only)
			AFTERBURNER	44.2	55.0 ¹²	.1 ¹²	16.5 ¹²	0.012	
T-56	GE-100	B-1	IDLE	Not for public release	17.2 ¹³	.9 ¹³	4.2 ¹³	.044 ¹³	
			APPROACH		3.2 ¹³	.3 ¹³	8.2 ¹³	.045 ¹³	
			MILITARY		.5 ¹³	.2 ¹³	23.9 ¹³	.05 ¹³	
			AFTERBURNER		65.0 ¹³	1.0 ¹³	8.0 ¹³	.052 ¹³	
O-470	A-7	C-130 B,E,F	IDLE	.548	28.10 ²	11.92 ²	3.93 ²		
			APPROACH	1.053	3.48 ²	.94 ²	7.38 ²		
			MILITARY	2.079	1.04 ²	.21 ²	10.98 ²		
10-360	A-15	C-130 H	IDLE	.493	18.05 ²	15.05 ²	2.45 ²		
			APPROACH	1.145	3.04 ²	.29 ²	6.38 ²		
			MILITARY	2.392	1.56 ²	.18 ²	11.66 ²		
10-360	C	O-1 A	IDLE	.01512	742.5 ²	191.4 ²	1.0 ²		
			APPROACH	.08555	691.7 ²	9.5 ²	9.4 ²		
			MILITARY	.13125	1155.8 ²	20.4 ²	1.1 ²		
10-360	C	O-2 AB	IDLE	.01517	848.2 ²	144.5 ²	1.1 ²		
			APPROACH	.06786	972.0 ²	17.4 ²	6.6 ²		
			MILITARY	.0887	1031.3 ²	22.5 ²	5.3 ²		

Footnotes:

¹¹Bahr, D. W., General Electric Aircraft Engine Group (GEAEG) Personal correspondence to Capt W. S. Blazowski, Air Force APL, August 16, 1973 and Mr. T. Lyon, GEAEG, personal telcon to Capt D. F. Naugle, 11 October 1974.

¹²Updated Final Environmental Statement for B-1 Aircraft Development, Dept of the Air Force, AFES-7-2F(1), October 1973.

¹³Orthman, Colonel Harry, F-15 SPO, ASD/YF, Personal correspondence to AFML using ASD/YFEJ adjustments to measured data in an Arnold Research Organization Inc. letter report dated 7 September 1973.

*Average sulfur emissions are 1.0 lb/1000 lbs fuel for turbine engines using JP-4 fuel and 0.6 lb/1000 lbs fuel for piston engines using "aviation gasoline."

*A Particulate measurement technique has not yet been standardized. These values do not include condensable particulates and are far lower than total particulates.

3. DESCRIPTION AND EVALUATION OF MATHEMATICAL MODELS

3.0 INTRODUCTION

The Air Quality Act of 1967 and the Clean Air Act Amendments of 1970 required an evaluation of the effects of various aircraft activities on air quality. As part of this evaluation, the Federal Aviation Administration (FAA) and the Environmental Protection Agency (EPA) have sponsored a number of programs aimed toward the development, validation and utilization of airport air pollution simulation models. These models are designed to simulate airport air pollution emissions, calculate the atmospheric dispersion and transport of the emitted pollutants, and estimate the concentration of pollutants over a given area of interest for specific time periods. Airport simulation models are thus a mechanism for determining the relationship between airport pollutant emission data and ambient air quality data (and relating it to national air quality standards). As such they are an invaluable tool for airport environment impact analysis, specifically as applied to:

- (1) the assessment of the impact of airport activities on local or regional air quality;
- (2) the prediction of "worst case" situations, based on specific meteorological conditions;
- (3) the evaluation of the possible effectiveness of various air pollution control strategies; and
- (4) the development of airport design criteria (aimed toward lessening possible environmental effects).

Atmospheric dispersion of air pollutants is a complex phenomena, and simulation models vary greatly in the mathematical techniques used to approximate dispersion. By far the most widely used methods today employ either the Gaussian technique or the Conservation of Mass approach. Gaussian models are based on the assumption that pollutant dispersion can be represented by a Gaussian distribution. Conservation of Mass models are based on the solution of the partial differential equations governing turbulent diffusion. Each of these techniques has inherent advantages and limitations, due primarily to the basic assumptions and simplifications required in their solution or application.

Aside from the complexities of modeling atmospheric dispersion in general, airports present a particularly difficult problem in air pollution simulation. This is due mainly to the multitude and variety of pollutant source configurations present at an airport and the intermittent and/or mobile nature of many of the emissions. Sources inside the airport boundaries which must be considered include aircraft, ground service vehicles, terminal access traffic, parking facilities, fuel storage and handling facilities, aircraft engine test facilities, and heating plants. Sources outside the specific airport boundaries but near the airport must also be considered, including highways, parking areas, and industrial, commercial or residential complexes. In many cases emissions from these sources are highly variable, depending upon the specific source type* and mode of operation. Additional complexities arise because many of these sources are not only mobile in two or even three dimensions, but also may operate in a number of different modes in a relatively short period of time. These factors, coupled with the inherently stochastic

* Vehicle sources, for example, may further be classed according to use, age, weight, etc.

nature of the governing meteorological conditions and the basic difficulties associated with describing turbulent atmospheric dispersion, make airport air quality modeling a particularly complex problem.

This report deals with the comparison and evaluation of eleven air quality simulation models as they apply to the study of airport air pollution. The eleven models considered are:

- The TRW Air Quality Display Model (AQDM)
- The Northern Research and Engineering Corporation (NREC) Model
- The GEOMET Model
- The Argonne National Laboratory (ANL) Airport Vicinity Air Pollution (AVAP) Model
- The ANL Air Quality Assessment Model (AQAM)
- The Systems, Science and Software (S³) Photochemical Model
- The Aerovironment Model
- The Walden-Research Model
- The Transportation Systems Center/Environmental Protection Agency (TSC/EPA) Model
- The California Department of Transportation (CALTRANS) Model
- The Environmental Research and Technology (ER&T) Model

The latter five of the models examined have been developed as highway air pollution models and because of the similarities in problems at airports and in urban areas they are being considered as potential models for estimating air quality levels near airports.

All but three of these models use the Gaussian approach to simulation of pollutant advection and diffusion. The S³ Photochemical Model is based upon the Conservation of Mass approach, and uses the "Particle-in-Cell" technique to describe pollutant dispersion. The Aerovironment and ER&T model is also a conservation of mass model. Because of this basic difference in approach, part of this report concerns itself with a discussion of the concepts, assumptions and limitations associated with each of these air quality modeling methods.

Four of the eleven models considered have been applied specifically to the problem of airport air quality. For these applications, certain modifications to the basic model concepts have been made to account for specific problems associated with airport modeling. In each of these cases considerable effort has gone into the evaluation (and sometimes modeling) of the complex emission parameters and/or meteorological data required in the analysis. As was indicated earlier, these considerations are of prime importance in the evaluation of airport air quality models. Thus, details as to the specific factors considered and the methods used in interpretation of these factors are presented (where applicable) as part of this report.

A particularly important factor which also must be considered in any evaluation of air quality simulation models is validation.* The last

* Here validation is taken to mean a study of the performance of a given model by examination of the individual portions of the model (i.e., the subroutines dealing with emissions, diffusion and advection, and meteorology) using detailed data from specifically applicable, controlled experimentation. Calibration, on the other hand, involves a statistical comparison between calculated and measured pollutant concentrations. On the basis of this comparison suitable adjustment factors can be incorporated into the model to give better agreement with measured values for a specific application.

section of this report concerns itself with the requirements associated with airport air quality validation and a discussion of the level of validation associated with each of the models considered.

3.1 BASIC MODEL CONCEPTS

One of the major complexities of airport air quality modeling is the multitude and variety of pollutant sources involved. These sources may be classified (according to their time dependent geophysical configuration) into three basic categories: point sources, line sources, or area sources. As a first approximation a number of airport air quality models consider all of these source types as some variation of one or more point sources.* Other models employ a true Gaussian line source representation, derived by integrating the basic Gaussian point source formulation in one dimension. Area sources may then be treated as a crosswind line source with a normal distribution of pollutant in the crosswind directions. Discussion of the specific approach used for each model considered may be found in Section 3.2. In this report, discussion of the basic phenomena involved and the model concepts used is presented in terms of point source emissions,** with modifications for more complex situations incorporated as they arise in consideration of specific models.

* The ramifications of this approximation will be discussed in a later section.

** Except for a brief discussion on Gaussian treatment of line and area sources.

3. 1. 1 The Problem

Aircraft are generally considered the most important emission sources associated with airports.* However, aircraft present one of the more complex emission source problems, because:

- (1) their position is variable in three dimensions;
- (2) their mode of operation (and thus their emission characteristics) may change several times over a matter of minutes;
- (3) their emissions are thermally excited; and
- (4) they impart to their emissions a momentum variable in magnitude and direction (again, in three dimensions).

In short, aircraft emissions are position variant, non-continuous, non-steady-state, possibly buoyant, and have an inherent variable velocity and direction upon release. Similar complexities also arise in consideration of other airport emission sources, particularly vehicles.

The least complex emission source associated with airport air quality simulation is that of the non-mobile point source (such as a power or heat generation plant). For purposes of initial discussion, consider the idealized case of emissions from a stationary, elevated, continuously emitting and steady-state point source. The coordinate system for this source may be defined in Figure 3.1.1-1. The origin is at ground level directly below the point of emission release. The x-axis is positioned to extend horizontally in the mean wind direction. The y-axis is horizontal in the cross-wind direction, and the z-axis is vertical.

* Here "most important" refers to the fact that aircraft are identified with the primary activity at airports, and does not necessarily imply most significant in terms of air quality impact.

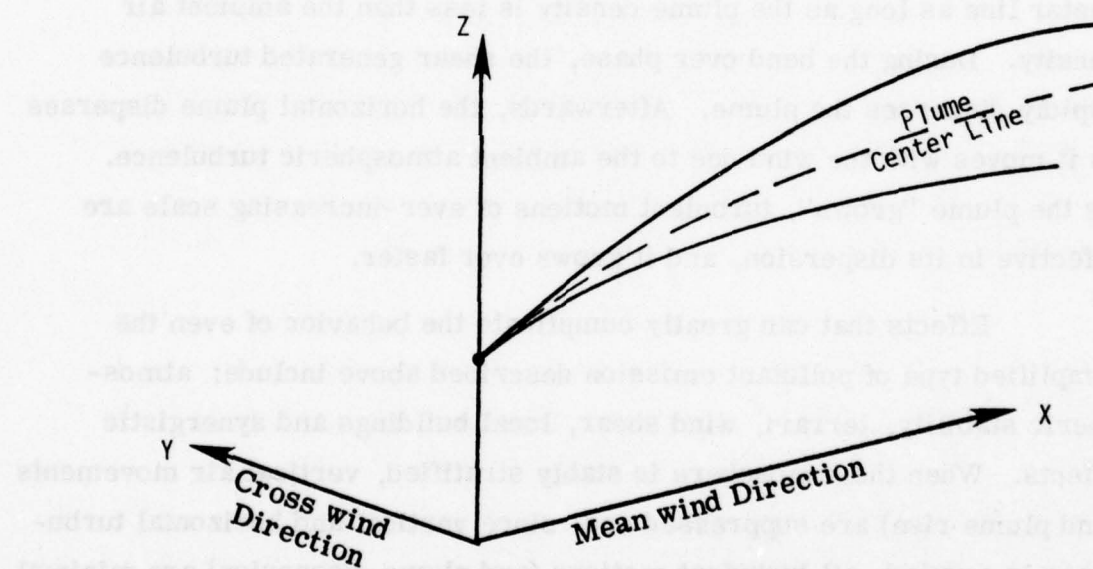


Figure 3.1.1-1. Elevated Point Source Emission.

As the effluent is emitted from the source into the atmosphere, a plume is formed whose initial behavior depends upon the specific conditions under which the effluent is released. If the effluent exists with a given vertical velocity (as in the case of a power plant stack emission), the plume will be lofted by its initial momentum and later by buoyancy (if its temperature is greater than that of the atmosphere). The plume will then slowly bend over toward the ambient wind direction (as illustrated in Figure 3. 1. 1-1). Bend over is caused by entraining ambient air (with its momentum) through the velocity shear generated turbulence at the plume "edge". This initial phase, exit to bend over, is dominated by the plume momentum rise, but thereafter buoyancy raises the plume center line as long as the plume density is less than the ambient air density. During the bend over phase, the shear generated turbulence rapidly disperses the plume. Afterwards, the horizontal plume disperses as it moves with the wind due to the ambient atmospheric turbulence. As the plume "grows", turbulent motions of ever-increasing scale are effective in its dispersion, and it grows ever faster.

Effects that can greatly complicate the behavior of even the simplified type of pollutant emission described above include: atmospheric stability, terrain, wind shear, local buildings and synergistic effects. When the atmosphere is stably stratified, vertical air movements (and plume rise) are suppressed and, since vertical and horizontal turbulence is coupled, all turbulent motions (and plume dispersion) are minimal. When the plume is in an unstable atmosphere, buoyant effects and dispersion are enhanced (see Figure 3. 1. 1-2).

Terrain affects both the wind and turbulence. The wind is generally channeled (increasingly with greater atmospheric stability) with

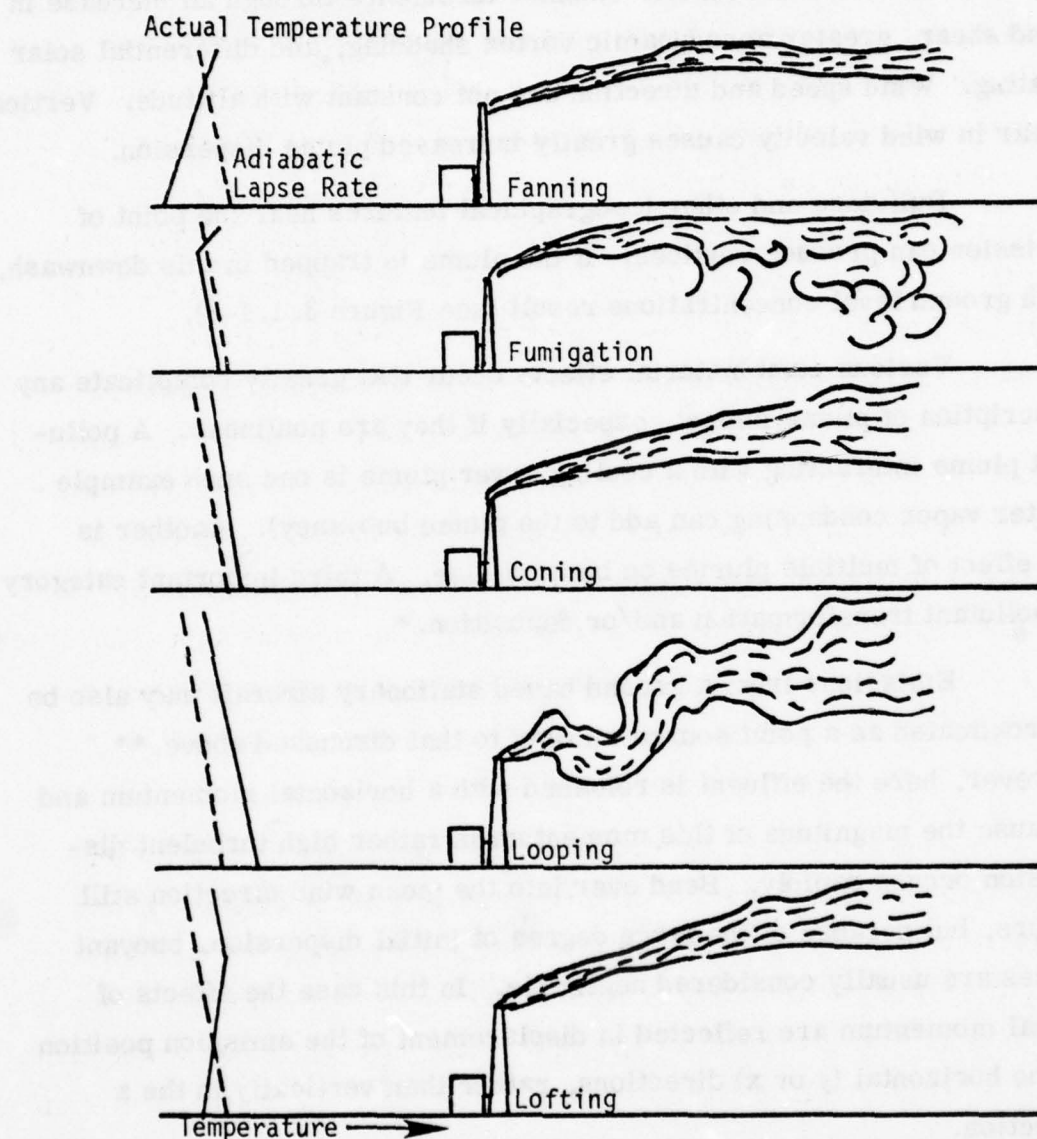


Figure 3.1.1-2. Effect of Temperature Profile on Plume Rise and Diffusion for a Point Source Stacks Emission^{301, 302}

the terrain. Terrain features enhance turbulence through an increase in wind shear, greater aerodynamic vortex shedding, and differential solar heating. Wind speed and direction are not constant with altitude. Vertical shear in wind velocity causes greatly increased plume dispersion.

Buildings and other topographical features near the point of emission can produce vortices. If the plume is trapped in this downwash, high ground level concentrations result (see Figure 3. 1. 1-3).

Various combinatorial effects occur that greatly complicate any description of plume impact, especially if they are nonlinear. A pollutant plume interacting with a cooling tower plume is one such example (water vapor condensing can add to the plume buoyancy). Another is the effect of multiple plumes on buoyant rise. A third important category is pollutant transformation and/or deposition.*

Emissions from a ground based stationary aircraft may also be approximated as a point source similar to that discussed above.** However, here the effluent is released with a horizontal momentum and because the magnitude of this momentum is rather high turbulent dispersion occurs rapidly. Bend over into the mean wind direction still occurs, but because of the large degree of initial dispersion, buoyant forces are usually considered negligible. In this case the effects of initial momentum are reflected in displacement of the emission position in the horizontal (y or x) directions, rather than vertically in the z direction.

* Transformation refers to a change of composition due to physical, chemical, or photochemical reactions. Deposition refers to any mechanism by which pollutants are returned to or retained by the ground, including: rain, snow, or ice effects; gravitational effects; and ground level impaction, adsorption, or absorption.

** Assuming steady-state and continuous emission conditions.

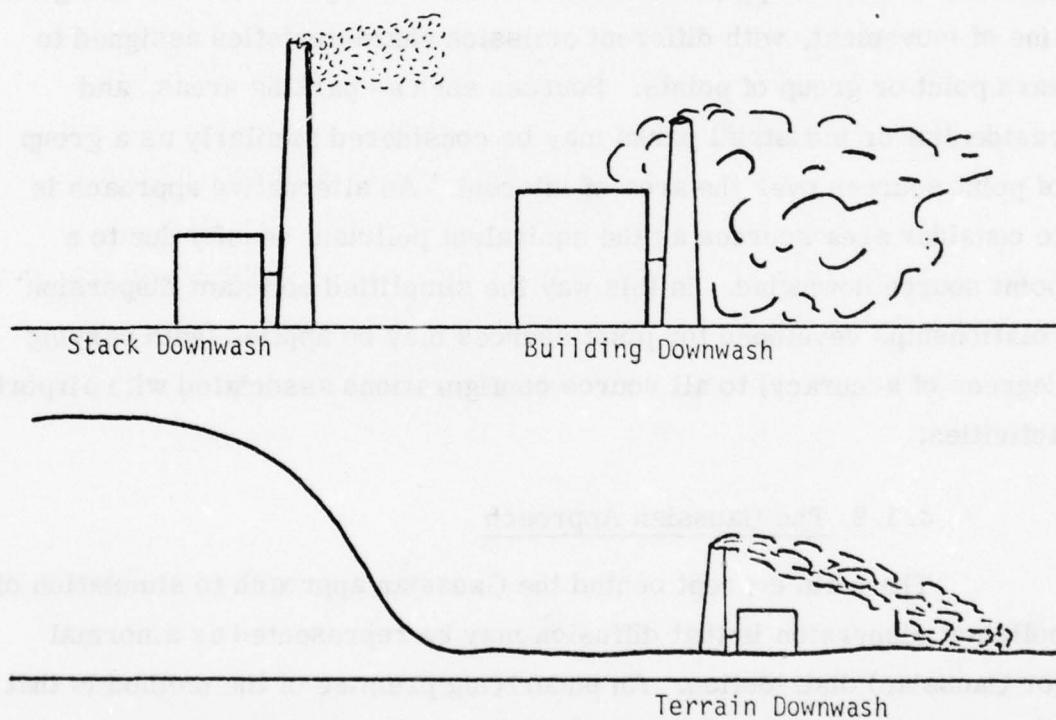


Figure 3. 1. 1-3. Undesirable Aerodynamic Effects on Stack Emissions^{301, 302.}

As was indicated earlier, for other types of airport emission sources the situation is generally much more complex. Aircraft go through a whole series of activities in which their emission characteristics may vary (start up and idle, taxi, engine checkout, takeoff and landing, climbout and approach, etc.). Vehicle emissions are a similar problem. When in motion both of these sources may be considered, to a first approximation, as a series of point sources along the line of movement, with different emission characteristics assigned to each point or group of points. Sources such as parking areas, and residential or industrial parks may be considered similarly as a group of point sources over the area of interest. An alternative approach is to consider area sources as the equivalent pollutant density due to a point source downwind. In this way the simplified pollutant dispersion relationships developed for point sources may be applied (with varying degrees of accuracy) to all source configurations associated with airport activities.

3.1.2 The Gaussian Approach

The main concept behind the Gaussian approach to simulation of pollutant dispersion is that diffusion may be represented as a normal (or Gaussian) distribution. An underlying premise of the method is that the complex behavior exhibited by pollutants as described above may be resolved into two distinct subproblems: (1) that of calculating the centroidal trajectory of emitted pollutants (the plume center-line) due to wind blown transport or advection and pollutant rise (where applicable), and (2) a separate calculation to obtain the spread of pollutants due to diffusion. This decoupling of pollutant motion into mean path and diffusion is graphically illustrated in Figure 3.1.2-1.

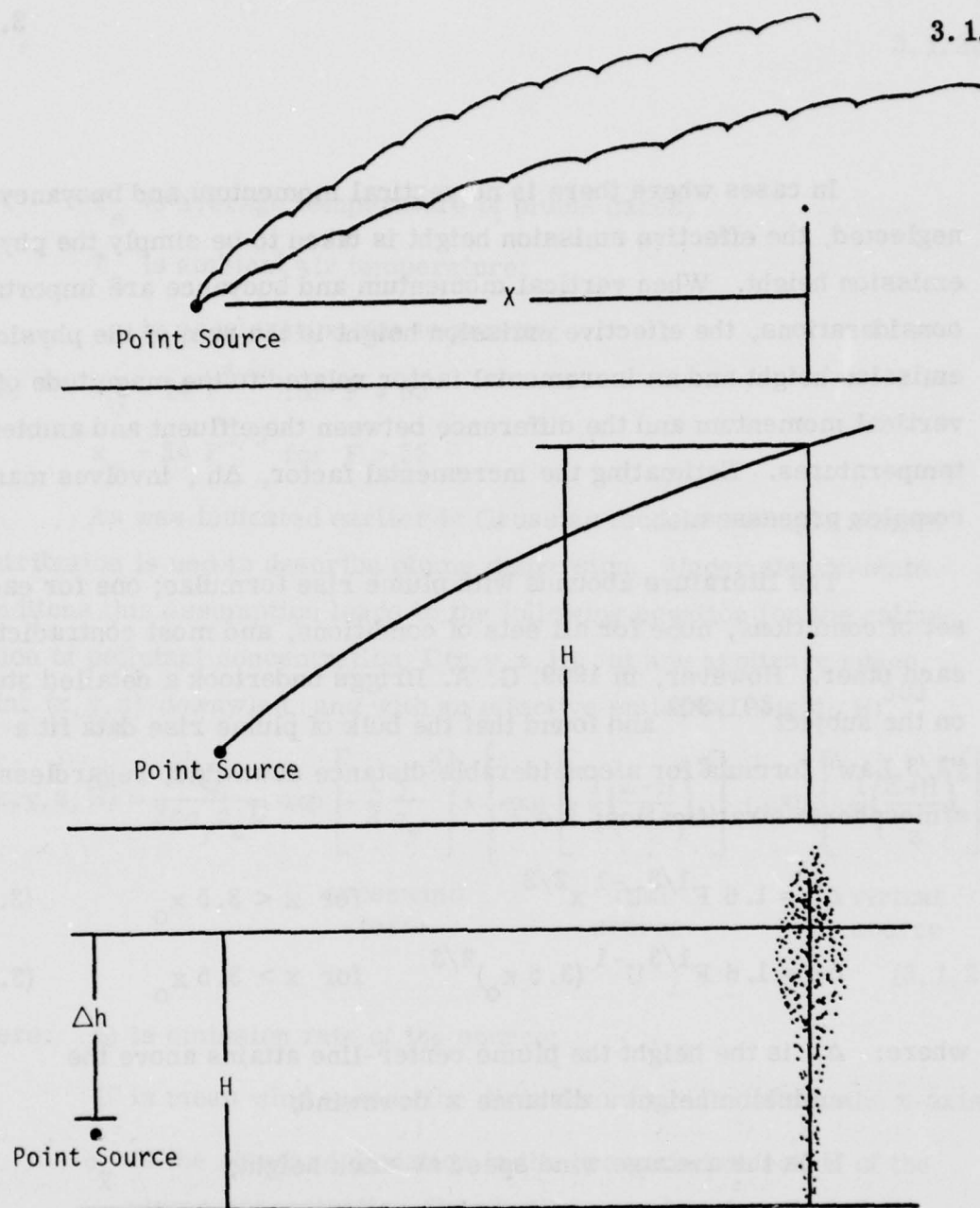


Figure 3.1.2-1. Gaussian Treatment of Centroidal Trajectory Calculation and Diffusion (assuming some plume rise due to initial vertical momentum and buoyance).
 H = effective emission height
 Δh = height plume center-line attains above emission height at a distance x downwind.

In cases where there is no vertical momentum and buoyancy is neglected, the effective emission height is taken to be simply the physical emission height. When vertical momentum and buoyance are important considerations, the effective emission height is the sum of the physical emission height and an incremental factor related to the magnitude of vertical momentum and the difference between the effluent and ambient temperatures. Estimating the incremental factor, Δh , involves many complex processes.

The literature abounds with plume rise formulae; one for each set of conditions, none for all sets of conditions, and most contradicting each other. However, in 1969, G. A. Briggs undertook a detailed study on the subject^{301, 302} and found that the bulk of plume rise data fit a "2/3 Law" formula for a considerable distance downwind, regardless of atmospheric stratification; i. e. :

$$\Delta h = 1.6 F^{1/3} U^{-1} x^{2/3} \quad \text{for } x < 3.5 x_0 \quad (3.1.2-1)$$

$$\Delta h = 1.6 F^{1/3} U^{-1} (3.5 x_0)^{2/3} \quad \text{for } x > 3.5 x_0 \quad (3.1.2-2)$$

where: Δh is the height the plume center-line attains above the emission height a distance x downwind;

U is the average wind speed at stack height;

x is the distance downwind.

$$F = g V_s R_s^2 \left[1 - \frac{T_a}{T_s} \right] \quad (3.1.2-3)$$

where: V_s is average exit velocity of emissions;

R_s is inner radius of the emission source;

T_s is average temperature of plume gases;

T_a is ambient air temperature;

g is acceleration due to gravity;

and: $x_o = 14 F^{5/8}$ for $F \leq 55$

$x_o = 34 F^{2/5}$ for $F > 55$

As was indicated earlier in Gaussian models a simple normal distribution is used to describe plume dispersion. Under steady-state conditions this assumption leads to the following equation for the calculation of pollutant concentration $C(x, y, z, H)$, at any arbitrary space point (x, y, z) downwind, and with an effective emission height, H :³⁰³

$$C(x, y, z, H) = \frac{Q}{2\pi\sigma_y\sigma_z U} \exp \left[-\frac{1}{2} \frac{y^2}{\sigma_y^2} \right] \cdot \left\{ \exp \left[-\frac{1}{2} \left(\frac{z-H}{\sigma_z} \right)^2 \right] + \exp \left[-\frac{1}{2} \left(\frac{z+H}{\sigma_z} \right)^2 \right] \right\}$$

crosswind
term

real
source

virtual
source

(3.1.2-4)

where: Q is emission rate of the source;

U is mean wind speed, the direction of which defines the x -axis;

σ_y is the standard deviation in the crosswind direction of the plume concentration distribution. σ_y is a function of x ;

σ_z is the standard deviation in the vertical of the plume concentration distribution. σ_z is a function of x .

The second exponential term is due to the "real" source, located at a height H above the ground surface. The third exponential term (following Sutton,³⁰⁴ and assuming that the ground surface acts as a perfect reflector

of pollutant) is due to the virtual image source located at a distance H below the ground surface. * Several of the variables of this equation are illustrated graphically in Figure 3.1.2-2.

For ground level concentrations (i.e., $z = 0$) Eq. (3.1.2-4) simplifies to:

$$C(x, y, 0; h) = \frac{Q}{\pi \sigma_y \sigma_z U} \exp \left[-\frac{1}{2} \left(\frac{y}{\sigma_y} \right)^2 \right] \cdot \exp \left[-\frac{1}{2} \left(\frac{H}{\sigma_z} \right)^2 \right] \quad (3.1.2-5)$$

The basic point source Gaussian formulation [Eq. (3.1.2-5)] may be modified to handle line sources by integration in one dimension. ³⁰⁶

Consider a finite line at height H extending from y_1 to y_2 ($y_1 < y_2$), perpendicular to the mean wind blowing in the x direction. If the line is considered to emit at a constant rate, Q , per unit length,

$$C(x, y, 0) = \frac{2Q}{\sqrt{2\pi} \sigma_z U} \exp \left[-\frac{1}{2} \left(\frac{H}{\sigma_z} \right)^2 \right] \int_{\xi_1}^{\xi_2} \frac{1}{\sqrt{2\pi}} \exp \left[-\left(\frac{p}{2} \right)^2 \right] dp \quad (3.1.2-6)$$

where: $\xi_i = \frac{y_i}{\sigma_y}$, $i = 1, 2$ and p is an integration variable

If the line source is at ground level,

$$C(x, y, 0) = \frac{2Q}{\sqrt{2\pi} \sigma_z U} \int_{\xi_1}^{\xi_2} \frac{1}{\sqrt{2\pi}} \exp \left[-\left(\frac{p}{2} \right)^2 \right] dp \quad (3.1.2-7)$$

For the case in which the line is considered of infinite length,

$$C(x, y, 0) = \frac{2Q}{\sqrt{2\pi} \sigma_z U} \exp \left[-\frac{1}{2} \left(\frac{H}{\sigma_z} \right)^2 \right] \quad (3.1.2-8)$$

* To simulate perfect reflection of pollutant at ground level.

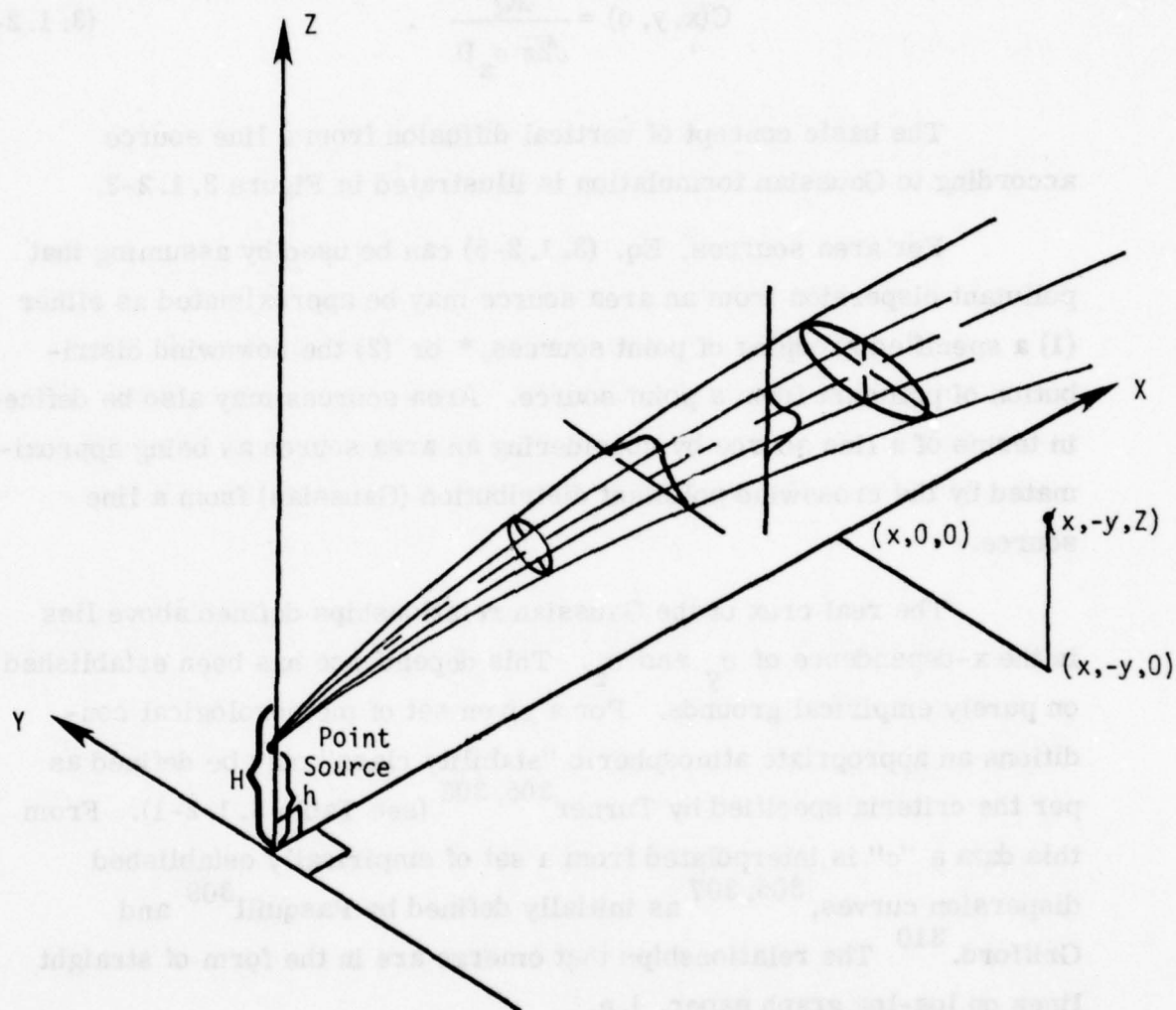


Figure 3. 1. 2-2. Coordinate System Showing Gaussian Distribution in the Horizontal and Vertical³⁰⁵.

and considering again a ground level system

$$C(x, y, o) = \frac{2Q}{\sqrt{2\pi} \sigma_z U} \quad (3.1.2-9)$$

The basic concept of vertical diffusion from a line source according to Gaussian formulation is illustrated in Figure 3.1.2-3.

For area sources, Eq. (3.1.2-5) can be used by assuming that pollutant dispersion from an area source may be approximated as either (1) a specified grouping of point sources,* or (2) the downwind distribution of pollutant from a point source. Area sources may also be defined in terms of a line source by considering an area source as being approximated by the crosswind pollutant distribution (Gaussian) from a line source.

The real crux of the Gaussian relationships defined above lies in the x-dependence of σ_y and σ_z . This dependence has been established on purely empirical grounds. For a given set of meteorological conditions an appropriate atmospheric "stability class" may be defined as per the criteria specified by Turner^{305,308} (see Table 3.1.2-1). From this data a " σ " is interpolated from a set of empirically established dispersion curves,^{305,307} as initially defined by Pasquill³⁰⁹ and Griford.³¹⁰ The relationships that emerge are in the form of straight lines on log-log graph paper, i.e.,

$$\sigma_y(x) = ax^b + c \quad (3.1.2-10)$$

where a, b, and c depend upon the stability category.

* Similarly, a line source may be considered as a linear array of point sources.

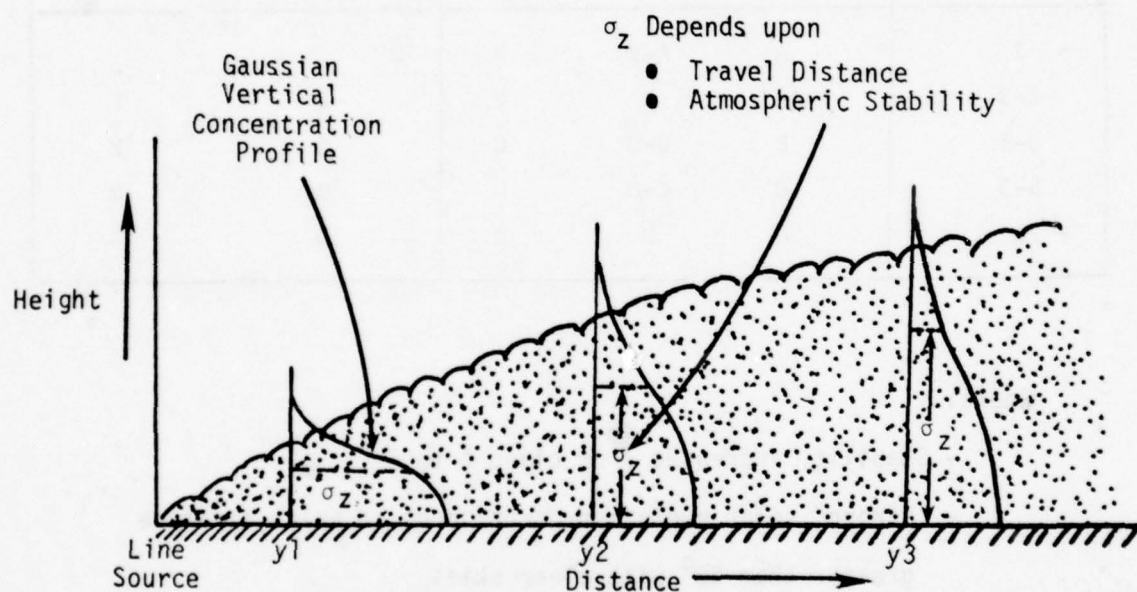


Figure 3.1.2-3. Vertical Diffusion According to the Gaussian Model.

Table 3. 1. 2-1

KEY TO STABILITY CATEGORIES^{305, 308}

Surface Wind Speed (at 10m) m sec ⁻¹	Day Incoming Solar Radiation			Night	
	Strong	Moderate	Slight	Thinly Overcast or ≥4/8 Low Cloud	<3/8 Cloud
< 2	A	A-B	B		
2-3	A-B	B	C	E	F
3-5	B	B-C	C	D	E
5-6	C	C-D	D	D	D
> 6	C	D	D	D	D

where:

- Stability increases from class A to F
- "strong" solar radiation corresponds to solar attitude greater than 60° with clear skies
- "slight" corresponds to 15° to 35° with clear skies
- the natural class ,D, should be assumed for overcast conditions during day or night.

As was mentioned in Section 3. 1. 1, the problem of determining pollutant concentrations can be complicated when an elevated stable layer occurs. Under these conditions, the estimated pollutant concentration can be calculated assuming the effluent remains within a mixing layer of height L , defined as the vertical distance from the ground to the base of the stable layer. If this "lid" and the ground surface are assumed to be perfect reflectors, repeated reflections of pollutant from the two parallel surfaces (the lid and the ground) can be represented in terms of a multiple image series:^{311, 312}

$$C(x, y, z) = \sum_{i=0}^N C_i(x, y, z) \quad (3. 1. 2-11)$$

where: C_0 = concentration contribution from the "real" source; and

C_i = concentration contribution from the i^{th} image source
(either above lid or below ground surface).

It can be shown that the mean concentration, \bar{C} , in the mixing layer between the ground and the lid is given by

$$\begin{aligned} \bar{C}(x, y) &= \frac{1}{L} \int_0^L \sum_{i=0}^{\infty} C_i(x, y, z) dz \\ &= \frac{1}{L} \int_{-\infty}^{+\infty} C_0(x, y, z) dz \\ &= \frac{Q}{\sqrt{2\pi} L U \sigma_y} \exp \left[-\frac{1}{2} \left(\frac{y}{\sigma_y} \right)^2 \right] \end{aligned} \quad (3. 1. 2-12)$$

and as $\sigma_z \rightarrow \infty$, $C(x, y, z) \rightarrow \bar{C}(x, y)$.

In practice the multiple image series is generally truncated, so as to include only the most significant image sources. A simple approximation, and one used in most of the airport air quality simulation models considered in this report, is to define a critical downwind distance X_L beyond which the lid significantly interferes with further vertical plume dispersion. At this distance the pollutant concentration at the lid, $C_0(x, y, L)$, is one-tenth of the value at the plume center-line, and

$$\sigma_z(X_L) = \frac{L - H}{2.15} \quad (3.1.2-13)$$

Up to this distance, the Gaussian vertical distribution is assumed and Eq. (3.1.2-4) is appropriate. At a distance X_L , the confinement effect of the elevated stable layer begins to be effective, and uniform mixing below the base of the stable layer is assumed to occur at a downwind distance of $2X_L$. Thus for distances $X \geq 2X_L$, the concentration is calculated using Eq. (3.1.2-12). For distances between X_L and $2X_L$, C is determined by a linear interpolation between Eq. (3.1.2-4), evaluated at X_L , and Eq. (3.1.2-12) evaluated at $2X_L$.

Equations (3.1.2-4) and (3.1.2-8) may be modified to yield estimates of annual average ground level concentrations by use of the so-called Martin-Tikvart technique. All of the five Gaussian models considered in this report employ this approach. The Martin-Tikvart technique or model^{313, 314} is based upon the assumption that the long term average concentration at a receptor from a given source is approximately equal to the weighted sum of calculated concentrations under all applicable meteorological conditions for the time period considered. Essentially the model calculates the effects of each source on each receptor for the observed combination of wind direction, wind speed, and stability class.

Wind direction is normally specified with respect to a sixteen point compass, corresponding to 22.5 degree circular sectors. * For each of the sixteen wind direction intervals, wind speed is defined in terms of six categories: 0-3, 4-6, 7-10, 11-16, 17-21, and > 21 knots.

For a given source-receptor configuration, an estimate of the pollutant concentration is obtained by choosing a representative wind speed for each wind speed class and solving the appropriate equation (3. 1. 2-4 or 3. 1. 2-12) for all wind speed and stability classes associated with the time period involved. ** The average concentration is determined by summing all concentrations and weighting each according to its frequency for the particular wind direction, wind speed class, and stability class:

$$C = \sum_{\theta} \sum_N \sum_S F(\theta, N, S) C(\theta, N, S) \quad (3. 1. 2-14)$$

where: $F(\theta, N, S)$ = the normalized frequency during the period of interest for wind direction interval θ , wind speed class N , and stability class S ; and

$C(\theta, N, S)$ = the average ground level concentration.

The total concentration at a specific receptor is then obtained by summing the results of Eq. (3. 1. 2-14) over all sources. †

* The 16 point compass approach is one method that is frequently used. However, wind direction has been similarly defined in terms of a variety of sector divisions, including 8 point and 4 point systems.

** For annual periods it is assumed that all wind directions within a given sector occur with equal frequency. To avoid discontinuities in the calculated concentrations at wind direction sector boundaries under these conditions, a linear interpolation between sector center-lines is used.

† The so called principle of superposition.

3.1.3 The "Particle-in-Cell" Technique

The "Particle-in-Cell" (PIC) technique forms the basis on which the so-called S³ Photochemical model* considered in this study is formulated.³¹⁵ PIC is based upon the use of Lagrangian mass points to simulate pollutant transport as described by the conservation of mass equation derived for turbulent atmospheric diffusion. K-theory approximations³⁰³ are used in developing the atmospheric diffusion equation used in PIC.

A proper beginning in a discussion of the PIC technique is with the equation expressing conservation of mass for a pollutant whose concentration is sufficiently small so as not to perturb ambient atmospheric flow. For this pollutant, the time rate of change of the instantaneous concentration, C , is due to motion with the ambient flow, and to molecular diffusion:

$$\frac{\partial c}{\partial t} = -\frac{\partial}{\partial x}(uc) - \frac{\partial}{\partial y}(vc) - \frac{\partial}{\partial z}(wc) + D_x \frac{\partial^2 c}{\partial x^2} + D_y \frac{\partial^2 c}{\partial y^2} + D_z \frac{\partial^2 c}{\partial z^2} \quad (3.1.3-1)$$

where: u, v, w = wind velocity components; and

D_x, D_y, D_z = molecular diffusion components.

The concentration and the velocity can be divided into mean (denoted by overbars) and fluctuations about the means** (denoted by primes):

$$\begin{aligned} c &= \bar{c} + c' \\ u &= \bar{u} + u' \end{aligned} \quad (3.1.3-2)$$

* Also called NEXUS/P (Numerical Examination of Urban Smog with Photochemistry).

** Subtleties arise depending upon the type of mean employed (spatial, temporal, or ensemble). For the purposes of this discussion these need not be considered here.

When these are substituted back into Eq. (3.1.3-1) and the resultant average, the following is obtained:

$$\begin{aligned} \frac{\partial \bar{c}}{\partial t} = & -\frac{\partial}{\partial x} (\overline{uc}) - \frac{\partial}{\partial y} (\overline{vc}) - \frac{\partial}{\partial z} (\overline{wc}) - \frac{\partial}{\partial x} \overline{u'c'} - \frac{\partial}{\partial y} \overline{v'c'} - \frac{\partial}{\partial z} \overline{w'c'} \\ & + D_x \frac{\partial^2}{\partial x^2} (\bar{c}) + D_y \frac{\partial^2}{\partial y^2} (\bar{c}) + D_z \frac{\partial^2}{\partial z^2} (\bar{c}) \quad . \end{aligned} \quad (3.1.3-3)$$

That is, the time rate of change in mean pollutant concentration is caused by transport of mean concentration by the mean wind, transport of concentration fluctuations by correlated velocity fluctuations, and by molecular diffusion.

The second group of terms on the right side of Eq. (3.1.3-3) represent turbulent diffusion. Since this term contains fluctuation terms for which there is usually little or no data, it is frequently modeled in terms of mean quantities. By analogy with molecular diffusion and other assumptions, the hypothesis is established that this term may be approximated by diffusion of mean concentration,

$$\overline{u'c'} = -K_x \frac{\partial \bar{c}}{\partial x} \quad (3.1.3-4)$$

where K_x = turbulent diffusivity tensor component in the x direction.* In addition, turbulent diffusion is much more important than molecular diffusion in atmospheric studies, so that in considering turbulent diffusion

* It should be noted that for convenience the coordinate axis have been assumed to be the principal axes for the diffusivity tensor. This is not a required assumption for application of the PIC technique, since PIC could actually be developed for tensor eddy diffusivity. ³¹⁶

phenomena molecular diffusion is usually negligible. With modification and substituting in Eq. (3. 1. 3-4), Eq. (3. 1. 3-3) becomes:

$$\begin{aligned} \frac{\partial \bar{c}}{\partial t} = & - \frac{\partial}{\partial x} (\bar{u}\bar{c}) - \frac{\partial}{\partial y} (\bar{v}\bar{c}) - \frac{\partial}{\partial z} (\bar{w}\bar{c}) + \frac{\partial}{\partial x} \left(K_x \frac{\partial \bar{c}}{\partial x} \right) + \frac{\partial}{\partial y} \left(K_y \frac{\partial \bar{c}}{\partial y} \right) \\ & + \frac{\partial}{\partial z} \left(K_z \frac{\partial \bar{c}}{\partial z} \right). \end{aligned} \quad (3. 1. 3-5)$$

This is the basic equation of "K-Theory". For simplicity, the turbulent diffusivity is usually considered constant, and the overbars denoting mean values are suppressed. The effect of pollutant emissions may be included by adding a source emission rate terms. Equation (3. 1. 3-5) can now be written:

$$\frac{\partial c}{\partial t} = - \frac{\partial}{\partial x} (uc) - \frac{\partial}{\partial y} (vc) - \frac{\partial}{\partial z} (wc) + K_x \frac{\partial^2 c}{\partial x^2} + K_y \frac{\partial^2 c}{\partial y^2} + K_z \frac{\partial^2 c}{\partial z^2} + S. \quad (3. 1. 3-6)$$

For a constant wind and diffusivity, and a continuous point source, Eq. (3. 1. 3-6) can be solved analytically to give the Gaussian plume formulation.

In the PIC method, the mass of pollutant is separated into individual elements, and centroids of these discrete masses ("particles") are tracked using a Lagrangian coordinate system. The advection and diffusion terms in Eq. (3. 1. 3-6) are combined by definition of a diffusion velocity (termed the "turbulent flux velocity"; U_d , V_d , and W_d), where:

$$\begin{aligned} U_d &= - \frac{K_x}{c} \frac{\partial c}{\partial x} \\ V_d &= - \frac{K_y}{c} \frac{\partial c}{\partial y} \\ W_d &= - \frac{K_z}{c} \frac{\partial c}{\partial z} \end{aligned} \quad (3. 1. 3-7)$$

These newly defined velocities may be interpreted as the effective velocity of diffusive transport. The total velocity involved in transporting pollutants (termed the "total equivalent transport velocity") is then:

$$U = u + u_d$$

$$V = v + v_d$$

$$W = w + w_d \quad . \quad (3. 1. 3-8)$$

With these definitions, Eq. (3. 1. 3-6) can be written as:

$$\frac{\partial c}{\partial t} = - \frac{\partial}{\partial x} (U_c) - \frac{\partial}{\partial y} (V_c) - \frac{\partial}{\partial z} (W_c) + S \quad . \quad (3. 1. 3-9)$$

This equation is identical in form with the equation of continuity for a general compressible fluid. It is this special fact that is the basis for the PIC method as applied to the problem of atmospheric diffusion. By the device of introducing the "turbulent flux velocity" and the artifact of the "total equivalent transport velocity", the original problem of turbulent atmospheric diffusion is transformed into one describing the advective changes of fluid density in a compressible fluid moving in the fictitious velocity field (U, V, W) of total equivalent transport velocities. In the compressible fluid problem the continuous field variable representing fluid density can be visualized in a discrete manner as the total mass of elementary fluid particles in a unit volume of space, while the changes of density may be considered in terms of changes in the number of elementary mass particles occupying the unit volume. Similarly, the mass particles in the atmospheric dispersion problem follow the fluid motion in the fictitious velocity field, and their number in any given unit volume will determine the concentration of pollutant in the volume.

In the PIC method the spatial distribution of pollutant is represented by means of a large number of Lagrangian mass particles, i.e., ones of constant mass of pollutant that are simply advected in the fictitious field of total velocity. Physical space is divided into cells of a fixed Eulerian grid and the particles carry pollution from cell to cell as they are moved by the fictitious velocity field. Since this field is a non-solenoidal one, it will cause particles to move apart or together, and thus uneven distributions may result. In order to simulate satisfactorily the spatial distribution of pollution, a sufficiently large number of particles must be used in each grid cell.

Concentrations in the PIC method are computed as cell averages. Two prescriptions for calculating cell concentrations from the particle masses have been employed. In the simplest prescription the cell concentration is the sum of the masses of all particles in the cell divided by the cell volume. Thus, when a particle crosses a cell boundary, the particle mass is added to the cell entered and subtracted from the cell it has left. The second prescription is equivalent to an area (or volume) apportionment of a particle's mass between cells based upon overlap considerations. For this purpose the particle mass is regarded as uniformly spread over an area (or volume) the size of a cell and centered on the particle position. The overlap with adjacent cells then determines the mass apportionment between them. In both cases the values of the cell concentration is associated with the cell center. Initially, the particles are placed at random within each cell. The number of particles in a cell is determined by the initial concentration in the cell.

The fictitious total velocity field that is used to transport the particles in the PIC method is defined by its values at the centers of the

cells. For each such center, the mean velocity vector (\bar{u} , \bar{v} , \bar{w}) for the original real velocity field must be specified and the turbulent flux velocity calculated utilizing Eq. (3.1.3-7) with the derivatives approximated by a finite difference algorithm. The fictitious total velocity at each cell center is then given by the sum of the original mean velocity and the turbulent flux velocity. Once this has been calculated for any elementary time-interval (t , $t + \Delta t$) the particles in the cells are then moved for this interval with a velocity obtained by linear interpolation according to the position of the particle between the centers of adjacent cells, using the velocity at each center.

In the PIC method the calculation to advance the particle configuration in time proceeds in steps or cycles, each of which calculates the desired quantities for time $t + \Delta t$ in terms of those at time t (an "explicit" time advancement procedure)

$$\begin{aligned}x(t + \Delta t) &= x(t) + U\Delta t \\y(t + \Delta t) &= y(t) + V\Delta t\end{aligned}\tag{3.1.3-10}$$

The velocities are the fictitious total velocities determined for the beginning of the time interval and interpolated to initial particle positions. These are held constant throughout any elementary time interval. It is evident that the magnitude of the time interval Δt must be restricted, as otherwise a particle could pass through many cells in a cycle and well out of the region for which its velocity was interpolated. This could result in inaccuracies and instabilities in the solution. Limiting the time step so that no particle moves more than four-tenths of a cell within any one cycle has been used as an empirical rule to avoid this problem.

Boundary conditions are introduced by modifications of the fictitious total velocities. Thus, impervious barriers are simulated by not allowing particles to be transported across these boundaries. Transmittive boundaries are permeable to particles which continue to pass through them with the total velocity.

Thus is completed one cycle by which the PIC method solves the diffusion equation for a time step. In each cycle the cellular concentrations are calculated from particle masses, the fictitious total velocity for each cell is calculated as the sum of mean wind velocity and the turbulent flux velocity and the particle positions are updated using an interpolated total velocity. Time is stepped along cycle by cycle and the position of each particle traces a trajectory of the pollutant mass.

As pollutants are emitted into the atmosphere, additional pollutant mass must be added to the simulation [as per the source emission term, S , in Eq. (3.1.3-9)]. The additional pollutant mass may be added to the mass associated with a pre-existing particle at the source location, or a new particle may be generated. The new particle would enter the simulation at the source location with pollutant mass equal to that physically generated during the time interval. Pollutant generation is treated separately for each cell of the grid. Thus point, line, area and volume sources can easily be simulated.

The simulation of the chemical reactions in PIC begins with a chemical mechanism -- a set of chemical reactions and their reaction rate constants -- assumed to be an adequate description of the relevant pollutant reactions. The chemical mechanism is then translated into a set of chemical kinetic rate equations -- coupled first-order differential equations describing the time rate of change of each reactant and

product pollutant species. The solutions of these equations determine the cell concentrations but the changes in concentrations have to be related back to particle masses. Within each cell the particle masses are re-weighted by the fractional change in concentration due to chemical reactions. For each chemical species and each cell the fraction is calculated. For the case of a pollutant species being initially generated in a cell by chemical reaction (where there is no pre-existing particle to re-weight) a new particle is introduced into the cell.

3.1.4 Comparison of Basic Concepts - Assumptions/Limitations

3.1.4.1 Gaussian

The main advantage of the Gaussian formulation of pollutant dispersion layer is its basic simplicity, ease of application, and flexibility. However, these advantages have been achieved at the expense of a number of significant assumptions which can greatly restrict the application of a Gaussian air pollution dispersion model.

The basic assumptions associated with the Gaussian formulation are as follows:

- (1) Steady-state conditions,
- (2) Homogenous flow,
- (3) Flat terrain,
- (4) An inert passive pollutant,
- (5) Perfect reflection of the pollutant at the boundary surfaces,
- (6) Statistical Gaussian forms for the crosswind and vertical distributions of pollutant, and
- (7) Negligible diffusion in the x direction in comparison to transport or advection by the wind.

The assumptions of steady-state conditions, homogenous flow, flat terrain require that there be no time or space fluctuations in effluent discharge, wind, or turbulence associated with the problem being modeled using the Gaussian equations. Obviously, this is an idealized situation, and application of the Gaussian formulation to real world situations must be predicted on the fact that, at best, calculated concentrations are approximations whose accuracy is dependent upon the significance of these and other factors not taken into account. Thus, Eqs. (3.1.2-4) through (3.1.2-12) apply strictly only to emissions which may be considered continuous for the time interval involved. This assumption is particularly troublesome for transportation related problems (i.e., aircraft, vehicles) which tend to vary in both space and time. Also, variations in wind speed and direction over the volume of interest are considered negligible, an assumption contrary to the known behavior of winds. Wind speed increases with altitude in the lower several hundred meters of the atmosphere, and a large wind shear exists near the ground and in some cases aloft. In addition, wind direction frequently contains low-frequency fluctuations which may be significant depending upon the averaging time involved. * Topographical factors are also considered negligible, i.e., no effects on wind or turbulence are exhibited due to terrain, buildings or other geophysical features. This too is an unrealistic assumption, since in many cases the landscape surrounding a given emission problem is usually not flat and often may contain significant irregularities.

* For example, if the wind veers slowly through 45 degrees over 15 minutes, returning to its original direction 15 minutes later, a steady-state condition can be assumed for the 30 minute period but not for the individual 15 minute intervals that might be used experimentally for estimating σ .

The assumption that only inert, passive pollutants are involved requires that no transformation, scavenging, or precipitation of pollutant take place. Thus, effects of chemical reaction, rain, ice or snow wash-out, and gravitation fallout* are considered negligible. In addition, the assumption that perfect reflection of pollutant occurs at the boundary surfaces requires that no ground adsorption or absorption occur and that there are no losses of pollutant through any inversion layer. It should be noted here that a number of Gaussian models³⁰³ have been developed which include an exponential parameter to account for pollutant transformation or deposition. However, it is almost impossible to develop an appropriate general time constant for use in this factor, and even if a proper empirical time constant could be defined the basic concept used with Gaussian models to relate pollutant contributions from various sources to the concentration at a given receptor (the principal of superposition) would be invalid under conditions of pollutant transformation and/or deposition. The assumption that statistical Gaussian forms apply for the crosswind and vertical distribution of pollutant implies that an averaging time of at least ten minutes is involved to insure that irregularities and instantaneous "peaks" are smoothed away.** The assumption that diffusion along the x-axis is negligible in comparison to

* The condition of no gravitation fallout can be translated into a requirement that no effluent have an equivalent diameter greater than 20 microns. For most cases, actual effluents meet this requirement.

** A number of authors (for example, Reference 303, p. 382) have indicated that the assumption of Gaussian distribution, although of practical importance, is not in itself a serious limiting factor since substantial departures from Gaussian distribution have been shown to have only minor impact on ground level pollutant concentration calculations.

transport or advection by the wind limits the application of the Gaussian formulations to moderate or high wind conditions. Under calm conditions or light winds the Gaussian equations (with the mean wind speed appearing in the denominator only) break down. It should be noted that predictions of air quality under calm wind conditions is one of the most important objectives of air pollution simulation studies, since in many cases the "worst case" situation required to correlate estimated pollutant concentrations with national air quality standards occurs under conditions of calm winds (or confining topography).

Other limiting factors associated with Gaussian pollution dispersion modeling include the empirical definitions of the standard deviation, limitations associated with input data (stability class, wind roses), and the considerations of plume rise (where applicable) and inversion layer effects. The standard deviation is assumed to be a function of downwind distance and atmospheric stability only. Stability factors used are empirical approximations, and wind rose data, at best, is generated from measurements taken on an hourly basis in the "vicinity" of the region under study. Plume rise considerations must still be considered a rough approximation, and inversion layer effects do not take into account the known intra-day variations.

3.1.4.2 PIC

The PIC method was developed as a modification of techniques designed to overcome many of the inherent limitations associated with Gaussian pollutant dispersion models. It is a method derived from first principles without required assumptions of steady-state conditions, homogenous flow, inert passive pollutants, perfect pollutant reflection at the boundary surfaces, negligible x direction diffusion, or Gaussian

distributions. However, certain assumptions are involved, including:

- (1) molecular diffusion is negligible in comparison to turbulent diffusion; and
- (2) atmospheric flow is incompressible.

Because of the cellular nature of the basic conservation of mass equations, PIC is widely able to accommodate considerations of variable emission, chemical reactions, and scavenging and precipitation effects. In addition, pollutant losses due to adsorption or absorption at the ground surface or passage through the emission layer may also be included.

Another advantage of the grid structure definition of PIC is that a separate wind may be incorporated for each cell. This data may also be updated during each cycle of the simulation. However, in practice this advantage is nullified by the fact that detailed, three-dimensional wind distribution data is rarely available. The existence of an inversion layer in the atmosphere (and its associated intra-day variations) does not pose a problem for PIC either, since the mixing level can simply be defined as a limited boundary condition and updated each computational cycle.

In PIC, the standard deviation terms (σ_y and σ_z) are replaced by the eddy diffusion coefficients (K_x , K_y , and K_z). Thus, the problem of defining σ has been replaced with the problem of defining K . In most cases, K is assumed to be a constant over the regime in question.

In summary, it is clear that the "Particle-in-Cell" approach overcomes many of the limitations inherent in Gaussian models. However, this advantage is obtained at the expense of complexity in terms of

required input data and computation time. Since the problem of simulation of air pollution dispersion is inherently complex in itself, it is not unexpected that a detailed theoretical simulation of the problem is also somewhat complex.

3.2 MODEL DESCRIPTIONS

3.2.1 Gaussian³¹⁷

3.2.1.1 AQDM³¹⁴

AQDM was developed for the Department of Health, Education and Welfare (HEW) by TRW as a general purpose air quality simulation model. It consists of two submodels: (1) a Gaussian atmospheric diffusion formulation based on the Martin-Tikvart approach; and (2) a statistical model designed to determine the geometric mean and expected maximum pollutant concentration values based on the annual arithmetic average concentration as calculated from (1). AQDM was not designed specifically for a particular airport air quality determination, and as such does not include an emission or meteorological inventory/model.

3.2.1.1.1 AQDM Atmospheric Diffusion Formulation

The AQDM atmospheric diffusion formulation is based upon a straightforward Martin-Tikvart model as described in Section 3.1.2. AQDM estimates the annual arithmetic average ground level pollutant concentration resulting from specified elevated, continuously emitting point sources using Eqs. (3.1.2-5) or (3.1.2-12) as appropriate. AQDM handles area sources (and ground reflections) by converting them to equivalent or "virtual" point sources. In the conversion process, both the downwind distance and the source strength are dependent on the particular source-receptor configuration.

The values for the standard deviation used in AQDM are those of Pasquill³⁰⁹ and Griford,³¹⁰ as per Eq. (3.1.2-10). The minimum value of x , the downwind distance, used in calculating " σ " is 100 meters.

The mixing layer depth, L , is determined by modifying the average afternoon mixing depth values (as tabulated by Holzworth³¹⁸) according to the stability class being considered. Stability category is defined on the basis of the criteria stated by Turner.³⁰⁸

The original AQDM formulation was developed prior to dissemination of Briggs' plume rise equations (Section 3.1.2). The plume rise equation used in AQDM is that due to Holland,³¹⁹ and is given by:

$$\Delta h = \frac{V_s d}{u} \left[1.5 + 2.68 \times 10^{-3} p \left(\frac{T_s - T_a}{T_s} \right) d \right] \quad (3.2.1-1)$$

where: V_s = emission gas exit velocity

d = emission exit diameter

u = mean wind speed

p = atmospheric pressure

T_s = emission gas exit temperature

T_a = ambient air temperature.

Equation (3.2.1-1) is applicable for the neutral stability condition only. To allow for a range of stability ($1.3 \Delta h$ for very stable conditions to Δh for neutral stability), AQDM modifies Eq. (3.2.1-1) using the following formulation:

$$h = h^* + \Delta h (1.4 - 0.1 S) \quad (3.2.1-2)$$

where: h^* = physical stack height

S = stability class (Turner³⁰⁸).

3.2.1.1.2 AQDM Statistical Formulation^{314, 320}

The statistical model used in the AQDM to define the distribution of pollutant concentration at each receptor as a function of averaging time, arithmetic average concentration, and standard geometric deviation is that described by Larsen.³²⁰ This model is used to convert arithmetic average concentration (the output of the diffusion model) to expected maximum concentration and expected geometric mean concentration for given averaging times. The model is based upon the assumptions (developed on empirical grounds) that:

- (1) concentrations are lognormally distributed for all pollutants in all regions under consideration for all averaging times; and
- (2) the median (geometric mean) concentration is proportional to average time raised to an exponent.

The assumption that pollutant concentrations are lognormally distributed leads to the result that only two parameters (a concentration for a given averaging time) are required to determine the concentration for any averaging period. Since a given averaging period corresponds to a fixed number of samples over a year, once the relative position of the lognormal distribution is specified it is possible to determine the expected maximum concentration for the year.

AQDM calculates the geometric mean for a given set of samples (i.e., averaging time) from the arithmetic mean and the

standard deviation for the same set of samples using the following relationship:

$$M_g = C / (S_g)^{(\frac{1}{2} \ln S_g)} \quad (3.2.1-3)$$

where: C = arithmetic mean

M_g = geometric mean for a set of samples

S_g = standard geometric deviation for the sample set of samples.

If S_g is defined for the desired averaging time, Eq. (3.2.1-3) may be used to provide the desired output. If the desired averaging time is different than the one associated with the input S_g , then S_g must be translated into the desired averaging time. The AQDM statistical model does this by assuming that the median concentration is proportional to averaging time to an exponent. Thus, the standard deviation for different averaging times may be related as per Eq. (3.2.1-4).

$$S_{g_n} = (S_{g_i})^k \quad (3.2.1-4)$$

where: S_{g_n} = standard geometric deviation at averaging period of n hours; and

S_{g_i} = standard geometric deviation of samples observed (usually corresponding to 24-hour averaging times).

The relationship between the arithmetic mean, geometric mean, and expected maximum concentration utilized in the AQDM statistical model is graphically illustrated in Figure 3.2.1-1.

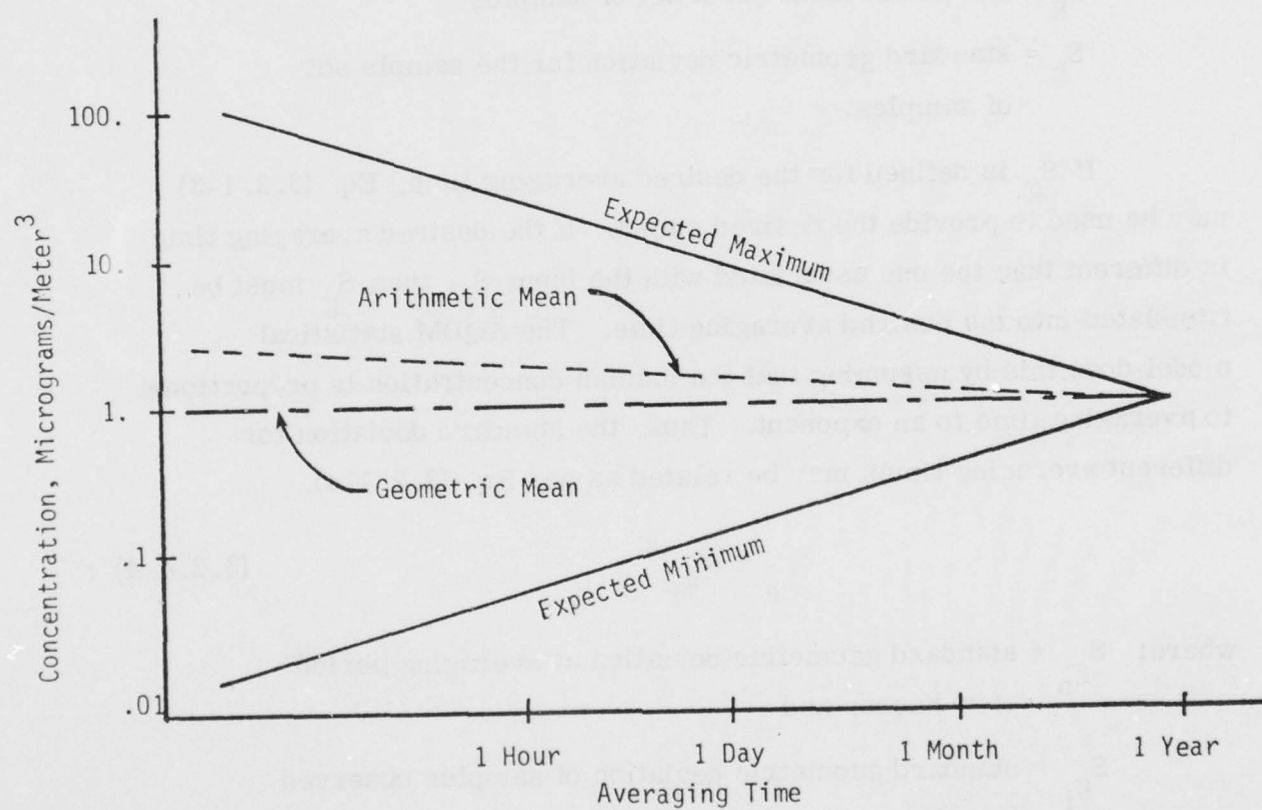


Figure 3.2.1-1. Graphic Representation of AQDM (Larsen)
Statistical Model Relationship³²⁰.

3.2.1.2 The NREC Model^{321, 322, 323}

The NREC Model was developed for the EPA for specific application to airport air quality determinations. It consists of two submodels, one dealing with airport emissions and the other with atmospheric dispersion. The atmospheric dispersion model contains two subroutines, concerned separately with short-term maxima dispersion and long-term average dispersion.

3.2.1.2.1 Short-Term Subroutine

The NREC short-term model is based upon the empirical Gaussian* plume solution to the diffusion equation as discussed in Section 3.1.2. In the NREC short-term model, Eq. (3.1.2-4) is modified to account for dispersion mechanism effects associated with the transformation and/or deposition of pollutants. This modification takes the highly simplified form of an exponential decay (dependent upon mean wind speed, u , and downwind distance, x):

$$\exp \left[- \frac{1}{k} \frac{x}{u} \right] . \quad (3.2.1-5)$$

However, the time constant, k , is assumed to be infinite in the NREC model, thus effectively eliminating chemical transformation and deposition from consideration.

In the NREC short-term subroutine, each point source is described as the arithmetic average of a set of point sources at the same

* Sometimes referred to as bivarient or double Gaussian to emphasize the assumption of Gaussian characteristics in both the vertical and crosswind plume spread directions.

location. Ground reflections, and area and line sources are simulated as virtual point sources as in the AQDM. Concentrations are calculated using a single set of meteorological conditions. This is done by dividing the time period for such calculations into intervals characterized by single values of wind-speed class and atmospheric-stability class, by a mean wind direction, and by a wind persistence as measured by the angular variation of the wind direction during the time period considered. Wind direction variability is incorporated by averaging the pollutant concentration over direction. Wind speeds are taken as the average speed of the wind speed class into which the true wind speed falls. This avoids a singularity in the model for calm conditions.

Atmospheric stability is categorized, as described by Martin,³²⁴ into six classes for rural areas and five classes for urban areas. Mixing height is also treated based on Martin³²⁴ and Holzworth³¹⁸ as discussed in Section 3.1.2. To allow for the use of wind-stability frequency distributions as prepared by the National Climatic Center (based on six stability classes), the number of stability classes for urban areas are reduced by combining the two most stable classes. Values of the parameters of vertical and horizontal plume spread, σ_z and σ_y , respectively, are based on data presented by Turner.³⁰⁸ Plume rise is assumed to be effectively zero for all emission sources in the NREC model, * based on Briggs.³⁰²

3.2.1.2.2 Long-Term Subroutine

The NREC long-term subroutine utilizes the Martin-Tikvart model (as discussed in Section 3.1.2) without modification. As with the

* Including sources having plume rise effects, i. e., power plants.

short-term model all sources are simulated as point sources. Mixing height, and vertical and horizontal plume spread parameters (σ_z and σ_y) are evaluated as in the short-term model. Plume rise is again considered negligible.

3.2.1.2.3 Emission Model

Three categories of emissions are evaluated in the NREC model: aircraft operations, non-aircraft airport operations, and airport surroundings. Eight pollutant types are considered: carbon monoxide, nitrogen oxides, sulfur dioxide, dry particles, lead, total hydrocarbon, reactive hydrocarbon, and aldehydes. Very little data is presented on reactive hydrocarbon emission, however. Each emission source, whether a point, line, or area, is represented as one or more continuously emitting point sources of constant strength (in time) distributed throughout the airport and its surroundings. Twelve aircraft classes and ten modes of aircraft operation are considered:

<u>Aircraft Class</u>	<u>Mode of Operation</u>
SST	Approach
Jumbo Jet	Landing
Long-Range Jet	Taxi
Medium-Range Jet	Idle & Shutdown
Turboprop Transport	Maintenance
Business Jet	Start-up and Idle
Utility (Piston Engine)	Delay at Runway
Military:	Take-off
Over 400,000 lbs	Climb-out
100,000 - 400,000 lbs	Fuel Venting
10,000 to 100,000 lbs	
Under 10,000 lbs	
Helicopter and V/STOL	

Emission rates for a given aircraft class are based upon measured emission rates for the most widely used engine in the class.³²⁵

Emission factors for the approach, idle and shutdown, maintenance, start-up and idle, climb-out, and fuel venting are characterized as total emissions of pollutant per aircraft. Emission factors for taxi and delay times are characterized as emission rates of pollutant per aircraft. Two emission factors are used to characterize both the landing and take-off modes, by linear variations of emissions of pollutants per aircraft per unit distance traveled.

Three specific non-aircraft airport operations are considered in the NREC model: ground vehicle travel within the airport, * airport power/heat generation, and airport fuel storage. Automobile travel within the airport are characterized by a constant emission of pollutant per vehicle per distance traveled. Number of automobiles and distance traveled are derived from (1) the average travel per automobile within the airport, (2) the fraction of automobiles entering the airport per passenger, (3) the average number of passengers per aircraft, and (4) aircraft activity data. Emission factors for heating plants are subdivided according to type of heating fuel. The emission factors are characterized as emission rates of pollutant per fuel flow rate. Fuel storage area emission factors are characterized as emission rates of pollutant per fuel storage area. Emission factors for airport surroundings are subdivided according to type of surroundings and characterized as per EPA area emission data (based on a study of the St. Louis area).

* Emissions from automobile activity on roadways adjacent to the airport are not explicitly included in the NREC analysis. Rather, they are assumed to be included in the surrounding emissions.

The distribution of emission sources throughout the airport and its surroundings are segmented as follows:

- (1) Aircraft emissions during the start-up and idle, and idle and shutdown modes at the terminals;
- (2) Aircraft emissions during the taxi mode at stations which divide each taxiway into a number of equal segments;
- (3) Aircraft emissions during the delay-at-runway mode at the heads of the runways;
- (4) Aircraft emissions during the landing and take-off modes at stations which divide each runway into a number of equal segments;
- (5) Aircraft emissions during the approach and climb-out modes at stations which divide a single approach and climb-out path for each runway into a number of segments which become successively larger as distance from the airport increases;
- (6) Aircraft emissions during the fuel-venting mode at a single point on the climb-out path of each runway;
- (7) Aircraft emissions during the maintenance mode at the hangers;
- (8) Motor vehicle emissions at stations which divide each roadway (including the parking areas) into a number of equal segments;
- (9) Heating plant emissions at the heating plants;

- (10) Fuel storage emissions at a point within each storage area; and
- (11) Surrounding emissions at a point within each sub-division of the surroundings.

3.2.1.3 The GEOMET Model^{326, 327, 328}

The GEOMET Model is a modified version of the NREC model. These modifications center around three areas that do not effect the basic concepts behind the model:

- (1) the substitution of a single wind direction in place of the superimposed wind direction variability parameter used in the NREC short-term subroutine;
- (2) calculation of the long-term average concentration from a large sample of individual short-term calculations, rather than the use of joint frequency distribution of meteorological conditions (as in the NREC model); and
- (3) modification of the NREC emission inventory.

The NREC short-term subroutine involves the use of a single wind direction, and a representation of wind direction variability superimposed on the primary direction (see Section 3.2.1.2). The specific values employed were chosen from observations of hourly meteorological data. The GEOMET model employs a single wind direction only, based on the conclusion that parameters measured over periods of the order of an hour already include the appropriate wind direction variability for any given stability class.

In the calculation of long-term concentrations, the NREC model has an option which employs the joint frequency distribution of meteorological conditions together with the emissions distribution. This approach assumes independence of meteorology and emissions. The GEOMET model avoids this assumption by calculating the long-term concentrations from a large sample of single short-term values. In addition, the procedure accounts for relationships which may exist between meteorological conditions and emission rates, such as diurnal and/or seasonal variations.

The principal modification to the NREC emission model implemented in the GEOMET emission inventory consists of:

- (1) Aircraft Classification - the GEOMET classification involves fifteen categories, based on the number of type of engines per aircraft;
- (2) Aircraft Operational Modes and Emissions - aircraft operational modes are selected to physically represent operational phases. Model assignments are made by aircraft class;
- (3) Environ Area Source Modeling and Emission Factors - increase in the number of point sources representing the area (from sixteen for the NREC model to sixty-four). Definition of specific environ emission characteristics;
- (4) Uniform Line Sources - increase in the number of point sources representing a line source, with point source spacing dictated by relative location of line source; and

- (5) Major Highways - inclusion of emissions associated with major highways near airport.

3.2.1.4 The AVAP Model^{329, 330, 331, 332}

The AVAP model, developed by Argonne National Laboratory for the Federal Aviation Administration (FAA), is a modified version of the NREC model. The AVAP model consists of two submodels: (1) a Gaussian atmospheric dispersion model, and (2) an emission inventory model. Unlike the NREC model, the AVAP model concerns itself with analyzing short-term (24-hour) air pollutant concentrations only. No attempt is made to estimate long-term concentrations (i.e., the Martin-Tikvart technique is not applied). Other than this the basic difference between the AVAP and the NREC model lies in the mathematical simplifications used to compute pollutant dispersion.

3.2.1.4.1 Dispersion Model

The AVAP dispersion model is based on the steady-state Gaussian plume expression as presented in Eq. (3.1.2-4). No attempt is made to preserve temporal causality in the model, i.e., regardless of whether the transit time exceeds the time step, the Gaussian expression is applied as though steady-state conditions existed. Dispersion parameters are calculated in AVAP from the equation

$$\sigma(S, T) = \max \left[\sigma_T(T), \sigma_d(uT) \right] \quad (3.2.1-6)$$

where: S = stability class (according to Turner³⁰⁸)
T = transit time from source to receptor
u = wind speed

$\sigma_T(T)$ = the time-dependent coefficient adapted from
Turner's St. Louis Study³³⁰

$\sigma_d(uT)$ = the distance-dependent coefficient adapted from
Turner's workbook³⁰⁵.

For a particular source-receptor pair, stability class, and wind speed, the maximum value obtained from these two families of curves is used. Up to five virtual image reflections are considered.

For boundary conditions, AVAP used a combination of the uniform mixing method and the virtual image technique, as described in Section 3.1.2.

In AVAP a special algorithm was developed to overcome the difficulties associated with application of the Gaussian formulation under conditions of calm winds. However this algorithm was developed for point sources only, and thus could not be applied legitimately (since line sources are also involved). As a default option for calm conditions the wind speed is set to 1 and the wind direction from the next finite wind speed period is used.

For wind speeds greater than 15 mph, AVAP sets the plume rise parameter, Δh , equal to zero (assuming here that at these speeds downwash accords). Otherwise, the Carson-Moses formula³³³ is used to calculate Δh .*

$$\Delta h = \frac{KQ_s^{\frac{1}{2}}}{u_2} \quad (3.2.1-7)$$

* The momentum term in the original formulation is omitted here under the assumption that its contribution is negligible in comparison to the thermal buoyancy term.

where: Q_s = BTU/hr emitted from the source

$$K = \begin{cases} 0.870 & \text{for stability class 3} \\ 0.354 & \text{for stability class 4} \\ 0.222 & \text{for stability class 5} \end{cases}$$

and u_2 is the wind speed at the emission height H_s , given by

$$u_2 = u \left(\frac{H_s}{H_o} \right)^\gamma \quad (3.2.1-8)$$

where: u = wind speed input data taken at some altitude H_o

γ = stability class dependent exponent (see Table 3.2.1-1)

Restrictions on the use of Eq. (3.2.1-7) are reproduced from Reference 331 in Table 3.2.1-1.

AVAP considers point, line, and area sources. Area sources are approximated by a pseudo upwind point source. Provisions are made to allow for an initial dispersion, σ_{y_o} , so that a receptor may be located inside the boundaries of a source. The initial value of σ_{y_o} is determined as the width of the area source, w , divided by 2.4.* A time, T_y , is then determined such that for the stability class involved

$$\sigma_{y_o} = \sigma_y(S, T_y) \quad (3.2.1-9)$$

The vertical coefficient is chosen so that the initial distribution is approximately uniform to a height z by selecting σ_{z_o} using the equation

* $w = 2.4 \sigma_{y_o}$ corresponds to the width of the normal curve at half maximum.

Table 3.2.1-1

DEFINITION OF AVAP WIND SPEED FORMULATION EXPONENT³³¹

Stability Class	γ
Very stable (≥ 6)	0.5
Stable (5)	0.4
Neutral (4)	0.3
Unstable (< 3)	0.2

Table 3.2.1-2

RESTRICTIONS ON CARSON-MOSES PLUME RISE FORMULATION³³¹1. Low Wind Speeds (U)

If U is estimated to be less than 4 mph, the value 4 is used in Eq.(3.2.1-4).

2. Stability Class and the Coefficient K

If the physical stack height (H_s) is equal to or greater than 200 ft, $K = 0.354$ (neutral) is used, even though the stability index indicates unstable conditions. ($K = 0.222$ if conditions are stable.)

3. Mixing-layer or Lid Height (L)

- a. If the physical stack height H_s is greater than the lid height L, an infinite value for L is assumed, with plume-rise and dispersion according to stable atmospheric conditions.
- b. If the physical stack height is not greater than the lid height, a minimum plume rise ΔH_{\min} (DEFIN in subroutine ISPDV) is calculated, based on the coefficients for stably stratified air. If this minimum effective stack height, $H = H_s + \Delta H_{\min}$, is greater than the lid height L, then H is taken as the effective stack height. As in the case 3a, the lid height L is assumed infinite, but a neutral atmospheric condition is used. Note that "infinite" lid height is represented as 10,000 ft.
- c. If $H_s + \Delta H_{\min} < L$ and if the plume rise ΔH based on the actual stability class yields an effective stack height greater than L, i.e., if $H_s + \Delta H_{\min} < L$ and $H_s + \Delta H \geq L$, the effective stack height is restricted to the lid height L.

4. Downwash

If the wind speed is greater than 15 mph, downwash occurs and there is no plume rise. For short stacks or stacks with poor aerodynamic design the wind speed is 6 mph. (Good aerodynamic design rule of thumb is that $H_s \geq 2.5$ times the neighboring building height).

$$\sigma_{z_o} = \frac{z}{1.2} \quad (3.2.1-10)$$

and solving the equation

$$\sigma_{z_o} = \sigma_z (S, T_z) \quad (3.2.1-11)$$

The point source equation is then employed with dispersion parameters evaluated based upon $T + T_y$ and $T + T_z$.

AVAP includes a line source model designed to handle either a finite or infinite line source of arbitrary spatial orientation. The model may be used to consider a line source with a uniform emission pattern and line sources whose emission pattern corresponds to uniform acceleration or deceleration (i.e., non uniform line source emission density). The model employs a Green's Function technique similar to that used in the so-called "puff models". The calculations associated with this subroutine are quite complex,^{331, 334} and it is in fact the most time consuming portion of the program.

3.2.1.4.2 Emission Model

The AVAP source emission model considers three separate classes of sources:

- (1) Aircraft sources (along taxiways, runways, in gate areas, etc.);
- (2) Airport non-aircraft (service and access vehicles, stationary sources, etc.); and
- (3) Environ sources.

AD-A067 242

SCIENCE APPLICATIONS INC LA JOLLA CALIF

F/G 1/5

DEVELOPMENT OF CRITERIA FOR MONITORING OF AIRPORT GROUND POLLUT--ETC(U)

NOV 78 C B LUDWIG, J R YODER

DOT-FA76WA-3725

UNCLASSIFIED

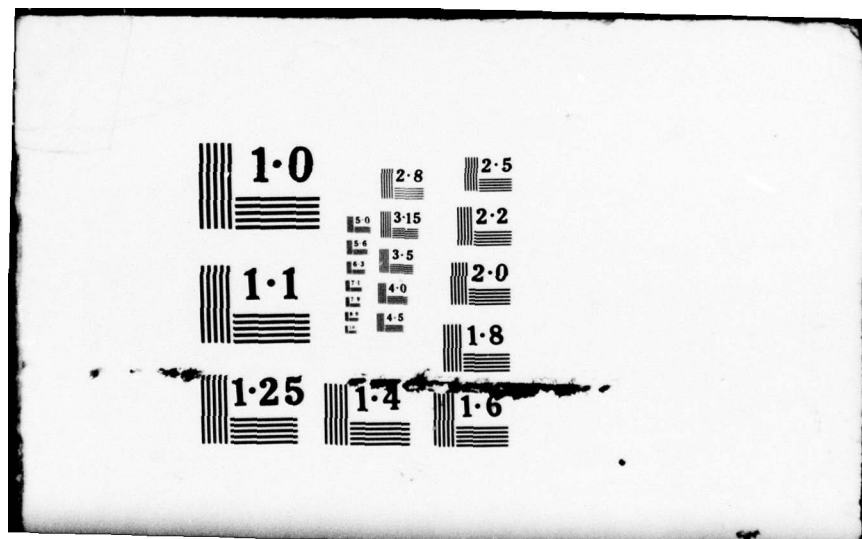
SAI-77-910-LJ-VOL-1-

FAA/RD-77-178-1

NL

2 OF 5
ADA
067242





Each of these classes is broken down into point, line, and area sources. Since all geometric source types are assigned initial values of dispersion they are all in fact treated as finite volume sources. Sources outside the airport, with the exception of major line and point sources are evaluated as a set of one square mile area sources. Two types of emissions for each grid square are considered. One is associated with a fixed plume rise, the other has no plume rise. In both cases the initial uniform vertical dispersion is assumed equal to the average building height (taken to be 30 feet). For environ sources with plume rise, Δh is set equal to the building height when the wind is less than 6 mph and 0 for greater speeds.

Sources inside the airport boundaries considered include: aircraft, access traffic, power/heating plants, service equipment, and fuel handling and storage facilities. In addition, an overall review of airport fuels received versus calculated fuel combustion was made to insure general agreement.* In AVAP, aircraft are grouped into four basic categories: jumbo, long range, medium range, and short range; and then further grouped into ten classes depending on number and type of engines. Six aircraft activity modes are considered (taxi, idle, landing, takeoff, approach, and climbout). The degree of aircraft activity per time interval is derived from (1) the hourly arrival rates, (2) the relative frequency of usage of each runway for landing and take-off, and (3) the relative frequency of usage of each taxiway. Associated with each runway is a set of arrival and departure velocities and angles, a runway roll time, and an exhaust plume length. Runway usage is dictated by wind direction.

* Some additions were made to allow reasonable agreement.

Airport access traffic is derived from information on the approximate number of vehicle trips per day, the class of vehicle, vehicle distance traveled, and the vehicle operational characteristics. Emission factors are developed from EPA published data on emissions associated with a standard urban driving cycle³³⁵ and considered as constants over the time interval of interest. Service vehicles are considered as either diesel or gasoline vehicles. Incinerators and heating/power plants are described as point sources with a given stack height and a heat of operation which induces additional plume rise (as mentioned earlier).

In applications after the initial development of AVAP,³³¹ several modifications were introduced. The primary changes involved the addition of:

- (1) a simulation of engine shutdown during taxi;
- (2) a simulation of runway queueing; and
- (3) an algorithm representing aircraft pauses prior to the crossing of active runways.

3.2.1.5 AQAM³³⁶

AQAM was developed by Argonne National Laboratory for the U. S. Air Force Weapons Laboratory. AQAM consists of four subprograms: (1) a meteorological data problem; (2) a source inventory program; (3) a short-term dispersion model; and (4) a long-term dispersion model. The dispersion models are based on the steady-state Gaussian plume formulation, with the short-term subroutine derived from the AVAP model and the long-term subroutine based on the AQDM.

3.2.1.5.1 Short-Term Model

The AQAM short-term subroutine is used to compute hourly average pollutant concentrations from the emission inventory and the corresponding hourly average values of the meteorological information. It is essentially the same model employed in AVAP, with the following exceptions:

- (1) Dispersion parameters employed in Eq. (3.2.1-6) are derived from those given in Turner's Workbook³⁰⁵ by multiplying by $(60/120)^{0.2} = 0.85$ to convert from two-hour to one-hour sample times;
- (2) Up to six virtual image reflections are considered in defining the effects of an inversion layer;
- (3) If a given receptor within the boundaries of a defined area source, the strength of the source is modified by a linear weighting factor:

$$\text{wt. factor} = \frac{R + x}{2R}$$

where: R = source radius

x = downwind distance from the center of
of the physical source to the receptor
(< 0 if the receptor is upwind of the
source center).

The dispersion coefficient is then taken at its initial value (i.e., no initial dispersion considered);

(4) In considering the effects of plume rise, sources are classified into five types:

- Area sources
- Point sources designated as having no plume rise
- Point sources with plume rise which is assumed to obey the Holland plume rise formula¹⁹
- Point sources with plume rise which is assumed to obey the Carson-Moses plume rise formula³³
- Special sources (training fires) requiring a special application of the Carson-Moses formulation.

For sources considered to have a plume rise, a downwash effect is calculated using a formula due to Briggs, dependent upon emission source height and diameter, wind speed at the altitude of emission release, and initial effluent velocity. If necessary, this factor is then adjusted for building wake effects based upon the building dimensions. Plume rise is then calculated using either the Holland or Carson-Moses formulation.

Plume rise associated with training fires is calculated by applying the Carson-Moses formulation to a ground level emission.

3.2.1.5.2 Long-Term Model

The AQAM long-term model is a modified version of the AQDM based on the Martin-Tikvart technique. The difference between the two models lies in the basic statistical approach used to compute the annual average of hourly pollutant concentrations. AQDM makes this calculation assuming a uniform annual average emission rate. AQAM calculates annual average concentrations using annual or monthly emission

rates. AQAM can also carry out computations based on one of seven diurnal time classes:

- (1) all hours of the day,
- (2) business hours,
- (3) morning rush hours,
- (4) mid-day,
- (5) evening rush hours,
- (6) late evening, and
- (7) nighttime.

The basic input parameters used in the long-term model are essentially the same as those in the short-term model. Plume rise effects are considered in the same manner in both. Consideration of line sources is the same, except that in the long-term model an angle averaging procedure is used to incorporate wind direction effects. In the treatment of dispersion from physical point and area sources, both models assume Gaussian distribution in the vertical direction, but only the short-term model considers Gaussian dispersion in the lateral direction as well. Furthermore, whereas both models treat the finite size of physical sources by the "pseudo upwind point source" method, the technique is used only for the horizontal dimension in the long-term model.

3.2.1.5.3 Emission Model

The AQAM emission model considers the airport emission inventory in a manner similar to that detailed in the AVAP model. Aircraft emissions are described by type of aircraft (up to fifty may be included).

Operations are detailed in terms of the following classes:

- (1) Arriving Aircraft - approach from 3000 feet to idle at shutdown;
- (2) Departing Aircraft - idle at start-up to climbout to 3000 feet;
- (3) Training Flights - (touch-go operation);
- (4) Associated ground service for arriving aircraft;
- (5) Associated ground service for departing aircraft;
- (6) Aircraft refueling emissions and associated spillage of fuel;
- (7) Fuel venting for arriving aircraft; and
- (8) Fuel venting for departing aircraft.

Traffic patterns are specified from monthly, daily, and hourly aircraft distribution data for each aircraft type together with a designation of runway usage patterns by wind direction and runway-taxiway usage. Vehicles are classified according to their gross weight. Emission factors are derived from activity distribution, number of vehicle miles traveled, and average vehicle speeds, with consideration for cold start emission effects. Power plant emissions are derived from fuel type and usage data, the furnace size, and the degree to which pollution controls have been implemented. Evaporation from fuel storage facilities is considered based on facilities design, usage, and meteorological factors. Emissions from training fires, engine tests and incinerators are also considered.

Environ emissions may be considered as per airport emission; by specific input of point, line, or area sources, or as in the NREC land use classification.

3.2.1.5.4 Meteorological Model

The meteorological model employed in AQAM was developed by the U. S. Air Force Environmental Technical Applications Center. The program essentially processes historical weather data and generates a climatological record consisting of a series of stability wind roses for the given geographic region. These stability wind roses are based on input for seven daily time period classifications, and are compiled on a monthly and annual basis.

3.2.1.6 Walden Research

The Walden Research highway model is a Gaussian model that is a modified version of AQDM which is described in detail in Section 3.3.1.1 of this document. The modifications are specific to highway applications and additional modifications would be required if the model were to be used as an airport model. The modifications consist of two major changes and other minor modifications for ease in use. The major modifications include the addition of a module to determine the emissions associated with the vehicle traffic along the highway source under consideration. The second modification is the implementation of a method for transforming the highway line sources into a series of point sources. This is accomplished by creating a virtual point source upwind of each traffic lane to represent an area of the lane by combining these sources a representation of a line source is developed. It appears that no significant improvement in air quality estimates could be obtained from modifying this model to be applicable to airport problems.

3.2.1.7 TSC/EPA Highway Model

The TSC/EPA highway model is a Gaussian model originally developed at EPA, Research Triangle Park, and is available in the EPA,

UNIMAP, model series as HIWAY. The staff at Transportant Systems Center (TSC) has modified the model to allow the treatment of a more complex arrangement of line sources so that multiple streets and interchanges can be modeled. In addition the model considers winds from several directions so that a worst case analysis can be made from a single computer run. The actual concentration at a receptor is determined by a sector average method assuming that the actual wind direction is variable. The concentration is computed from

$$C_{SA} = \frac{1}{4} \left[C(\theta_n - 22.5^\circ) + 2C(\theta_n) + C(\theta_n + 22.5^\circ) \right] \quad (3.2.1-12)$$

where: C_{SA} = the sector-average pollutant concentration for a principal wind direction;

$C(\theta)$ = the calculated concentration for wind direction; and

θ_n = the nominal angle for the principal wind direction.

The TSC/EPA model is basically a line source Gaussian model. Modification would be required for application to airports both from a geometrical point of view and the addition of appropriate emission factors.

3.2.1.8 Cal/Trans

The California Division of Highways (Cal/Trans) model is a model very specific to highways. The model is based on the Gaussian diffusion equation with several assumptions to account for the localized non-Gaussian behavior that is experienced near roadways. In particular a mixing cell is located at the highway to account for the turbulent field generated by the vehicles moving along the roadway.

The basic model assumptions, method of analysis and input-output parameters are based on a highway application and generalization of this model to an airport would require a significant effort. Because of the nature of the model and its formulation it does not appear to be a good candidate for an airport model.

3.2.2 Conservation of Mass Models

3.2.2.1 ERT Model

The ERT highway model EGAMA³³⁷ is a two-dimensional model using a grid system to describe the transport and dispersion of pollutants. Equation (3.2.1-13) describes the conservation equation used to determine pollutant concentrations.

$$\frac{\partial \chi}{\partial t} = -u \frac{\partial \chi}{\partial x} - w \frac{\partial \chi}{\partial z} + \frac{\partial}{\partial z} \left(K \frac{\partial \chi}{\partial z} \right) + Q \quad (3.2.2-1)$$

where: χ = concentration
 u, w = horizontal, vertical winds
 K = vertical diffusivity
 x = horizontal coordinate
 z = vertical coordinate .

The wind fields are determined internally in the model by assuming conservation of mass and that the undisturbed flow entering the left hand side of the grid is a horizontal power law wind field

$$u = u_0(z)$$

$$w = 0 \quad (3.2.2-2)$$

The turbulent diffusivity is computed to be a function of position throughout the grid.

The model uses a moment method³³⁸ for computing the advection terms in the transport equation, thereby reducing the artificial or pseudo diffusion due to the numerical differencing of the transport equation.

The methods developed in this model are applicable to line sources with flow perpendicular to the source. This limits the applicability to airport problems where the source distribution is complex and sources of types other than a line source must be considered. Many of the techniques used in this model are applicable to 3-D models and should be considered if a 3-D airport model is developed in the future.

3.2.2.2 Aerovironment

The Aerovironment model³³⁹ has been developed for transport of pollutants in the atmosphere according to

$$\frac{\partial c}{\partial t} + u \frac{\partial c}{\partial x} = \frac{\partial}{\partial x} \left(K_x \frac{\partial c}{\partial x} \right) + \frac{\partial}{\partial y} \left(K_y \frac{\partial c}{\partial y} \right) + \frac{\partial}{\partial z} \left(K_z \frac{\partial c}{\partial z} \right) \quad (3.2.2-3)$$

where:

c = concentration

x, y, z = coordinates

U = mean velocity in x direction

K_x, K_y & K_z = represent diffusivities or transfer coefficients.

The uniqueness of the model is in the method of determining the transfer coefficients. The coefficients are assumed to be of the form $K = a\sigma$ where a is the dispersion speed and σ is the scale of dispersion. σ is assumed to change with space and time while a is assumed to be invariant. A method of relating these parameters to surface heat flux and roughness is presented.

The equation can be solved for many cases analytically thus resulting in closed form solutions and eliminate the need for extensive numerical solutions and the associated numerical errors. Particular cases with closed term solutions are point sources and line sources. These solutions have been examined for a limited number of cases and appear to provide answers in reasonable agreement with measurement; however, the applicability of the model has not been generally verified. The concepts and ideas presented in this model warrant further investigation but its direct usefulness as an airport model is limited.

3.2.2.3 The S^3 · Photochemical Model

Since the development of the S^3 · photochemical model involved the initial definition of the "Particle-in-Cell" technique, much of the description of this model is contained in Section 3.1.3.

The S^3 · photochemical (or NEXUS) model involves an extension of PIC to include consideration of chemically reactive pollutants. In PIC each particle has a fixed mass, set when the particle is introduced into the calculation. Chemical reactions occurring in the atmosphere have the effect of removing primary pollutants and/or forming secondary ones. The net effects are changes in the concentrations of the reactant and product pollutants. Thus, in considering reactant and product species the mass represented by the PIC particles must be changed and new particles must be created.

The turbulent atmospheric diffusion equation solved in NEXUS can be written as

$$\frac{\partial c_s}{\partial t} = -\bar{u} \frac{\partial c_s}{\partial x} - \bar{v} \frac{\partial c_s}{\partial y} - \bar{w} \frac{\partial c_s}{\partial z} + \frac{\partial}{\partial x} \left(K_x \frac{\partial c_s}{\partial x} \right) + \frac{\partial}{\partial y} \left(K_y \frac{\partial c_s}{\partial y} \right) + \frac{\partial}{\partial z} \left(K_z \frac{\partial c_s}{\partial z} \right) + \sum_{r,t} B_{srt} c_r c_t + \sum_{r,t} P_{sr} c_r, \quad (3.2.2-4)$$

where the concentration subscripts have been used to emphasize different chemical species and the two new terms represent bi-molecular and photochemical reactions (B and P, respectively). There is a separate differential equation for each species being simulated. The differential equations are no longer linear and are coupled together through the chemical terms.

In the PIC method as used in NEXUS, the equations are rewritten as

$$\frac{\partial c_s}{\partial t} = -\frac{\partial u c_s}{\partial x} - \frac{\partial v c_s}{\partial y} - \frac{\partial w c_s}{\partial z} + S_s, \quad (3.2.2-5)$$

where the fictitious total velocity is used for pollutant transport and the chemical terms have been grouped into a source or sink for the "sth" species, S_s . Equation (3.2.2-5) is solved assuming the effects of pollutant transport and of chemical reactions are separable. Pollutant transport is simulated for the same interval. That is, the transport and reactions are calculated in sequence.

In simulating pollutant reactions the NEXUS model uses the so-called "Lumped Parameter" approximation, i.e., instead of considering the overwhelming number of possible pollutant reactions involved, NEXUS employs a chemical mechanism based on the lumping together of many similar species into a single "effective" species and many similar reactions into a single "effective" reaction. For the particle application for which NEXUS was developed (Los Angeles photochemical smog

simulation) a set of reactions based on the lumped parameter approximation and reported by Schenroeder and Martinez³³⁷ were employed. Eschenroeder's chemical mechanism is given in Table 3.2.2-1.

The set of chemical reactions considered can be translated into a set of coupled, non-linear, first-order differential equations -- the chemical kinetic rate equation. These rate equations are all of the form

$$\frac{\partial c}{\partial t} = F - Rc \quad (3.2.2-6)$$

where F is a summation of the rate of all reactions forming species c , and Rc is a summation of all those reactions removing c . F and R are called the formation and removal rates, respectively.

In NEXUS a small "chemical reaction" subroutine is used to solve these differential equations. The solution is based on the analytic solution of Eq. (3.2.2-5) for a time step, Δt , assuming constant F and R

$$c(t + \Delta t) = F/R + [c(t) - F/R]e^{-R\Delta t} \quad (3.2.2-7)$$

For a sufficiently small Δt , R and F are almost constant and the solution is a good approximation. In NEXUS, the species concentrations are predicted as indicated by Eq. (3.2.2-7). Then F and R are recalculated using the predicted concentrations, c_p , and new "corrected" concentrations, c_c , are calculated again using Eq. (3.2.2-7). A desired fractional error limit, ER , is used to compute the appropriate time step, Δt , from a trial time step t'

$$\Delta t = ER \left| \frac{\frac{c_p + c_c}{c_p - c_c}}{\frac{c_p - c_c}{c_p - c_c}} \right| \Delta t' \quad (3.2.2-8)$$

An initial time step of 10^{-9} seconds is used to insure starting accuracy.

Table 3.2.2-1

RATE COEFFICIENTS FOR ESCHENROEDER'S MODEL OF
THE HYDROCARBON/NITRIC OXIDE MECHANISM

(Stoichiometry imbalances may occur because of
lumped parameter assumptions.)

REACTION	RATE COEFFICIENTS
1. $(h\nu) + NO_2 \rightarrow NO + O$	0.4 min^{-1}
2. $O (+ O_2)(+ M) \rightarrow O_3 + M$	$2.64 \times 10^6 \text{ min}^{-1}$
3. $O_3 + NO \rightarrow NO_2 (+ O_2)$	$40 \text{ ppm}^{-1} \text{ min}^{-1}$
4. $O + HC \rightarrow 2RO_2$	$6100 \text{ ppm}^{-1} \text{ min}^{-1}$
5. $OH + HC \rightarrow 2RO_2$	$80 \text{ ppm}^{-1} \text{ min}^{-1}$
6. $RO_2 + NO \rightarrow NO_2 + 0.5 OH$	$1500 \text{ ppm}^{-1} \text{ min}^{-1}$
7. $RO_2 + NO_2 \rightarrow PAN$	$6 \text{ ppm}^{-1} \text{ min}^{-1}$
8. $OH + NO \rightarrow HNO_2^*$	$10 \text{ ppm}^{-1} \text{ min}^{-1}$
9. $OH + NO_2 \rightarrow HNO_3^*$	$30 \text{ ppm}^{-1} \text{ min}^{-1}$
10. $O_3 + HC \rightarrow RO_2$	$0.0125 \text{ ppm}^{-1} \text{ min}^{-1}$
11. $(H_2O +) NO + NO_2 \rightarrow 2HNO_2^{**}$	$0.01 \text{ ppm}^{-1} \text{ min}^{-1}$
12. $(h\nu) + HNO_2 \rightarrow NO + OH$	0.001 min^{-1}

*Rate constant incorporates third body concentration.

**Water vapor incorporated into rate coefficient.

RO_2 is used as the chemical symbol for a free radical lumped species.

HC stands for the hydrocarbon lumped species.

Parentheses are used to indicate species concentrations that are not chemically changing and are incorporated into the rate coefficient.

The solar flux is represented by " $h\nu$," the maximum solar flux is incorporated into the first rate coefficient.

The chemical reaction subroutine is incorporated as a subroutine into the PIC model for chemical simulation to form the quantity S_g in Eq. (3.2.2-5). An intermediate subroutine was also developed to call up the chemical subroutine for each cell in which chemical reactions are significant. The chemical reaction subroutine calculates new cell concentrations due to chemical reactions for a time interval equal to the PIC time step. The chemical reaction subroutine returns the fractional change in concentration for each species (CF)

$$CF = \frac{c(t + \Delta t)}{c(t)} \quad . \quad (3.2.2-9)$$

If the initial cell concentration of a species produced by chemical reactions were zero, the chemical reaction subroutine would return the negative of the concentration produced

$$CF = - c(t + \Delta t) \quad (3.2.2-10)$$

The negative sign is used as a flag to indicate that CF is the new concentration instead of the fractional change.

3.3 MODEL ASSESSMENT AND COMPARISON

3.3.1 Model Assessment

A review of all the models considered indicates that two types of models are available for use in the assessment of air quality problems in the vicinity of airports. The types are generic of the two generally available air quality models. By far the largest group available are Gaussian models which use a form of the equations developed by Pasquill³⁰³ as the basis for determining concentrations. The other

category of models are the conservation of mass models which require more detailed input and are usually computationally more complex than the Gaussian models.

Of the models considered in this review only some of the Gaussian models have been developed specifically for airport applications. Specific routines for emission factors and pollutant release information have been incorporated into these models. This type of data significantly improves the model usefulness. It makes it much easier to employ the model and to correctly interpret the model output.

One major limitation of many of these models at the present time is their inapplicability in their present form to the general airport problem. Many of these models have been developed for highways and predict concentrations downwind of a line source. The additional problem of appropriate emission factors mean that significant modification would be required before these models could be used for airport air quality projections. In addition, the geometrical complexity of the airport emissions would require major modification or restructuring of several of the models.

Three of the models (Walden, TSC/EPA, and Cal/Trans) are Gaussian formulations and offer little, if any, improvement over the existing models. Given the amount of work required to convert these models so they would be applicable to airport problems, and realizing that the formulation is very similar to the existing family of Gaussian airport models (GEOMET, NREC, AVAP and AQAM) it appears that major modification of these models is not appropriate or efficient in terms of developing an adequate model.

Two models (Aerovironment and ER&T) are both two-dimensional and would require significant modification to represent airport problems. Both of these models incorporate unique features which may be significant contributions to the development of air quality models and should be carefully reviewed as part of any development program. The Aerovironment model contains a unique method for determining dispersion coefficients that may be applicable in more general models. The ER&T model contains a unique advection methodology that reduces artificial dispersion due to numerical truncation errors. Neither of these models contain the necessary emission data or geometrical source configurations that would allow for direct application of these models to the airport problem.

Using a methodology developed for other air quality models³⁴⁰ Table 3.3.1-1 has been developed to compare some of the desirable attributes of models already constructed; the models have been compared ranking them as to the relative ability to exhibit each of the attributes.

The attributes considered are: (1) dynamic or time dependent, (2) horizontal wind field, (3) wind shear, (4) variable dispersion coefficients, (5) terrain effects, (6) photo-chemistry, (7) inclusion of emission factors, (8) data input requirements, (9) data preparation, and (10) ability to handle three-dimensional problems.

Each of the attributes is briefly described and its importance to the airport pollution problem discussed.

The ability to treat dynamic or time varying problems is crucial to determining the time dependent behavior of pollutant concentrations. While this is not essential in determining maximum impact or expected concentration levels, it may be essential to obtain good comparison with model results and with measured air quality parameters near existing airports.

TABLE 3.3.1-1
DESIRABLE MODEL ATTRIBUTE COMPARISON

	ATTRIBUTES										COMMENTS
	Dynamic	Hor. Wind Field	Wind Shear	Dispersion Coefficient	Terrain	Chemistry	Emission Factors	Data Requirements	Data Preparation	3-D	
AQDM	3	3	3	3	3	3	3	1	3	2	Long Term
NREC	3	3	3	3	3	3	1	2	2	2	Gaussian
GEOMET	3	3	3	3	3	3	1	2	2	2	Gaussian
AVAP	3	3	3	3	3	3	1	2	2	2	Gaussian
AQAM	3	3	3	3	3	3	1	2	2	2	Gaussian
PIC	1	1	1	2	1	1	3	3	3	1	3-D Particle
Aerovironment	2	3	1	1	2	2	3	2	2	2	2-D (Diffusion Package)
Walden Research	3	3	3	3	3	3	3	1	2	2	Gaussian + Source
TSC/EPA	3	3	3	3	3	3	3	1	2	2	Gaussian + Source
CAL TRANS	3	3	3	3	3	3	3	1	2	2	Gaussian + Calibration
ER&T	1	2	1	2	2	2	3	3	3	2	2-D

1 - Best Treatment
2 - Partially Treated
3 - Not Treated

Changing horizontal wind fields frequently occur particularly when terrain effects or thermal effects dominate the wind field. The ability to adequately treat these phenomena can be of importance.

Wind shears in the vertical can strongly influence atmospheric dispersion. Since much of the airport emissions occur at heights near the ground, but not on the ground, variation in wind speed with height become important in determining dispersion of the pollutants.

Variable dispersion coefficients which may change as a function of time and position can be important near airports. A great amount of turbulent mixing can be caused by the aircraft and this influences the mixing of the pollutants into the ambient air.

Terrain effects frequently are important as they distort the air flow and can entrain pollutants into the lee of buildings or obstacles causing large concentrations.

Photochemistry is an important parameter because many of the criteria pollutants are involved in photochemical reactions and to predict the air quality impact it is necessary to estimate these effects.

A significant amount of effort can be used to incorporate appropriate emissions into a model. The inclusion of these factors into the model can reduce the input required, the ease with which the model can be used and the number of errors that may occur.

The data requirements of the model are an important consideration in determining the ease with which a model can be used. Large amounts of data input reduce the model usefulness. The ease with which the data can be input (i. e. , manual preparation of data) also strongly influences the usefulness of a model. For example, if the input is in terms of aircraft type, it would be easier to use than an input requirement of exhaust temperature, emission rate, aircraft speed and other parameters.

The final attribute is the three-dimensional nature of the problem. The airport problems are very complex and can have major three-dimensional effects which need to be adequately treated if the model will realistically reflect the actual conditions at or near the airport.

3.3.2 Validation and Calibration

One of the basic questions regarding air quality models is "How well does the model work?". Much time, effort and money has been used to collect the necessary data and attempt to validate and calibrate air quality models. Frequently these efforts have not met with success and many people have become discouraged with this complex problem.

The major difficulty associated with the validation and calibration effort is the inability of man to control the atmosphere so that data can be obtained under controlled conditions. Without this control it is frequently impossible to collect data with which to test the model.

Some factors such as aircraft and vehicle emission factors can be measured under laboratory conditions that are controlled. The conditions can be varied so that a spectrum of operational situations can be obtained and a reasonable estimate of pollutant emissions obtained. This portion of any model would be relatively easy to validate.

Other model parameters such as dispersion parameters can only be obtained by deductive analysis of dispersion data and are influenced by the meteorological data collected during the dispersion tests. Wind shear, non-homogeneity of winds, thermal stratification, and mechanical turbulence frequently cause the data to be scattered and determination of dispersion coefficients extremely difficult.

Another major problem is the inability of the models to accept sufficient meteorological data to accurately reflect conditions during experiments and this frequently causes difficulties such as wind shifts and shears occur.

The problem of overall model calibration frequently results in data comparison between model prediction and actual measurements. These comparisons usually are not such that confidence can be placed in the model as an estimation of ambient air quality levels. Figure 3.3.2-1 shows a typical plot from the AVAP model study³³¹ at National Airport in Washington, D.C. As can be easily seen, there appears to be limited correlation between the model and reality.

Many factors can enter into this apparent lack of correlation. These factors include (1) inability to monitor at low ambient levels, (2) inability to separate "background" levels (i.e., those pollutant concentrations that are not directly attributable to the airport emissions), and (3) inability to appropriately model conditions at the airport.

The first two problems can be overcome to some extent by using a tracer gas to simulate actual emissions. Since costs to release from all sources would be prohibitive, normally tests would be conducted for a range of emitter-receptor configurations and these results compared with the model.

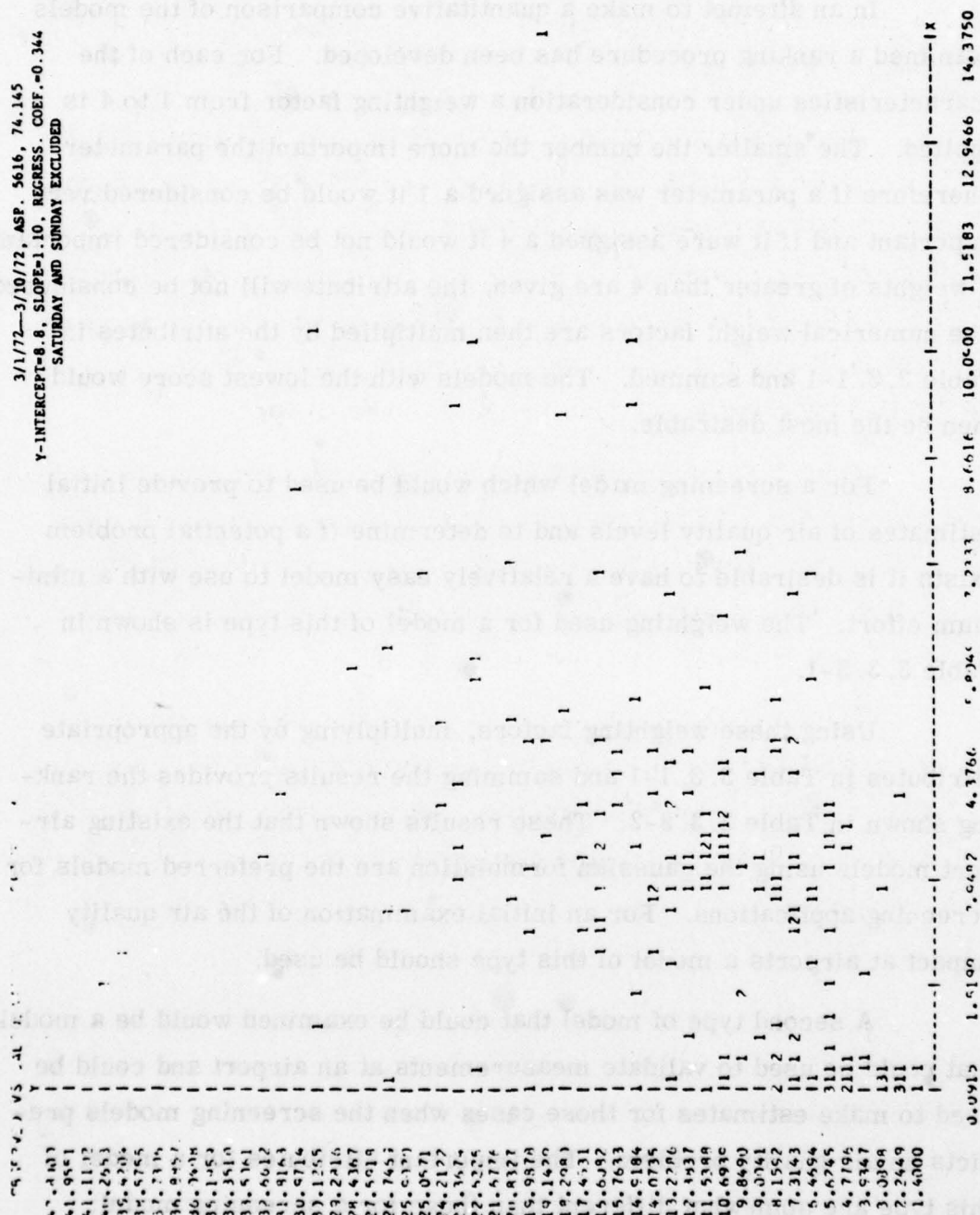


Figure 3.3.2-1 Scatter Plot of Hourly Observed vs Calculated CO Concentrations at Site 3 for the March Test Period with Regression Analysis Results. Saturday and Sunday Data Points were Excluded.

3. 3. 3 Model Ranking

In an attempt to make a quantitative comparison of the models examined a ranking procedure has been developed. For each of the characteristics under consideration a weighting factor from 1 to 4 is applied. The smaller the number the more important the parameter. Therefore if a parameter was assigned a 1 it would be considered very important and if it were assigned a 4 it would not be considered important. If weights of greater than 4 are given, the attribute will not be considered. The numerical weight factors are then multiplied by the attributes in Table 3. 3. 1-1 and summed. The models with the lowest score would then be the most desirable.

For a screening model which would be used to provide initial estimates of air quality levels and to determine if a potential problem exists it is desirable to have a relatively easy model to use with a minimum effort. The weighting used for a model of this type is shown in Table 3. 3. 3-1.

Using these weighting factors, multiplying by the appropriate attributes in Table 3. 3. 1-1 and summing the results provides the ranking shown in Table 3. 3. 3-2. These results shown that the existing airport models using the gaussian formulation are the preferred models for screening applications. For an initial examination of the air quality impact at airports a model of this type should be used.

A second type of model that could be examined would be a model that could be used to validate measurements at an airport and could be used to make estimates for those cases when the screening models predicts an air quality problem. The important attributes for a model of this type are somewhat different than those for a screening model;

TABLE 3. 3. 3-1
WEIGHT FACTORS FOR A SCREENING MODEL

Dynamic	5
Horizontal Wind Field	5
Wind Shear	5
Dispersion Coefficients	5
Terrain	5
Chemistry	5
Emission Factors	1
Data Requirements	1
Data Preparation	1
3-D	3

TABLE 3. 3. 3-2
RANKING OF MODELS FOR USE
AS A SCREENING MODEL

<u>Model</u>	<u>Score</u>
NREC	11
GEOMET	11
AVAP	11
AQAM	11
Walden Research	12
TSC/EPA	12
CALTRANS	12
PIC	12
AQDM	13
Aerovironments	13
ER&T	15

therefore, a new set of weighting factors is required. The weighting factors are shown in Table 3. 3. 3-3 and the resulting model ranking is shown in Table 3. 3. 3-4. These results indicate that for these purposes a more detailed model with the complexities of 3-D is better suited to the use. A model of this type will require considerable development in terms of incorporation of emission factor and appropriate geometrical factors such as runway patterns and flight paths.

3. 4 SUMMARY AND CONCLUSIONS

In reviewing all of the air quality models considered as candidate models for determining the air quality impact associated with airports and airport operations, SAI has concluded that two types of models should be used to accomplish these analyses.

The first model would be a "screening model" to estimate the ambient air quality levels in the vicinity of the airport. This model should provide a reasonable estimate of the concentration levels but may not provide a detailed distribution in time and space that can be validated by ambient measurements. The model should be relatively easy to use. If the model results indicate air quality levels significantly below ambient standards then further detailed analysis would not be required. If on the other hand, the results indicated potential problems with elevated pollutant levels then a more rigorous method should be applied.

The second model would be capable of completing detailed analysis of the expected air pollution problems at the airport and would be properly validated so that the results could confidently be used as good estimates of the ambient concentration levels in the vicinity.

TABLE 3. 3. 3-3

**WEIGHT FACTORS FOR A VALIDATION
AND APPLICATION MODEL**

Dynamic	1
Horizontal Wind Field	2
Wind Shear	2
Dispersion Coefficients	2
Terrain	3
Chemistry	3
Emission Factors	2
Data Requirements	3
Data Preparation	4
3-D	1

TABLE 3. 3. 3-4

RANKING OF MODELS FOR USE AS A VALIDATION
AND APPLICATION MODEL

<u>ModelQ</u>	<u>Score</u>
PIC	43
Aerovironment	46
ER&T	53
NREC	57
GEOMET	57
AVAP	57
AQAM	57
Walden Research	58
TSC/EPA	58
CALTRANS	58
AQDM	62

A screening model is presently available in the form of one of the Gaussian models developed for airports. The AVAP model developed by Argonne for the FAA has the proper characteristics. A sufficient amount of data has been collected to indicate that this model roughly provides predictions of ambient concentrations that are comparable to those measured. Other candidate screening models would be the NREC and Geomet models for airports.

At the present time a good detailed model for airports does not exist. The effort to develop this model would require incorporation of emission factors and geometrical factors into an existing three-dimensional model.

4.0 DESCRIPTION OF POINT SAMPLERS

4.1 Introduction

EPA has used the concepts of "reference methods" and "equivalent methods" to standardize measurement methodologies. Although not yet specified, remote monitors will eventually be included in these measurement methodologies. It is the purpose of this section to review EPA's standardization procedures for the point samplers (manual as well as automatic analyzers) and to extend these procedures to the remote monitors. Of special interest is the concept of "equivalent method" which makes it possible to accept pollutant measurements taken by an analyzer whose measurement principle is different from that of the reference method.

Originally, reference methods were specified for manual instruments that embodied a given technique. These were described in the Appendices A through F of Chapter I of Part 50, Title 40 of Code of Federal Regulations. They dealt with the manual measurements of total suspended particles (TSP), CO, SO₂, NO₂ and photochemical oxidants. Subsequently, EPA has adopted a new concept for some of these pollutants, which is described in Part 53 of Title 40, Chapter I. Instead of specifying reference methods, measurement principles and calibration procedures are designated. For example, the NDIR becomes the measurement principle for CO. Any analyzer using the NDIR principle and calibration procedure and meeting the appropriate performance tests is designated as a reference method. As a consequence, there could be as many reference methods for CO as there are models of CO analyzers utilizing the NDIR measurement principle⁽²⁰⁸⁾. Other methods, utilizing a different measurement principle, can be designated as equivalent method as long as equivalency to the reference methods can be demonstrated. In the case of CO, an equivalent method could be a manual or automatic flame ionization method, or potentially, a remote long-path method (see Section 6.1.1).

To obtain an overview of the different methods in actual use, we follow the discussion given by Hoffman et al. ⁽²⁰⁸⁾ about the status of the air quality monitoring by the states. Table 4-1 presents a national summary of the total number of stations in the state networks for monitoring each of the five NAAQS pollutants as of the end of 1974. These networks were established according to the "State's Implementation Plans (SIP)".

TABLE 4-1. National Summary of Air Monitors, 1974⁽²⁰⁸⁾

Pollutant	Total reporting*	Federal Register requirements	Percent completed†	SIP obligated	Percent completed‡
TSP	3683	1341	92	3521	86
SO ₂					
Continuous	503	213	64	698	50
Bubbler	1648	656	80	1434	80
CO	326	137	82	457	58
O ₃	331	214	80	455	65
NO ₂ ‡	1215	0		0	
Total§	6491	2561	85	6556	77

*Unacceptable methods not included. †Percentages are less than 100 because several states are below minimum network size, although others are operating networks larger than the minimum requirement. ‡The reference method has been withdrawn. Thus, there are technically no requirements until a new method is named. §NO₂ not included in totals.

Table 4-2 identifies the number of stations monitoring each pollutant according to the method or principle being used. Most air monitoring is being conducted with reference methods or principles. These are the sole members of the "approved" category at present. Other methods that are not reference methods but are considered reasonable candidates for passing equivalency tests are listed as "unapproved." The last category, "unacceptable," includes those methods or measurement principles that are generally acknowledged to be inaccurate and obsolete.

TABLE 4-2. Pollutant Method/Station Summary, 1974⁽²⁰⁸⁾

Pollutant	Method or principle*	No. of stations	Percent of total	Approved	Unapproved	Unacceptable
TSP	High volume (FRM)*	3683	100	X		
CO	NDIR (FRM)	316	96	X		
	Coulometric	2	n†			X
	Flame ionization	10	4		X	
	Total	328				
SO ₂	Colorimetric	122	6		X	
	Conductimetric	93	4		X	
	Coulometric	223	10		X	
	Flame photometric	59	3		X	
	Sequential conductimetric	6	n		X	
	Pararosaniline (FRM)	1648	77	X		
	Total	2151	100			
NO ₂	Colorimetric	139	11		X	
	Coulometric	5	1		X	
	Chemiluminescence (FRM)‡	49	4	X†		
	Salzman bubbler	5	1			X
	Sodium arsenite (orifice)	294	24		X	
	Sodium arsenite (frit)	730	59		X	
	TEA				X	
	TGS				X	
	Total	1220	100			
O ₃	Alkaline KI	10	3			X
	Coulometric	34	9		X	
	Neutral KI	71	19		X	
	Phenolphthalein	1	n			X
	Alkaline KI bubbler	18	5			X
	Ferrous oxidation	20	5			X
O ₃	Chemiluminescence (FRM)	225	59	X		
	Coulometric	1	n		X	
	Ultraviolet				X	
	Total	380	100			

*FRM, Federal reference method or principle.
replace Jacobs-Hochheiser procedure.

†n = negligible.

‡Proposed measurement principle to

In the meantime, several candidate instruments have been approved by EPA as reference or equivalent methods. These are described in Section 4.2.3.

4. 2 Ambient Air Monitoring Reference and Equivalent Methods and Measurement Principles

4. 2. 1 Definitions and Requirements

Measurement methodologies need be standardized so that all agencies use the optimum procedures (in terms of cost and ease of operation). Thus, EPA has specified procedures that can be used by the local and state air pollution control agencies in their air quality monitoring networks in the fulfillment of 40CFR51 ("Requirements for Preparation, Adoption, and submittal of Implementation Plans") and in the reporting of a daily air quality index (according to the "Pollutant Standards Index (PSI)" - 41FR37660, September 7, 1976). The procedures specified by EPA involve "reference methods" and "equivalent methods". A reference method is a field-tested and proven technique or instrument that is reasonable in cost and is relatively easy to operate and maintain. Measurement instruments that might be extremely precise and accurate, yet are costly, difficult to operate, or not field-tested would not be considered for designation as a reference measurement principle. Such instruments can, however, be used in research projects. ⁽²⁰⁸⁾ An equivalent method has been defined as a method that can be shown to meet certain performance specifications and give measurements having a consistent relationship to a reference method. Each method is based upon a measurement principle. If the measurement principle involves a manual method, this method becomes the "reference method". Manual reference methods are specified for sulfur dioxide (40CFR50, App. A) and for total suspended particles (40CFR50, App. B). If the measurement principle can be realized by a continuous or automated analyzer, no "reference method" is specified. Thus, any continuous or automated analyzer using the specified measurement

principle and associated calibration procedure and meeting the performance specifications can be designated as a reference method. Measurement principles are specified for carbon monoxide (40CFR50, App. C), photochemical oxidants (40CFR50, App. D) and nitrogen dioxide (40CFR50, App. F). For a continuous or automated analyzer to be designated as a reference method, the requirements of 40CFR53, Subparts B and C must be met. Equivalent methods can be manual or continuous. If they are manual, they have to meet the requirements of 40CFR53, Subpart C only. If they are continuous, they have, of course, to meet both Subparts B and C. Summaries of the above discussion are given in Tables 4-3 and 4-4.

The important performance specifications for continuous or automated analyzers are reproduced from 40CFR53, Subpart B in Table 4-5 and the procedures for determining a consistent relationship between candidate methods and reference methods are reproduced from 40CFR53, Subpart C in Table 4-6. The complete text of 40CFR50 and 53 are given in the Appendix I and II.

4. 2. 2 Measurement Principles and Reference Methods for the Six Primary Pollutants

4. 2. 2. 1 Sulfur Dioxide

The measurement principle for the determination of SO_2 in the ambient atmosphere consists of a quantitative chemical analysis and is described in 40CFR50, App. A. Basically, air is drawn through a sample of potassium tetrachloromercurate (KHgCl_4) solution, whereupon any SO_2 in the air is absorbed. The solution is returned to the laboratory, and formaldehyde and pararosaniline are added, forming a pink color. The intensity of this color, as measured by a colorimeter, is proportional to the SO_2 concentration in the sampled air. Since this is a

TABLE 4-3. Summary of Reference and Equivalent Methods⁽²⁰⁸⁾.

Pollutant	Measurement principle or method	Reference method	Equivalent methods
TSP	High-volume sampler (manual method)	High-volume sampler	None possible
SO ₂	Pararosaniline (manual method)	Pararosaniline	Manual or continuous
CO	Nondispersive infrared	•	Manual or continuous
O ₃	Chemiluminescence	•	Manual or continuous
NO ₂	Chemiluminescence **	•	Manual or continuous

*None specified. Manufacturer must submit data documenting that the analyzer meets performance specifications.

TABLE 4-4. Applicability of 40CFR50 and 53.

	Reference Method	Equivalent Method
Manual	Those methods as given in the Appendices to Part 50, except App. C (for CO), App. D (for oxidants) and App. F (for NO ₂)	Any method that satisfies the requirements in Subpart C of Part 53.
Automatic	Those methods whose "measurement principles and calibration procedures" are specified in the Appendices of Part 50 (namely App. C, D and F).	Any method that satisfies the requirements in Subparts B and C of Part 53.

TABLE 4-5. Performance Specifications for Automated Methods.

Performance parameter	Units ¹	Sulfur dioxide	Photochemical oxidants	Carbon monoxide	Nitrogen dioxide	Definitions and test procedures
1. Range.....	Parts per million.	0-0.5	0-0.5	0-50	0-0.5	Sec. 53.23(a).
2. Noise.....	do.	.005	.005	.50	.005	Sec. 53.23(b).
3. Lower detectable limit.....	do.	.01	.01	1.0	.01	Sec. 53.23(c).
4. Interference equivalent.....	do.	±.02	±.02	±1.0	±0.2	Sec. 53.23(d).
Each interferent.....	do.	±.02	±.02	±1.0	±.04	
Total interferent.....	do.	±.02	±.02	±1.0	±.02	Sec. 53.23(e).
5. Zero drift, 12 and 24 hour.....	do.	±.02	±.02	±1.0	±.02	Do.
6. Span drift, 24 hour.....	do.	±20.0	±20.0	±10.0	±20.0	
25 percent of upper range limit.....	Percent	±5.0	±5.0	±2.5	±5.0	
50 percent of upper range limit.....	do.	±5.0	±5.0	±2.5	±5.0	
7. Lag time.....	Minutes	20	20	10	20	Do.
8. Rise time.....	do.	15	15	5	15	Do.
9. Fall time.....	do.	15	15	5	15	Do.
10. Precision.....	do.	Do.	Do.	Do.	Do.	Do.
25 percent of upper range limit.....	Parts per million.	.01	.01	.5	.02	
50 percent of upper range limit.....	do.	.015	.01	.5	.02	

TABLE 4-6. Test Concentration Ranges, Number of Measurements Required, and Maximum Discrepancy Specification.

Pollutant	Concentration range, parts per million	Simultaneous measurements required				Maximum discrepancy specification, parts per million
		1-hr		24-hr		
		First set	Second set	First set	Second set	
Oxidants.....	Low 0.05 to 0.10.....	5	6			0.02
	Med 0.15 to 0.25.....	5	6			.02
	High 0.35 to 0.45.....	4	6			.04
Total.....		14	18			
Carbon monoxide.....	Low 7 to 15.....	5	6			1.0
	Med 20 to 30.....	5	6			2.0
	High 35 to 45.....	4	6			2.0
Total.....		14	18			
Sulfur dioxide.....	Low 0.02 to 0.05.....			3	3	0.02
	Med 0.10 to 0.15.....			2	3	.02
	High 0.20 to 0.50.....	7	6	2	2	.04
Total.....		7	6	7	8	
Nitrogen dioxide.....	Low 0.02 to 0.05.....			3	3	0.02
	Med 0.10 to 0.20.....			2	3	.02
	High 0.25 to 0.35.....			3	3	.02
Total.....				7	9	

manual method, it becomes necessarily the reference method. Equivalent methods can consist of an automated method, involving the same chemical analysis, or any other method, such as the non-dispersive infrared method, as long as it fulfills the requirements described in the previous section.

4. 2. 2. 2 Total Suspended Particles

The measurement principle for the determination of the total suspended particles (TSP) in the ambient atmosphere consists of a high-volume sampling method and is described in 40CFR50 (App. B). Basically, air is drawn through a weighed glass-fiber filter for a known period of time. After being returned to the laboratory, the filter is conditioned at constant humidity and then reweighed. The difference in weights is the amount of particulate matter in the sampled air. This weight, divided by the known volume of air drawn through the filter, is the average particulate density and is normally expressed in micrograms per cubic meter of sampled air. Since this is a manual method, it becomes necessarily the reference method. Equivalent method for TSP is not possible since in this case the pollutant is defined as the material collected by the high-volume sampler during the sample-collection phase of the reference method.

4. 2. 2. 3 Carbon-Monoxide

The measurement principle for the determination of CO in the ambient atmosphere is based upon the non-dispersive infrared method and is described in 40CFR50 (App. C). Basically, air is passed continuously through a sample cell where some of the infrared radiation from a lamp is absorbed by the CO. The signal from this cell is

compared with that from a reference cell. The ratio of these two signals is a measure of the CO concentration in the sampled air. Any instrument that is based upon this measurement principle can become a reference method, as long as the instrument fulfills the requirements of 40CFR53 (Subpart B and C). Examples are described in Section 4.2.3. Any instrument that is not based on this measurement principle, but fulfills the requirements of 40CFR53 (Subpart C) can become an equivalent method.

4. 2. 2. 4 Photochemical Oxidants

The measurement principle for the determination of photochemical oxidants (O_3) in the ambient atmosphere is based upon a chemiluminescence method and is described in 40CFR50 (App. D). Basically, air is drawn continuously through a sample cell simultaneously with ethylene gas. Any ozone in the air reacts immediately with the ethylene, thereupon emitting light. The amount of light emitted and measured by a photomultiplier tube is proportional to the ozone concentration in the sampled air. Any instrument that is based upon this measurement principle can become a reference method as long as the instrument fulfills the requirements of 40CFR53 (Subpart B and C). Examples are described in Section 4.2.3. Any instrument that is not based on this measurement principle, but fulfills the requirements of 40CFR53 (Subpart C), can become an equivalent method.

4. 2. 2. 5 Hydrocarbons

The measurement principle for the determination of total hydrocarbon (THC) in the ambient atmosphere is based upon the flame ionization method and is described in 40CFR50 (App. E). Measured volumes

of air are delivered semi-continuously (4 to 12 times per hour) to a hydrogen flame ionization detector to measure its total hydrocarbon (THC) content. An aliquot of the same air sample is introduced into a stripper column which removes water, carbon dioxide, and hydrocarbons other than methane. Methane and carbon monoxide are passed quantitatively to a gas chromatographic column where they are separated. The methane is eluted first, and is passed unchanged through a catalytic reduction tube into the flame ionization detector. The carbon monoxide is eluted into the catalytic reduction tube where it is reduced to methane before passing through the flame ionization detector. Between analyses the stripper column is backflushed to prepare it for subsequent analyses. Hydrocarbon concentrations corrected for methane are determined by subtracting the methane value from the total hydrocarbon value. No procedures to establish reference or equivalent methods have yet been proposed for inclusion in 40CFR53.

4. 2. 2. 6 Nitrogen Dioxide

The measurement principle for the determination of NO_2 in the ambient atmosphere is based upon the chemiluminescent method and is described in 40CFR50 (App. F). Basically, this is a continuous method that draws in air over a heated catalytic converter to reduce any NO_2 to NO . The NO is reacted with ozone, generating light in proportion to the NO concentration. The original NO_2 concentration is obtained by subtracting the concurrent NO concentration measured by the same technique in a parallel air sample that has not passed over the converter. Any instrument that is based upon this measurement principle can become a reference method, as long as the instrument fulfills the requirements of 40CFR53 (Subpart B and C).

Examples are described in Section 4.2.3. Any instrument that is not based on this measurement principle, but fulfills the requirements of 40CFR53 (Subpart C), can become an equivalent method.

4.2.3 Designated Reference and Equivalent Methods

As of September 1977, several instruments have been designated as either reference or equivalent methods, after a test analyzer representative of each of the methods had been tested in accordance with the test procedure specified in 40CFR53.

- (1) SO₂ Ambient Monitor - Equivalent Method. It is an automated method which utilizes a measurement principle based on "second derivative spectroscopy" and is available from Lear Siegler Inc., Environmental Technology Division, Englewood, Colorado (Model No. SM1000). It operates in the 0.5 ppm range, at a wavelength of 229.5 nm, and with the "slow" (300 seconds) response time. (41FR3893, January 27, 1976; 41FR32946, August 6, 1976; 42FR13044, March 8, 1977).
- (2) Sulfur Dioxide Analyzer - Equivalent Method. It is an automated analyzer utilizing the "flame photometric detection" measurement principle and is available from Meloy Laboratories, Inc., Instrument and Systems Division, Springfield, Virginia (Model No. SA185-2A). It operates with a scale range of 0-0.5 ppm. (41FR3893, January 27, 1976).
- (3) Ozone Analyzer - Reference Method. It is an automated method which utilizes the chemiluminescent reaction with ethylene and is available from Bendix Corporation, Process Instruments Division, Lewisburg, West Virginia (Model No. 8002). It operates in the 0-0.5 ppm range with a time constant of 40 seconds. (41FR5144, February 4, 1976).

- (4) Infrared CO Analyzer - Reference Method. It is an automated method based on the NDIR principle and is available from Bendix Corporation, Process Instruments Division, Lewisburg, West Virginia (Model No. 8501). It operates in the 0-50 ppm range with a time constant from 5 to 16 seconds. (41FR7450, February 8, 1976).
- (5) Pulsed Fluorescent SO₂ Analyzer - Equivalent Method. It is an automated method based on the pulsed fluorescent detection of SO₂ and is available from Thermo Electron Corp., Environmental Instr. Division, Waltham, MA (Model No. 43). It operates in the 0-0.5 ppm range. (41FR8531, February 27, 1976; 42FR20490, April 20, 1977).
- (6) SO₂ Analyzer - Equivalent Method. It is an automated method based on the measurement principle of coulometric titration and is available from Philips Electronic Industries, Inc., Mount Vernon, N. Y. (Model Nos. PW9755 and 9700). They operate in the 0-0.5 ppm range (41FR26252, June 25, 1976; 41FR34105, August 12, 1976).
- (7) Ambient CO Monitoring System - Reference Method. It is an automated method based on the NDIR measurement principle and is available from Beckman Instruments, Inc., Process Instruments Division, Fullerton, CA (Model No. 866). It operates in the 0-50 ppm range with a 13 second time response (41FR36245, August 27, 1976).

- (8) Sulfur Monitor - Equivalent Method. It is an automated method based on flame photometry for the detection of SO_2 and is available from Monitor Labs, Inc., San Diego, CA (Model No. 8450). It operates in the 0-0.5 ppm range with a time response of 5 seconds. (41FR36245, August 27, 1976).
- (9) Ozone Meter - Reference Method. Three instruments that are automated methods based on the chemiluminescent reaction with ethylene and that are available from McMillan Electronics Corp., a subsidiary of Columbia Scientific Industries, Austin, Texas (Model Nos. 1100-1, -2, -3). They operate in the 0-0.5 ppm range (41FR46647, October 22, 1976).
- (10) Ozone-Analyzer - Reference Method. It is an automated method based on the chemiluminescent reaction with ethylene and is available from Monitor Labs, Inc., San Diego, CA (Model No. 8410E). It operates in the 0-0.5 ppm range with a time constant of 5 seconds. (41FR43684, December 8, 1976).
- (11) CO Analyzer - Reference Method. It is an automated method based on the NDIR, using a regenerative dryer, and is available from Mine Safety Appliances Corp., Pittsburgh, Penn. (LIRA Model 202S). It operates in the 0-50 ppm range with a "slow response amplifier". (42FR5748, January 31, 1977).
- (12) NO_2 Analyzer - Reference Method. It is an automated method using the gas phase chemiluminescence and is available from Monitor Labs, Inc., San Diego, CA (Model No. 8440R). It operates in the 0-0.5 ppm range with a time constant of 20 seconds. (42R37434, July 21, 1977).

- (13) NO_2 Analyzer - Reference Method. It is an automated method using the gas phase chemiluminescence and is available from Bendix Corporation, Process Instruments Division, Lewisburg, West Virginia (Model No. 8101-C). It operates in the 0-0.5 ppm range (42FR37435, July 21, 1977).
- (14) O_3 Analyzer - Equivalent Method. It is an automated Method using chemiluminescence of the Rhodamine B organic dye and is available from Philips Electronic Instruments, Mahwah, N. J. (Model No. PW9771). It operates in the 0-0.5 ppm range (42FR38931, August 1, 1977).
- (15) SO_2 Analyzer - Equivalent Method. It is an automated method, based on the increase in the electrolytic conductance of a chemical solution from absorption of SO_2 , and is available from ASARCO Inc., Salt Lake City, Utah (Model No. 500). It operates in the 0-0.5 ppm range (42FR44264, September 2, 1977).

4. 2. 4 Brief Description of Various Measurement Principles

A list of instruments that are based on the following measurement principles and are being marketed by the different instrument companies (without being designated yet as reference or equivalent method) is given in Appendix VI. In the following subsections, we give a brief description of the measurement principles involved.

4. 2. 4. 1 Colorimetric Method

In this method, the characteristic wavelength present in the products of chemical reactions is measured. The air sample is passed through a liquid absorbent containing an appropriate reagent. Then light is transmitted through the sample and compared with that through a reference path. Comparison is made by visual matching ⁽²⁹⁵⁾ or by spectrophotometric analysis. A typical schematic is shown in Figure 4. 2. 4-1, taken from Ref. 299. The method can be applied to many pollutants and is flexible and sensitive. The reference method for the manual determination of SO_2 , using KHgCl_4 as as absorber and formaldehyde and pararosaniline as reagent, is based on this principle. The disadvantages are the delay in the color development, stringent requirements in the reagent preparation, transport and storage and sensitivity to temperature, pH, reaction time, reagent purity and age, and atmospheric interference ⁽²⁹⁵⁾.

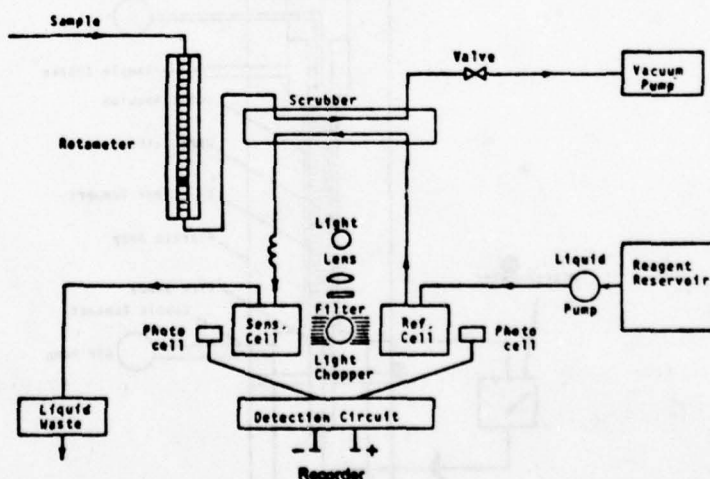


Figure 4. 2. 4-1. Schematic Diagram of a Typical Colorimetric Monitor

4. 2. 4. 2 Coulometric Method

An analyzer based on this method measures the generating current necessary to maintain a constant halide concentration in a solution into which an air sample has been absorbed. The magnitude of the current required is proportional to the amount of absorbed pollutant (SO_2 , NO_2 , oxidant). Although commonly called coulometric analyzers, they are actually "amperometric" devices, because it is the current and not the charge that is measured (296). A schematic diagram of a typical amperometric monitor is shown in Fig. 4. 2. 4-2, taken from Ref. 299. If, on the other hand the quantity of electrons is measured that are required to oxidize or reduce the pollutant quantity, the analyzer is truly based on the coulometric principle (Faraday's Law). A schematic diagram is shown in Fig. 4. 2. 4-3, taken from Ref. 299.

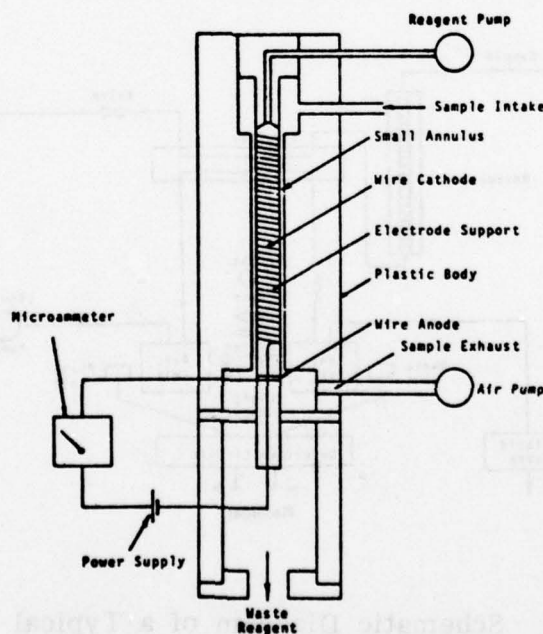


Figure 4. 2. 4-2. Schematic Diagram of a Typical Amperometric Monitor

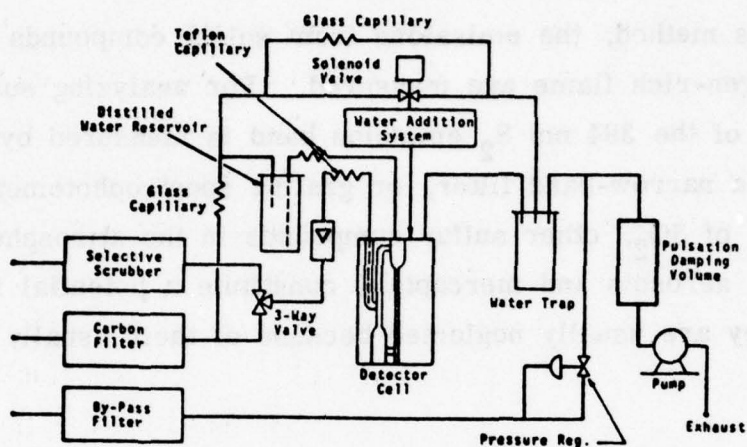


Figure 4. 2. 4-3. Schematic Diagram of a Typical Coulometric Monitor

4. 2. 4. 3 Flame Photometric Method

In this method, the emissions from sulfur compounds introduced into a hydrogen-rich flame are measured. For analyzing sulfur compounds, the intensity of the 394 nm S_2 emission band is measured by a photomultiplier, using a narrow-band filter, or grating spectrophotometer. For the measurement of SO_2 , other sulfur compounds in the atmosphere such as H_2S , H_2SO_4 , aerosols and mercaptans constitute a potential interference (296) However, they are usually neglected because of their usually small contribution.

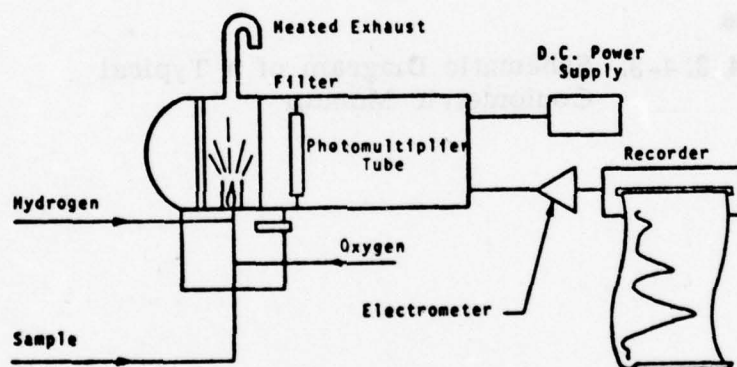


Figure 4. 2. 4-4. Schematic Diagram of a Typical Flame Photometric Sulfur Monitor

4. 2. 4. 4 Flame Ionization Method

This method is used in monitoring hydrocarbons. The sample is introduced into a combustion region created by the reaction of H_2 and O_2 , occurring between two electrodes. The ionization of the hydrocarbon fragments results in a current which is related to the concentration (296). To separate different hydrocarbons, a gas chromatograph is utilized (see Section 4. 2. 4. 5). Fig. 4. 2. 4-5 (Ref. 299) shows a schematic diagram of a flame ionization monitor.

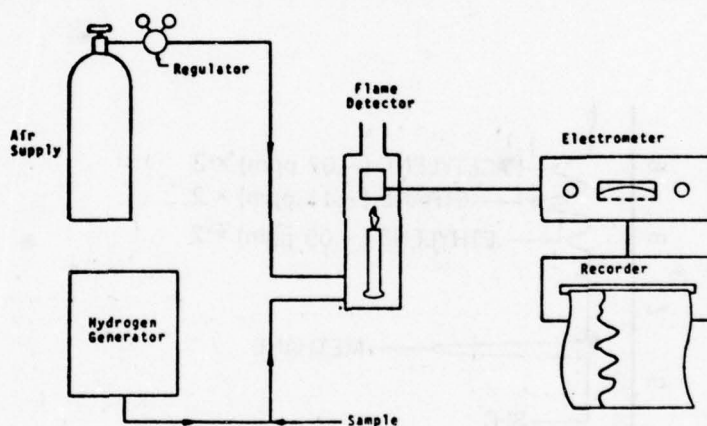


Figure 4. 2. 4-5. Schematic Diagram of a Typical Flame Ionization Monitor

4. 2. 4. 5 Gas Chromatographic Method

Gas Chromatographs utilize columns of granular materials, through which the air sample is passed. The different gas species are absorbed selectively by the material in the columns so that the sample constituents are separated and the stream is released as a series of components. Chromatographs are flexible and sensitive. Their main disadvantage is that they are complex and are used mostly in the laboratory. However, some automated on-site models are available ⁽²⁹⁵⁾. A typical GC trace, using a flame ionization detector for the emanating gas is shown in Fig. 4. 2. 4-6.

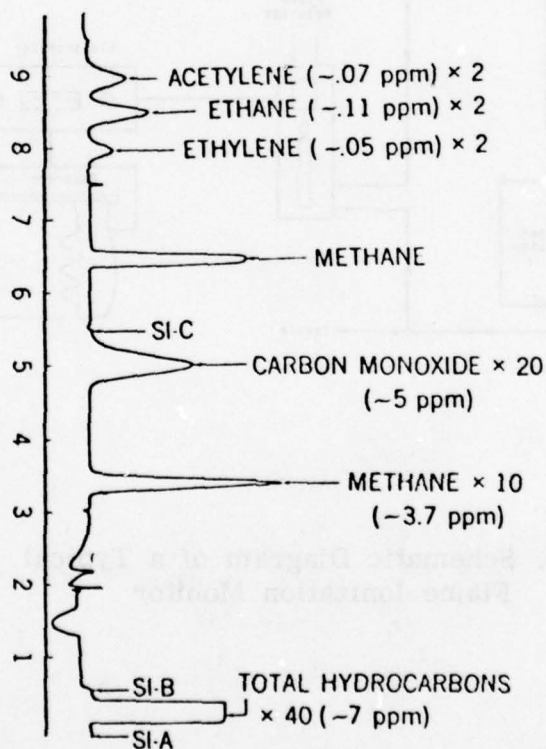


Figure 4. 2. 4-6. Typical GC Trace

4. 2. 4. 6 Non-Dispersive Infrared Method

This method can be used for monitoring CO, NO, CO₂ and hydrocarbons. It has been widely applied to the measurement of CO and is the EPA-designated measurement principle for the CO reference method. It is based on the differential absorption of infrared energy, using a double beam infrared source, a balanced optical system, and a low pressure Luft detector charged with the specific gas of interest (for example, carbon monoxide).

Two infrared sources are used, one for the sample energy beam, the other for reference energy beam. The beams are continuously and momentarily interrupted by a device called a "chopper." In the uninterrupted condition each beam simultaneously passes through the associated cell and into the detector. The sample cell is a metal tube which receives and exhausts a continuous stream of sample gas. The reference cell is a sealed tube filled with a reference gas. This gas is selected for negligible absorption of infrared energy of those wavelengths absorbed by the sample component of interest.

The detector consists of two sealed chambers separated by a flexible metal diaphragm. Each chamber has an infrared-transmitting window to permit entry of the corresponding beam. Both chambers are filled, to the same partial pressure, with vapor of the component of interest (for example, CO). The detector responds only to that portion of net difference in radiant energy due to the presence of the measured component (for example, CO).

A schematic of the NDIR is shown in Fig. 4. 2. 4-7 taken from Ref. 299. A recent development is the so-called "Gas Filter Correlation (GFC)" instrument, which was pursued by different research groups ⁽¹⁸⁾⁽¹⁹⁾⁽²⁰⁾. A schematic of an instrument utilizing a grating spectrophotometer, GFC and long sample cells for improved sensitivity and specificity is shown in Fig. 4. 2. 4-8.

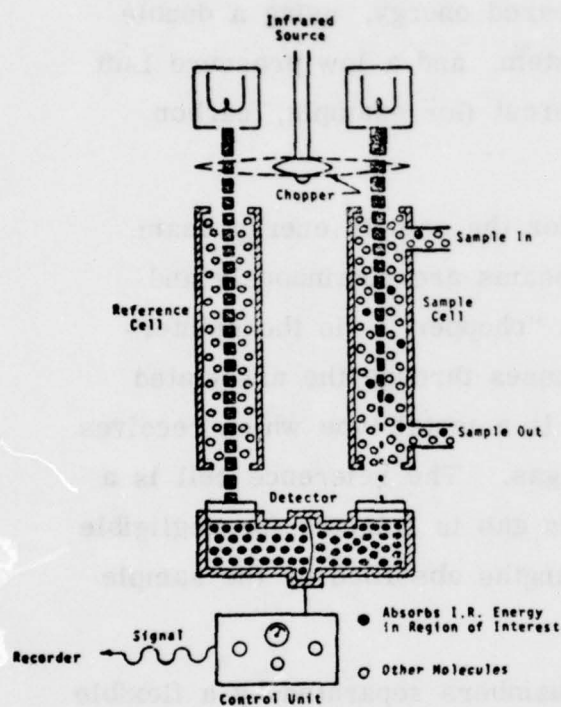


Figure 4.2.4-7. Schematic Diagram of a Typical Nondispersive Infrared CO Monitor

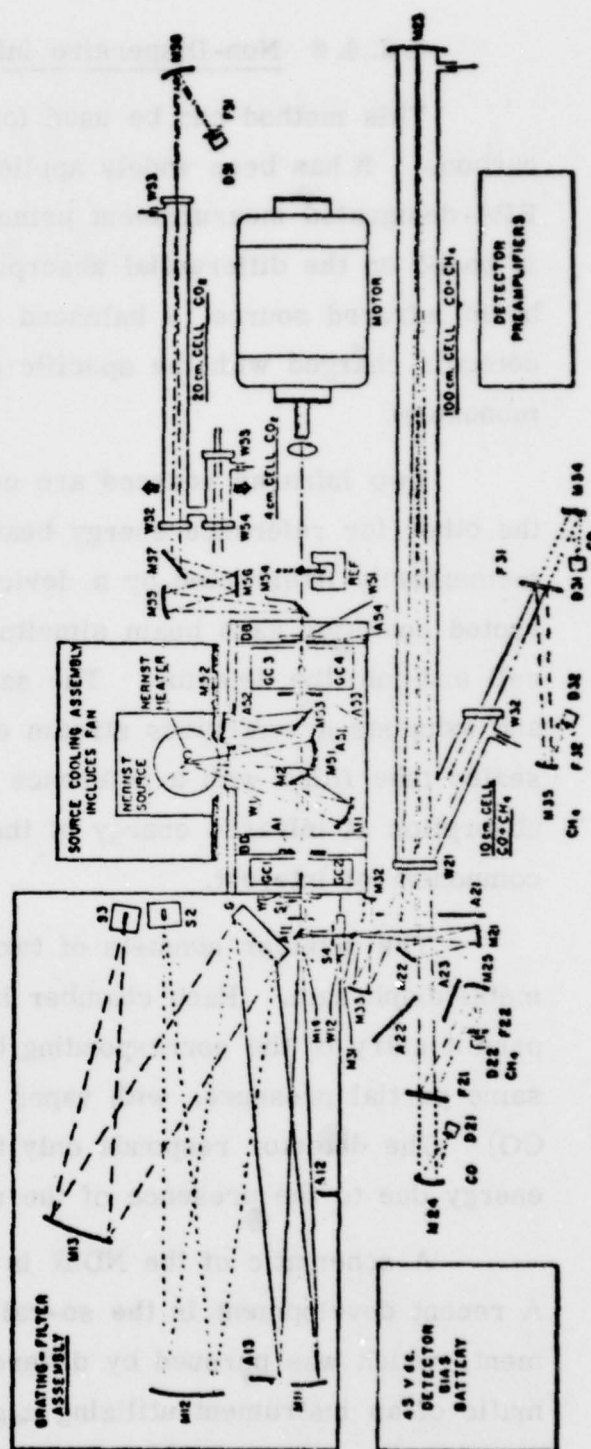


Figure 4.2.4-8. Schematic of a GFC Instrument (Ref. 19)

A different version of the non-dispersive infrared analyzer was introduced by Dimeff of the NASA Ames Research Center ⁽²⁹⁸⁾. A schematic of the device is shown in Fig. 4. 2. 4-9. Two windowed cells are used, one containing the unknown gas, the other containing a specific reference gas. The two cells are pressure modulated at separate frequencies f_1 and f_2 by mechanically driven bellows. Blackbody radiation traverses the two cells then falls on a detector. The detector signal component at the difference frequency ($f_1 - f_2$) is proportional to the concentration of the specific gas in the unknown.

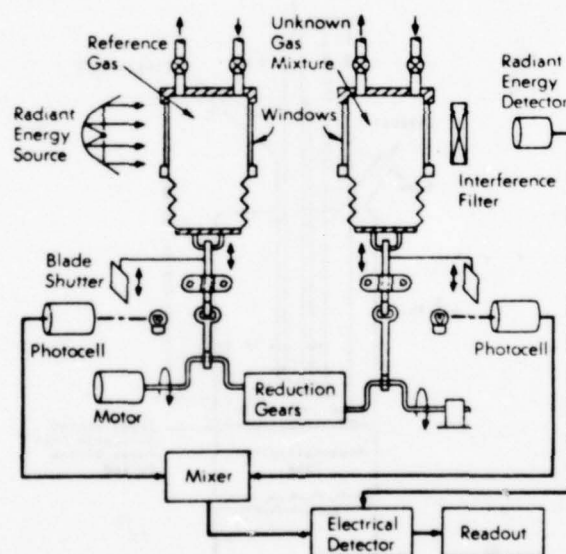


Figure 4. 2. 4-9. Schematic of Pressure Modulated Gas Correlation Monitor (Ref. 298)

4. 2. 4. 7 Chemiluminescent Method

In this method, the emission resulting from reactions between chemical compounds is measured by a photomultiplier tube. The air sample is introduced into a chamber together with the reactant gas. Of importance is the constancy of the air flow rate, adequate supply of the reactant gas and properly designed chambers ⁽²⁹⁵⁾. These analyzers are used for determining ozone, and oxides of nitrogen, and have been designated by EPA as reference methods. A schematic diagram is shown as Fig. 4. 2. 4-10 (from Ref. 299).

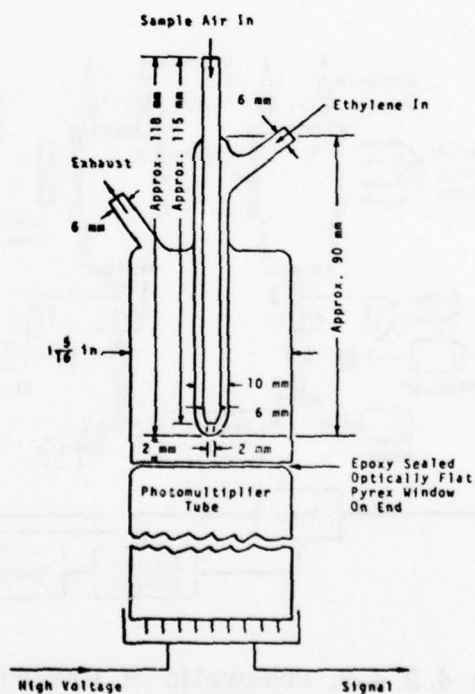


Figure 4. 2. 4-10. Schematic Diagram of a Typical Gas-Phase Chemiluminescent Ozone Detector

4. 2. 4. 8 Tunable Diode Laser Method

Using different combinations of lead salts, diode lasers can be fabricated that cover a wide range in the infrared⁽²⁴⁾. The nominal wavelength regions of three lead salt semiconductors, operating at 12°K, are shown in Figure 4. 2. 4-11, together with the spectral location of strongly absorbing pollutant bands of O₃, CO, NO, NO₂ and some hydrocarbons. A very recent development was discussed by Reid, et al.⁽²⁹⁴⁾

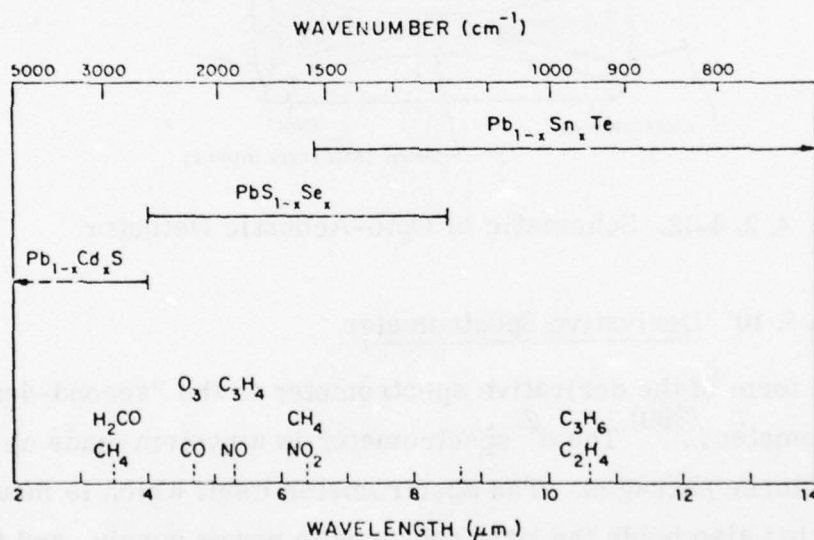


Figure 4. 2. 4-11. Range of Several Tunable Diode Lasers

The tunable narrow-band source is used in combination with an absorption cell and a broad-band receiver to accomplish special measurement of a point sample.

4. 2. 4. 9 Opto-Acoustic Method

In this method, radiation is passed through a cell containing the pollutant gas. The radiation at resonant wavelengths is transferred into translational energy of the gas, thus increasing the pressure which is detected by a microphone⁽²⁵⁾. The schematic of such a detector is shown in Figure 4. 2. 4-12.

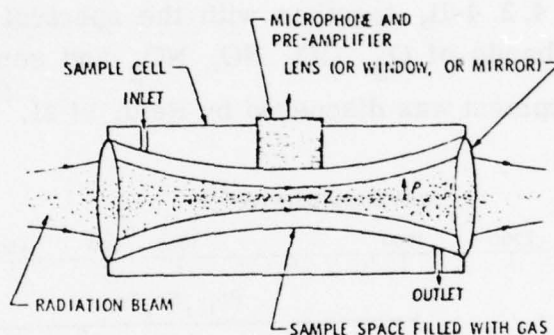


Figure 4. 2. 4-12. Schematic of Opto-Acoustic Detector

4. 2. 4. 10 Derivative Spectrometer

One form of the derivative spectrometer is the "second-derivative (d^2) Spectrometer"⁽²⁹⁰⁾. The d^2 spectrometer is a system made up essentially of three packages. The spectrometer itself which is mounted in a board that also holds the light source with power supply, and the absorption cell. This cell is placed between the fixed exit slit of the spectrometer and the photomultiplier tube. The wobbler carrying the oscillating slit is shown behind the light source; it replaces the fixed entrance slit of the monochromator. (See Figure 4. 2. 4-13.)

4. 2. 4. 10b

4. 2. 4. 12a

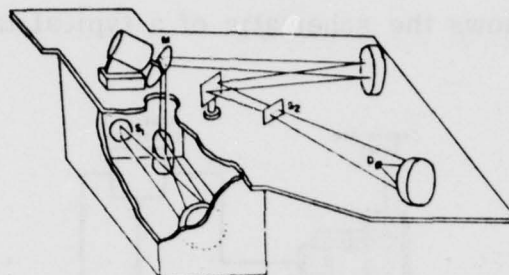


Figure 4. 2. 4-13. Optical Path for the Derivative Spectrometer. S_1 is monochromator exit slit plane, S_2 is exit slit, M is schizophrenic mirror, D is detector.

4. 2. 4. 11 Titration

A simple variation of colorimetry, titration uses standard chemicals for qualitative determinations of pollutants. Detection is based on absorption of the contaminant, followed by chemical reaction to produce a colored product. Titration requires only basic apparatus, and can be performed by relatively unskilled technicians.

4. 2. 4. 12 Particle Samplers

Using the principles of reflectance and transmittance, the tape sampler is used to measure suspended particulates in ambient air. Air is drawn through a section of white filter paper. The most generally accepted sampling parameters for this measurement are: a 1 inch diameter spot, 7.07 l. /min. (0.25 ft.³ /min.) flow rate and a two hour sampling period. At the end of the sampling period, the tape advances automatically by means of a timing mechanism, placing a clean section of filter tape at the sampling port. The collected spot is automatically positioned under a photoelectric reflectance or transmittance head which evaluates the density of the spot by measuring the light reflected from or transmitted through the spot to the cell (Ref. 17).

Figure 4. 2. 4-14 shows the schematic of a typical tape sampler.

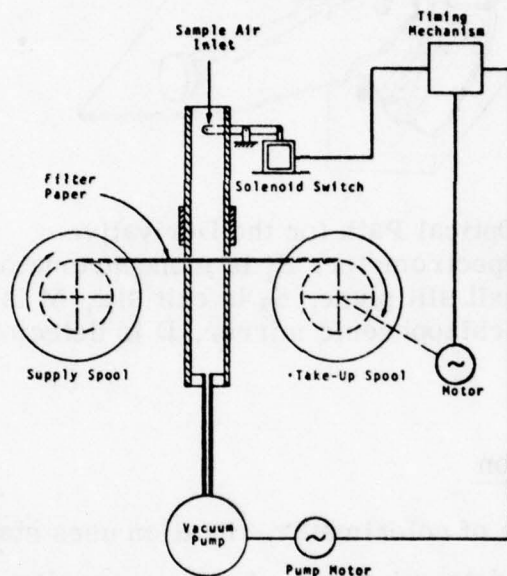


Figure 4. 2. 4-14. Schematic Diagram of a Typical Tape Sampler

Another measuring device for particles is the nephelometer which is based upon the principle that a common effect of particulate air pollution is the reduction of visibility. Small particles suspended in the air scatter light out of the line of vision, making distant objects appear less distinct. The air sample is drawn into the detection chamber where it is illuminated by a pulsed-flash lamp. The scattered light is measured over a range of scattering angles of 9° to 170° by means of a photomultiplier tube (see Figure 4. 2. 4-15). The signal produced by the photomultiplier tube is averaged and compared with a reference voltage from another phototube illuminated by the flash lamp (Ref. 17).

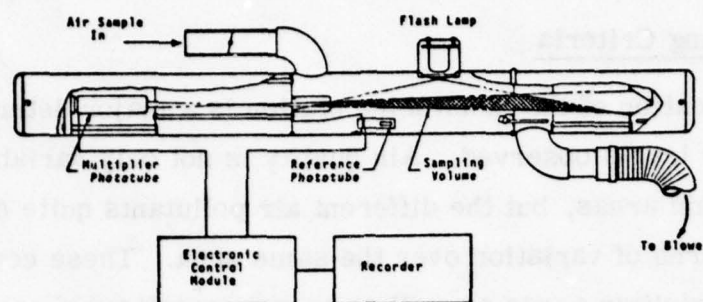


Figure 4. 2. 4-15. Schematic Diagram of a Typical Integrating Nephelometer

4. 2. 5 Calibration Standards

The Environmental Protection Agency requires that calibration standards used in reference methods of concern to air pollution measurements be traceable to certified Standard Reference Materials (SRM) available from the National Bureau of Standards. The Environmental Protection Agency and the National Bureau of Standards both desire that the mechanism establishing the traceability link between working calibration standards and the appropriate SRM be reliable (see Discussion in Appendix V). Protocols for traceability in air pollution measurements do not exist and the Environmental Protection Agency and the National Bureau of Standards have held a workshop (September 30-October 1, 1976) for the purpose of discussing the problems, advantages, disadvantages, and other features of traceability protocols. Of particular concern are the protocols to be used for establishing traceability of commercially available compressed gases used as working standards in air pollution measurements. No formal summary report was issued, but protocols of traceability are being worked on by EPA. (291)

4. 3 Sampling Criteria

The location of the monitoring station is a major determinant in the air quality levels observed. Air quality is not only variable within most geographic areas, but the different air pollutants quite often have different patterns of variation over the same area. These considerations apply to metropolitan areas as well as to more confined areas such as airports. Thus, we will discuss first the sampling criteria for metropolitan networks and second, those that should apply to airport environs.

4. 3. 1 Metropolitan Networks

According to the pollutant standards index (PSI, 41FR37660, September 7, 1976), the sites selected should generally meet two basic criteria:

(1) Sites should be representative of population exposure--that is, not unduly influenced by a single emission point or background-oriented, and

(2) sites should be located in areas of maximum concentration for the pollutant of interest, but should not be unduly influenced by any single source. Areas suitable for monitoring, by pollutant are:

TSP - populated areas substantially downwind of large sources or in the midst of numerous area sources.

SO₂ - populated areas substantially downwind of large sources or in the midst of numerous area sources.

CO - densely populated, high-traffic volume areas, including areas in the center city.

O₂ - populated areas substantially downwind of areas of maximum hydrocarbon emissions density, such as the central business district. The site should be 100 meters or more removed from major traffic arteries or parking lots.

NO₂ - populated areas downwind of areas of high traffic density.

If a pollutant(s) is (are) measured at several locations within a metropolitan area, it would be desirable (if possible) to base the air quality index on the site showing the highest reading on a given day. This would mean that different sites would be used on different days.

For large metropolitan areas comprised of many smaller cities and suburbs where significant air quality differences may exist, the air pollution control agency may wish to report separate index values for each community. This has the additional advantages of showing the public how air pollution varies over the larger metropolitan area. Furthermore, for example, the photochemical pollutants tend to be higher in the suburban fringe.

In addition to the pollutant-related data (source locations, physical source characteristics and emissions, atmospheric physiochemical transfer-motion processes, air quality measurements and trends) meteorological data are needed. The types of meteorological information that could be used for forecasting the PSI have been rather well defined through past experience with forecasting methods developed in support of air pollution control activities. This support has largely dealt with forecasting indices and episodic conditions. The meteorological features and parameters that are most often utilized in forecasting air quality indices at the present time are:

- Character and movement of air masses and fronts
- Areas of air mass subsidence
- Incidence, intensity, and height of inversions
- Mixing layer height
- Prevailing wind direction

Mean wind speed (surface and mixing layer)

Ventilation (mixing layer mean wind speed x mixing height)

Precipitation

Temperature

Total sky cover

4. 3. 2 Airport Environs

Based upon the regulations and guidelines discussed in the previous sections, an outline of sampling criteria for air enforcement monitoring in airport environs is given in the following.

- The analyzers employed must be reference or equivalent methods that have been designated as such by the EPA;
- The analyzers must be employed according to the manufacturers specifications, e. g. , no moving platforms if not specifically designed for it;
- The personnel using the analyzers must be qualified and trained in their operation;
- The site selection must be considered in terms of freedom from spurious emission, avoidance from point sources in the immediate sampling vicinity, wind direction, and non-interference with airport operations;
- For recording single events, the site selection must also be considered in terms of the frequency at which aircraft passed the monitoring sites⁽²⁹²⁾;
- Recording of meteorological data must be made to determine the interference by the pollutant sources in the vicinity of the airport environs.

5.0 DESCRIPTION OF REMOTE MONITORS

5.1 Introduction

This technology and its subsets, as applied to air pollution monitoring, are a recent development. Some of the methods, physical phenomena and techniques utilized are unfamiliar to many workers involved in air pollution monitoring. Thus, we define first some of the terms used in this technology.

5.1.1 Definitions of Terms Used in Remote Monitoring

Active System - Consists of two basic units: a transmitter and a receiver. The transmitter emits a beam of energy, which interacts with the atmosphere by scattering, absorption and/or stimulated emission, which is subsequently observed by the receiver.

Passive System - Consists of one basic unit: a receiver which observes the radiation from the atmosphere, either emitted by thermal radiation or scattered solar radiation.

Bistatic System - An active system, in which transmitter and receiver are separated by a distance, and are, in general, not on the same platform.

Description of System	Location	Active/Passive	Single Word Name
Receiver only	1	P	Passive
Receiver and transmitter at same location	1	A	Monostatic
Receiver one location transmitter elsewhere	2	A	Bistatic

Monostatic System - An active system, in which transmitter and receiver are located close to each other. In this system, the transmitted energy must be backscattered by either a natural reflector (wall, hillside), an artificial reflector (mirror, corner-cube reflector) or the atmosphere itself.

Line Integral - The integrated value of the parameter along a line-of-sight (LOS) through the atmosphere with no specified endpoint. Units are ppm-m.

Line Average - The average of the measured parameter along the LOS, having a known length. Units are ppm.

Line Profile - The distribution of the measured parameter along the LOS. Units are ppm.

Atmospheric Radiative Transfer - A process in which the amount of energy at the receiver is given by two contributions: (1) the transmitted source energy, reduced by absorption and scattering of the atmosphere and (2) self-emission and scattering of the atmosphere. For a non-pulsed system (active or passive), the relevant expression is

$$P_{\lambda} = (\eta_{\lambda} A_o \Omega_o) \int_x N_{\lambda}^o(T, x) d\tau_{\lambda}(x) \quad (5.1.1-1)$$

where η_{λ} is the efficiency of the instrument, A_o is the entrance area, Ω_o is the solid angle, $N_{\lambda}^o(T, x)$ is the blackbody radiance ($W/cm^2 sr-\mu m$) at the temperature $T(K)$, $\tau_{\lambda}(x)$ is the transmission, and x is the position along the line-of-sight. For a source at $x = 0$, Eq. (1) can be written as

$$P_{\lambda} = (\eta_{\lambda} A_o \Omega_o) [N_{\lambda}(T_s) \tau_{\lambda} + \int_{x=0}^{x_1} N_{\lambda}^o(T, x) d\tau_{\lambda}(x)] \quad (5.1.1-1a)$$

In the case of a pulsed laser system,

$$P(R) = \eta_o P_t L N(R) \beta A_o R^{-2} \tau_A(R) \tau_G(R) \text{ per pulse} \quad (5.1.1-2)$$

where $P(R)$ is instantaneous received energy from resolution element L at range R , P_t is transmitted energy (generally given in joules or photons) at t_0 , L is effective pulse length, ($L = c\Delta t/2$, where c is the velocity of light and Δt is pulse duration; it is the range interval from which signals are simultaneously received at time t), R is range, $R = c(t-t_0)/2$, where t_0 is the time of transmission of pulse, A_o is the effective receiver aperture, η_o is the optical efficiency of the system, $N(R)$ is the number density of the relevant pollutant, β is the backscattering cross-section appropriate to the scattering phenomenon under consideration, and $\tau_A(R)$ is the atmospheric attenuation by interferent along the laser path, and $\tau_G(R)$ is the pollutant attenuation, both at range R .

Atmospheric Transmission - The general expression for the transmissivity is given by $\tau_\lambda = \tau_a \tau_s$, where τ_a is the transmissivity of gases, and τ_s is the transmissivity of particles. Then,

$$\tau_a = \prod_i \tau_{ai}(\lambda) = \exp \left[- \int \sum_i \kappa_i(\lambda) C_i(x) p_t(x) dx \right] \quad (5.1.1-3)$$

where $\kappa_i(\lambda)$ is the spectral absorption coefficient, $C_i(x)$ is the concentration (mixing ratio) of species i at location x , and p_t is the total pressure, and

$$\tau_s = \exp \left[- \int \sum_i \sigma_i n_i(x) dx \right] \quad (5.1.1-4)$$

where σ_i is the sum of the absorption and scattering cross sections, $n_i(x)$ is the number density of species i at location x .

Absorption - A molecule absorbs energy by being raised to a higher energy state. Absorptivity and transmissivity of gases are related by $\alpha_a = 1 - \tau_a$. According to Kirchoff's law, the absorptivity is equal to the emissivity. For molecular absorption to take place, there must always be "resonance" between the frequency of the incoming energy and the quantum states of the molecule. Thus, the term "resonant absorption" is a tautology. The absorbed energy is isotropically re-emitted with a probability of emission described by the radiative lifetime.

A special phenomenon occurs at the short wavelengths (ultraviolet/visible region), where electronic transitions take place. Because of the high transition probabilities (much higher than in the infrared), more energy is absorbed in the UV than in the IR. As a consequence, more energy is also re-emitted in all directions, mostly over a wide spectral range, because of the many possible vibration-rotation transitions between electronic states. This re-emission is called "fluorescence". Since the fluorescence is not instantaneous, but occurs within the radiative lifetime, quenching (de-activation by collision) takes place which greatly reduces the intensity of the fluorescence. (A more detailed theoretical treatment of the absorption processes will be given in Section 5. 3. 1. 1).

Scattering - Scattering from spherical particles is described by the theory of Mie scattering, or in the limiting case of long wavelengths, Rayleigh scattering. Molecules also exhibit Rayleigh scattering as well as an inelastic (Raman) scattering. In inelastic scattering, a portion of the incoming energy is retained by the molecule so that the scattered energy is at a different frequency than the incoming energy. The shift in frequency

is determined by the molecular constants and, thus, very specific to the scatterer. The phenomenon was discovered by Raman. The intensity of the Raman scattering is several orders of magnitude smaller than the Rayleigh scattering. A much higher intensity can be achieved by "resonant Raman scattering", in which the incoming energy is close to the required resonant frequency of an electronic transition. However, it is found that this process is heavily interfered by the fluorescence process (see above). (A more detailed treatment of the scattering processes is given in Section 5.2.1.1.)

Differential Absorption Technique - A technique developed especially for near-monochromatic laser systems, in which two wavelengths are observed at the same time. One wavelength is near a pollutant absorption line, providing I_0 , the other is on the pollutant absorption line, providing I . (A detailed treatment of this powerful technique is given in 5.2.2.1.)

Heterodyne Technique - A method used with lasers, where the transmitted frequency is beat against the received frequency, resulting in information about the Doppler shift and, thus, about the velocity of the moving medium. The same term applies to the passive "Heterodyne radiometer", in which the radiation of a local oscillator (laser) is mixed with the incoming radiation, resulting in a beat frequency.

5.1.2 Active (pulsed) Systems

These are monostatic systems that can provide "line profile" data and are, thus, well suited to map out a volume. They are complex and expensive. The systems presently in the theoretical and experimental development and/or testing stage are:

- (i) Differential absorption by scattering (DAS) laser system, using multiple wavelengths;
- (ii) Raman scattering laser system;

- (iii) Resonance Raman/Fluorescence laser system;
- (iv) *Lidar system.

5. 1. 3 Active CW (non-pulsed) Systems

These are the systems that provide "line average" values. They are slightly less complex than the pulsed systems. These systems can be bistatic or monostatic, using a retroreflector. The spectral discrimination is obtained by using either a broadband transmitter (illuminator) and wavelength-dependent receiver or a wavelength-dependent transmitter (laser, narrow-line source) and a broadband receiver. Systems in the first category include blackbody sources with receivers such as

- (i) Dispersive monochromator;
- (ii) Fourier transform spectrometer;
- (iii) Gas Filter Correlator;
- (iv) Filterwheel receiver;
- (v) Optical correlation devices (matched filter).

Systems in the second category include mode-locked CW lasers with appropriate broadband detector systems.

5. 1. 4 Passive Systems

These systems can provide both "line averaged" data, when looking at a boundary, and "line integral" data, when looking along a LOS with no end point. They are the least complex, because they do not require a man-made source. However, since the receivers utilize the energy from

* Lidar - Light Detection and Ranging

natural sources, they must be more sensitive, in general, than those listed above in Section 5.1.3 under wavelength-dependent receivers. Up-looking systems operating in the UV/visible to measure SO_2 and NO_2 do exist, while systems operating in the infrared are under development. Their greatest utility appears to be in the perimeter monitoring mode.

5.1.5 Summary

The applicability of the different systems for the three different "line" data is shown in the following matrix:

System Data	Active Pulsed (monostatic)	Active CW		Passive
		monostatic	bi-static	
Line Integral				●
Line Average	● (a)	●	●	○ (b)
Line Profile	●	○ (c)	○ (c)	○ (d)

(a) derived from averaging line profile data.

(b) definitive if end point is a solid surface; less definitive if "end point" is the mixing layer.

(c) taking many spectral data, line profile data may be obtained by inversion techniques (limited to a few points).

(d) same as in (c) with the additional possibility of taking spatial data and inverting those.

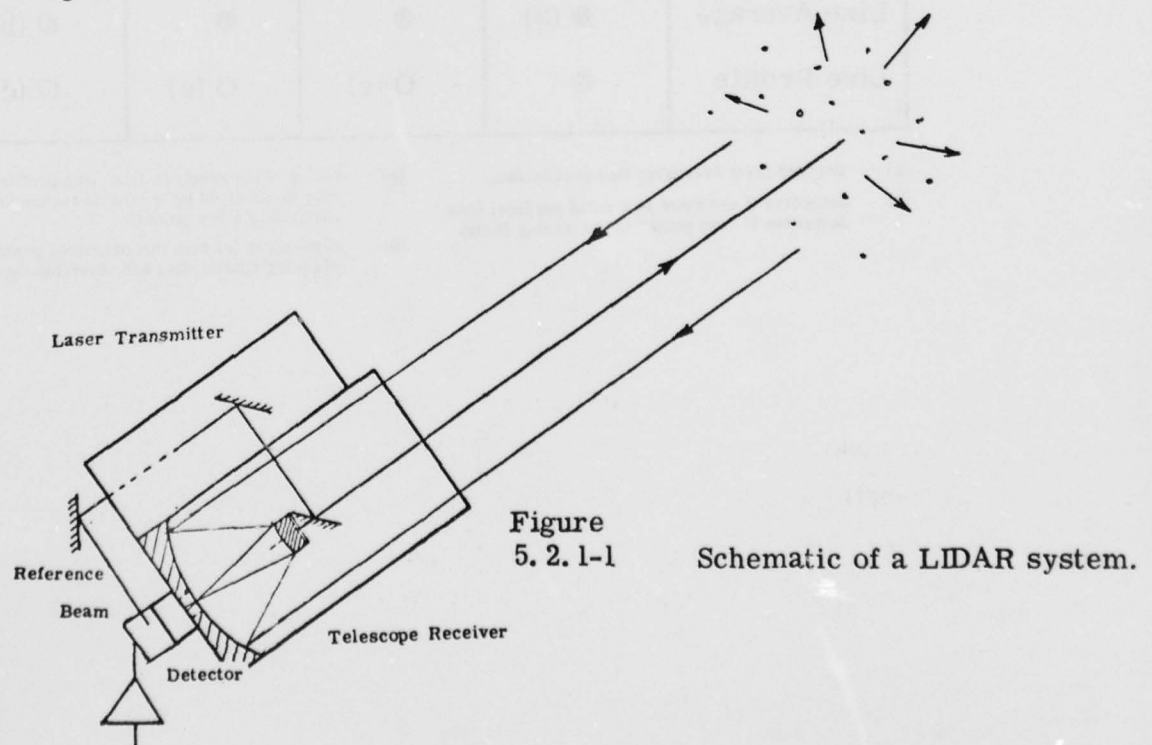
5. 2 DESCRIPTION OF ACTIVE PULSED SYSTEMS (Subsets Within Remote Sensing Technology)

There are six items included in the description of subsets, namely principle of operation, state-of-the-art, advantages/disadvantages, system and operational requirements, and analysis and critique.

5. 2. 1 Active (Pulsed) System: LIDAR

5. 2. 1. 1 Principle of Operation

LIDAR is a monostatic system (in a few cases it has also been used in a bistatic mode), using a laser at fixed wavelength. It measures the Mie backscattering from particulate matter in the atmosphere. By gating the detection system, different arrival times can be observed, thus obtaining spatially resolved signals. This is analogous to a RADAR system. Instead of using Radiowaves, a LIDAR is using Lightwaves. Thus, LIDAR stands for "Lightwave Detection And Ranging". The "reference beam" used for measuring the time interval can be taken from the other end of the laser.



Since the laser is emitting energy in a narrow spectral band, optical filters at the detector can be used to reduce noise from extraneous sources.

The LIDAR equation for the received power $P(R)$ from Mie scatterers at distance R is given by

$$P(R) = \eta_o P_t L N(R) \beta A_o R^{-2} \tau_A(R) \text{ per pulse} \quad (5.2.1-1)$$

where $P(R)$ is received power from resolution element L at range R , P_t is transmitted power (but generally given in total pulse energy, $U_t = P_t \Delta t$, joules or photons) at t_0 , L is effective pulse length, ($L = c\Delta t/2$, where c is the velocity of light and Δt is pulse duration; it is the range interval from which signals are simultaneously received at time t), R is range, $R = c(t-t_0)/2$, where t_0 is the time of transmission of pulse, A_o is the effective receiver aperture, η_o is the optical efficiency of the system, $N(R)$ is the number density of the relevant pollutant, β is the backscattering cross-section appropriate to the scattering phenomenon under consideration, and $\tau_A(R)$ is the atmospheric attenuation along the laser path, given by

$$\tau_A(R) = \exp\left[-2 \int_0^R \sigma(r) dr\right] \quad (5.2.1-2)$$

where σ is the volume extinction coefficient composed of a scattering and an absorption component. Both β and σ are dependent upon the wavelength λ , the number, size, shape and refractive properties of the particles. When the scatterers are small compared with the wavelength (molecules and the smaller particles), Rayleigh scattering applies and

the relationship between β and σ is given by⁽¹⁰⁾

$$\beta N(R) = \frac{1.5}{4\pi} \sigma \quad (5. 2. 1-3)$$

However, when the scattering particles are comparable with the wavelength, Mie scattering applies and the relationship of Eq. 5. 2. 1-3 does not hold. Calculations based upon the Mie theory have been made extensively and Collis and Uthe⁽³⁴⁾ show results for the backscattering efficiency (i. e., the ratio of the computed backscatter cross section to the geometrical cross section).

The results of these calculations are limited to idealized size distributions, assumed complex index of refractions and idealized particle shapes (mostly spherical). For realistic situations, the solution appears to be very difficult. However, it is found that the volume backscattering and volume extinction coefficients are actually less critically dependent upon particle size distribution than the exact theory shows⁽³⁴⁾. Nevertheless, some uncertainty between β and σ remains. These uncertainties may be overcome by making comparative observations. For atmospheric conditions, the ratio $\beta N(R) / \sigma$ can be assumed to remain constant and σ may be determined by LIDAR measurements using a calibrated target. It is then possible to solve for $\beta N(R)$. However, in order to be meaningful in terms of particulate pollution, it must be related to a mass concentration.

Measures and Pilon^(34a) give

$$\beta N(R) = 0.04 \sigma \quad (5. 2. 1-4)$$

as a typical relationship for Mie scattering. Representative values for β and $N(R)$ are given in the following:

	<u>Rayleigh</u>	<u>Mie</u>
$\beta(\text{cm}^2 \text{sr}^{-1})$	10^{-27}	10^{-8}
$N(R) (\text{cm}^{-3})$	10^{19}	10^2
$\beta N(R) (\text{cm}^{-1} \text{sr}^{-1})$	10^{-8}	10^{-6}

As will be shown in 5.2.1.5, the determination of the mass density $\rho(\mu\text{g}/\text{m}^3)$ by optical methods depends on many parameters. Much research needs to be done before they are all adequately known. Nevertheless, it is possible to derive approximate relationships that can serve as the basis for future work. In this subsection we derive approximate relationships between $\rho(\mu\text{g}/\text{m}^3)$ and Mie scattering coefficient $\beta_M(\text{km}^{-1})$ as a function of wavelength in the visible (4000-7000Å) spectrum.

Koschmieder⁽²⁵⁹⁾ theory states that at 5500 Å, using his nomenclature defined below,

$$V_\eta = 3.91/\beta_{\text{ext}}$$

where

$$\beta_{\text{ext}} = \beta_R + \beta_M$$

V_η is the meteorological range (km), β_{ext} is the total extinction coefficient (km^{-1}) and β_R and β_M are the Rayleigh and Mie scattering coefficients. The meteorological range $V_\eta(\text{km})$ and mass density has been related by Fett⁽²⁶¹⁾ at $\lambda = 5500 \text{ Å}$ through

$$\rho = 4.6 \times 10^2 \beta_{\text{ext}} \text{ at } \lambda = 5500 \text{ Å}$$

Based on the work of Curcio et al. ⁽²⁶²⁾ Elterman ⁽²⁶³⁾ has shown that a family of distributions for $\beta_M(V_\eta, \lambda)$ can be computed if the $\beta_M(V_4, \lambda)$ values are used so that

$$\beta_M(V_\eta, \lambda) = \frac{(3.91/V_\eta) - \beta_R(\lambda = 5500)}{(3.91/V_4) - \beta_R(\lambda = 5500)} \beta_M(V_4, \lambda)$$

Introducing the relationship between ρ and V_η one obtains

$$\beta_M(\rho, \lambda) = \frac{2.17 \times 10^{-3} \rho - 0.012}{.965} \beta_M(V_4, \lambda)$$

Representative values of V_η , ρ , β_R , β_M and β_{ext} are given in Table 5. 2. 1-1 for $\lambda = 5500 \text{ \AA}$. The values for $\beta_M(V_4, \lambda)$ are taken from Curcio et al. ⁽²⁶²⁾. These values can be fitted to a very good approximation by

$$\beta_M(V_4, \lambda) = [5337.5/\lambda(\text{\AA})] - 0.028$$

Thus, the equation for $\beta_M(\rho, \lambda)$ becomes

$$\beta_M(\rho, \lambda) = \left[\frac{12.0}{\lambda(\text{\AA})} - 6.3 \times 10^{-5} \right] \rho - \frac{64.0}{\lambda(\text{\AA})} + 3.36 \times 10^{-4}$$

As a consistency check, the calculated values of $\beta_M(\rho, \lambda)$ for a meteorological range of 4 km are compared with those of Curcio et al. in Table 5. 2. 1-2.

TABLE 5. 2. 1-1 Surface Meteorological Ranges and Corresponding Parameters (Refs. 263, 263a) at $\lambda = 5500 \text{ \AA}$ (Nomenclature per Ref. 259)

$V_{\eta}(\text{km})$	$\rho(\mu\text{g}/\text{m}^3)$	$\beta_R(\text{km}^{-1})$	$\beta_M(\text{km}^{-1})$	$\beta_{\text{ext}}(\text{km}^{-1})$
2	900	0. 012	1. 943	1. 955
4	450	0. 012	0. 966	. 978
6	300	0. 012	0. 640	. 652
8	225	0. 012	0. 476	. 488
10	180	0. 012	0. 379	. 391
13	138	0. 012	0. 289	. 301
23	78	0. 012	0. 158	. 170
50	36	0. 012	0. 066	. 078
100	18	0. 012	0. 027	. 039

TABLE 5. 2. 1-2 Comparison of Calculated and Measured Values of $\beta_M(\rho, \lambda)$ at V_4

$\lambda(\text{\AA})$	4000	4500	5000	5500	6000	6500	7000
β_M (Curcio)	1. 30	1. 15	1. 05	. 966	. 860	. 780	. 730
β_M (Calculated)	1. 31	1. 16	1. 04	. 942	. 861	. 793	. 734

Having completed the consistency check, we have calculated $\beta_M(\text{km}^{-1})$ as a function of λ and ρ . The results are given in Table 5. 2. 1-3. Since the Rayleigh attenuation coefficients are needed later, they are listed in Table 5. 2. 1-4.

TABLE 5. 2. 1-3. Calculated Surface Aerosol Attenuation Coefficients $\beta_M(\text{km}^{-1})$ as a Function of Mass Density ($\mu\text{g}/\text{m}^3$) and Wavelength (\AA)

$\lambda(\text{\AA})$	$\rho = 10$	30	100	300	1000($\mu\text{g}/\text{m}^3$)
4000	1.37^{-2}	7.24^{-2}	2.78^{-1}	8.65^{-1}	2.92
4500	1.22^{-2}	6.42^{-2}	2.46^{-1}	7.67^{-1}	2.59
5000	1.09^{-2}	5.76^{-2}	2.21^{-1}	6.89^{-1}	2.32
5500	9.89^{-3}	5.23^{-2}	2.01^{-1}	6.24^{-1}	2.11
6000	9.04^{-3}	4.78^{-2}	1.83^{-1}	5.71^{-1}	1.93
6500	8.32^{-3}	4.40^{-2}	1.69^{-1}	5.25^{-1}	1.77
7000	7.71^{-3}	4.07^{-2}	1.56^{-1}	4.87^{-1}	1.64

TABLE 5. 2. 1-4. Rayleigh Scattering Coefficient $\beta_R(\text{km}^{-1})$ (Ref. 263a)

$\lambda(\text{\AA})$	$\beta_R(\text{km}^{-1})$
4000	0.043
4500	0.026
5000	0.017
5500	0.012
6000	0.008
6500	0.006
7000	0.004

5. 2. 1. 2 State-of-the-Art

In describing the present state-of-the-art of lidar systems, we distinguish between measurements of smoke plumes and hazy atmospheres (turbidity). The method of measuring smoke plumes may be applied to measuring the particulate emission of aircraft engines.

Cook et al.⁽³⁵⁾ report a method in which the plume transmittance is measured by comparing the clear air lidar return from the near side of the plume with that from the far side. They made field measurements on a power plant smoke plume with a van-mounted ruby laser system at a range of 487 m. A comparison was made with the passive telephotometer⁽³⁶⁾ which makes a contrast measurement and relies on having a target with contrast (e. g., sky and hillside) behind the plume. The passive technique is somewhat sensitive to the illumination conditions (e. g., sun position, cloud cover). The lidar accuracy is limited by the PM^{*} tube afterpulsing, but within the error limits both methods agreed. The lidar system errors are estimated to be $< 12\%$ for an opacity of < 0.5 , and $< 2.5\%$ for opacity < 0.2 .

This system has been recently improved by replacing the PM tube and hence eliminating the afterpulsing. Conner⁽³⁷⁾ considers that in good atmospheric conditions the method can now measure the opacity within 2%. Good atmospheric conditions mean that the atmospheric aerosol content is the same on both sides of the plume. Under poor atmospheric conditions, readings are variable and must be averaged over a period of time.

* PM - Photomultiplier

The technique of Cook et al. is basically the same as that of Nakahara et al.⁽³⁸⁾ who used the Raman signal from N_2 in front and through the plume. Nakahara et al. considers their method to be more accurate since the N_2 concentration and Raman backscatter are better known than the atmospheric particle concentration and backscatter. This latter technique appears advantageous since the signal is readily obtained from a Raman system for gases, so that a separate system for particle observations is not required. However, due to the low Raman signals, the range capability would be less, and sky background noise would be more significant.

It should be noted that optical techniques,* as presently known, cannot separate the scattering by particles and by water droplets. The remote sensor will have to examine the plume some distance from the stack exit where visual observation indicates that the droplets have evaporated.

Measurements of atmospheric turbidity by lidar were reported as early as 1969⁽³⁹⁾, as a result of the Barbados Oceanographic and Meteorological Experiment (BOMEX). Lidar return signals indicated the turbidity in the atmosphere (see Fig. 5.2.1-2). This figure shows a computer generated representation of ranges normalized signal returns in logarithmic form that are corrected for instrumentation transfer anomalies and any pulse-to-pulse lidar performance variation. The indicated layer at 1.8 km was interpreted as the stream of dust carried by the north-east trade winds to the Caribbean area from the Sahara Desert. The data were taken from an aircraft flying at 3 km (10,000 ft) altitude with the lidar at a fixed downward angle of -60° elevation. The data reduction procedure appeared to be quite complex, as indicated by the description given by Collis⁽⁴⁰⁾:

"The raw data consisted of Polaroid records of the A-scope traces of signal intensity vs. range, each terminating in a return from

* Optical techniques refer to techniques in the UV, Visible and IR.

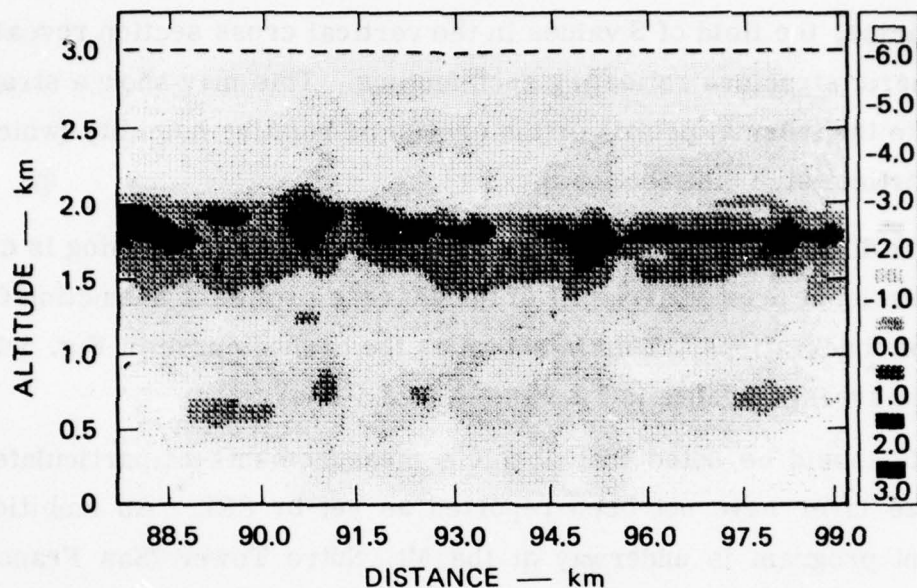


Figure 5. 2. 1-2 Digital Presentation of Lidar Observed Aerosol Structure⁽¹⁰⁾.

the sea surface or a cloud. These data were converted to digital records on computer cards using graphical/manual techniques. Thereafter processing was carried out by computer. Initially this consists of deriving a field of S values in the form of a vertical cross section. S values represent range-normalized signal returns in logarithmic form that are corrected for instrumentation transfer function anomalies and any pulse-to-pulse lidar performance variations. They thus evaluate, in relative terms, the atmospheric dependent parameters of the lidar equation: $\beta \exp(-2 \int \sigma dr)$. Where σ is small, as in the clear air of the Caribbean area, attenuation may be ignored and the S function essentially represents the backscattering properties of the atmosphere, i.e., $S \propto 10 \log_{10} \beta$. Since the backscattering coefficient, β , varies with particle number density, size distribution, and the refractive properties of

the particles, the field of S values in the vertical cross section reveals an atmospheric structure reflecting such factors. This may show a stratification related to the thermal profile or the profile of relative humidity (which may affect particle size distributions).

To display such information, further computer processing is carried out to develop a least squares fit of the average profile of S-function from each series of observations. This is shown as the dashed curve in Fig. 5. 2. 1-3 which the average profile is also shown (solid line).

It should be noted that absolute measurements of particulate pollution in a haze layer have not been reported as yet by SRI. * An ambitious measurement program is underway at the Mt. Sutro Tower (San Francisco)⁽⁴²⁾, in which the effects of aerosol pollution on atmospheric radiation and temperature are to be continuously monitored. Figure 5. 2. 1-4 gives a good overview of that program.

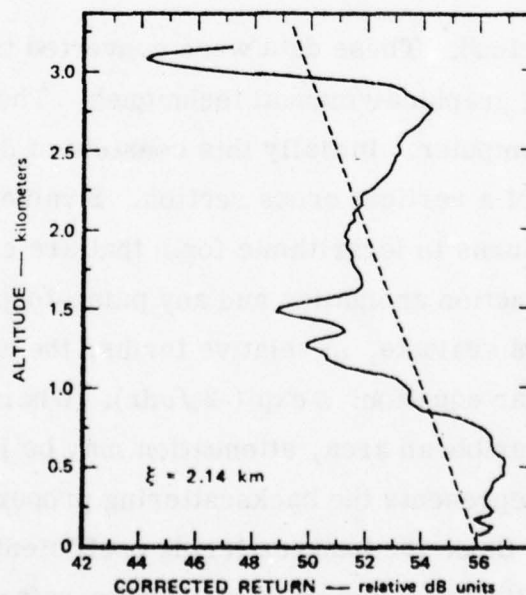


Figure 5. 2. 1-3 Average Vertical Profile of Corrected Lidar Return (S-function) (solid) and Least-Squares Fit (dashed).

* SRI - Stanford Research Institute

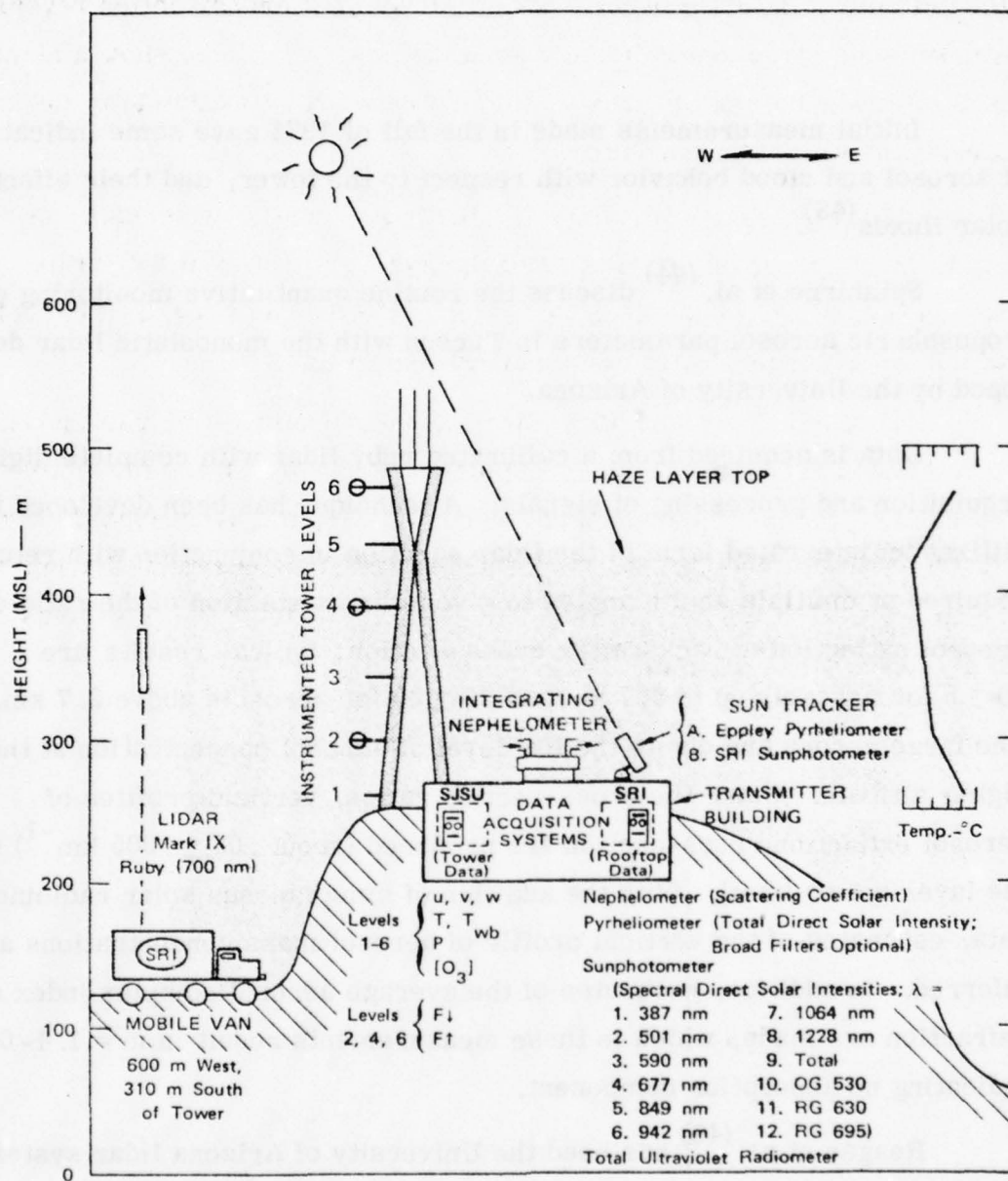


Figure
5. 2. 1-4

Schematic of the SRI Aerosol and
Radiation Study at the Mt. Sutro Tower

Initial measurements made in the fall of 1974 gave some indication of aerosol and cloud behavior with respect to the tower, and their effects on solar fluxes⁽⁴³⁾.

Spinhirne et al.⁽⁴⁴⁾ discuss the routine quantitative monitoring of tropospheric aerosol parameters in Tucson with the monostatic lidar developed by the University of Arizona.

Data is acquired from a calibrated ruby lidar with complete digital acquisition and processing of signals. A technique has been developed that utilizes an integrated form of the lidar equation in conjunction with returns acquired at multiple zenith angles to give a direct solution of the ratio of aerosol extinction to backscatter cross-section; typical results are 30 ± 5 for aerosols up to 2.7 km and 20 ± 20 for aerosols above 2.7 km. The large errors are due to the low level of aerosol concentration at the higher altitude. Using the cross-section ratios, vertical profiles of aerosol extinction cross-section are produced (about $.02 \pm .005 \text{ km}^{-1}$) for the layer below 3 km). With the addition of simultaneous solar radiometer data, estimates of the vertical profile of aerosol mass concentrations are inferred. In addition, estimates of the average aerosol complex index of refraction are made, which in these measurements result in $m = 1.4 - 0i$, indicating no absorption component.

Reagan et al.⁽⁴⁵⁾ has used the University of Arizona lidar system in a bistatic mode to permit angular scattering measurements.

Observations show that the aerosol number density fluctuates both temporally and spatially, creating uncertainties in the data reduction. Several sets of bistatic measurements were analyzed to obtain angular scattering curves of the parallel and perpendicular Stokes components,

and combinations thereof, due to aerosol scattering for scattering angles ranging from approximately 100 to 160°. These angular scattering measurements can be related to theoretical Mie scattering calculations to obtain information about the size distribution and imaginary component of refractive index of the aerosol scatterers. Typical results indicate that $m = 1.40 - 0.01i$, the real part of which agrees with the monostatic measurements by Spinhirne et al.⁽⁴⁴⁾, but shows a non-zero imaginary part.

Reagan et al.⁽⁴⁶⁾ also compared these lidar measurements with in-situ aircraft measurements. Both the bistatic lidar and solar radiometer measurements revealed that the particulate size distributions were non-Junge, as was also revealed by the aircraft measurements. Vertical profiles of particulate backscatter and extinction extracted from the slant path lidar returns displayed relative variations with height that were in excellent agreement with the aircraft Optical Particle Counter and Integrating Nephelometer measurements. Absolute values of the particulate mass loading versus height inferred from the slant path lidar returns agreed with the aircraft Particle Mass Monitor measurements to within the estimated measurement errors. For example, the lidar data indicated values of mass/unit volume ranging from 8.8 to 18.2 $\mu\text{g}/\text{m}^3$, while the in-situ values ranged from 17.2-21 $\mu\text{g}/\text{m}^3$.

Patterson et al.⁽⁴⁷⁾ described the use of lidar for the measurements of the time variation in height of the mixed layer during a rural boundary layer experiment. Aerosols were also collected a few meters above the ground and above the field site by an impactor located on the NCAR Electra aircraft to characterize as completely as possible the size and spatial distribution and the optical properties of the aerosols within the mixed layer under conditions that are regarded to be representative of rural areas.

It was found that the radii of the typical urban derived aerosols (mostly spheres) ranged from $.01$ to $1\text{ }\mu\text{m}$, and that soil dust particles (irregular shapes) had effective radii from 1 - $10\text{ }\mu\text{m}$.

New developments of improved lidar systems include multiwavelength application and polarization. The multiwavelength lidar can be used to separate the aerosol from molecular scattering. A feasibility study was conducted by DeLuise et al.⁽⁴⁸⁾, who concluded that the measurements must be made at more than one wavelength at fairly wide separation and that the solutions are sensitive to error noise and relative signal strength of both components and also depend on the required spatial and temporal resolutions.

Shipley and Weinman⁽⁴⁹⁾ discuss a possible experimental approach, the schematic of which is shown in Figure 5. 2. 1-5. The detection system can achieve high contrast by means of a three Fabry-Perot etalon train (FP1, FP2, FP3) which suppresses background radiation ($\delta\sigma_{123}$) outside of its passband of full width at half maximum at the wavenumber of maximum receiver transmission (σ_r). The etalon FP4 is used to achieve very high resolution with $\delta\sigma_4$ at σ_r . When $\sigma_r = \sigma_0$, where σ_0

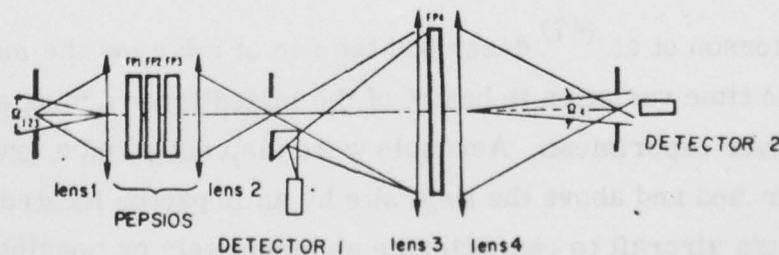


Figure
5. 2. 1-5

A Schematic Representation of an HSRL
Receiver System Incorporating a PEPSIOS
High Resolution Spectrometer.

is the laser output wavenumber maximum, most of those photons scattered by aerosols reach detector #2, and a large fraction of those photons scattered by molecules (Doppler shifted) reach detector #1. These signals can be used to obtain the molecular and aerosol components through the inversion of a set of linear equations. Characteristic parameter values are given in Table 5. 2. 1-5. The proposed instrument is theoretically feasible for aircraft deployment using present technology.

TABLE 5. 2. 1-5 System Parameters for a Model Instrument

Wavelength	4880 Å
PEPSIOS FWHM	$\delta\sigma_{123} = \delta\sigma_D (\text{at } 250^\circ\text{K}) = .086 \text{ cm}^{-1}$ ($\delta\lambda \sim 20 \text{ mÅ}$)
	$\delta\sigma_4 = 1/5 \delta\sigma_D = .017 \text{ cm}^{-1}$ ($\delta\lambda \sim 4 \text{ mÅ}$)
Laser Output FWHM	$\delta\sigma_o = 1/10 \delta\sigma_D = .009 \text{ cm}^{-1}$ ($\delta\lambda \sim 2 \text{ mÅ}$)
	$\delta\sigma_D$ is the Doppler FWHM

Polarization studies using linearly polarized transmitted signals are discussed by McNeil and Carswell⁽⁵⁰⁾. They found that in hazy atmospheres (visibility 3-5 km, humidity 80%), depolarization takes place. It is stated that for dust particles in the atmosphere, a greater depolarization should be expected because of their irregular shapes (in contrast to the spherical liquid condensation droplets). Thus, the authors surmise that a differentiation between these species should be possible.

Several papers were recently presented in which the depolarization was briefly discussed⁽⁵¹⁻⁵³⁾. A compilation of measured linear depolarization ratios (the ratio of returned energies in the planes of polarization

perpendicular and parallel to that of the source) are given in Figure 5. 2. 1-6, as obtained by Sassen⁽⁵³⁾.

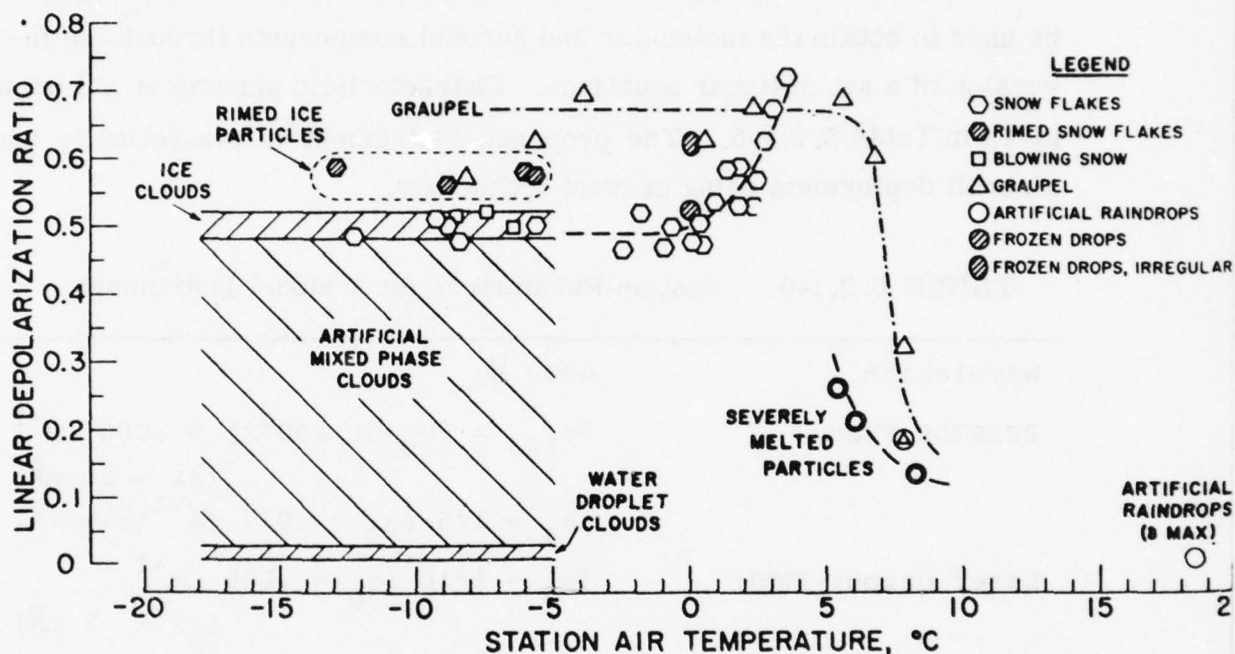


Figure 5. 2. 1-6 Linear Depolarization Ratio for Different Particles, using a CW HeNe Laser (6328 Å).

5. 2. 1. 3 Advantages and Disadvantages

The obvious advantage of lidar systems for the measurement of particulate matter in a polluted atmosphere is the rapid and real-time coverage of the air volume enveloping the airport and its vicinity. It will be seen later that this advantage is universally enjoyed by all remote monitoring sensors, especially when compared with isolated in-situ sensors placed on the ground.

The three-dimensional coverage can significantly contribute to the--

- (a) validation and verification of atmospheric pollution models for airports,
- (b) determination of engaging emergency measures for airport operations in situations when the NAAQS are exceeded,
- (c) determination of the mixing depth for an independent estimate of the total pollution level, using dispersion models and emission factors, and
- (d) determination of the effectiveness of abatement measures in "normal" as well as in episode situations.

As will be seen later, there are other methods of remotely determining the particulate concentration. We will then discuss some more advantages/disadvantages in relationship to these other methods.

The disadvantages of a lidar system to measure particulate pollution in the air volume in the vicinity of an airport are:

- (a) Operational limitations due to requirement of non-interference with airport operation and of eye safety regulations;
- (b) difficult requirements for functional checks because of the complexity of the data reduction system, performance checks and field calibration;
- (c) the validity underlying the assumptions that relate the particulate mass per unit volume (the parameter to be determined according to the NAAQS, (see section 2)

to the three unknowns contained in the lidar equation, namely the volume extinction coefficient, the back-scattering coefficient and the number density;

- (d) the validity underlying the assumptions that account for the interfering effects such as humidity, polarization/depolarization, and multiple scattering.

5. 2. 1. 4 System and Operational Requirements

5. 2. 1. 4. 1 System Requirements

The system requirements are dictated by the NAAQS in relationship to the airport environ, i. e., range, repetition rate, sensitivity, specificity, etc. The system parameters include laser power output, pulse length and repetition rate, beam expansion, receiver optics, detector characteristics, electronic processing, data reduction system, etc.

5. 2. 1. 4. 2 Operational Limitations due to Airport Operations

Monitoring operations must be carried out without significant interference with airport operations. Remote sensor installations do not require location which obstruct, impede or endanger airport operations. Access to instrument sites may require passage across runways and taxiways which must be governed by traffic control, preferably at off-peak hours.

Monitoring installations in the vicinity of radio, radar and electronic navigation and landing system antennas require consideration of possible RF interference emitted by the monitor (not likely in properly designed monitors). The monitor installation must not alter the antenna beams pattern or phase.

5. 2. 1. 4. 3 Operational Limitation due to Eye Safety Requirements

This topic is discussed in Section 6. 1. 3. 2 where figures are presented showing maximum permissible exposure versus wavelength and minimum permissible beam diameter.

5. 2. 1. 5 Analysis and Critique

In this section we analyze the assumptions used in relating the particulate mass per unit volume to the three unknowns contained in the lidar equation and in accounting for the interfering effects such as humidity, polarization/depolarization and multiple scattering.

Consider the lidar equation (5. 2. 1-1). The three unknown quantities are β , $N(R)$ and $\sigma(r)$. With one measurement, none of the unknowns can be determined. A further requirement is the relationship between $N(R)$ (number of particles per cm^3) and $\rho(R)$, the mass density ($\mu\text{g}/\text{m}^3$). This latter quantity is the one for which the NAAQS has been established. By conducting several independent experiments one can obtain, of course, more information about the unknowns. For example, several bistatic experiments may be conducted to obtain the angular distribution of the backscattered signals, multiwavelengths lidar measurements may be used to learn something about size distribution, and polarized laser beams may be used to obtain information about the depolarization of the scattering medium. In fact, these measurements are currently being carried out by different groups in order to determine some of the scattering parameters in the atmosphere. However, it is unlikely that these relatively sophisticated experiments would be undertaken in routine monitoring operations. The complexity of the problem can be appreciated by listing all variables that enter the determination of the particulate mass density. The backscattering coefficient β consists of the Rayleigh and Mie components. Methods of

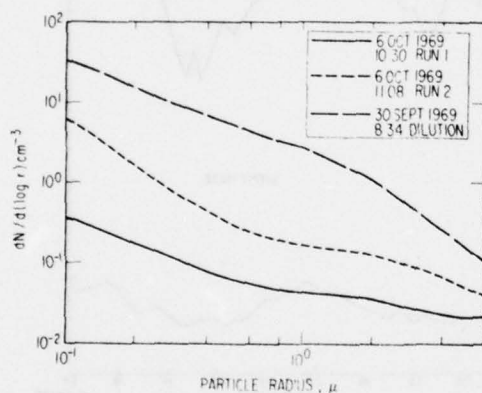
separating the two have already been mentioned^(48, 49). The coefficients are dependent upon the size parameter, size distribution, particle shape, the real part of the index of refraction, and the wavelength. The same dependencies are encountered for the volume extinction coefficient σ with additional ones. The first is the number density of the particulate matter as a function of range, the second is the particulate absorption, which in turn required knowledge of the imaginary part of the complex index of refraction, and the third is the molecular absorption, which requires the knowledge of the absorption coefficients and the optical path of the molecular species present. For the conversion of particulate number density (cm^{-3}) measured at range R to the mass density ($\mu\text{g}/\text{m}^3$), one needs again the size distribution.

The range in which size distributions may vary in one general area within a time lapse of 1 month was shown by Harris⁽⁵⁵⁾. Table 5. 2. 1-6 shows the conditions for those distributions that were chosen. The measurement system consisted of a Royco 220 particle counter, a Technical Instruments

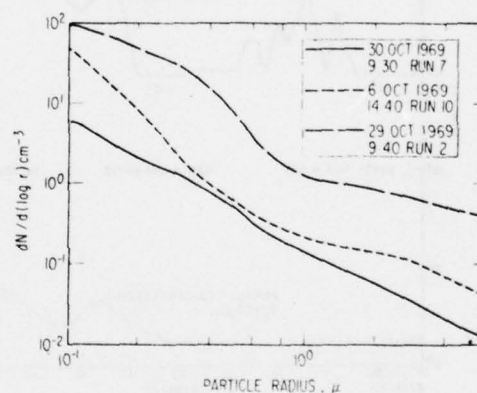
TABLE 5. 2. 1-6 Los Angeles Aerosol Size Distribution Types Arranged Roughly in Order of Increased Slope of Curve

Case	Date	Location	Run	Temperature (°C)	Relative humidity (%)	Wind (km/h)	Remarks
1	6 Oct. 1969 10:30	Mt. Wilson	1	20	13	1.6 at 180°	Slightly hazy over city
2	6 Oct. 1969 11:08	Mt. Wilson	2	21	7	8 at 180°	Slightly hazy over city
3	30 Sept. 1969 8:34	Eaton Canyon	Dil	—	43	3 at 160°	Sunny and clear
4	30 Oct. 1969 9:30	Sunland	7	23	19	3 at 90°	Some haze
5	6 Oct. 1969 14:40	Mt. Wilson	10	20	10	5 at 180°	Haze over city
6	29 Oct. 1969 9:40	Marineland	2	16	81	16 at 270°	Foggy out to sea
7	30 Oct. 1969 7:25	Granada Hills	3	20	13	10 at 135°	Smell of smoke
8	30 Sept. 1969 11:30	Eaton Canyon	12	31	27	7 at 160°	Sunny, hazy
9	30 Oct. 1969 6:55	Newhall	2	8	29	8 at 135°	Clear
10	29 Oct. 1969 10:00	Marineland	3	18	73	16 at 270°	Fog clearing
11	29 Oct. 1969 12:45	Torrance Beach	9	19	65	5 at 270°	Vis. 1.6 km on sea side

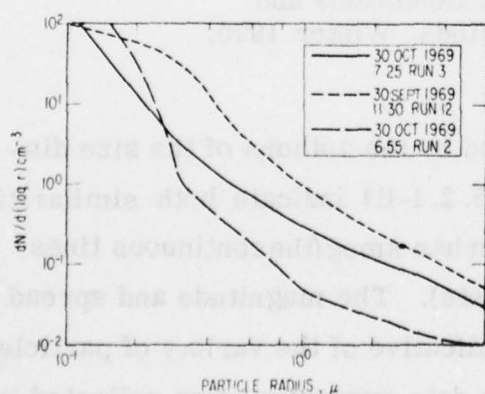
Incorporated pulse converter, a TII model 102 Gammascope 100-channel pulse height analyzer, a TII model 535 type-punch read unit, a 1500-W alternator as power source unit, and a voltage regulator. The paper tape output data were processed by computer to plot the size distribution on a $dN/d(\log r)$ vs. log radius chart. When the particle count rate was higher than 10,000 counts/min., clean filtered air was used for dilution to avoid coincidence counting distortion. The results of the size distributions are shown in Figures 5. 2. 1-9.



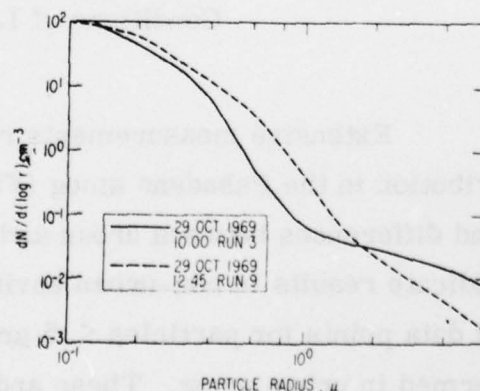
Cases 1, 2 and 3



Cases 4, 5 and 6



Cases 7, 8 and 9



Cases 10 and 11

Figure
5. 2. 1-9.

Los Angeles Atmospheric Aerosol Size Distributions

The ability of the Los Angeles atmosphere to vary strongly in aerosol content depending on meteorological conditions was observed by Hidy and Friedlander^(55a). Figure 5.2.1-10 shows a time series of Aitken nuclei counts from the GE instrument, and the large particle fraction from the Royco output.

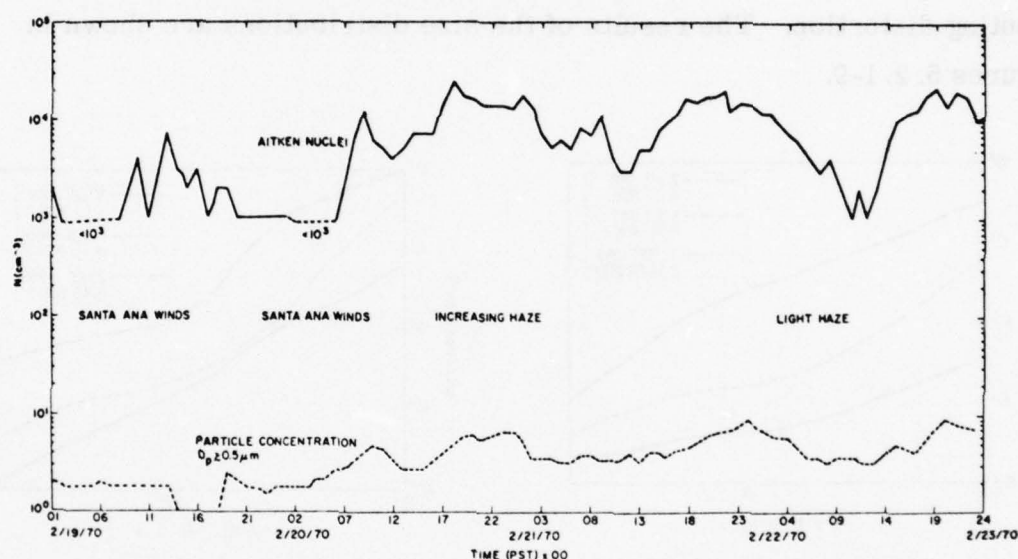


Figure 5. 2. 1-10. Comparison Between Aerosol Concentrations under Santa Ana Wind Conditions and Conditions of Light Winds, Winter 1970.

Extensive measurements reported by the authors of the size distribution in the Pasadena smog (Figure 5.2.1-11) indicate both similarities and differences between urban and non-urban smog (the continuous lines indicate results in non-urban environments). The magnitude and spread of data points for particles $< .5 \mu\text{m}$ is indicative of the variety of particles formed in urban smog. These and other data currently being collected in

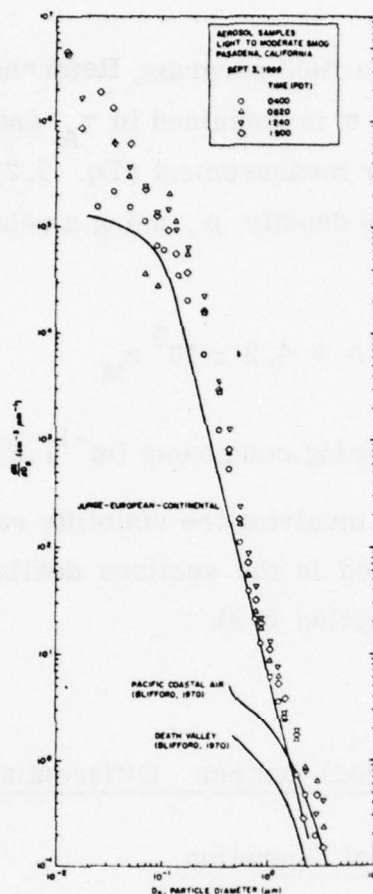


Figure
5. 2. 1-11.

Comparison between Aerosol Size Spectra in Different Geographical Locations and Spectra taken for Light to Moderate Smog in Pasadena, California. (Data for Pasadena courtesy of K. T. Whitby). [Taken from Ref. (55a).]

laboratory and field measurements together with theoretical calculations will yield the basis on which empirical relationships between the mass density and backscattered lidar signals can be based.

As examples of some relationships established so far, we have given already the one between the backscattering and extinction coefficients in Section 5. 2. 1. 1. The inverse of that is $\sigma/\beta N(R) = 25$. This value was

recently confirmed during a field program, Reference No. 44 (see Section 5. 2. 1. 2). Since σ is contained in τ_A and the product $\tau_A \beta N(R)$ can be deduced from a lidar measurement (Eq. 5. 2. 1-1), it is therefore possible to deduce the mass density ρ , using a relationship given by Griggs⁽⁵⁶⁾, i. e.,

$$\rho = 4.2 \times 10^5 \sigma_M$$

where σ_M is the Mie scattering component (m^{-1}) of the extinction coefficient.

Other relationships involving the visibility range and extinction coefficients⁽⁵⁷⁾, are discussed in the sections dealing with systems that measure line averages (Section 5. 3).

5. 2. 2 Active (Pulsed) System: Differential Absorption

5. 2. 2. 1 Principle of Operation

Differential absorption and scattering (DAS) is a monostatic system, utilizing a two-wavelength laser system and the elastic backscattering (Rayleigh and Mie) from the atmosphere. It is used to obtain range-resolved measurements of gaseous pollutants. By gating the detector, different arrival times can be observed, thus obtaining spatially resolved signals. This is very similar to the LIDAR system described in the previous sections. Hence, the acronym DIAL (differential absorption by LIDAR) is also used.

The two wavelengths can either be transmitted simultaneously, using two lasers at fixed lasing frequency (see Figure 5. 2. 2-1), or transmitted

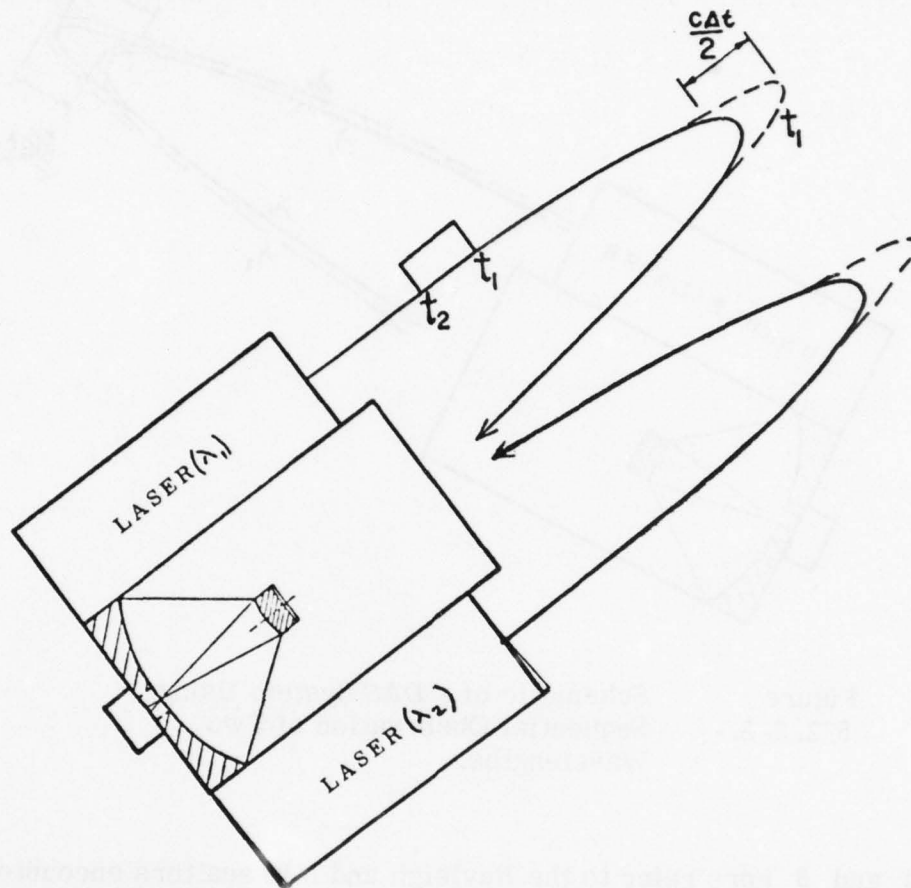


Figure
5. 2. 2-1.

Schematic of a DAS System Using
Simultaneous Observation of Two
Wavelengths.

sequentially, using one tunable laser (see Figure 5. 2. 2-2). Provided the atmosphere is relatively homogeneous, many of the uncertainties contained in a single measurement such as in LIDAR disappear as is shown in the following.

In DAS the laser radiation is transmitted (and received) at the line center (wavelength 1) and at the wing (wavelength 2). The values of

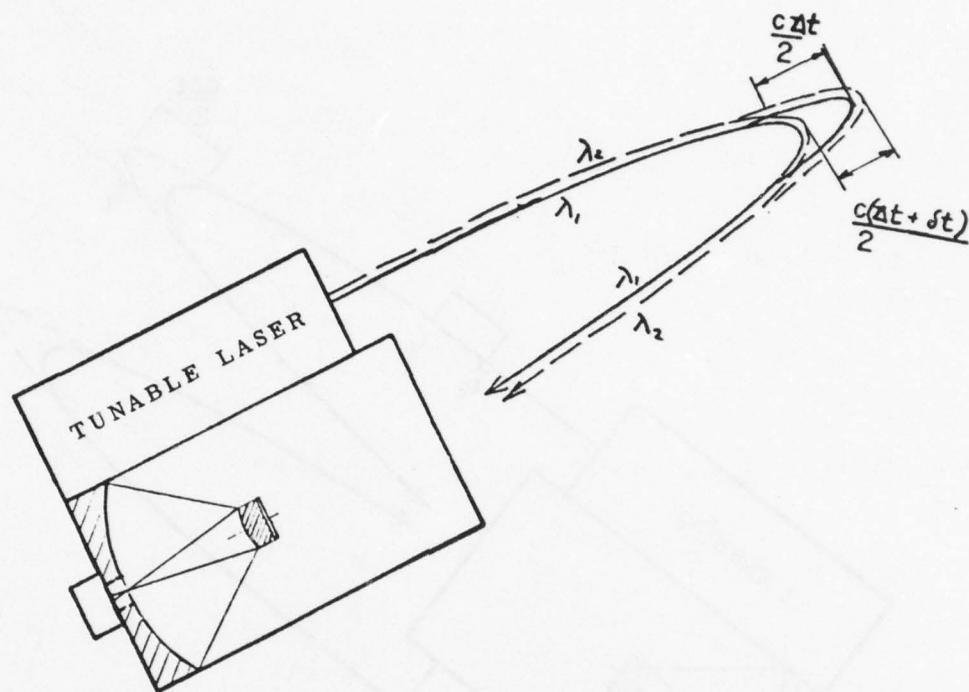


Figure
5. 2. 2-2.

Schematic of a DAS System Using
Sequential Observation of Two
Wavelengths.

$N(R)$ and β here refer to the Rayleigh and Mie scatters encountered by the same pulse at time t_1 and at time t_2 and are assumed constant during the measurements. The LIDAR equation may then be written as

$$P(R) = F R^{-2} \tau_A(R) \quad (5. 2. 2-1)$$

or

$$\ln P(R) = \ln F - 2 \ln R - 2 \int_0^R \sigma(r) dr$$

where

$$F = \eta P_t L N(R) \beta A .$$

At time t_2 and range $R + \Delta R$

$$\ln P(R + \Delta R) = \ln F - 2 \ln(R + \Delta R) - 2 \int_0^{R+\Delta R} \sigma(r) dr$$

Differencing the two equations for wavelength 1 and 2

$$\left. \begin{aligned} \ln P_1(R) - \ln P_1(R + \Delta R) &= 2 \ln \frac{(R + \Delta R)}{R} + 2 \bar{\sigma}_1(R) \Delta R \\ \ln P_2(R) - \ln P_2(R + \Delta R) &= 2 \ln \frac{(R + \Delta R)}{R} + 2 \bar{\sigma}_2(R) \Delta R \end{aligned} \right\} \quad (5. 2. 2-2)$$

where $\bar{\sigma}(R)$ is the mean volume extinction coefficient over the distance ΔR . The volume extinction coefficient may be expressed as

$$\sigma = \sigma_s + \sigma_a = \sigma_s + k p_p$$

where σ_s is the scattering and σ_a the absorption component, k is the absorption coefficient ($\text{cm}^{-1} \text{atm}^{-1}$), and p_p is the partial pressure of the pollutant. Since the two wavelengths are close, the scattering coefficient does not change, thus

$$\sigma_s(\lambda_1) = \sigma_s(\lambda_2)$$

Introducing these expressions into Equations 5. 2. 2-2 and differencing those, we obtain

$$\ln Q = 2 (k_1 - k_2) \bar{p}_p(R) \Delta R \quad (5. 2. 2-3)$$

AD-A067 242

SCIENCE APPLICATIONS INC LA JOLLA CALIF

F/G 1/5

DEVELOPMENT OF CRITERIA FOR MONITORING OF AIRPORT GROUND POLLUT--ETC(U)

NOV 78 C B LUDWIG, J R YODER

DOT-FA76WA-3725

UNCLASSIFIED

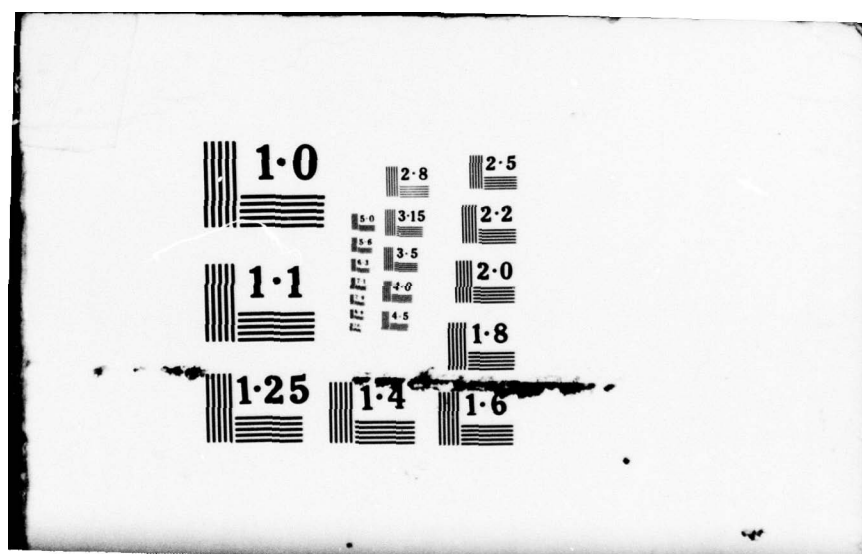
SAI-77-910-LJ-VOL-1-

FAA/RD-77-178-1

NL

3 OF 5
ADA
067242





where

$$Q = \frac{P_1(R) P_2(R + \Delta R)}{P_2(R) P_1(R + \Delta R)} \quad (5. 2. 2-4)$$

The partial pressure \bar{p}_p can be expressed as

$$\bar{p}_p = \bar{C} p_t = 10^{-6} \bar{\xi} \quad (5. 2. 2-5)$$

where \bar{C} is the concentration, p_t is the total pressure and $\bar{\xi}$ is the concentration in ppm by volume at 1 atm pressure. *

Thus

$$\bar{\xi}(R) = \frac{10^6 \ln Q}{2 \Delta R (k_1 - k_2)} \quad (5. 2. 2-6)$$

In deriving Equation 5. 2. 2-6 it was assumed that the atmospheric and pollutant properties are constant while the data are taken at the two wavelengths. This is true if they are taken simultaneously, but if it takes more than 1 msec to tune the laser between wavelengths, then atmospheric scintillation and air motion adds an error term to Eq. (5. 2. 2-6). Schotland⁽⁵⁸⁾ discussed these errors but did not provide an estimate of their magnitudes. It is clear that simultaneous measurements at the two wavelengths are preferred.

Only two of the primary pollutants, SO_2 and NO_2 , have spectral bands in the UV. All others have to be measured in the infrared.

* Other conversions are $\xi_w(\text{ppm-weight}) = \frac{\text{Mol. Wt.}}{28.8} \xi(\text{ppm-vol})$

and $\rho(\mu\text{g}/\text{m}^3) = \frac{\text{Mol. Wt.}}{0.02404} \xi(\text{ppm-vol})$

5. 2. 2. 2 State-of-the-Art

Part of this material was prepared for a previous program⁽⁵⁹⁾.

The differential absorption method has been used to measure NO_2 in urban atmospheres (Rothe et al.)⁽⁶⁰⁾ and in stack emissions (Rothe et al.)⁽⁶¹⁾. They used a tunable dye laser in the 4600 Å region. For the urban measurements, a mean concentration of 0.23 ppm of NO_2 was found over the distance 1.73 to 3.74 km. The measurement was made at nighttime and took about 13 minutes; no comparison was made with other data. The same laser system was used to measure NO_2 in stack emissions in a chemical factory. Measurements were made 300 m from the stack exit at a range of 750 m. The distribution across the plume indicates that 1 ppm was detectable. Again the measurement time was long, being about 33 minutes. The same publication shows ambient air contours of NO_2 over the chemical factory, and indicate a measurement sensitivity of 0.5 ppm at a range of 500 m with each data point requiring 20 seconds measurement time. No comparison with other data or a discussion of accuracy is given.

Grant et al.⁽⁶²⁾, using a tunable dye laser in the 4500 Å region, made nighttime measurements of NO_2 in a closed chamber at a range of 365 m. A sensitivity equivalent to 5 ppm with a 10 m resolution element at this range was determined, but no discussion of the integration time required was given. The results showed good agreement with independent transmissometer readings across the chamber.

Igarashi⁽⁶³⁾ reported a differential absorption measurement of NO_2 using the 4480 Å region, and SO_2 using the 3000 Å region. Details of the experiment are not given, but 0.1 ppm of the gases were measured at a range of 300 m, with a resolution element of 100 m, using a 1 mJ laser output.

An interesting variation of this technique due to Zaromb⁽⁶⁴⁾ does not require a tunable laser. It uses the Raman backscattered signals from oxygen and nitrogen, which coincide with absorption bands of NO_2 and SO_2 . A system is presently being built to measure 20-70 ppm of SO_2 and 5-25 ppm of NO_2 at a range of 200 m. The same system will also measure 1000 ppm of CO_2 using the direct Raman signal of CO_2 . No further details are presently available.

Another similar technique (Granatstein et al.)⁽⁶⁵⁾ uses the backscatter of laser radiation from droplets (or smoke particles) in a stack effluent. Laboratory measurements of CH_4 and CO_2 were made by tuning a He-Ne laser at either 3.391 μm or 4.217 μm , respectively. Measurements were made using gas concentrations greater than 1000 ppm, and it was concluded that the attenuation properties of the scatterers are needed to interpret the data. It would appear that two adjacent wavelengths are needed for each gas, instead of just one, and then of course, the method is the same as the other differential absorption methods which use the visible/UV.

Feasibility studies have been conducted by Ahmed⁽⁶⁶⁾ and Byer and Garbuny⁽⁶⁷⁾. Ahmed estimates a sensitivity of 0.4 ppm for NO_2 in a 100 m resolution element at a range of 1 km for a 1 mJ laser in the 4000 \AA region. Byer and Garbuny, for NO_2 , estimate .85 ppm in 15 m, at 1 km range, using 1 pulse from a 100 mJ laser; they also estimate that .14 ppm of CO can be determined under the same conditions. Schotland⁽⁵⁸⁾ discusses the errors involved in the differential absorption, and using the example of measuring vertical water vapor profiles estimates errors of less than 6% for altitudes below 3 km.

Grant and Hake⁽⁶⁸⁾ have recently made DAS measurements of SO_2 and O_3 at 2900 \AA using a 15 mJ dye laser which can meet the Federal eye safety requirements with the addition of a 2 in. diameter beam expander.

The gas was contained in a 2.5 m chamber at about 250 m range. Averaging eight pulses, they found an uncertainty of ± 60 ppm-m for SO_2 and ± 130 ppm-m for O_3 . These large errors are attributable to variations in the atmospheric backscatter since the measurements were spread over one hour. They estimate that ± 10 ppm-m for SO_2 and ± 13 ppm-m for O_3 can be achieved by taking all the data within one minute.

Two preliminary reports from the Radio Research Laboratories in Tokyo [Inomata and Igarashi⁽⁶⁹⁾, Asai and Igarashi⁽⁷⁰⁾] discussed the development of two systems suitable for making the two DAS wavelength measurements simultaneously or within 1 nsec of each other, to minimize scintillation effects. The simultaneous measurement uses two linearly polarized components (independently tunable) of a dye laser cavity. The other report (Asai and Igarashi)⁽⁷⁰⁾ concerned the measurement of O_3 using a CO_2 laser and a retroreflector in a long-path measurement. The P(14) and R(14) lines of a single laser were used, and alternately transmitted through the atmosphere at 130 Hz. In controlled tests, they determined a sensitivity of 12.4 ppm-m, but by improving the stability of the laser and by using digital processing, they anticipate a sensitivity of about 5 ppm-m.

A new approach has been analyzed theoretically by Kobaysi and Inaba⁽⁷¹⁾, using an infrared heterodyne laser scheme. This approach is of importance because most pollutants have absorption bands in the infrared, while only SO_2 and NO_2 have bands in the UV. The sensitivity in the IR is, of course, lower than in the visible, but the authors state that the heterodyne sensitivity is 10^3 to 10^6 times better than that achieved by the conventional direct detection. Heterodyne detection of radiation will be discussed in the section dealing with CW systems. The authors conclude that this method offers the spatial-resolved detection of pollutants (less than ppm) up to several km with an average laser power of 100 W.

Recently, Hoell et al. ⁽⁷²⁾ have described measurements in which atmospheric measurements of SO₂ were performed using a single flash-lamp-pumped dye laser whose wavelengths were switched from λ_{on} to λ_{off} on a time scale of approximately 15 seconds. Further measurements were described by Wade et al. ⁽⁷³⁾ in which the time scale between λ_{on} and λ_{off} is less than 1 ms, thereby reducing noise effects due to atmospheric turbulence and scintillation.

The authors emphasize that an important feature of the UV lidar system is the system calibration technique in which a known quantity of SO₂ located in the path of the transmitting beam is used to simulate a known column content of SO₂. This technique was used to verify linearity of the detection system and to calibrate the sensitivity of the system, on line. Measurements of SO₂ concentrations in the atmosphere using a single laser system were made for 300-meter range cells, at total ranges of nearly 2 km, with a measurement sensitivity of 10 ppb of SO₂. The measurements obtained in the plume of a local steam generating plant showed excellent correlation with plant operations and the direction of local winds used to direct the SO₂ into the fixed path of the DIAL system. The return signal was collected with a 0.25-meter Dall-Kirkham telescope and an EMI9558 photomultiplier tube. The output of the phototube was analyzed by range-gated sample and hold circuits which provided the capability of obtaining the spatial distribution of SO₂ in the atmosphere. Real time data analysis was achieved through use of a PDP-8 minicomputer. An interesting application of the method to Space Shuttle operation is being explored by NASA-Langley Research Center ⁽⁷⁴⁾, based upon the theoretical findings by SRI ⁽⁷⁵⁾. System parameters for these simulations were Shuttle altitude, 200 km; laser energy, 0.1 joule/pulse; telescope area, 1 m²; system receiving efficiency, 10%; range cell size, 2 km; and no averaging of pulses.

For the preceding parameters, off-line returns at ruby wavelengths can be measured to better than 10% accuracy from the surface to an altitude of 25 km. By considering additional realistic constraints, such as noise due to conventional detectors, inadequate laser power in the UV, and short wavelength absorption by ozone and oxygen, only wavelengths from about 0.3 to 1.0 micrometers are feasible for off-line measurements with currently demonstrated LIDAR system technology. Off-line measurements to better than 10% for altitudes up to 60 km are possible if the laser energy is increased to 10 joules/pulse or 0.1 joule energy averaged over 100 laser firings.

An application of the DIAL system in the near infrared was discussed by Bair and Allerio⁽⁷⁶⁾. It applies to the detection of anhydrous HCl in the ground cloud of solid rocket motors and for profiling atmospheric pollutants in the atmosphere. To evaluate the feasibility of DIAL for detecting HCl in the ground cloud, a computer simulation was performed in which a dual wavelength laser transmitter was assumed. Absorption and scattering coefficients for a typical rocket ground cloud were calculated using Mie theory. Primary constituents of the ground cloud are CO₂, H₂O, N₂, CO, HCl, H₂O aerosols, and Al₂O₃ particulates. The computer simulation developed for the ground cloud problem was also used to evaluate the near IR DIAL technique for measuring SO₂ emissions in smoke stacks and comparing it to the UV DIAL technique. To account for the distribution of constituents in the cloud and change of composition in time as the cloud drifts away from the launch pad, a previously developed molecular Multilayer Diffusion Model⁽⁷⁷⁾ was assumed. For typical ground cloud concentrations of HCl and Al₂O₃ particles obtained from the Multilayer Diffusion Model, and for a range of 2 km from the transmitter to the edge of the cloud, typical detectable concentrations of HCl are smaller than

1 ppm with a sensitivity of ± 0.1 ppm. Authors believe that considerable improvement in sensitivity can be obtained by increasing the laser energy, pulse repetition rate, and area of the receiver. For a 75-meter range cell, typical penetration depths into the cloud exceed 400 meters. Assuming a typical cloud diameter of 1 km, and assuming the cloud constituents are symmetrically distributed about the centerline of the cloud, the near IR DIAL technique should be capable of generating a near total profile of the concentration of anhydrous HCl in the cloud. Large concentrations of H_2O aerosols in the cloud (e.g., 100 particles/ cm^3 at the center of the cloud distributed as a Gaussian) can degrade the measurement sensitivity by a factor of 5.

Another system being funded by NASA-Langley Research Center and developed by University of Maryland was described by McIlrath et al. (78) and its calibration by Wilkerson et al. (79).

The laser is shown schematically in Figure 5. 2. 2-3. The ruby laser generates up to 2 joules of which .5 to .7 joules is used to pump the dye

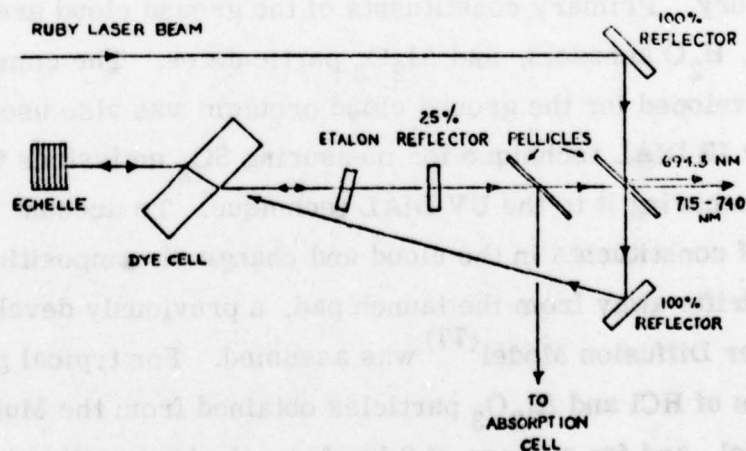


Figure 5. 2. 2-3. Ruby Pumped IR Dye Laser—View from Above (78)

laser. The dye laser is pumped nearly longitudinally, approximately 7° off axis, with an uncoated dye cell oriented at Brewster's angle relative to the cavity axis. The tuning elements are a 79 g/mm echelle grating used in 34th order and a single Fabry-Perot etalon having a free spectral range of 2.5 cm^{-1} . The present limitation of 30 mJ on the dye laser output is due to the onset of damage to the diffraction grating. Authors state that a conversion to an all etalon system will allow much higher output energies. The dye laser operates from 7150 Å to 7430 Å using DTDC* dissolved in DMSO.** The output is continuously tunable by rotation of the grating and etalon, and the output line width is .01 nm with a wavelength stability of better than 5%, the beam diameter is 1 cm, and the beam divergence is less than 3 mr. The output has been tuned through water lines at 724.3 nm and absorption of the signal observed with a multiple pass absorption cell described in the adjacent abstract. The laser and absorption cell are now being integrated with the Lidar and data handling equipment of NASA-Langley Research Center for observations of differential absorption in the atmosphere. The overall lidar experiment includes a calibrating absorption cell, which receives a sample of each laser pulse to determine its extinction by a known column content of H_2O on every shot. Path-lengths are $\sim 300 \text{ M}$ at 50-70% humidity for $T \sim 24^\circ \text{C}$. The cell consists of two large spherical mirrors 4 M apart. A "perturbing mirror" allows a choice between simple or re-entrant optical paths⁽⁸⁰⁾. Input/output PMTs are PCA 4832, driving the data cables through IC buffer amplifiers so as to keep overall response time $\leq 5 \text{ n sec}$. Authors state that for atmospheric ranging, the extinction observed in the cell will be helpful in interpreting the on-line lidar return in terms of absolute humidity as a function of range.

* 3, 3'-Diethylthiatricarbocyanine iodide
 ** Dimethyl sulfoxide

The usefulness of a DAS or DIAL system operating in the infrared was already mentioned. SRI⁽⁸¹⁾ has constructed such a system. The transmitter consists of a multi-gas TEA laser operating on CO₂ (10 μ m) at energy levels of 1 J/pulse at 0.5 Hz PRF with a pulse width of 100 ns (FWHM) and beam divergence of 0.7 mrad (FWHM). The receiver consists of a 30 cm diameter Newtonian telescope with a 1.8 mrad field-of-view (FWHM) and a 1 x 1 mm mercury-cadmium-telluride detector with a D* of $2(10^{10})$ cm Hz^{1/2}/watt. The first species to be measured remotely using this IR dial system is ambient water vapor. The results show a backscattered signal on the absorbed line greater than the system noise level for a range of at least 1.5 km on a single-pulse basis. The differential signal between the absorbed and nonabsorbed wavelengths was easily discernible. Authors state that general good agreement was obtained between the DIAL results and those from a calibrated recording hygrothermo-

Murray⁽²⁴⁹⁾ reports further use of discretely tunable infrared gas lasers for remote measurement of gases. Integrated concentrations of HCl, CH₄ and N₂O were measured between the lidar and a topographic target. Range-resolved profile of water vapor was determined using a CO₂ laser and backscattering from natural aerosol. Performance data are presented which appear to be better by orders of magnitude than those indicated in this study. It is therefore important to examine and compare the two results. This is done in section 5.2.2.5.

5. 2. 2. 3 Advantages and Disadvantages

The obvious advantage of the differential absorption by pulsed lidar for the measurement of the gaseous pollutants is the rapid and real-time coverage of the air volume enveloping the airport and its vicinity.

The three-dimensional coverage can significantly contribute to the

- (a) validation and verification of atmospheric pollution models for airports,
- (b) determination of engaging emergency measures for airport operations in situations when NAAQS are exceeded,
- (c) determination of the effectiveness of abatement measures in "normal" as well as in episode situations.

In addition, the differential absorption has the advantage of having very little dependence on the backscattering and extinction coefficients of the atmosphere and dependence only (in theory) on the optical parameters and concentration of the pollutant gas, with the exception of a possible coincidence of line absorption by another molecule.

The disadvantages of the differential absorption by pulsed lidar to measure gaseous pollutants in the air volume in the vicinity of an airport are:

- (a) operational limitations due to requirements of non-interference with airport operations and of eye safety regulations; however the limitations due to eye safety regulations are somewhat less restrictive than in the case of lidar for particulate measurements since measurements will not be made in the visible spectrum;
- (b) difficult requirements for functional system checks because of the complexity of the data reduction system, performance checks and field calibration;

- (c) the data reduction involves four independent measurements which increases the noise and reduces the signal-to-noise ratio (SNR);
- (d) the complexity of the system is greater than for a lidar system that was described in Section 5.2.1, since either rapid tuning of one laser or the simultaneous firing of two lasers is required.

These four items will be discussed in greater detail in the following sections.

5. 2. 2. 4 System and Operational Requirements

5. 2. 2. 4. 1 System Requirements

The system requirements are dictated by the NAAQS in relationship to the airport environ, i.e., range, repetition rate, sensitivity, specificity, etc. The system parameters include laser power output, both frequencies, pulse length and repetition rate, beam expansion, receiver optics, detector characteristics, electronic processing, data reduction system, etc.

5. 2. 2. 4. 2 Operational Limitations due to Airport Operations

Monitoring operations must be carried out without significant interference with airport operations. Remote sensors installations do not require location which obstruct, impede or endanger airport operations. Access to instrument sites may require passage across runways and taxiways which must be governed by traffic control, preferably at off-peak hours.

Monitoring installations in the vicinity of radio, radar and electronic navigation and landing system antennas require consideration of possible RF interference emitted by the monitor (not likely in properly designed monitors). The monitor installation must not alter the beam or phase pattern of the antenna.

5. 2. 2. 4. 3 Operational Limitation due to Eye Safety Requirements

In general, everything applies as discussed already in Section 5. 2. 1. 4. 3. However, since the visible and the near infrared spectral region from 7000 Å to 14000 Å (1.4 μm) are of no or little importance for measuring gaseous pollutants, the strict requirements for MPE as indicated by (c) and (d) in Figures 5. 2. 1-7 and 5. 2. 1-8 will not apply.

5. 2. 2. 5 Analysis and Critique

In Equation 5. 2. 2-6 the absorption coefficients may be uncertain by as much as $\pm 20\%$ (Schotland)⁽⁵⁸⁾, but this would be merely a systematic error which could be eliminated by careful calibration. Random errors in the absorption coefficient can arise by variation of pressure and temperature of the pollutant, and by fluctuations in the laser wavelength. The other errors in using the equation to deduce $\xi(R)$ occur in the measurement of the received power as a function of range and wavelength. The received power can possibly be measured to within 1% (implying a signal-to-noise ratio of 100), but since four power outputs must be measured in Equation 5. 2. 2-6, Q has an error of 4%, and when Q is close to unity, then the error in $\ln Q$, and hence, in $\xi(R)$ is large.

This latter conclusion is verified by Inomata and Igarashi⁽⁶⁹⁾, who have developed a DAS system with simultaneous wavelength oscillation of a dye laser. Two linearly polarized components of a dye laser cavity were independently tuned and used to measure 85 ppm-m of NO₂ in a test cell. The laser power fluctuates by more than 10%, and it was necessary to monitor the output power at each wavelength. Their results are shown

in Figure 5. 2. 2-3 which shows the standard deviation of a series of measurements. $(V/P)_0$ and (V/P) correspond to $P_2(R)/P_1(R)$ and $P_2(R + \Delta R)/P_1(R + \Delta R)$ respectively, in Equation 5. 2. 2-4. These errors also include those due to wavelength instabilities of the laser, although the authors measured them and found them to be negligible.

The advantage of simultaneous wavelength measurements is demonstrated by the reduction in the fluctuations in (c) and (f) compared with (a), (b), (d) and (e). The error in Q for this set of data is only 4% [(c) + (d) errors], but translates strikingly into a 47.5% error in the measurement of pollutant optical thickness. This error will be even larger if the SNR is less than the apparent value 100 for each power measurement, as will occur for increasing range. Of course, for larger optical thicknesses is error is reduced. For 850 ppm-m, which might be more representative of a plume, and 4% error in Q , the error in the optical thickness is about

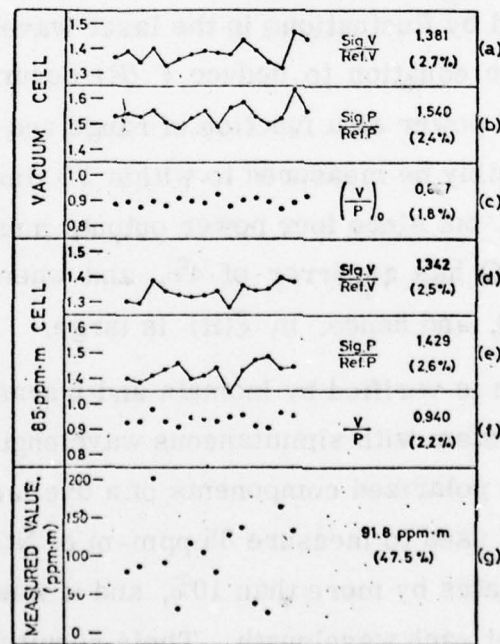


Figure 5. 2. 2-3. DAS Experimental Errors (after Inomata and Igarashi)⁽⁶⁹⁾

25%. For increasingly larger optical thicknesses, the transmission of the plume will decrease so that the resulting return signal decreases and the measurement errors increase, and finally cannot be measured due to system or background noise. It should be noted that these measurement errors could be reduced by averaging more pulses [$\text{SNR} \propto (\text{number of pulses})^{1/2}$], but a long averaging time may not always be practicable, particularly if the source and atmosphere are fluctuating.

The question of atmospheric fluctuations was investigated by Grant et al.⁽⁸²⁾ Schotland⁽⁵⁸⁾ had predicted that the atmosphere can be considered stationary for periods up to 1 ms, but so far no experimental confirmation has been made of this prediction, and the seriousness of the effect for delays longer than 1 ms had not been explored. Thus, Grant et al. have conducted experiments with a variable delay dual-pulse lidar employing two coaxial-flashlamp dye lasers⁽⁸³⁾ to determine the magnitude of this DIAL error source as a function of interpulse time delay. The lasers transmit 20 to 100 mJ per pulse with a 0.5 to 10 Å spectral width at 450 nm in a 1/4-μs, 1-mrad divergence beam. The two beams are made coaxial by the use of mirrors, and are transmitted through a 5X beam expander. It was found that in a relatively calm atmosphere, no trend in uncertainty was discerned for time delays between 10 μsec and 10 sec. More experiments in less calm atmospheres are planned.

We now analyze the basic sensitivities of a DAS instrument. It is recalled that the measurement of the pollutant concentration requires four signals. The appropriate expression was given by Equation 5. 2. 2-6. The expression for the signal-to-noise ratio is given by

$$\text{SNR} = \frac{\ln Q}{\text{NEP} \sqrt{(1/P_1)^2 + (1/P_1')^2 + (1/P_2)^2 + (1/P_2')^2}} \quad (5. 2. 2-7)$$

where

$$\ln Q = \ln \frac{P_1 P_2'}{P_1' P_2}$$

$$P_1 = (G/R^2) e^{-2k_1 C_1 R}$$

$$P_1' = (G/(R + \Delta R)^2) e^{-2k_1 C_1 (R + \Delta R)}$$

$$P_2 = (G/R^2) e^{-2k_2 C_2 R}$$

$$P_2' = (G/(R + \Delta R)^2) e^{-2k_2 C_2 (R + \Delta R)}$$

$$G = \eta_o P_t L N(R) \beta A_o$$

$$dP = \text{NEP} = (A_d \Delta f)^{1/2} (D^*)^{-1}$$

Introducing all of these expressions result in

$$SNR = \frac{\eta_o P_t L N(R) \beta A_o 2 \Delta R (k_1 C_1 - k_2 C_2) D^*}{\sqrt{A_d \Delta f} R^2 e^{2k_1 C_1 R} S}$$

where

$$S = \left\{ \left(1 + \exp[4R(k_2 C_2 - k_1 C_1)] \right) + \left(\frac{R + \Delta R}{R} \right)^4 \exp[4k_1 C_1 \Delta R] \right. \\ \left. \left(1 + \exp[4(R + \Delta R)(k_2 C_2 - k_1 C_1)] \right) \right\}^{1/2}$$

The following instrument parameters were chosen:

$$\begin{aligned} \eta_o &= 0.01 \\ P_t &= 1.4 \times 10^5 \text{ W} \\ \Delta t &= 10^{-7} \text{ sec} \\ L &= 15 \text{ m} \\ A_o &= 700 \text{ cm}^2 \\ D^* &= 10^{10} \text{ W}^{-1} \text{ Hz}^{1/2} \text{ cm (detector performance parameter)} \\ A_d &= 10^{-4} \text{ cm}^2 \text{ (detector area)} \\ \Delta f &= (10^{-7} \text{ sec/pulse} \times 100 \text{ pulse/sec} \times 60 \text{ sec} \times 4)^{-1} = 417 \text{ Hz} \\ &\quad \text{(electrical bandpass required to process signal)} \end{aligned}$$

The following atmospheric parameters were assumed

$$\begin{aligned} k &= 10 \text{ cm}^{-1} \text{ atm}^{-1} \\ C_1 &= C_{\text{poll}} = 10^{-5} - 10^{-9} \text{ cm-atm} \\ k_2 C_2 &= (kC)_{\text{atm}} = 0.9 (kC)_{\text{poll}} \end{aligned}$$

It should be noted that a D^* of $10^{10} \text{ W}^{-1} \text{ Hz}^{1/2} \text{ cm}$ is reasonable for the entire infrared region because of the requirement of fast time response ($\sim .1 \mu\text{sec}$).

The results in terms of pollutant concentration versus range are shown in Figure 5. 2. 2-4 as the left-hand curve(a). It is seen that there is a maximum range, due to atmospheric absorption. This maximum range is about 240 m and the range for pollution concentrations at NAAQS levels is less than 200 m. Thus, the DAS system, using "direct detection" (see below), is not very practical for ambient air monitoring.

In contrast to the "direct detection (dd)", "heterodyne detection (hd)" offers the potential of greater range. The improvement can be seen most easily by expressing the SNR of the heterodyne detection in terms of the SNR of direct detection and a factor which takes into account the NEP of the two systems and their entrance areas:

$$(\text{SNR})^{\text{hd}} = F (\text{SNR})^{\text{dd}}$$

$$F = \frac{(A_o)^{\text{hd}}}{(A_o)^{\text{dd}}} \times \frac{(\text{NEP})^{\text{dd}}}{(\text{NEP})^{\text{hd}}}$$

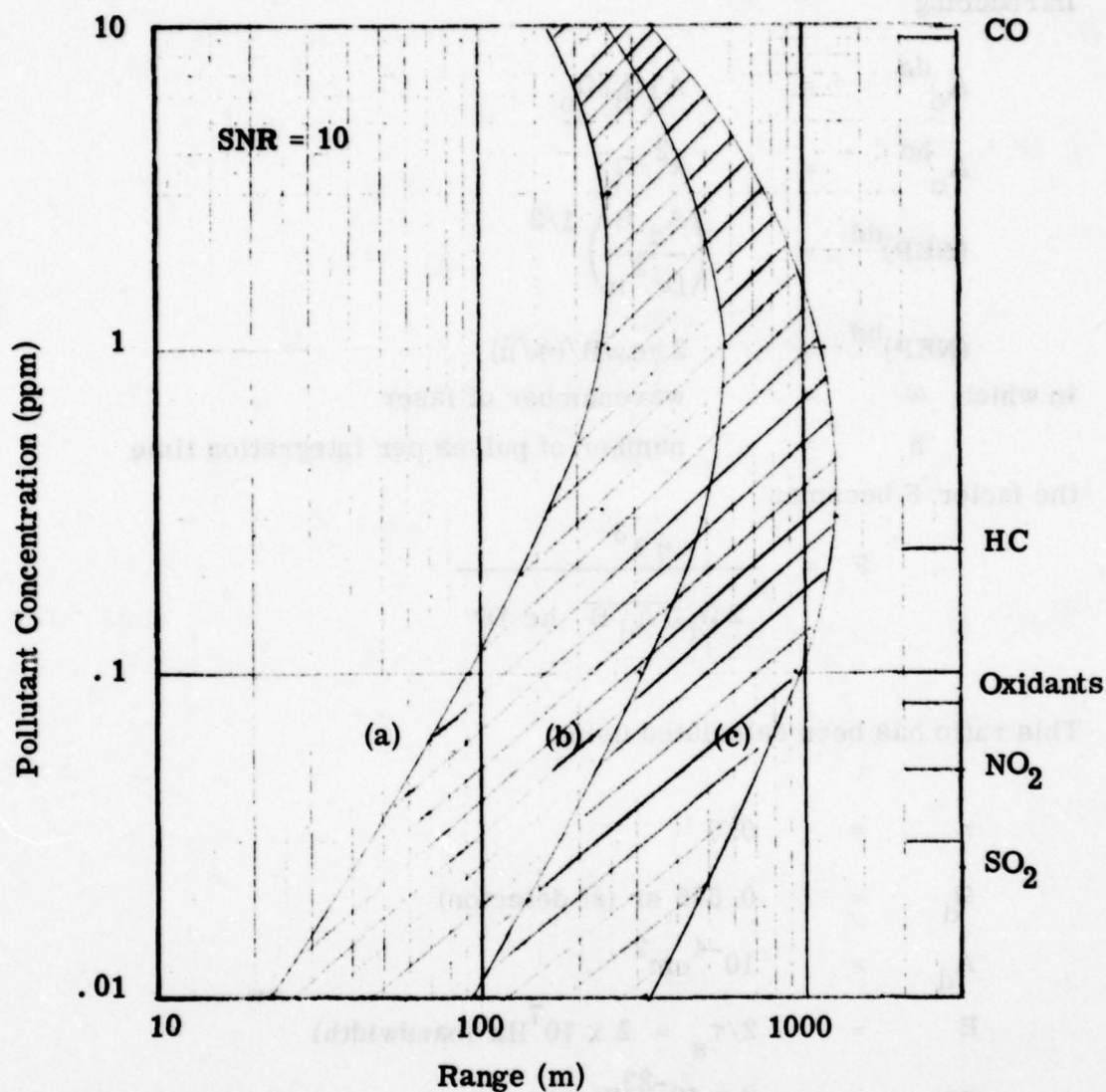


Figure
5. 2. 2-4.

Pollutant Concentration Versus Range, Using $k = 10 \text{ cm}^{-1}\text{atm}^{-1}$. Curve (a) is for Direct Detection and for Heterodyne Detection at $\lambda = 2.9 \mu\text{m}$. Curves (b) and (c) are for Heterodyne Detection at $\lambda = 6$ and $13 \mu\text{m}$, Respectively.

Introducing

$$A_o^{dd} = A_d \Omega_d / \Omega_o$$

$$A_o^{hd} = \lambda^2 / \Omega_o$$

$$(NEP)^{dd} = \left(\frac{A_d B}{D^{*2} n} \right)^{1/2}$$

$$(NEP)^{hd} = 2 hc \omega B / (\eta \sqrt{n})$$

in which ω = wavenumber of laser

h = number of pulses per integration time

the factor F becomes

$$F = \frac{\eta \lambda^3}{2 \Omega_d \sqrt{A_d B} hc D^*}$$

This ratio has been calculated using

$$\eta = 0.5$$

$$\Omega_d = 0.625 \text{ sr (at detector)}$$

$$A_d = 10^{-4} \text{ cm}^2$$

$$B = 2/\tau_s = 2 \times 10^7 \text{ Hz (bandwidth)}$$

$$hc = 2 \times 10^{-23} \text{ W sec cm}$$

$$D^* = 10^{10} \text{ W}^{-1} \text{ Hz}^{1/2} \text{ cm}$$

The results of F versus λ are shown in Figure 5. 2. 2-5. It is seen that for $\lambda > 2.9 \mu\text{m}$, the heterodyne detection is superior to the direct detection.

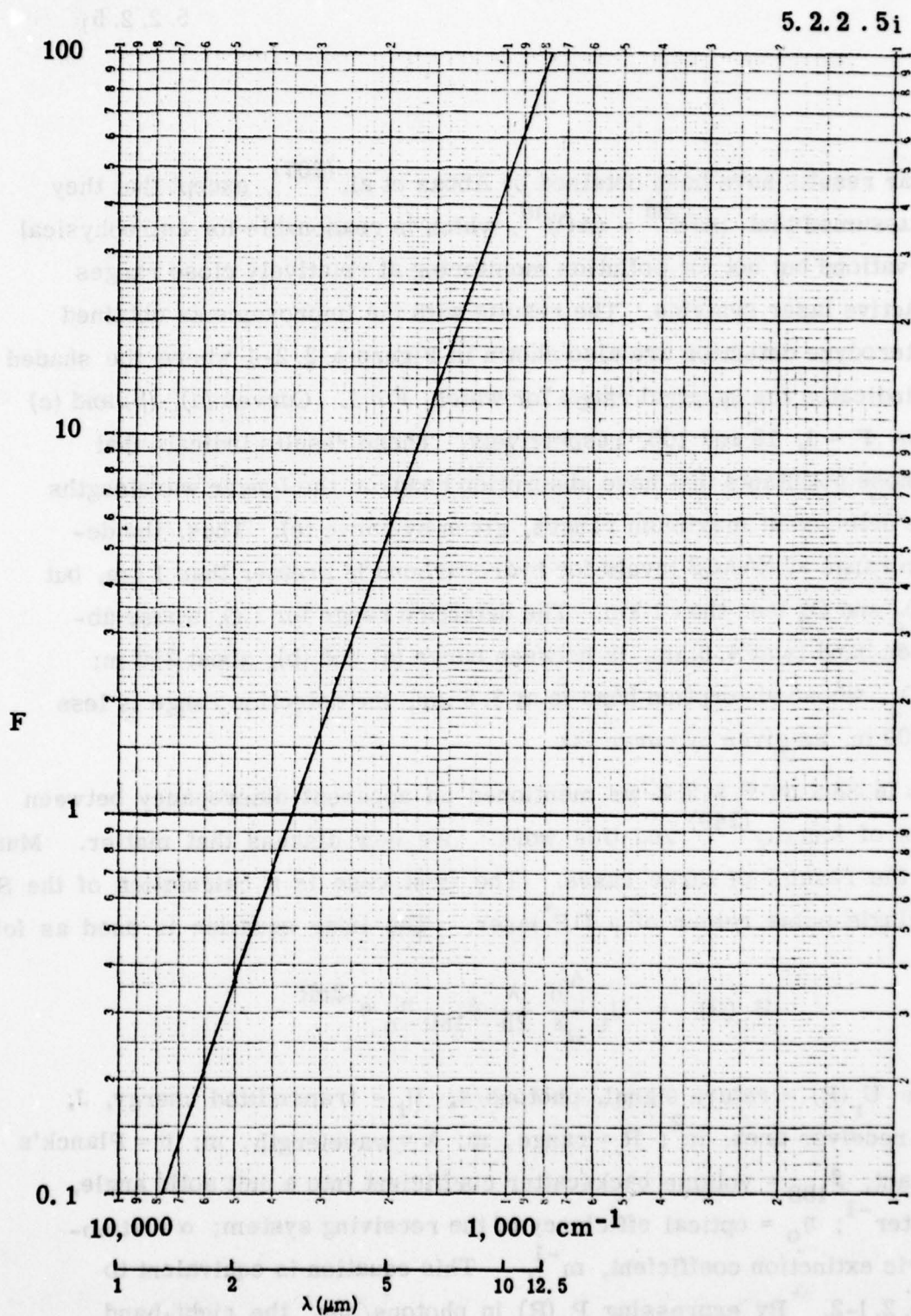


Figure
5.2.2-5.

The Ratio F Versus Wavenumber
(wavelength). For $F > 1$ the Heterodyne
Detection is Advantageous

Similar results have been obtained by Abbas et al.⁽²⁰⁷⁾, except that they have assumed that $(A\Omega)^{dd} = (A\Omega)^{hd}$, which is reasonable for astrophysical observations but not for pollution monitoring at relatively close ranges with active laser systems. The results with the improvements obtained by heterodyne detection are also shown in Figure 5. 2. 2-4 where the shaded area indicates the spectral range for which $F \geq 1$. Curves (a), (b) and (c) are for $F = 1, 10$ and 100 , respectively. These results indicate that only those pollutants that have absorption bands at the longer wavelengths can be detected at maximum ranges, given by curve (c). Thus, the detection range at NAAQS levels for hydrocarbons is greater than 1 km, but for SO_2 and O_3 less than 1 km. The detection range for CO, whose absorption band is at $4.6 \mu m$, is between curve (a) and (b), about 250 m; for NO_2 , whose absorption band is at $3.3 \mu m$, the detection range is less than 100 m, as given by curve (a).

In Section 5. 2. 2. 2 we mentioned an apparent discrepancy between results of Murray⁽²⁴⁹⁾ and this work. We now discuss that matter. Murray gives the results of three cases. The first case is a calculation of the SNR of a single pulse return of a DF^* laser. The lidar equation is used as follows:

$$U_r(R) = U_t \frac{A_o}{R^2} \frac{\lambda}{2h} \beta_{180} \eta_o e^{-2\alpha R}$$

where $U_r(R)$ = return signal, photons/s; U_t = transmitted energy, J; A_o = receiver area, m^2 ; R = range, m; λ = wavelength, m; h = Planck's constant; β_{180} = volume backscatter coefficient into a unit solid angle, $m^{-1}ster^{-1}$; η_o = optical efficiency of the receiving system; α = atmospheric extinction coefficient, m^{-1} . This equation is equivalent to Eq. 5. 2. 1-2. By expressing $P_r(R)$ in photons/sec, the right-hand side of the equation must be divided by $\Delta t h \nu = \Delta t hc/\lambda$, thus resulting in the above equation. The noise-equivalent-power is expressed as

* Deuterium Fluoride

$$\text{NEP} = \frac{\sqrt{\Delta f A_d}}{D^*} \frac{\lambda}{hc} \text{ Photons/sec}$$

The instrument and atmospheric parameters used by Murray are given in Table 5. 2. 2-1, together with values we have used (page 5. 2. 2. 5e). In the last column the ratio between Murray's and our values is given. One can see that Murray used instrument parameters that are more optimistic and/or indicate a larger system. The utilization of a laser with 1J energy output requires a beam expansion to almost 2m, according to Figure 5. 2. 1-8.

TABLE 5. 2. 2-1. DAS Instrument Parameters Used by Murray in Case 1 and This Work

Parameter	Murray	This Work Page 5. 2. 2. 5e	(Murray) This Work
η_o	. 5	. 01	50
$A_r(\text{cm}^2)$	11, 700	700	16. 7
$U_t(\text{J})$	1	. 014	71. 4
$\Delta t(\text{nsec})$	100	100	1
$L(\text{m})$	15	15	1
$\beta_{180}(\text{cm}^{-1}\text{sr}^{-1})$	8×10^{-9}	10^{-7}	8×10^{-2}
$\alpha(\text{cm}^{-1})$	$6. 57 \times 10^{-7}$	$10^{-4}-10^{-8}$	---
$D^*(\text{cm}\sqrt{\text{Hz}}/\text{w})$	10^{11}	10^{10}	10
$1/\sqrt{\Delta f}(1/\sqrt{\text{Hz}})$	$1/\sqrt{417}$	$1/\sqrt{2. 5 \times 10^6}$	$1. 3 \times 10^{-2}$
$1/\sqrt{A_d}$	$1/10^{-1}$	$1/10^{-2}$	10^{-1}

On the other hand, the backscattering coefficient used by Murray is more conservative than our assumed value. By multiplying all ratios of the last column, Murray has an advantage of about 60. The SNR based on his values is 115 for a horizontal range of 10 km, while it is about 2 for our values. Although some of our values can be improved (β_{180}), others, we feel, cannot be improved, such as η_0 and U_t . The reason is that (a) our experience indicates an overall efficiency of 1% being more realistic than 50% (Murray relates η_0 only to the optical efficiency of the receiving system, but neglects to incorporate other deficiencies, such as non-ideal response of the detecting, gating, amplifying and recording subsystems), and (b) a realistic beam diameter of 10 cm limits the laser energy to 0.014 J. Projecting these results to the DAS/DIAL mode, where four signals are ratioed and differenced, one can easily see why our projections are more pessimistic than Murray's.

We turn now to case 2, where Murray discusses the actual performance of a prototype CO₂ DIAL system. The results obtained with a mercury-cadmium-telluride detector having a time response of 0.98 μ sec are shown in Figure 5. 2. 2-6.

The absorption coefficients of H₂O for these three CO₂ laser lines are given in Table 5. 2. 2-1.

TABLE 5. 2. 2-1. Water-Vapor Absorption Coefficients

Line	ν , cm ⁻¹	α , 10 ⁻⁴ cm ⁻¹ atm ⁻¹
R(12)	970.547	1.60
R(18)	974.622	0.935
R(20)	975.931	8.65

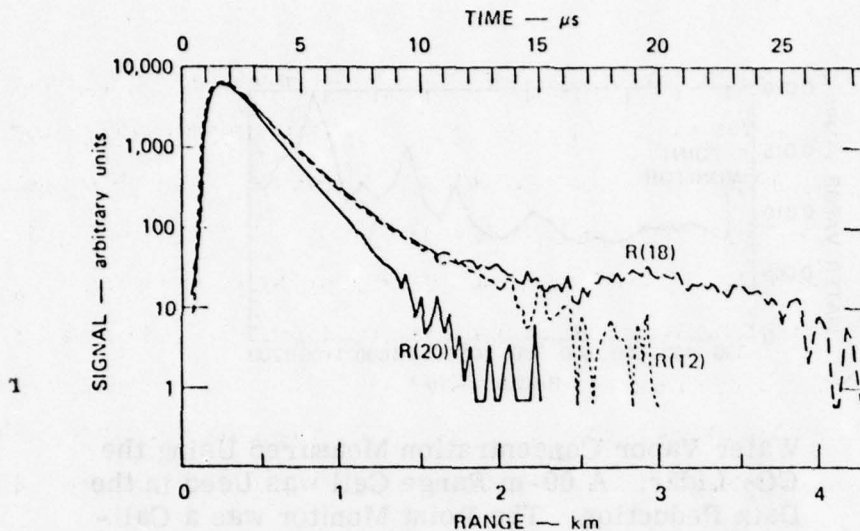


Figure
5. 2. 2-6.

Signal Backscattered from Atmospheric Aerosols for the R(12), R(18), and R(20) Lines on the 10- μ m Band of CO_2 . The R(20) Line is More Strongly Absorbed by Ambient H_2O than is the R(12) or R(18). The 0.98- μ s Detector was Used for These Results (Ref. 249)

Murray describes the appearance of the signal in Figure 5. 2. 2-6 and the data analysis as follows.

"The sharply rising aerosol return is characteristic of the geometric overlap of the transmitter and receiver. Following system convergence, the $1/R^2$ and the atmospheric attenuating losses decrease the signals, causing them to drop into the noise near 1.5 to 2.0 km. The differential between the R(20) and either the R(18) or R(12) line is readily apparent. The rate of change of the differential between these lines is proportional to the concentration of the absorbing species. The water vapor concentration was calculated from the DIAL concentration equation using the data of Figure 5. 2. 2-6. The resulting water vapor profile is shown in Fig 5. 2. 2-7 as a function of range. The point monitor was a recording hygrothermograph located on the roof of a building at a range of 300 m near the lidar

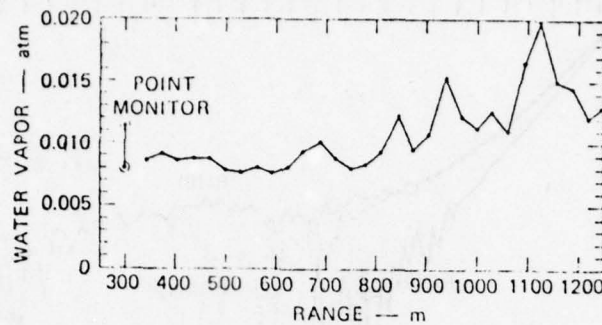


Figure
5. 2. 2-7.

Water Vapor Concentration Measured Using the CO_2 Lidar. A 60-m Range Cell was Used in the Data Reduction. The Point Monitor was a Calibrated Recording Hygrothermograph Located Near the Lidar Line-of-Sight.

line-of-sight. Good agreement is obtained between the point monitor and the lidar values for short ranges. The lidar-determined concentration appears to undergo random fluctuations at less than 1 km, whereas the return signal was relatively noise-free to a range of 1.5 km. This is indicative of the propagation of noise from the return signal through the concentration equation for the DIAL method. This demonstrates the distinction between the differential SNR and the SNR on the return signal."

Murray states that after those initial tests, changes have been made that improved the system by a factor of 2. That means that the concentration of water vapor can be observed in a DAS/DIAL mode up to about 1.2 km with the improved system. The absorption coefficients of H_2O as given in Table 5. 2. 2-1 are about 4 to 5 orders of magnitude smaller than those of pollutants, but this is compensated by the much smaller pollutant concentrations (4 to 5 orders). These results are significant. They show that Murray has successfully demonstrated with the present system that pollutants at concentration levels of interest to the NAAQS can be measured in a range-resolved mode up to distances

of about 1 km. This distance is significant for air pollution monitoring in the vicinity of airports. Of course, further optimization of the system is possible. However, some optimization is still needed for the present system to improve the range resolution and to reduce the laser energy to less than 1J/pulse.

In the third case discussed by Murray, he predicts the performance of an optimized range-resolved performance of the CO₂ laser lidar system. By using the following parameters

$$\begin{aligned}
 U_t &= 15 \text{ J/pulse} \\
 A_r &= 1.17 \text{ m}^2 \\
 \lambda &= 10.0 \text{ } \mu\text{m} \\
 \eta_o &= 0.5 \\
 \beta_{180} &= 1.2 \times 10^{-7} \text{ m}^{-1} \text{ ster}^{-1} \\
 \alpha &= 0.0927 \text{ km}^{-1} \\
 D^* &= 2(10^{10}) \text{ cm}\sqrt{\text{Hz}}/\text{W}
 \end{aligned}$$

he obtains a SNR of 50 for a single pulse at a range of 10 km. From this he concludes that high-sensitivity range-resolved measurements are feasible at 10 km. Longer range or higher sensitivity can be obtained using multipulse integration. Murray then calculated the sensitivity of the CO₂ laser lidar system to different gases based on a system SNR of 200. He calculated the sensitivity values of 16 representative compounds that are shown in Table 5. 2. 2-2. As can be seen the absorption coefficients vary widely. Those for carbon dioxide and water vapor are relatively small, which is necessary to permit long-range transmission of the beam. The absorption coefficient

TABLE 5. 2. 2-2. Calculated CO₂ Lidar System Sensitivities

Species		Absorption Coefficient (cm ⁻¹ atm ⁻¹)	Sensitivity (ppb-km)
Name	Formula		
Ammonia	NH ₃	120.0	0.42
Benzene	C ₆ H ₆	2.3	22.
1,3 butadiene		3.45	15.
Carbon dioxide	CO ₂	1.8 (10 ⁻³)	28000.
Ethylene	C ₂ H ₄	33.0	1.5
Freon 113	C ₂ Cl ₃ F ₃	19.2	2.6
Freon 11	CCl ₃ F	31.0	1.6
Freon 12	CCl ₂ F ₂	92.0	0.55
Methanol	CH ₃ OH	19.4	2.6
Ozone	O ₃	12.7	4.0
Perchloroethylene	C ₂ Cl ₄	28.5	1.8
Sulfur dioxide	SO ₂	6.73	7.5
Sulfur hexafluoride	SF ₆	800.0	0.063
Trichloroethylene	C ₂ HCl ₃	14.0	3.6
Vinyl chloride	C ₂ H ₃ Cl	6.79	7.4
Water vapor	H ₂ O	8.36 (10 ⁻⁴)	60000.

of many other gases is quite high, yielding a sensitivity of a few parts per billion in a kilometer. Murray concludes that range-resolved multigas monitoring of these gases appears feasible at 10 km range with commercially available components.

We do not agree with these predictions, because

- the assumed laser energy is too high by a factor of about 10³ (eye safety),
- no overall efficiency factor is included in the calculation, which may degrade the performance by a factor 50,
- pollutant absorption along the line-of-sight becomes significant beyond 1 km, a fact not considered by Murray (he confined the pollutant into a slab whose depth is apparently the resolution length), and

- the calculations were based on the lidar performance of a detector-noise limited system. In reality, the ratio of two differenced signals (using thus four signals) has to be evaluated, where the atmospheric scintillation will most probably be the dominant noise.

5. 2. 3 Active (Pulsed) System: Raman Scattering

5. 2. 3. 1 Principle of Operation

The Raman effect is an inelastic scattering process in which the energy of the scattered photon is either greater (anti-Stokes) or less (Stokes) than the incident photon, because the scattering molecule has either lost or gained energy from the incident photon. The scattered radiation follows the angular distribution of the Rayleigh elastic scattering. A schematic of the different Raman scattering processes (including rotational Raman) is given in Figure 5. 2. 3-1. (Note, that these Raman processes are only for molecules whose electronic angular momentum Λ is zero. For molecules with $\Lambda \neq 0$, additional transitions $\Delta J = \pm 1$, are allowed).

Figure 5. 2. 3-2 shows a typical Raman spectrum at 300°K. The spectrum is for a (00°0) to (10°0) transition in CO₂. The Q branch has the same rotational fine structure as the O and S branches, but the displacement between the lines is very small. For example, for CO₂ the width of the Q branch is only 0.3 cm⁻¹, and the line strength is about ten times larger than for the O and S branches. ⁽⁸⁴⁾

A set of parameters for ground-state Q-branch Raman is shown in Table 5. 2. 3-1, as measured by different investigators ⁽⁸⁵⁻⁸⁸⁾ and given by DeLong ⁽⁸⁹⁾. The relative cross sections are in respect to nitrogen, which is given as $\sigma_{N_2}(3471.5 \text{ \AA}) = 3.03 \times 10^{-29} \text{ cm}^2/\text{molecule}$.

Another list was compiled by Inaba and Kobayasi ⁽⁹⁰⁾, which is given in Table 5. 2. 3-2, using data from various investigators.

5. 2. 3. 1b

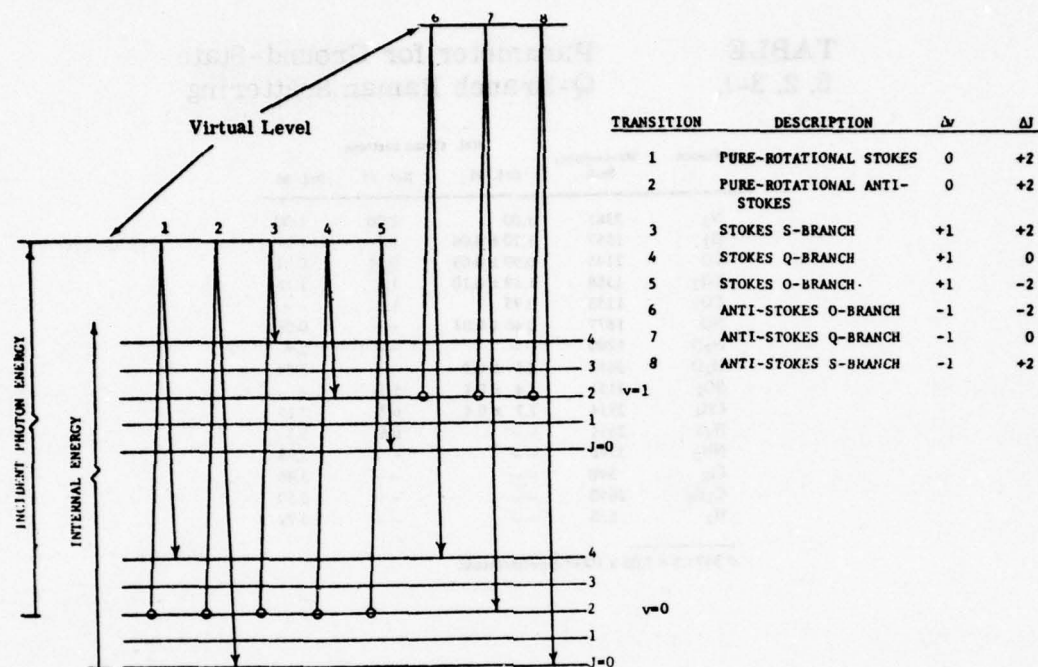


Figure
5. 2. 3-1.

Molecular Vibration-Rotation
Transitions in Raman Scattering

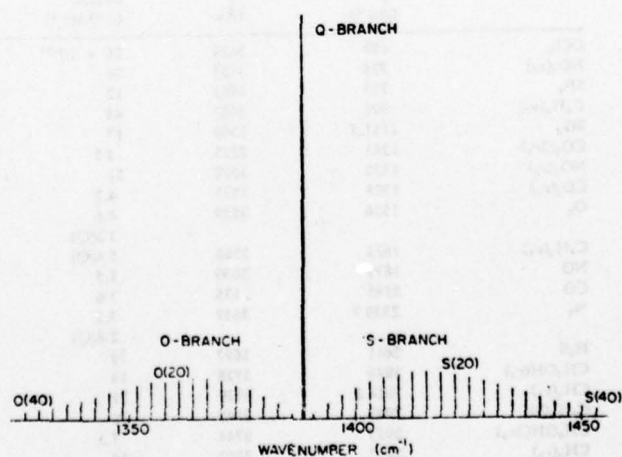


Figure
5. 2. 3-2.

Calculated Raman Spectrum for CO_2 for the
(00°0) to (10°0) Transition at 300°K.

TABLE
5. 2. 3-1. Parameter for Ground-State
Q-Branch Raman Scattering

Pollutant	Wavenumber Shift	Rel. Cross Sections		
		Ref. 86	Ref. 87	Ref. 88
N ₂	2381	1.00	1.00	1.00
O ₂	1557	1.20 ± 0.06	1.2	1.21
CO	2145	0.99 ± 0.05	0.91	0.81
CO ₂	1388	1.49 ± 0.10	1.5	1.18
CO ₂	1288	0.95	1.0	--
NO	1877	0.46 ± 0.03	--	0.08
N ₂ O	1290	--	--	2.9
H ₂ O	3652	2.5 ± 0.3	--	3.24
SO ₂	1151	5.4 ± 0.5	5.5	--
CH ₄	2914	7.7 ± 0.4	6.7	7.15
H ₂ S	2611	--	6.6	5.5
NH ₃	3340	--	--	3.98
Cl ₂	540	--	--	3.46
C ₂ H ₆	2650	--	--	5.50
H ₂	530	--	--	6.29

$\sigma_{3471.5} = 3.03 \times 10^{-29} \text{ cm}^2/\text{molecule.}$

TABLE
5. 2. 3-2

List of Raman Frequency Shifts and Measured Differential Raman Backscattering Cross Sections of Various Gaseous Molecules Present in the Atmosphere. These Data are Referred to the Incident Wavelength of 3371 Å.

Molecule	ν_j (cm ⁻¹)	λ_r (Å)	$d\sigma/d\Omega$ (cm ² str ⁻¹)
CCl ₄	459	3424	26 × 10 ⁻³⁰
NO ₂ (ν_2)	754	3457	24
SF ₆	775	3461	12
C ₆ H ₆ (ν_2)	991	3487	44
SO ₂	1151.5	3508	17
CO ₂ (2 ν_2)	1285	3525	3.1
NO ₂ (ν_1)	1320	3528	51
CO ₂ (ν_1)	1388	3537	4.2
O ₃	1556	3559	4.6
C ₂ H ₄ (ν_2)	1623	3566	3.3(Q)
NO	1877	3600	5.4(Q)
CO	2145	3635	1.5
N ₂	2330.7	3659	3.6
			3.5
			2.8(Q)
H ₂ S	2611	3697	19
CH ₃ OH(ν_2)	2846	3728	14
CH ₄ (ν_1)	2914.2	3739	21
C ₂ H ₅ OH	2943	3742	19
CH ₃ OH(2 ν_2)	2955	3744	7.5
CH ₄ (ν_2)	3017	3752	14
C ₂ H ₄ (ν_1)	3020	3753	16(Q)
C ₂ H ₆ (ν_1)	3070	3760	30
NH ₃	3334	3798	11
H ₂ O	3651.7	3844	7.8(Q)
H ₂	4160.2	3922	8.7

Note that the cross sections are given at a wavelength λ_0 . They change with wavelength according to

$$\sigma_{\lambda} = \sigma_0 \left(\frac{\lambda_0}{\lambda} \right)^4$$

In comparison with Rayleigh cross sections, the Raman cross sections are smaller by 3 to 4 orders of magnitude.

The schematic of a co-axial Raman system is similar to the one shown in Figure 5. 2. 1-1. The difference is in the details of the detection system, which must be able to detect backscattered signals at a different wavelength than the transmitted one. One such schematic is shown in Figure 5. 2. 3-3. (85)

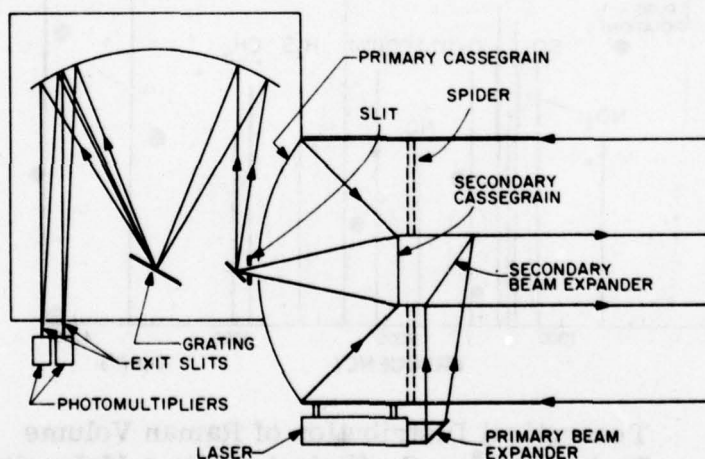


Figure 5. 2. 3-3. Schematic of Remote Raman System (Ref. 35)

The lidar equation 5. 2. 1-1 is directly applicable, except for substituting the backscattering coefficient β with the differential Raman cross section $d\sigma_R/d\Omega$, and introducing additional terms corresponding to the transmitted and backscattered wavelengths. Thus,

$$P(R) = \eta_o P_t L N(R) \frac{d\sigma_R}{d\Omega} A R^{-2} \tau_A(\lambda_t, R) \tau_A(\lambda_{Ram}, R) \quad (5. 2. 3-1)$$

As an example, Inaba and Kobayasi⁽⁹⁰⁾ have presented a theoretical plot of the distribution of Raman volume backscattered coefficient due to a mixture contained in a typical oil smoke as a function of Raman shifted frequency (cm^{-1}) (see Figure 5. 2. 3-4).

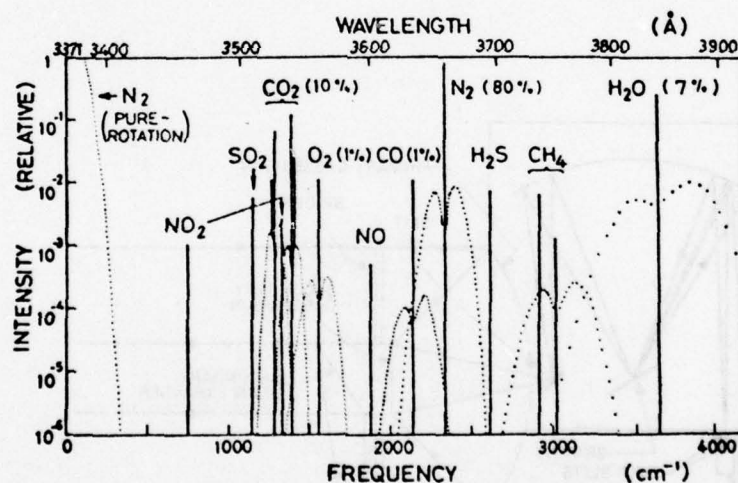


Figure
5. 2. 3-4

Theoretical Distribution of Raman Volume
Backscattering Coefficient due to a Molecular
Mixture Contained in a Typical Oil Smoke as a
Function of Raman-Shifted Frequency

This theoretical distribution may be compared with measured ones for "clean air" (Fig 5. 2. 3-5), "oil smoke" (Fig 5. 2. 3-6) and "automobile exhaust" (Fig 5. 2. 3-7).

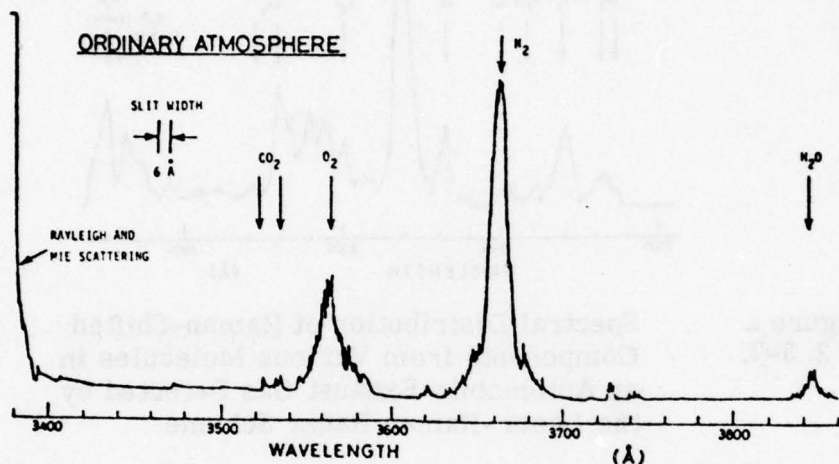


Figure
5. 2. 3-5.

Measured Spectrum of Raman-Shifted and Unshifted Backscatters from the Ordinary Atmosphere

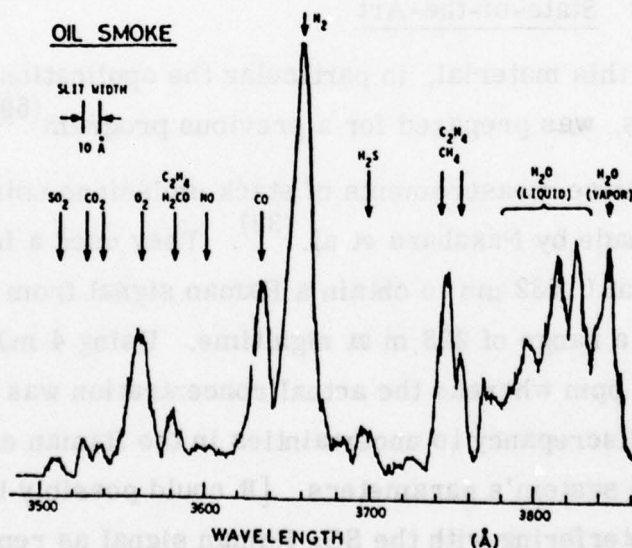


Figure
5. 2. 3-6

Spectral Distribution of Raman-Shifted Components from a Variety of Molecular Species in an Oil Smoke Plume Remotely Analyzed by the Laser-Raman Radar Method

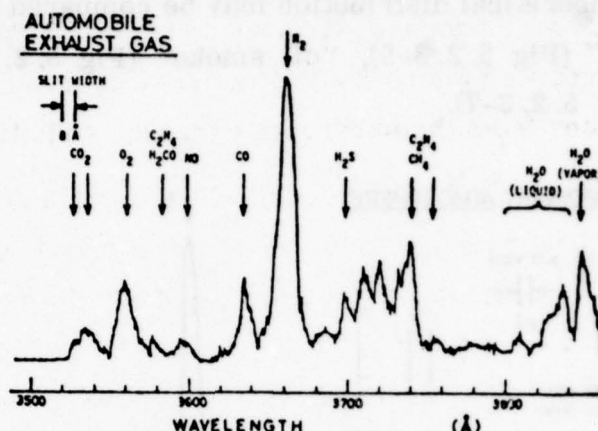


Figure 2
5. 2. 3-7.

Spectral Distribution of Raman-Shifted Components from Various Molecules in an Automobile Exhaust Gas Detected by the Laser-Raman Radar Scheme

5. 2. 3. 2 State-of-the-Art

Part of this material, in particular the application of measurements to stack plumes, was prepared for a previous program⁽⁵⁹⁾.

Quantitative measurements of stack emissions using the Raman method were made by Nakahara et al.⁽³⁸⁾. They used a frequency doubled Nd: YAG laser at 0. 532 μ m to obtain a Raman signal from SO₂ in a smoke-stack plume at a range of 228 m at nighttime. Using 4 mJ pulses, they measured 1850 ppm whereas the actual concentration was 1000 ppm. They attributed the discrepancy to uncertainties in the Raman cross-section for SO₂, and in the system's parameters. [It could possibly be due to NO₂ fluorescence interfering with the SO₂ Raman signal as reported by three of the authors in the later paper (Reference 116)]. They calculate that 80 ppm of SO₂ can be detected at nighttime with a 10 mJ laser, at a range of 283 m, with a resolution element of 9 m, using an integration time of

about 4 minutes. In addition to measuring SO_2 , they use the Raman signal from N_2 to measure the scattering optical thickness (opacity) of the plume, by observations from the same range through and off the plume.

Melfi et al.⁽⁹¹⁾ made a qualitative nighttime observation of SO_2 in a plume 5 m above the top of the stack using a ruby laser at 6943 Å. Using 1.5 J pulses at a repetition rate of 1 pps averaged over 100 seconds, they detected SO_2 at a range of 210 m with a 3.7 m resolution element. They found good qualitative agreement between the SO_2 Raman intensity and the plant's electrical power output.

Although the two Raman systems discussed above were designed for SO_2 , Inaba and Kobayasi⁽⁹⁰⁾ report on a N_2 laser (3371 Å) demonstration system with a monochromator rather than a filter system. Using this system at a range of 30 m and a resolution of 3 m they analyzed the Raman spectrum from oil smoke and automobile exhaust gas. Using 0.2 mJ pulses with a repetition of 50 pps and a 5 sec integration time, they identified signals from SO_2 , C_2H_4 , H_2CO , NO , CO , H_2S , CH_4 , in addition to the usual CO_2 , O_2 , N_2 and H_2O .

Other field measurements using the Raman method were made by groups from Block Engineering and Edgewood Arsenal [DeLong⁽⁸⁹⁾]. The system uses a frequency doubled ruby laser (0.347 μm) operating with 80 to 160 mJ per pulse at two pulses per second. Daytime field tests have measured controlled amounts of SO_2 (30 ppm), kerosene (1.7 ppm), HNO_3 (7 ppm) and organo phosphate (.04 ppm) at a range of 200 m with a resolution length of 10 m, using an integration time of about 1 minute. Based on these measurements and relative Raman cross-sections, DeLong⁽⁸⁹⁾ projected the sensitivity of the present system to other gases, and compared them with calculated values as shown in Table 5. 2. 3-3. Note that the nighttime sensitivities are about a factor of two better than those in daytime.

TABLE
5. 2. 3-3.Projected and Calculated Sensitivities
and System Parameters (Ref. 89)

Material	Spectral Shift (cm ⁻¹)	Spectral Position (Å)	Projected Day Sensitivity		Calculated Sensitivity	
			(ppm)	Ref. (21)	Day (ppm)	Night (ppm)
N ₂	2331	3777	313		215	124
O ₂	1557	3670	262		179	103
CO	2145	3751	317	86	217	125
CO ₂	1388	3647	210	62	144	83
CO ₂	1288	3634	330		227	130
NO	1877	3713	682		468	269
N ₂ O	1290	3634	108		74	43
H ₂ O	3652	3976	125	19	86	49
SO ₂	1151	3616	58	5	39	23
CH ₄	2914	3862	41	9	28	16
H ₂ S	2611	3818	57	12	39	22
NH ₃	3340	3927	79		54	31
Cl ₂	540	3538	91		62	36
C ₂ H ₆	2650	3823	57		39	22
H ₂	530	3536	50		34	20

Present Instrument Parameters	
Collector Diameter, cm	91.4
Transmitter Efficiency	0.9
Receiver Efficiency	0.075
Detector Quantum Efficiency	0.3
Laser Energy @ 3471.5 Å, J	0.083
Receiver Bandwidth, u	0.0005
Receiver Field of View, sr	1 x 10 ⁻⁶
Atmospheric Transmission	0.89
Range, cm	2 x 10 ⁴
Range Gate, cm	10 ³

Smith⁽⁹²⁾, Barrett⁽⁹³⁾, and Klainer⁽⁹⁴⁾ have suggested a method of enhancing the Raman sensitivity by using a Fabry-Perot interferometer in conjunction with the rotational Raman lines instead of the vibrational lines used in the systems discussed above. The rotational lines are periodically spaced and may be multiplexed by using the Fabry-Perot as a filter with similar periodic transmission peaks. Klainer suggests an increased sensitivity factor over vibrational Raman of 50 for HCl and 150 for CO₂.

Gelbwachs and Birnbaum⁽⁹⁵⁾ have suggested a problem with the Raman technique due to fluorescence of aerosols which they observed in some in-situ measurements. They estimate that the aerosol fluorescence signal can be equivalent to the Raman signal from 600 ppm of SO₂, or 6000 ppm of NO, or 3000 ppm of CO.

Leonard and Caputo⁽⁹⁶⁾ have used the Raman shifted backscattered signal from N₂ to determine the atmospheric transmission. As already pointed out, a major difficulty in the interpretation of pulsed lidar backscatter data is that unless a priori information is available concerning the relationship between the volume backscattering coefficient and the attenuation coefficient, the received intensity cannot be easily evaluated as transmittance. The backscatter coefficient for Raman scattering, however, depends only on the Raman cross-section of the specific molecule used and the number density of that molecule. In the lower atmosphere the density of atmospheric nitrogen is constant. A measurement of Raman scattering from nitrogen will therefore give a direct determination of transmission as a function of range. Authors report about experiments conducted over a 1/4-mile range that produced consistent results for transmissions down to as low as 2 percent when compared with simultaneous double-ended reference transmissometer data. Typical results as obtained by the authors are shown in Figure 5.2.3-8. The square of the transmission (T^2) through the smoke bank is obtained by taking the ratio of the change in Raman scattering intensity level at the range gates beyond the smoke bank. As shown, the T^2 value is 0.021 corresponding to a transmission, T of 0.145 or 14.5 percent. Estimates of remotely detecting acid aerosols by Raman backscattering are presented by Dylis⁽⁹⁷⁾. A detectivity of 60 ppb at 6 km (night) is calculated for a system with a collecting diameter of 91.4 cm and 1 J/pulse laser power at 3472 Å.

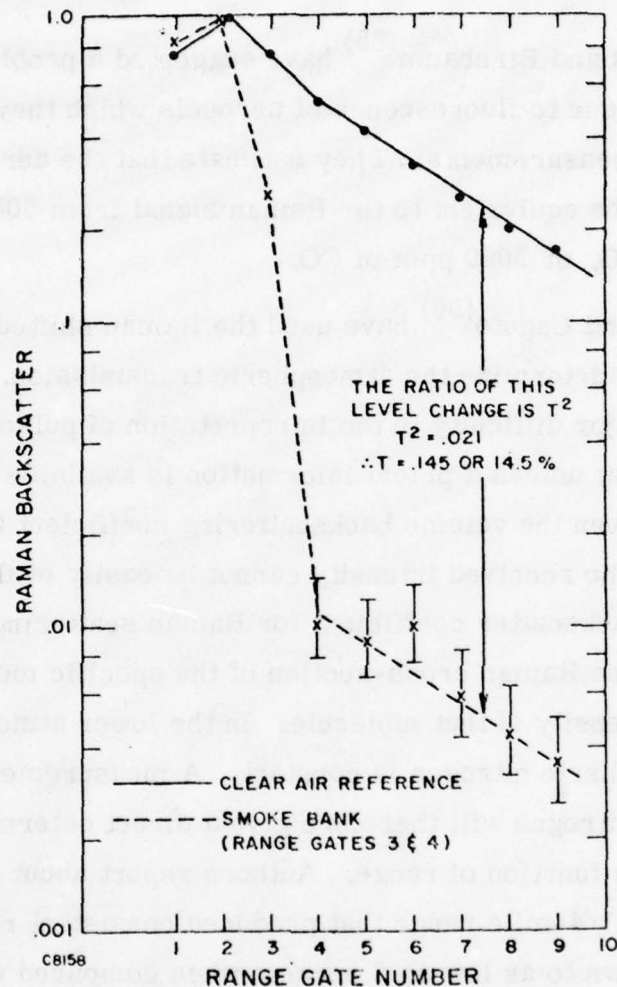


Figure
5. 2. 3-8

Raman Backscatter as Function of Range (Ref. 96).

Field data were recently obtained by Poultney et al. ⁽⁹⁸⁾, who made ten percent measurements of 1.2×10^3 ppm SO_2 in 15 minutes using a 1.5 J ruby laser at 30 pulses/min, and an 8-inch receiver. Certainty of measurement accuracy was checked, by measuring known concentrations of SO_2 in a tank, by tuning the filters on and off the specific Raman

line, by varying the CO_2 concentration to very high levels while in SO_2 operation, and by viewing the tank through aerosol veils typical of plumes from stacks with efficient precipitators. The results are presented in Figure 5. 2. 3-9.

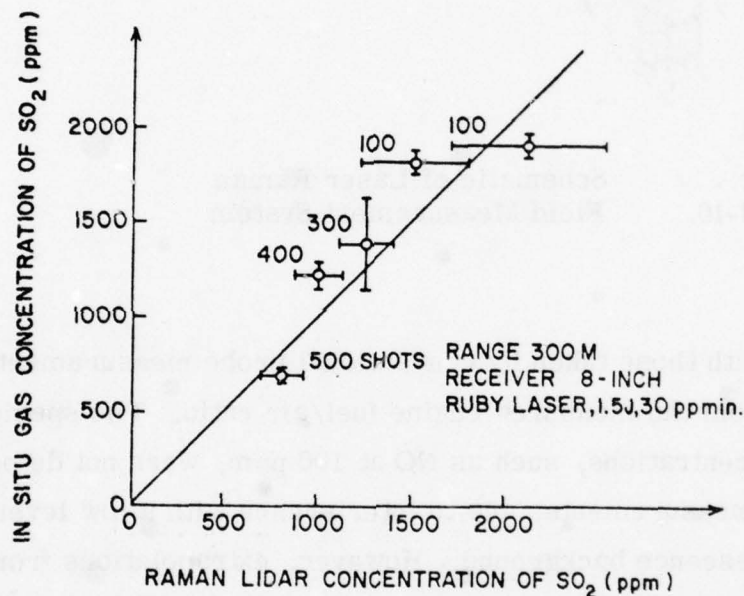


Figure 5. 2. 3-9. Comparison of Raman Scattered Signal from SO_2 in Tank vs. In-Situ Values

Although the system developed by Leonard^(99, 100) is not for remote sensing over large distances, it is nevertheless a system that is designed to measure the species concentrations in jet exhausts on a non-interfering basis, as shown in Figure 5. 2. 3-10. Leonard obtained data for the concentrations of O_2 and CO_2 which were in excellent

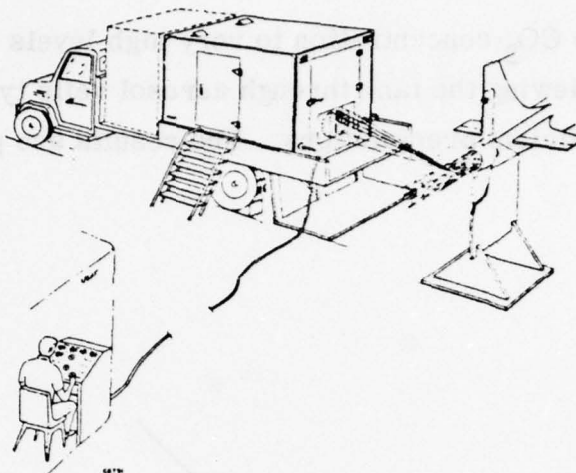


Figure 5. 2. 3-10. Schematic of Laser Raman Field Measurement System

agreement with those taken by conventional probe measurements and calculated from the measured engine fuel/air ratio. The species present at lower concentrations, such as NO at 100 ppm, were not detected in actual field measurements, due to interference with a low level hydrocarbon fluorescence background. However, extrapolations from the data obtained indicate that a refurbished optical system operating at its nominal design throughput could detect NO at 100 ppm in less than 5 minutes integration time. Temperature profiles of the engine exhaust were also obtained from the Raman spectra (see Fig 5. 2. 3-11) which were in good agreement with thermocouple measurements, although at higher power levels the Raman data are higher than the (uncorrected) thermocouple data⁽⁹⁹⁾.

5. 2. 3. 2h

5. 2. 3. 3a

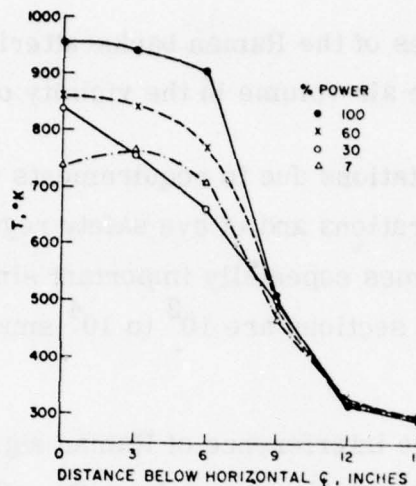


Figure
5. 2. 3-11.

Temperature Profiles of T-53
Engine Exhaust Using Raman
Density Method

5. 2. 3. 3 Advantages/Disadvantages

Basically, the advantages using a remote Raman backscattering system to measure gaseous pollutants are similar to those listed for the differential absorption system in Section 5. 2. 2. 3. However, a definite advantage of the Raman system is that it does not require tuning (similar to the LIDAR system described in Section 5. 2. 1) and many pollutants will exhibit Raman signals simultaneously without having to use different laser frequencies. The systems complexity is somewhat less than for a DIAL/DAS system. On the other hand, while the advantages clearly outweighed the disadvantages for the DAS/DIAL systems, this is not the case for the Raman system as will be apparent in the enumeration of the disadvantages. The use of Raman signals backscattered from atmospheric N_2 for the measurement of atmospheric transmission and, thus, the determination of the particulate concentration or mass loading, could potentially be more advantageous than the LIDAR system.

The disadvantages of the Raman backscattering system to measure gaseous pollutants in the air volume in the vicinity of an airport are:

- (a) Operational limitations due to requirements of non-interference with airport operations and of eye safety regulations; the latter restriction becomes especially important since the Raman back-scattering cross sections are 10^2 to 10^4 smaller than the Rayleigh cross sections.
- (b) potentially severe interference of Raman signals between the abundant molecules in the atmosphere (N_2 , O_2 , H_2O , CO_2) and pollutants;
- (c) excitation of other processes such as molecular and aerosol fluorescence, masking the Raman signals;
- (d) large photon flux (noise) from sun scattered light during daytime, if not used in the solar-blind spectral region ($\lambda \leq 3000 \text{ \AA}$).

5. 2. 3. 4 System and Operational Requirements

The systems requirements and operational limitations due to airport operations will, in general, be the same as for the LIDAR and DAS/DIAL systems. However, because of the small backscattering cross sections, more laser power is required to receive signals with a signal-to-noise ratio (SNR) greater than unity. But because of the eye safety regulations, the laser power cannot be employed. More details are given in the next section.

5. 2. 3. 5 Analysis and Critique

As already mentioned, the small Raman cross section make the system not usable for measuring pollutants in the ambient air, except in the case where the N_2 signal is used for the measurement of particulate matter. The magnitude of the problem may be appreciated by recalling the field data obtained by Poultney et al.⁽⁹⁷⁾, who used a ruby laser with 1.5 J to measure ~ 800 ppm of SO_2 at a distance of 300 m within ± 12 percent error. For an (assumed) pulse length of 100 nsec, the beam would have had to be expanded to over 20 m to meet the eye safety regulations, according to curve (d) in Figure 5.2.1-8, since the laser wavelength is in the visible. For a more reasonable beam diameter of 20 cm, the laser power would have to be lowered to about 10^{-4} J, resulting in a noise-equivalent-concentration (SNR = 1) of about 20,000 ppm at a distance of 10 m during daytime, rapidly increasing with range. Thus, it is seen that a Raman system working in the visible is much too insensitive to be useful.

We will now estimate the performance of a system which takes advantage of many optimized instrument parameters, such as working in the solar blind region ($\lambda < 3000 \text{ \AA}$) and using large collecting optics (2 ft. diameter). It will be shown that even for such a system, the achievable sensitivities are not good enough to make it a practical system.

The signal-to-noise ratio (SNR) in a photon counting device is given by the expression⁽¹⁰¹⁾

$$SNR = \frac{\eta' U(R) n}{\sqrt{\eta' n U(R) + \eta' n U_B + N_D}} \quad (5.2.3-2)$$

where η' is the quantum efficiency of the photomultiplier, n is the number of pulses, $U(R)$ is the count of the signal photons, U_B is the count of the background photons, and N_D is the dark current equivalent noise input.

The signal photons are expressed through Eq. 5. 2. 3-1, where the conversion between Joules and photons is as follows:

$$U(\text{photons}) = U(J)/h\nu = U(J) \lambda(\text{cm})/hc$$

$$\text{where } hc = 6.62 \times 10^{-34} \times 3 \times 10^{10} = 2.0 \times 10^{-23} \text{ J cm.}$$

The dark current equivalent noise input N_D may be neglected in comparison with signal noise, particularly when the photomultiplier is cooled. During night or in the sun-blind spectral region, the background noise is also negligible in comparison with the signal noise. Thus, Eq. (5. 2. 3-2) may be written as

$$\text{SNR} = \sqrt{n \eta' U(R)} \quad (5. 2. 3-3)$$

Introducing Eq. (5. 2. 3-1) and solving for $N(R)$ we obtain

$$N(R) = \frac{(\text{SNR})^2 R^2}{Q' \tau_A(\lambda_t, R) \tau_A(\lambda_{\text{Ram}}, R)} \quad (5. 2. 3-4)$$

$$\text{where } Q' = \eta \eta' n P_t L \frac{d\sigma_R}{d\Omega} A \lambda_t / \lambda_{\text{Ram}}.$$

Assuming $\eta = .1$, $\eta' = .2$, $n = 100$, $U_t = 1.5 \times 10^{-2} \text{ J} = 2.3 \times 10^{16}$ photons at 3000 \AA (derived from the MPE and an assumed beam diameter of 20 cm), $L = 15 \text{ m}$, $d\sigma_R/d\Omega \approx 10^{-29} \text{ cm}^2 \text{-sr}^{-1}$, $A = 2.92 \times 10^3 \text{ cm}^2$ (2 ft. diameter) and $\lambda_t \approx \lambda_{\text{Ram}}$, the numerical value for Q' becomes

$$Q' = 2.015 \times 10^{-6} \text{ photons} \times \text{cm}^5$$

The values for the atmospheric transmission can be much less than unity, but are set here equal to unity. Thus, for a 10% measurement (SNR = 10), Eq. (5. 2. 3-4) becomes

$$N(R) \approx 5 \times 10^{11} R^2 \quad (R \text{ in m, } N(R) \text{ in cm}^{-3})$$

In order to express $N(R)$ in ppm, this expression is referenced to the number of molecules per cc, at atmospheric pressure and temperature, i. e., $2.7 \times 10^{19} \text{ cm}^{-3}$. Thus,

$$N'(R) \approx 1.8 \times 10^{-2} R^2 \quad (R \text{ in m, } N'(R) \text{ in ppm})$$

The results are shown in Figure 5. 2. 3-12. Also indicated are the levels of the NAAQS for the different prime gaseous pollutants. It can be seen that the sensitivity extends to a range of less than 30 m for all pollutants. Thus, it is clearly demonstrated in these simplified but optimistic calculations that even an optimized Raman system would not be a useful tool for remote monitoring.

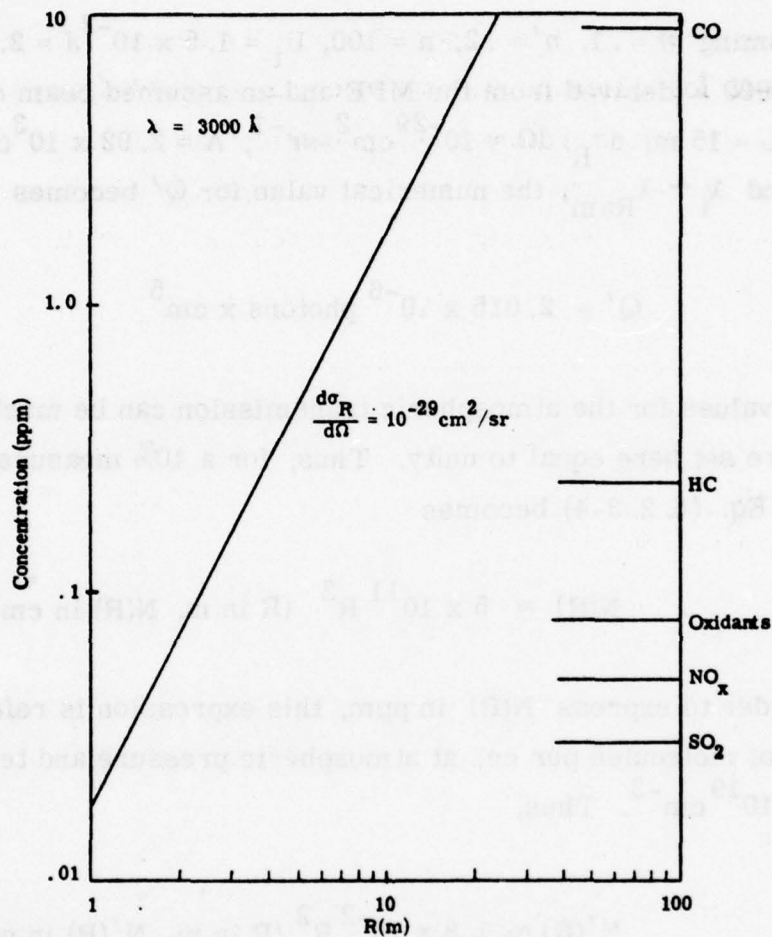


Figure 5. 2. 3-12. Determination by Raman of Concentration within 10% versus Range, using 100 Pulses and a Gate Length of 15 m.

Similar results were obtained by Derr and Little⁽¹⁰¹⁾, who calculated the number of photoelectrons per 10 m range increment for a single pulse as a function of range. The peak power was assumed to be 100 kW, pulse width was 10 nsec, the filter bandwidth was 10 Å at 3371 Å, the receiver diameter was 25 cm and the optical and detector quantum

efficiencies were 75% and 18%, respectively. The results are shown in Figure 5. 2. 3-13 for different atmospheric gases. Of particular interest in this figure are the levels of background photoelectrons during different sky conditions. At the right-hand side of this figure are indicated the levels of noise photoelectrons for some common photomultipliers.

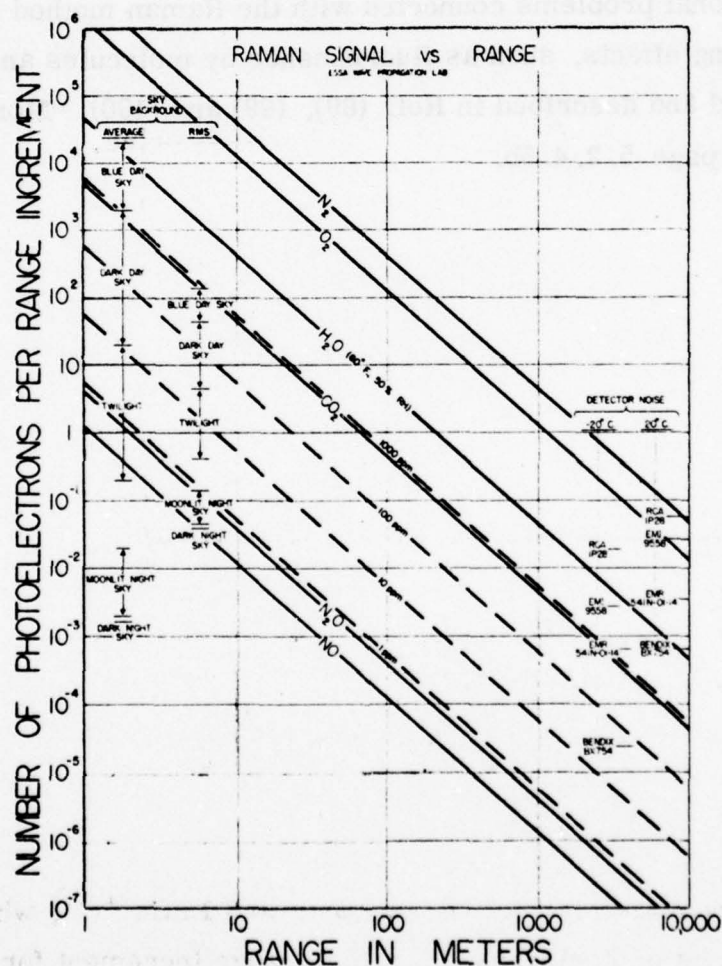


Figure
5. 2. 3-13.

Raman Lidar Signal versus Range, and
Background and Detector Noise Magnitudes

The experimental results shown by Hirschfeld et al. ⁽¹⁰²⁾ for daylight observations of 30 ppm SO₂ at a distance of 200 m appear to be better by approximately a factor of 5 than the theoretical results shown in Fig 5. 2. 3-12. Unfortunately, Hirschfeld et al. do not present enough details to compare their instrument parameters with the ones we have used.

Additional problems connected with the Raman method have to do with interfering effects, such as fluorescence by molecules and aerosols, already quoted and described in Ref. (89), (99) and (100). More details are given on page 5. 2. 4. 5b.

5. 2. 4 Active (Pulsed) System: Resonant Raman/Fluorescence

5. 2. 4. 1 Principle of Operation

The weak Raman scattering discussed in Section 5. 2. 3 can be enhanced by moving the incident laser wavelength close to a single isolated absorption line. The characteristics of this inelastic-scattered radiation, now called "resonant Raman", is the same as the non-resonant Raman, except that the magnitude of the signal is increased. If the wavelength of the incident laser beam is too close and, in the limit, overlaps completely, then absorption will occur. This absorption will be followed by fluorescence. The characteristics of this radiation are different, because the two-step process (absorption-emission) is subject to collisional quenching. Note that the two processes, resonant Raman and fluorescence, may occur simultaneously, but in varying degrees, depending upon many conditions, besides the closeness of the incident and absorbing wavelengths. It is clear that it is very difficult to distinguish experimentally between the two processes. Therefore, many workers^(103, 104) do refer to the two processes as one phenomena that may conveniently be called "resonance scattering*". However, it should be remembered that in any given situation either of the two processes may dominate so that the experimental observation may be concerned with that process only⁽¹⁰⁵⁻¹⁰⁹⁾.

Wright et al.⁽¹¹⁰⁾ have identified four resonant processes, instead of the two described above. They have differentiated between resonant Raman, "off-resonance fluorescence", "resonant fluorescence" and "broad fluorescence". These processes, together with the non-resonant Raman, are schematically shown in Figure 5. 2. 4-1. A description of these processes is taken from Reference 110.

* Strictly speaking, fluorescence is not a scattering process since absorption of the incident photon takes place.

"In each case, some vibrational levels of the ground electronic state and of an excited electronic state are shown. The initial, final, and intermediate molecular states are labeled i, f, and m, respectively. ω_L and ω_s are the energies of the incident and scattered photons. Case (a) is ordinary Raman scattering (ORS), where the laser photon energy falls far below the excited band. Many intermediate states are excited, but only weakly because of the large energy mismatch between the excited-state energies of the molecule and the photon energy of the laser. Case (b) represents resonance Raman scattering (RRS), where the laser photon energy falls near the electronic absorption band. Many intermediate states are again excited, but more strongly than in case (a) because of the smaller energy mismatch. In process (c), the laser line falls within the absorption band, but outside the linewidths of all molecular levels. The contribution from the few intermediate states that are nearest to the laser photon energy dominates in the scattered intensity. This process will be called "off-resonance fluorescence" (ORF). It is often referred to as "resonance Raman scattering," however. Case (d) is resonance fluorescence (RF), where the laser photon energy falls within the width of a molecular level. This single intermediate state will dominate the scattered intensity. In case (e), the laser photon energy again falls within the absorption band, but the excited molecule undergoes one or more inelastic collisions before it can reradiate. Because of the possible transfer of energy to translation and rotation, ω_s can take on a nearly continuous range of values, so that this process gives rise to a broad continuum in the scattered spectrum. Therefore, it will be called "broad fluorescence" (BF). In contrast, ω_s in processes (a), (b), (c), and (d) takes on discrete values, so that these processes yield "spikes" in the scattered spectrum."

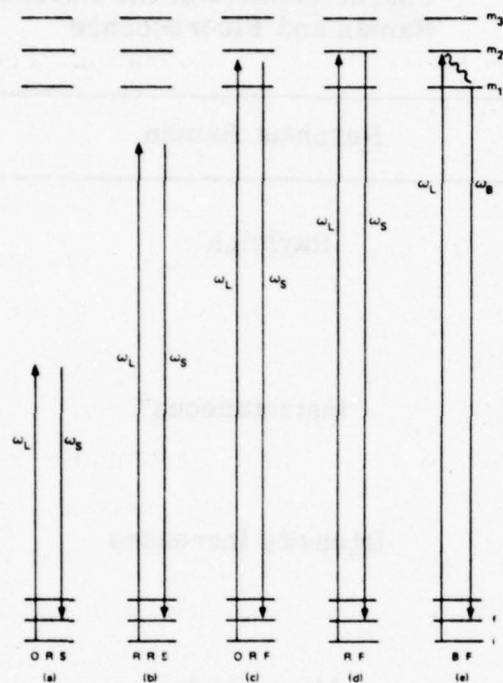


Figure 4 Energy-Level Diagrams for
5. 2. 4-1. Inelastic Light-Scattering
Processes (Ref. 110)

Careful experimental measurements and theoretical considerations lead to a formal distinction between the resonant-Raman- and the fluorescence-type scattering. These are summarized in Table 5. 2. 4-1.

The value for the "spontaneous radiative lifetime" of the fluorescence scattering given in Table 5. 2. 4-1 is for the case of no quenching. At atmospheric pressures, quenching is significant and the following relaxation processes must be considered:

TABLE
5. 2. 4-1Characteristics of the Resonant
Raman and Fluorescence

	Resonant Raman	Fluorescence
Distribution of scattered/emitted radiation	Rayleigh	4π
Spontaneous radiative lifetime	"instantaneous"	$10^{-1} - 10^{-5}$ sec
Effect of increased foreign gas pressure	Intensity increases	Intensity decreases
Depolarization	Many bands polarized	Depolarized
Dependency on state (Ref. 109)	Ground state only	Ground and upper state
Band envelope (Ref. 105)	Broad regular Q-branch and rotational wings	Very sharp doublet lines at low pressure
Overtone pattern (Ref. 105)	Continuous broadening of the Q-branch and continuous decrease in peak intensity with higher order	Irregular overtone sequence of doublets, some lines might be completely missing

Rotational relaxation	$\sim 10^{-9}$ sec
Spontaneous radiation decay (ir)	$10^{-1} - 10^{-2}$ sec
(uv)	$10^{-4} - 10^{-5}$ sec
Collisions per sec at atm pressure	$\sim 10^{10}$ sec $^{-1}$
Quenching factor	$\sim 10^{-5}$

Multiplying the quenching factor with the spontaneous radiation decay results in an "effective fluorescence decay time at atmospheric pressure" of about $10^{-6} - 10^{-7}$ sec in the infrared and $10^{-9} - 10^{-10}$ sec in the ultraviolet. This shortening of the spontaneous radiation decay time improves the range resolution, but reduces the effective fluorescence cross section at the same time. Since the rotational relaxation time is fast, it gives the molecule time to reach rotational equilibrium before it decays to the ground state. The radiative portion of that decay (fluorescence) is thus emitted over a wide spectral band.

From the above discussion, it is clear that the expression for the received signal $P(R)$ resulting from resonant Raman processes must be the same as that given for the non-resonant Raman process, except for the differential cross section $(d\sigma_{RR}/d\Omega)$. The enhancement is approximately⁽⁸⁴⁾

$$\left(\frac{d\sigma_{RR}}{d\Omega}\right) \sim \left(\frac{d\sigma_R}{d\Omega}\right) \frac{\omega_0^2}{(\omega_1 - \omega_0)^2 + \left(\frac{\Delta\omega}{2}\right)^2} \quad (5. 2. 4-1)$$

where ω_1 is the laser frequency, ω_0 is the electronic transition frequency and $\Delta\omega$ is the line width of the electronic transition.

A detailed expression for the received signal $P(R)$ resulting from the fluorescence process, applicable both in the ir and uv was developed by Kildal and Byer⁽⁸⁴⁾, and reformulated by Byer⁽¹¹¹⁾. This expression contains a dimensionless integral which reflects the increased time over which fluorescence returns to the detector due to the finite radiation decay time of the fluorescence in the infrared. Since the radiation decay time is very short in the uv, the integral can be greatly simplified. The resulting expression for $P(R)$ applicable in the uv is essentially the same as given for the Raman process, except that the differential Raman cross section $(d\sigma_R/d\Omega)$ is replaced by the fluorescence cross section $\sigma_F/4\pi$. This cross section is equal to the absorption cross section $\sigma_a/4\pi$, modified by a quenching factor q . Thus

$$\sigma_F/4\pi = q \sigma_a/4\pi \quad (5. 2. 4-2)$$

5. 2. 4. 2 State-of-the-Art

The first field measurements using resonant backscattering were made^(112, 113) in 1969 to observe sodium in the upper atmosphere. The measurements were extended to daytime⁽¹¹⁴⁾ in 1972 and to the measurements of potassium⁽¹¹⁵⁾ in 1973.

The use of resonant scattering processes in the troposphere has been limited to some measurements of NO_2 by Nakahara et al.⁽¹¹⁶⁾, who apparently obtained them as a result of NO_2 fluorescence interfering with their Raman measurement of SO_2 in the visible region, and to several laboratory measurements and theoretical investigations.

Fowler and Berger⁽¹¹⁷⁾, under EPA sponsorship, investigated the feasibility of measuring SO_2 in stack emissions using fluorescence and resonance Raman methods. In laboratory measurements they found a resonance Raman signal 1.8 times greater than the fluorescence signal around 3000 Å; this ratio could be improved with a narrower spectral bandpass (they used 24 Å). The authors also confirm the problems of fluorescence from other species and particles making quantitative measurements unlikely.

Laboratory measurements of the resonance Raman cross-sections have been reported for SO_2 by Rosen et al.⁽¹⁰⁴⁾.

It is clear from this and the preceding discussion in Section 5. 2. 4. 1 that there are problems in the interpretation of fluorescence and Raman signals. In addition, Kildal and Byer⁽⁸⁴⁾ state that there is no straightforward relationship between the fluorescence intensity and the pollutant concentration, making quantitative measurements very difficult. Presumably this latter problem can be overcome with careful laboratory studies, and, in fact, has been investigated in the infrared by Robinson and Dake⁽¹¹⁸⁾. They found that at atmospheric pressure the IR fluorescence intensity is linearly related to the laser power, and to the 6/5 power of the concentration, suggesting that remote monitoring of fluorescence is possible at least in the IR. The same authors⁽¹¹⁹⁾ extrapolate some laboratory measurements of ethylene fluorescence using a CO_2 laser to infer that 0.1 ppm of ethylene could be detected at 10 km, or 100 ppm at 1000 km. (Their graphs actually appear to give 0.2 ppm at 10 km and 1000 ppm at 1000 km.) They suggest this latter sensitivity would allow satellite monitoring of stack effluents. However, it appears that they have not considered problems such as the field-of-view being greater than the stack plume dimensions, and background noise.

Pikus et al.⁽¹²⁰⁾ have also considered a satellite-borne system for detecting NO based on fluorescence at 5.19 μm . The calculations assume a 5 J pulse CO laser and compute a threshold NO concentration sensitivity of $2 \times 10^{11} \text{ cm}^{-3}$ (7.4 ppb) at sea level. Even assuming that a 5 J laser were available for satellite use, these results may be optimistic since the calculations neglect detector and system noise sources, 80 cm diameter collecting optics are required, a 50% optical efficiency is assumed, and interferences due to other species are neglected. (At 5.19 μm , H_2O is a strong absorber over the 0.1 micron band pass assumed.)

Another estimate by Menzies⁽¹²¹⁾ of the capability of remote sensing of NO fluorescence in the infrared using a 1 mJ pulse CO laser and sensitive heterodyne detection indicates that 0.1 ppm in a 300 m path can be measured at a 1 km range, if the relative humidity is 50% (quenching by H_2O is faster than that of other constituents for this case). Also detection of SO_2 and CO is discussed.

For fluorescence in the visible/UV region, Kildal and Byer⁽⁸⁴⁾ have estimated that at nighttime about 0.5 ppm of NO_2 and SO_2 in a 15 m path can be detected at a range of 100 m using a 0.1 mJ pulse laser. They state that this sensitivity drops by a factor of 200 during the day.

Penney et al.⁽¹²²⁾ have made laboratory observations of NO_2 and O_3 fluorescence using a 0.488 μm argon laser, and of SO_2 fluorescence using a dye laser tuned near 0.3 μm . They found SO_2 fluorescence to be strongest, and estimate that it should be feasible to measure 10^{-3} ppm of SO_2 with a resolution element of 100 m at a range of 1 km.

Gelbwachs et al.^(123, 124) have also made laboratory observations of NO_2 fluorescence using laser excitation at 4416 and 4880 Å. They then

developed an in-situ fluorescence technique to measure ambient NO_2 . They do not discuss the possibility of extending the method to remote sensing, except to point out that they observed aerosol fluorescence which may interfere with remote sensing applications.

Fouche and Chang⁽¹²⁵⁾ reported on an enhancement of Raman scattering of iodine by tuning through an absorption line. These results could not be confirmed by St. Peters et al.⁽¹²⁶⁾, based on their experiments using different foreign gas pressures. However, Williams et al.⁽¹⁰³⁾ have pointed out that quenching data cannot be used unambiguously to study the transition from fluorescence to resonance Raman, since both inelastic and elastic collision broadening are involved for these transitions in molecular iodine. According to St. Peters and Silverstein⁽¹²⁷⁾, quenching data to measure the scattering time is valid only if elastic collisional broadening is unimportant. Other laboratory studies involving resonant Raman and fluorescence of the halogen molecules were conducted by Holzer et al.⁽¹⁰⁵⁾, Berjot et al.⁽¹²⁸⁾, and Robrish et al.⁽¹²⁹⁾.

Fluorescence cross sections of OH have been measured by Baardsen and Terhune⁽¹³⁰⁾ and Wang and Davis⁽¹⁰⁶⁾. The latter authors were able to measure in the laboratory the atmospheric concentrations of OH at a level of 2 parts in 10^{13} .

5. 2. 4. 3 Advantages/Disadvantages

The advantages using a remote resonant backscattering system to measure gaseous pollutants are similar to those listed for the differential absorption system in Section 5. 2. 2. 3. An additional advantage is that it does not require two frequencies to operate. But it does need a tunable laser source, thus losing the advantage of a non-resonant Raman

system. (See Section 5. 2. 3. 3.) However, this disadvantage is compensated for by the enhancement of the scattering cross section and, thus, in an increased signal.

The disadvantages of the resonant Raman/fluorescence backscattering system to measure gaseous pollutants in the air volume in the vicinity of an airport are:

- (a) Operational limitations due to requirements of non-interference with airport operations and of eye safety regulations; the latter restriction is not as severe as in the case for non-resonant Raman because of the enhanced cross section;
- (b) Potentially severe interference of broad fluorescence by molecules and aerosols that may be excited regardless of the frequency of the laser beam, thus masking the resonant Raman/fluorescence signals from the pollutants.

5. 2. 4. 4 System and Operational Requirements

The systems requirements and operational limitations due to airport operations will, in general, be the same as for the LIDAR and DAS/DIAL systems (Sections 5. 2. 1. 3 and 5. 2. 2. 3).

5. 2. 4. 5 Analysis and Critique

Based on the fact that resonant Raman and fluorescence (quenched) cross sections are enhanced by many orders of magnitude, theoretical predictions of the usefulness of resonant backscattering in the UV made over the last few years and listed in Section 5. 2. 4. 2 have been encouraging.

Results obtained by Kildal and Byer⁽⁸⁴⁾ in 1971 indicate a minimum sensitivity (SNR = 1) of 0.5 ppm at night at a range of 100 m for SO₂ and NO₂, using a 100 μ J laser with a range resolution of 15 m and assuming a visibility of 10 km. The minimum sensitivity was estimated to increase by a factor of 200 during the day.

Results by Penney et al.⁽¹²²⁾ reported in 1973 showed a sensitivity of 10 ppb of SO₂ at a range of 1 km with a resolution of 100 m. However, these results are per Joule of transmitted energy, which is beyond the eye safety limits.

Estimates by Rosen et al. first reported in 1974 and published in 1975⁽¹⁰⁴⁾ are more realistic since a moderate laser energy of 50 mJ has been used. They made the following assumptions: SNR = 10, integration over 10,000 pulses and a range resolution of 10 m. The scattering cross sections used were 10^{-25} , 6×10^{-27} , and 10^{-23} cm²/sr for SO₂, NO₂ and NO, respectively. The results are reproduced in Figure 5.2.4-2, together with the level of the NAAQS for NO_x and SO₂. It can be seen from this figure that monitoring of ambient pollutant concentration even at night at distances in the order of 1 km does not appear to be feasible.

An additional consideration, which was deliberately left out by Rosen et al., is the potential of exciting aerosol fluorescence. Gelbwachs and Birnbaum⁽¹²⁴⁾ anticipate a fluorescence signal due to aerosols corresponding to an equivalent NO₂ concentration of 1 ppm. Thus, the authors state that if aerosol concentration of the magnitude similar to that observed in Los Angeles is present, remote fluorescence of NO₂ may be severely hindered. The authors propose a two-wavelength method (similar to the DAS/DIAL method) to separate the contributions to the fluorescence signal from the pollutant molecule and from the aerosols. However, the errors increase due to the necessity of two measurements.

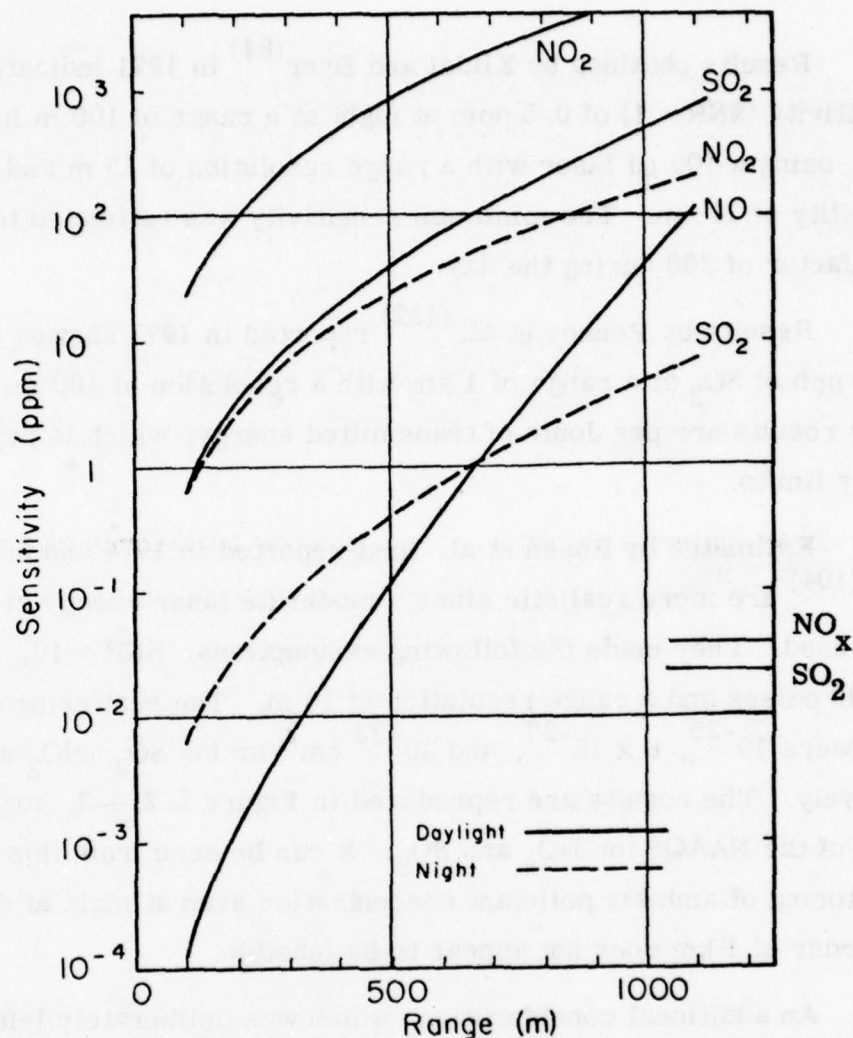


Figure
5. 2. 4-2.

Resonant Backscattering Sensitivity vs.
Range for $E = 0.05$ mJ and $N = 10^4$ Pulses
Assuming a SNR of 10, a Range Resolution
of 15 m, and a Visibility of 10 km (Ref. 104)

To date, backscattering measurements in polluted atmospheres have not disclosed aerosol fluorescence⁽¹²⁴⁾. If it can be excited, fluorescence may potentially be a useful means for aerosol monitoring.

The estimates by Menzies⁽¹²¹⁾ for resonant backscattering of NO in the IR using a heterodyne receiver, show very good sensitivity.

5. 3 DESCRIPTION OF NON-PULSED SYSTEMS (Subsets Within Remote Sensing Technology)

There are six items included in the description of subsets, namely principle of operation, state-of-the-art, advantages/disadvantages, system and operational requirements, and analysis and critique.

5. 3. 1 Active CW System: Long-Path With Laser Source

5. 3. 1. 1 Principle of Operation

Although these systems may employ pulsed lasers for various reasons (such as tuning or minimizing atmospheric turbulence effects), only "line average" values (ppm-m) of pollutants will be obtained in general. The two arrangements using different reflectors are shown in Figure 5. 3. 1-1.

The equation for the arrangements given in Figure 5. 3. 1-1 is basically the same as was given for the LIDAR system in Equation (5. 2. 1-1), viz.

$$P_r(\lambda) = \eta P_t \frac{\rho'}{\pi} A R^{-2} \tau_A(\lambda, R) \quad (5. 3. 1-1)$$

where P_t is the laser output (watts) and ρ' is the reflectivity of the topographical reflector assuming a Lambertian surface (uniformly diffuse). The corresponding expression for a retroreflector is given by

$$P_r(\lambda) = \eta P_t \Gamma(R) \tau_A(\lambda, R) \quad (5. 3. 1-2)$$

where $\Gamma(R)$ is an efficiency factor, to be defined later on (page 5. 3. 1. 5c)

The unknown to be determined is

$$\tau_A(\lambda, R) = \exp \left[-2 \int_0^R [\sigma_s(\lambda) + \sigma_a(\lambda)] N dr \right]$$

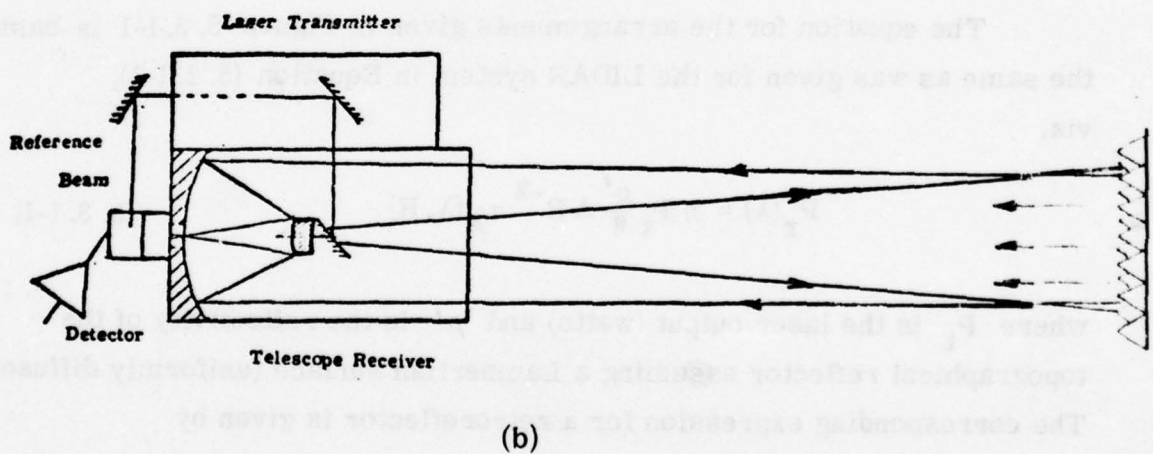
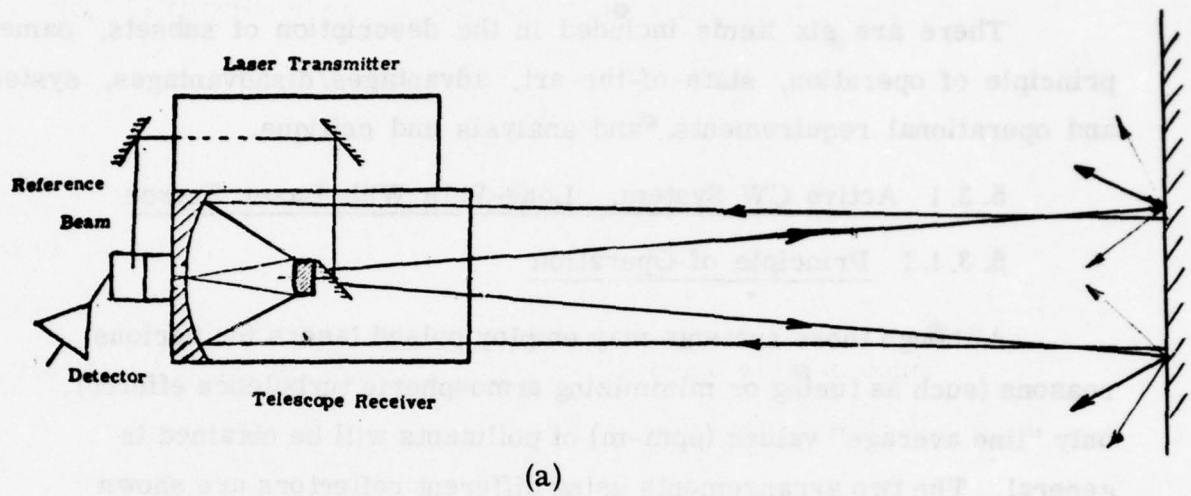


Figure 5. 3. 1-1. Two Arrangements of an Active CW System;
 (a) Using a Topographic Reflector; (b) Using
 Corner-Cube Retroreflector.

where σ_s is the scattering cross section and σ_a the absorption cross section. When the scattering processes can be neglected as in the infrared, the expression for the transmission can be simplified, viz.

$$\tau_A(\lambda, R) = \exp \left[-2 \int_0^R k(\lambda) C p_t dr \right]$$

where $k(\lambda)$ is the absorption coefficient, C is the concentration, and p_t is total pressure (usually 1 atm).

Since in these schemes only line-averaged values are measured, the integration is replaced and we write

$$\tau_A(\lambda) = \exp [-2 k(\lambda) \bar{C} p_t R] \quad (5. 3. 1-3)$$

If there are more than one species absorbing at wavelength λ , Eq. (5. 3. 1-3) must be expanded to include the other species i :

$$\begin{aligned} \tau_A(\lambda) &= \exp \left[-2 p_t R \sum_{i=1}^n k_i(\lambda) \bar{C}_i \right] \\ &= \exp \left[-2 p_t R (k_1(\lambda) \bar{C}_1 + k_2(\lambda) \bar{C}_2 + \dots) \right] \end{aligned} \quad (5. 3. 1-4)$$

Because of the many unknowns entering these equations, the method of differential absorption, as already discussed in Section 5. 2. 2, is usually employed, except that here only two measurements (instead of four) are required; one "on" the absorption line (at λ_1), and one "off" the absorption line (at λ_2).

From 5.2.1-1 and 5.3.1-3,

$$\ln P_r(\lambda_1) = \ln K - 2 p_t R [k_1(\lambda_1) \bar{C}_1 + k_2(\lambda_1) \bar{C}_2 + \dots]$$

$$\ln P_r(\lambda_2) = \ln K - 2 p_t R [k_2(\lambda_2) \bar{C}_2 + \dots]$$

where $K = \eta P_t \frac{\rho'}{\pi} AR^{-2}$

Assuming $i=1$ to be the pollutant of interest and, further, $k_2(\lambda_1) \bar{C}_2 = k_2(\lambda_2) \bar{C}_2$, $k_3(\lambda_1) \bar{C}_3 = k_3(\lambda_2) \bar{C}_3$, ..., the difference becomes

$$\ln P_r(\lambda_1) - \ln P_r(\lambda_2) = -2 p_t R k_1(\lambda_1) \bar{C}_1$$

and

$$p_t \bar{C}_1 R = \frac{\ln Q_c}{2 k_1(\lambda_1)}$$

with $Q_c = P_r(\lambda_2)/P_r(\lambda_1)$. Replacing [as in Eq. 5.2.2-5] $\bar{C}_1 p_t$ by $10^{-6} \bar{\xi}_1$, we obtain

$$\bar{\xi}_1(\text{ppm}) R = \frac{10^6 \ln Q_c}{2 k_1(\lambda_1)} \quad (\text{ppm-m}) \quad (5.3.1-5)$$

One of the crucial assumptions is that the interfering species have the same absorption coefficients at λ_1 and λ_2 . By judiciously selecting the pollutant line, this is usually the case. On the other hand, if the pollutant line is interfered by a species belonging to the "normal, clean" atmosphere, its absorption characteristics are generally known and can be accounted for.

An example of an atmospheric spectrum showing an isolated pollutant line is shown in Figure 5. 3. 1-2, indicating possible locations for λ_1 and λ_2 .

Recording Fourpaper

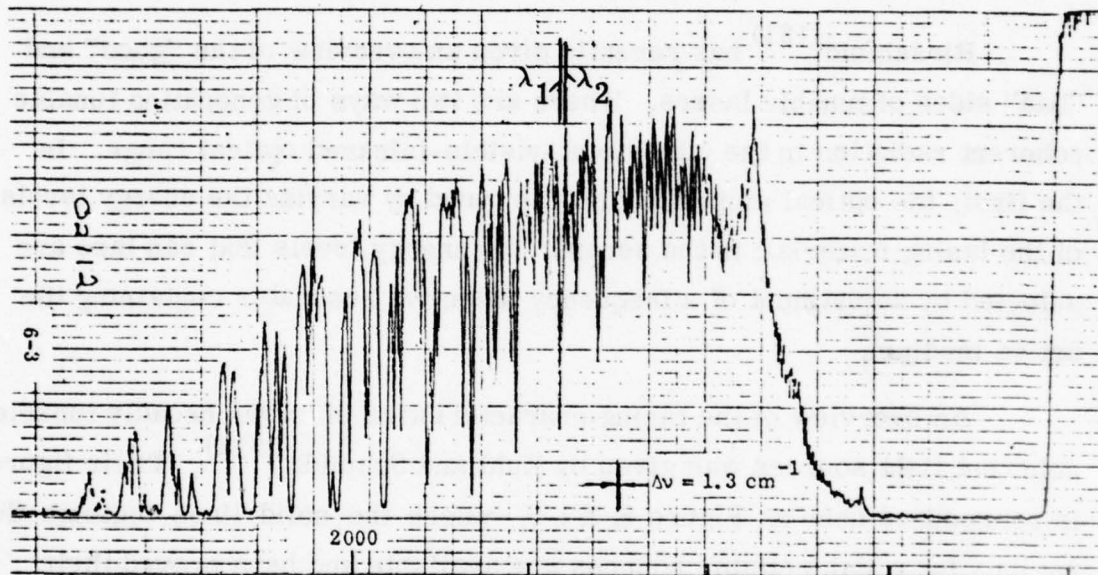


Figure 5. 3. 1-2 Atmospheric Transmission in Polluted Atmosphere over a Pathlength of 400 m (Ref. 130a) λ_1 is position "on" CO line, λ_2 "off" CO line.

5. 3. 1. 2 State-of-the-Art

5. 3. 1. 2. 1 Tunable Laser Development

For all laser resonance systems, tunable lasers are essential. For this reason we give here an overview of the recent development of tunable laser sources. They include both CW and pulsed lasers. Both types are covered here, even though this section deals with CW systems.

Hirschfeld⁽¹³¹⁾ has recently given an overview of the "good" and "bad" sides of tunable lasers. There are two ways of generating tunable coherent radiation in the ultraviolet-visible-infrared optical range. In the first, the optical emission itself is tuned by varying the energy levels of the lasing material; in the second, the energy levels that can lase are selected by adjustment of a frequency selective resonator containing the active medium.

An overview of the tuning characteristics of known broadly tunable coherent light sources was given by Kuhl and Schmidt^(131a). Their figure is reproduced here as Figure 5. 3. 1-3, where the solid lines indicate the regions for which reliable sources are available and have proved their potential, and the dashed lines indicate the regions for which sources are being developed.

An estimate of future capabilities of some of the tunable lasers was also given by Wright et al.⁽⁷⁵⁾ and is shown in Figure 5. 3. 1-3.

A brief description of the laser systems mentioned in Figure 5. 3. 1-4 is given in the following:

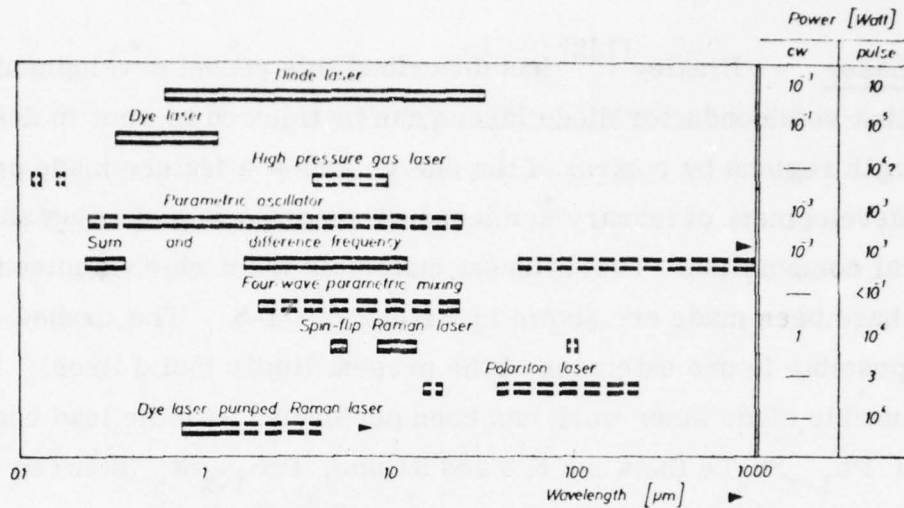


Figure 5. 3. 1-3 Summary of Tuning Characteristics of Known Laser Sources

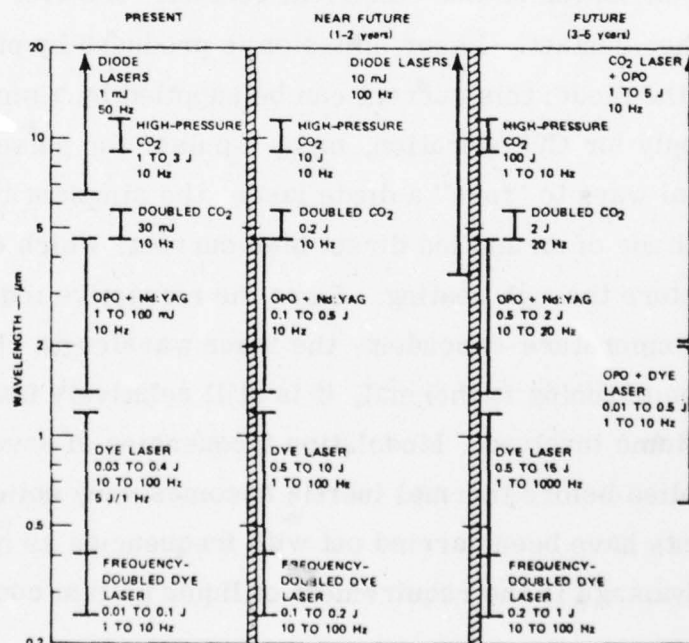


Figure 5. 3. 1-4 Estimates of Future Capabilities of Lasers

Diode Laser - Hinkley⁽¹³²⁾ has described this recent development. He states that semiconductor diode lasers can be tailored to emit in desired wavelength regions by control of the energy gap — a feature made possible by the development of ternary semiconductor compounds of adjustable chemical composition. The different materials from which semiconductor lasers have been made are shown in Figure 5. 3. 1-5. The dashed lines indicate possible future extension of the present limits (solid lines). Most of the tunable diode laser work has been performed with the lead chalcogenides $\text{Pb}_{1-x}\text{Sn}_x\text{Te}$ (between 6.5 and 34 μm), $\text{PbS}_{1-x}\text{Se}_x$ (between 4.0 and 8.5 μm), and $\text{Pb}_{1-x}\text{Cd}_x\text{S}$ (between about 2.5 and 4 μm).

Figure 5. 3. 1-6 is a drawing of a semiconductor diode laser in its standard package, approximately the same size as an average transistor. The diode crystal, nominally 0.12 x 0.05 x 0.03 cm, is mounted on a copper stud, which serves as one electrical contact. A silver ribbon serves as the other contact. Laser emission is produced by passing a current through the diode; this current can be supplied by a small battery or DC power supply for CW operation, or by a pulser for pulsed operation. There are several ways to "tune" a diode laser, the simplest being to change the magnitude of an applied direct bias current, which changes the junction temperature through heating. Since the refractive index within the laser cavity is temperature-dependent, the laser wavelength changes. Although this type of tuning is thermal, it is still relatively fast because of the limited volume involved. Modulation frequencies of several hundred Hertz can be applied before thermal inertia becomes very noticeable, and useful experiments have been carried out with frequencies as high as 10 kHz. The major disadvantage is the requirement of liquid helium cooling.

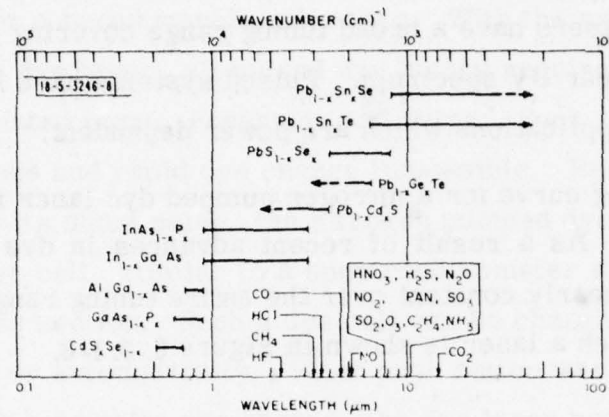


Figure 5. 3. 1-5. Wavelength Ranges which can be Covered with Alloyed Semiconductor Lasers. The Arrows indicate Possible Further Extension Beyond Present Limits. Some of the Gases of Environmental Concern are also shown

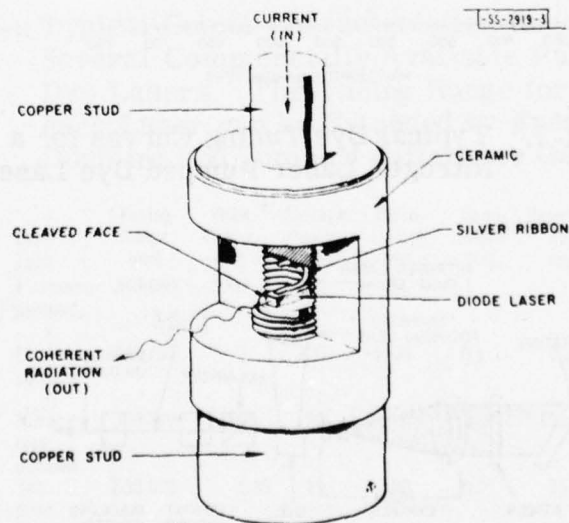


Figure 5. 3. 1-6. Semiconductor Diode Laser Mounted in its Standard Package. Over-all Package Size is approximately 1 cm.

Dye-Laser - Klauminzer⁽¹³³⁾ has recently given an overview. He states that dye lasers have a broad tuning range covering extremes of the visible and near UV spectrum. Pulsed systems have high peak and rms power for applications which are power dependent.

The tuning curve for a nitrogen pumped dye laser is shown in Figure 5. 3. 1-7. As a result of recent advances in dye technology, the output power is nearly constant over the entire tuning range. The optical schematic for such a laser is shown in Figure 5. 3. 1-8.

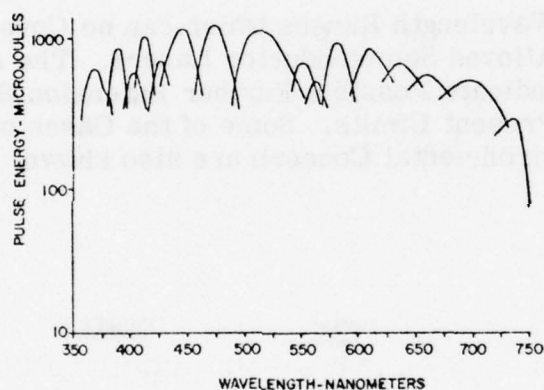


Figure 5. 3. 1-7. Typical Dye Tuning Curves for a Nitrogen Laser Pumped Dye Laser

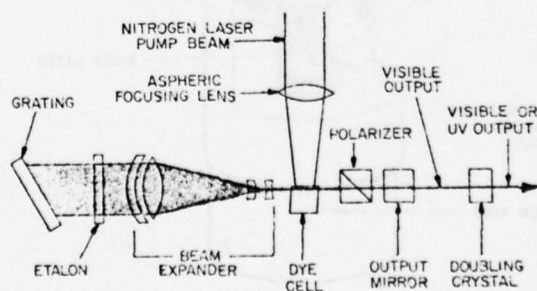


Figure 5. 3. 1-8. Optical Schematic for a Nitrogen Pumped Dye Laser

From the tuning curves it is clear that several different dyes are required to cover a broad wavelength range. With the exception of the nitrogen pumped dye laser, all pulsed dye lasers require rapid-flow dye cells with associated pump, reservoir and filter. Such a system makes dye change tedious and rapid dye change impossible. Because it has very high gain during its short pulse, the nitrogen pumped dye laser can use a small cuvette dye cell, similar to a spectrophotometer sample cell 10 mm x 10 mm in cross section. Such a dye cell can be changed in a few seconds either manually or automatically. When push button wavelength scanning is combined with automatic dye change, the dye laser begins to take on the convenience aspects of a spectrophotometer source.

Klauminzer predicts that dye lasers will become more reliable and easier to use. The wavelength range of a single laser will extend from 2,000-10,000 Å. A partial list of available pulsed dye lasers is given in Table 5. 3. 1-1.

TABLE 5. 3. 1-1. Typical Output Characteristics for Several Commercially Available Pulsed Dye Lasers. The Tuning Range for each Laser can be Extended by Frequency Doubling and Sum and Difference Generation

Laser Type	Tuning Range (nm)	Peak Power (kW)	Average Power (mW)	Pulse Length (ns)	Band-width (nm)	Repetition Rate (pps)
Flashlamp pumped I	340-950	1000	400	400	1	1
Flashlamp pumped II	445-700	7	200	1000	0.1	30
Nitrogen laser pumped	360-750	150	30	6	0.01	100
YAG laser pumped	530-670	0.35	25	80	0.05	75

High-Pressure Gas Laser - A review of these lasers at pressure greater than 1 atm and high energies (> 10 J) was recently given by Wood⁽¹³⁴⁾. Their applications to remote sensing of pollutants has been explored by Hess and Seals⁽¹³⁵⁾. Authors state that the lasers can be tuned across the pressure broadened lines which can be made wider than atmospheric species absorption lines. Their studies indicate that absorption lines of several species (O_3 , NH_3 , C_2H_4 , SO_2) are within 1.5×10^9 Hz tuning range from line centers of $C^{12}O_2^{16}$ and $C^{12}O_2^{18}$ lasers.

Wave-Guide Lasers - Abrams and Bridges⁽¹³⁶⁾ have discussed the characteristics of sealed-off waveguide CO_2 lasers. The reduction in discharge tube diameter and the corresponding increase in gas pressure (over 300 torr) implies a pressure-broadened line width in excess of 1.5 GHz, where frequency tuning may be applied to heterodyne detection. Authors studied the gain, output power and efficiency in sealed-off CW capillary-bore CO_2 laser, using the tube wall as an optical waveguide. The experimental set up is shown in Figure 5. 3. 1-9.

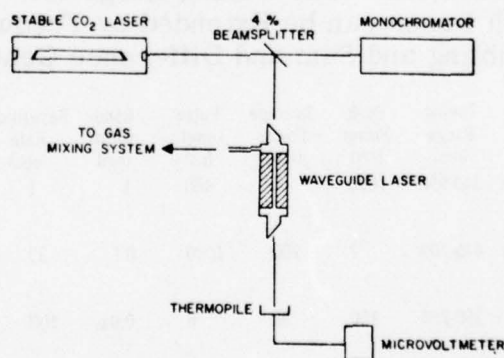


Figure 5. 3. 1-9. Experimental Arrangement for Measurement of Waveguide Laser Gain

Construction of a beryllium oxide capillary-bore laser is shown in Figure 5. 3. 1-10, and typical results of gain and power versus gas pressure in Figures 5. 3. 1-11 and 12, respectively.

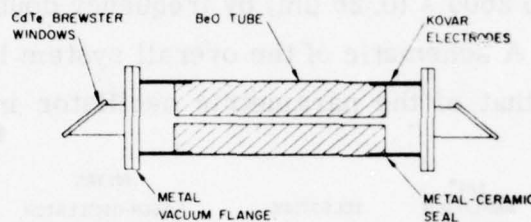


Figure 5. 3. 1-10. Construction Details of BeO Capillary Bore Laser

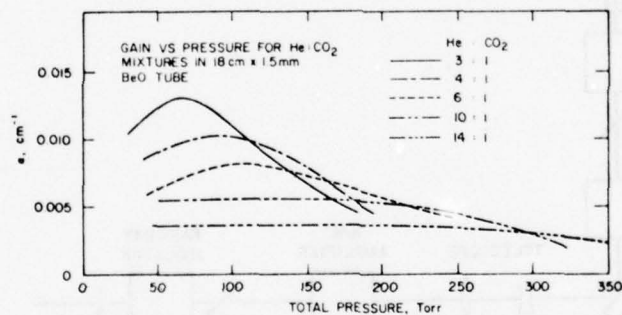


Figure 5. 3. 1-11. Gain versus Total Pressure for Various Sealed-Off He:CO₂ Mixtures in an 18-cm x 1.5-mm BeO Tube

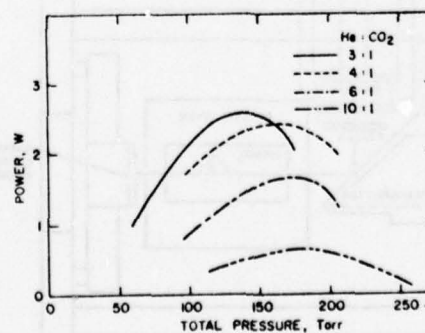


Figure 5. 3. 1-12. Output Power versus Total Pressure for He:CO₂ Mixtures in 18-cm x 1.5-mm BeO Tube

Parametric Oscillator - Byer⁽¹³⁷⁾ has discussed the use of parametric oscillators in spectroscopy. Recently, Byer, Herbst and Fleming⁽¹³⁸⁾ have constructed a breadboard model of a Nd:YAG laser pumped LiNbO₃ parametric oscillator whose basic range extends from 1.4 to 4.2 μm that can be extended to 2600 Å (0.26 μm) by frequency doubling and to 25 μm by frequency mixing. A schematic of the overall system is shown in Figure 5.3.1-13 and that of the parametric oscillator in Figure 5.3.1-14.

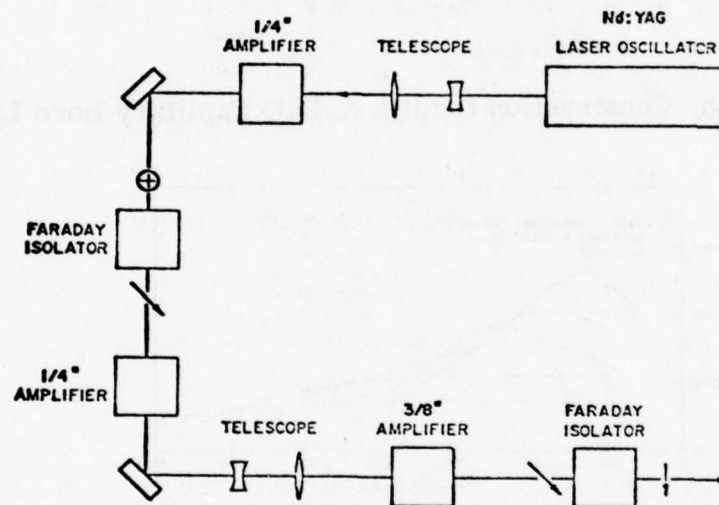


Figure 5.3.1-13. Schematic of a 0.5 J Per Pulse Nd:YAG Oscillator-Amplifier System

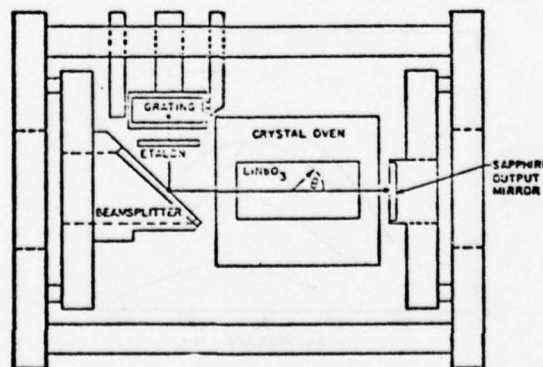


Figure 5.3.1-14. Schematic of the 1.06 μm Pumped, Angle Tuned LiNbO₃ Singly Resonant Parametric Oscillator

For high conversion efficiency and narrow linewidth operation, stringent temporal, spatial, spectral and pulse energy requirements are placed on the pump laser. Also, good overall alignment is essential.

Sum and Difference Frequency Technique - This is used to extend the basic range of a system (see Figure 5. 3. 1-14). However, the output power is decreased due to losses in the crystals. As an example, Hirschfeld et al.⁽¹⁰²⁾ report an experimentally measured efficiency of 8% versus a theoretical one of 40% in a crystal used for frequency doubling.

Four-Wave Parametric Mixing - In this process, anti-Stokes side-bands are generated in stimulated Raman scattering and the laser pump and the Stokes wave are coupled in the sample gas. The method can be applied only to in-situ probing. A simplified description is given by Klauminzer⁽¹³³⁾.

Spin-Flip Raman Laser - The development of the spin-flip Raman (SFR) laser is due to Patel⁽¹³⁹⁾. It is tunable over a wide wavelength range in the infrared below 5μ and has been shown to have output linewidths considerably narrower than 1 kHz ($3 \times 10^{-8} \text{ cm}^{-1}$). A CW CO laser beam of about 0.7 W is focused on an indium antimonide sample in a magnetic field of a large magnet; the radiation passing through the material is the tunable spin-flip Raman radiation. Its application to stratospheric in-situ sampling of NO by NBS was briefly reported⁽¹⁴⁰⁾.

5. 3. 1. 2. 2 Laser Systems

Several theoretical predictions of system sensitivities have been made over the years. Byer and Garbuny⁽⁶⁷⁾ have calculated that pollutants of less than 0.01 ppm for ranges up to 10 km can be measured, using topographical reflectors. With retroreflectors, the sensitivity may be increased by several orders of magnitude.

McClenny et al.⁽¹⁴³⁾ have discussed the methodology for comparison of long-path data with those of point monitors. Their conclusions are relevant to the subject of "Operational Requirements" and will be discussed in Section 5. 3. 1. 4.

Hirschfeld⁽¹⁴⁴⁾ discussed the application of long-path infrared detection of atmospheric pollutants and found that bi-static "remote instruments can do the job now, but restrict measurements to a small number of line-of-sight paths, over which they give an average value. This is probably the most sensitive technique now operational, especially in its correlation mode. . . . Laser backscatter techniques will become important with further laser development to render them operational, which may extend laser methods also to the bi-static systems".

Ball and Keller⁽¹⁴⁵⁾ predicted that concentrations of NO_2 less than 1 ppm could be determined in a 1 km optical path, using multiple lines of a CW Argon ion laser. These predictions were based on laboratory measurements with a 48 m multipass cell (see Figure 5. 3. 1-15). The authors state that some of the Ar^+ laser wavelengths occur close to absorption maxima while others occur close to absorption minima. In this respect, the Ar^+ laser is as good as a dye laser. The substitution of an Ar^+ laser for a dye laser in this technique has several advantages: 1) Wavelength measurement and control is not as convenient in a dye laser as it is in an Ar^+ laser; 2) most commercial Ar^+ lasers have servo mechanisms to

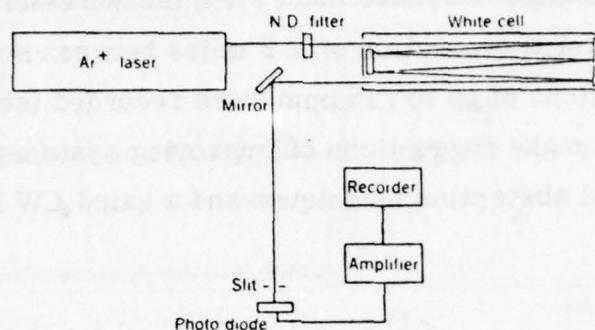


Figure 5. 3. 1-15. Apparatus for the Detection of Ar⁺ Laser Emission by Gaseous NO₂

maintain constant intensity outputs. In contrast to this, the output from a dye laser can vary considerably from pulse to pulse and over longer periods due to bubbles, thermal changes, and dye degradation; 3) the operator skill required to operate an Ar⁺ laser is minimal while the skill required to operate presently available dye lasers can be considerable. A serious disadvantage of the Ar⁺ laser is the less than ten wavelengths available for tuning in contrast to the continuous range of wavelengths available from the dye laser.

An argon ion laser emits at several wavelengths throughout the visible region. The cross sections for absorption by gaseous NO₂ are larger for some of these wavelengths than for others. Concentrations of NO₂ can be determined by measuring the ratio of transmitted or scattered intensities at two different wavelengths once the difference in absorption coefficients at these two wavelengths is known. To obtain accurate measurements of concentration it is necessary to have accurate values of the absorption coefficients.

O'Shea and Dodge⁽¹⁴⁶⁾ have made field measurements with a pulsed Ar^+ laser over a separation of 2.2 miles between source and receiver. Fluctuations of up to .15 ppm were recorded (see Figure 5. 3. 1-16. Authors make suggestions of improving system performance by using differential absorption techniques and a gated CW laser system.

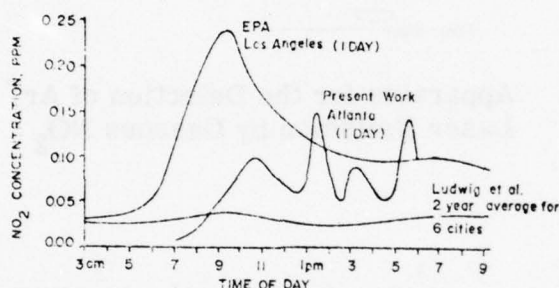


Figure 5. 3. 1-16. Comparison of Diurnal Variation of NO_2 Concentration in Some Urban Environments (Ref. 146). (Ludwig, et al., Ref. 146a).

Kucеровsky et al.⁽¹⁴⁷⁾ discussed the measurement of methane over long distances. They used two CW helium-neon lasers, one working at 6328 \AA (as a visible guide beam) and the other at $3.392 \text{ }\mu\text{m}$. As a receiver, an 8" Newton telescope coupled to a triglycine sulphate pyroelectric detector was used (see Figure 5. 3. 1-17).

Authors state that the sensitivity of the method is relatively high, and that it is possible to use the laser transmitter not only to measure integral absorption by methane homogeneously mixed in the atmosphere, but also to detect localized sources of methane such as point leaks. This could be important for application of the system for monitoring

leaks in storage containers, drill sites, etc. To produce the record of transmission of the type shown in Figure 5. 3. 1-18, the beam was aimed parallel with the ground at a height of 1 m. A point leak was simulated in still air inside the laboratory by releasing about 1 cm^3 of methane at a rate of $100 \text{ cm}^3 \text{ min}^{-1}$ at ground level directly below the transmitted beam. This amount of methane produced about a 5% decrease in the level of the signal. The measurement was performed with a separation between the laser transmitter and retro-reflecting mirror of 20 m. The decrease in level of the signal depends in this case only on the intensity of the localized leak, and the way the gas migrates and not on the length of the path being surveyed.

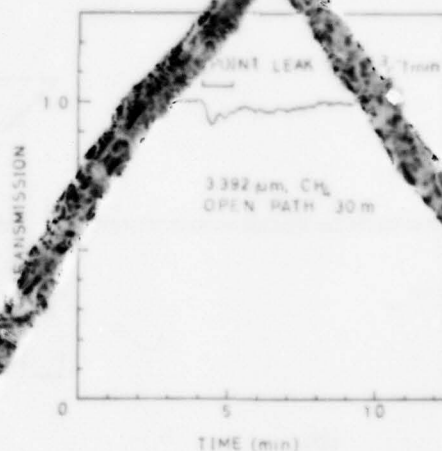
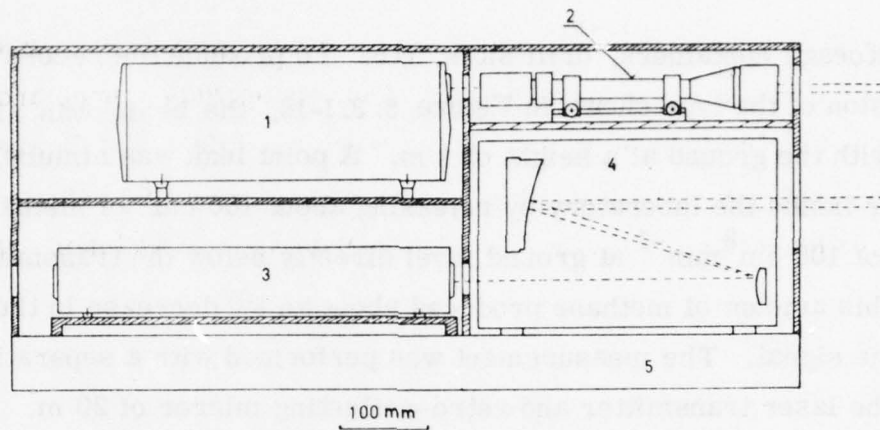
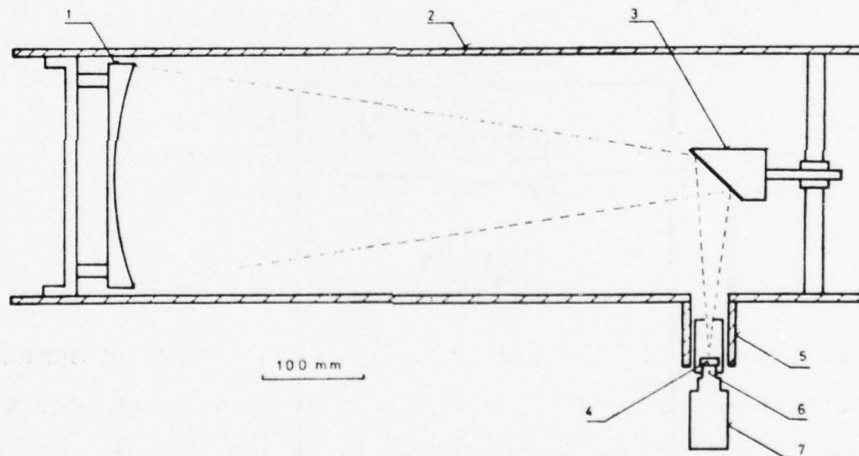


Figure 5. 3. 1-18. Detection of a Point Leak of Natural Gas Using the Long-Path Laser Absorption Method.



(a)



(b)

Figure 5. 3. 1-17:

- (a) Laser Transmitter: 1, 0.6328- μm Laser; 2, Beam Expander Telescope; 3, 3.392- μm Laser; 4, Off-Axis Telescope Beam Expander; 5, Aluminum Base Plate
- (b) Laser Receiver: 1, Primary 8-Inch Spherical Mirror; 2, Telescope Body; 3, Secondary Mirror; 4, Detector; 5, Eyepiece Holder; 6, High-Input Impedance Pre-amplifier; 7, Low-Noise Preamplifier (6-60 dB).

leaks in storage containers, drill sites, etc. To produce the record of transmission of the type shown in Figure 5. 3. 1-18, the beam was aimed parallel with the ground at a height of 1 m. A point leak was simulated in still air inside the laboratory by releasing about 100 cm^3 of methane at a rate of $100 \text{ cm}^3 \text{ min}^{-1}$ at ground level directly below the transmitted beam. This amount of methane produced about an 8% decrease in the level of the signal. The measurement was performed with a separation between the laser transmitter and retro-reflecting mirror of 20 m. The decrease in level of the signal depends in this case only on the intensity of the localized leak, and the way the gas migrates and not on the length of the path being surveyed.

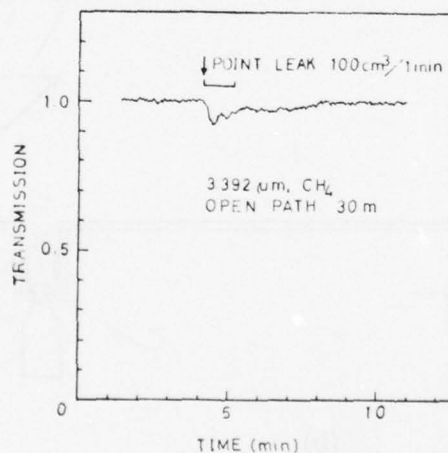


Figure 5. 3. 1-18. Detection of a Point Leak of Natural Gas Using the Long-Path Laser Absorption Method.

Two field programs, sponsored by EPA and NSF, were conducted during 1973. Craig et al.⁽¹⁴⁸⁾ discuss the modification of a CO₂ gas laser system required to monitor ozone and McClenny et al.⁽¹⁴⁹⁾ the field evaluation of the system. The system is called "Infrared Laser Atmospheric Monitoring System (ILAMS)" and is housed in a van (Figure 5. 3. 1-19); the laser optical layout is shown in Figure 5. 3. 1-20.

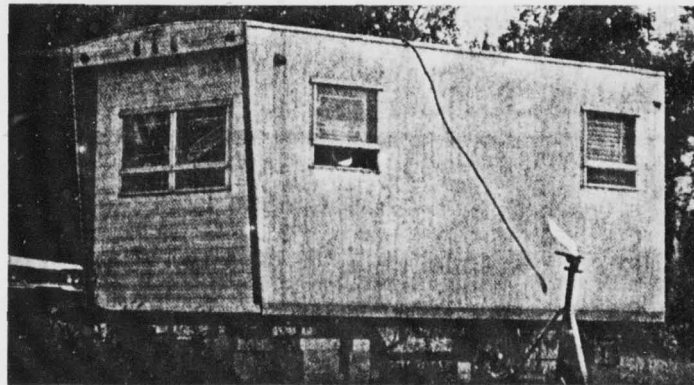


Figure 5. 3. 1-19. Photograph of Van Housing Laser and Signal Processor

The test site in the GE plant, located in Syracuse, New York, is shown in Figure 5. 3. 1-21.

The long-path measurements were also compared with point monitors. An example of such a comparison is shown in Figure 5. 3. 1-22. The erratic behavior of the ILAMS during the morning hours has not been definitely identified, but is believed to be related to the alignment of the laser beam at the retroreflector. Spurious absorptions result whenever the relationship between return and reference signals were

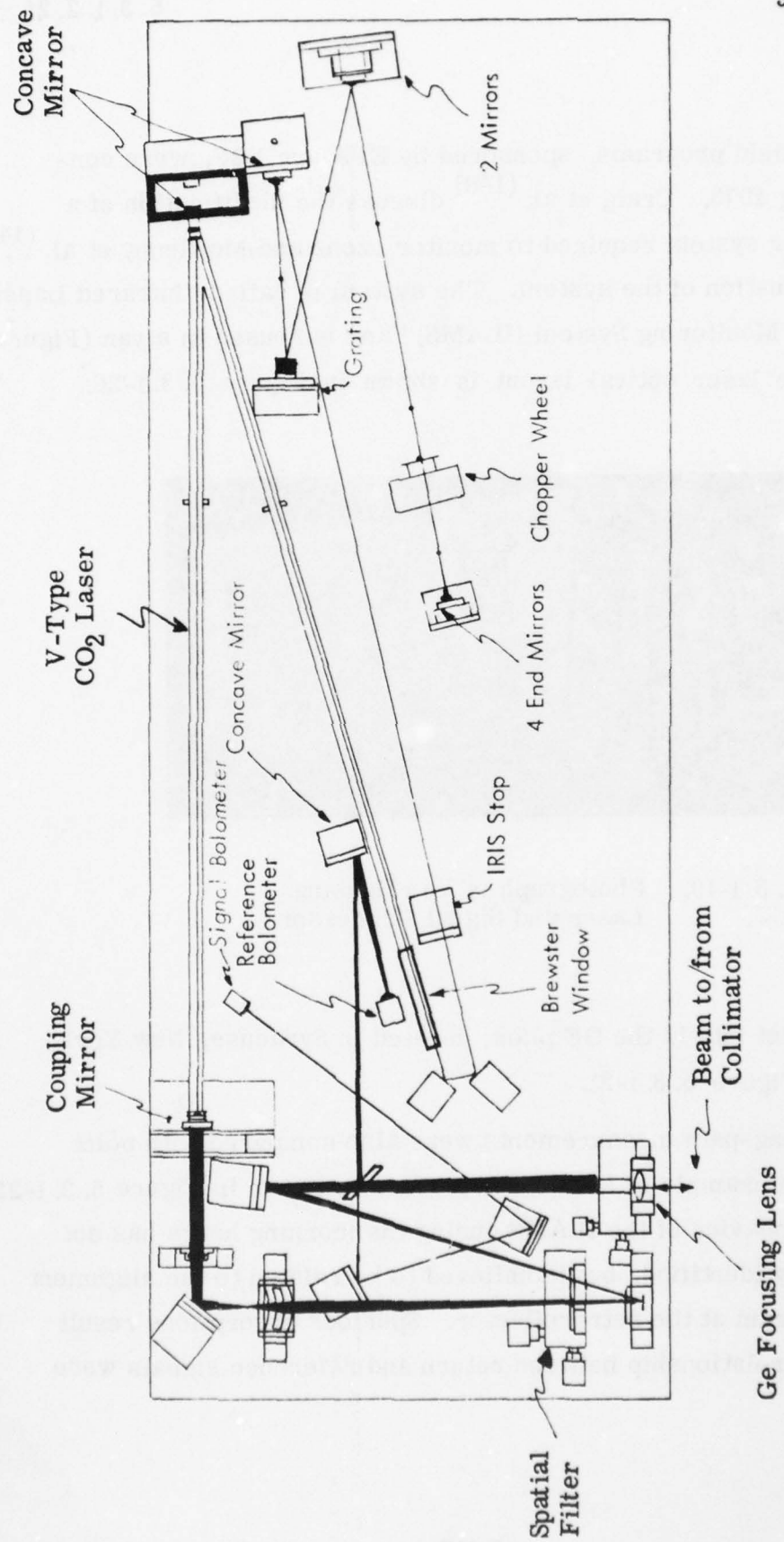


Figure 5. 3. 1-20. Optical Layout of Laser System

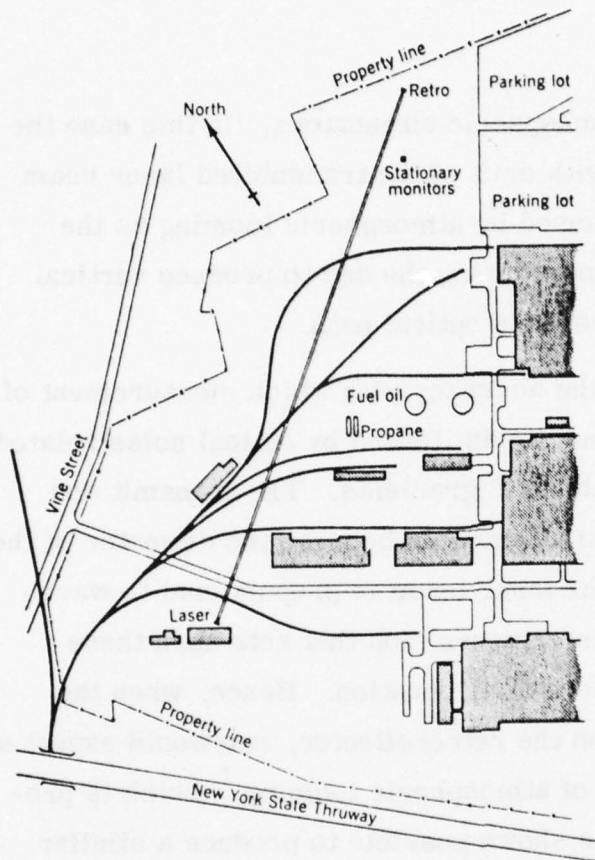


Figure 5. 3. 1-21

Schematic of Open-Path Measurement Site (G. E., Syracuse, N. Y.); Shaded Areas are Buildings, Several Railroad Tracks and One Roadway Intersect the Measurement Path. The Total Length of the Measurement Path was 670 m.

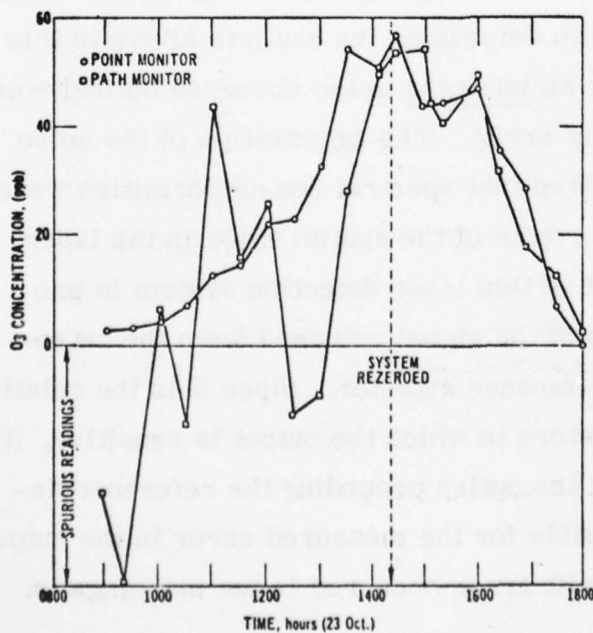


Figure 5. 3. 1-22.

Comparison Between Long-Path and Point Monitors.

changed by other than known atmospheric attenuators. In this case the spurious absorption coincided with drift of the transmitted laser beam away from the retroreflector caused by atmospheric looming as the ground warmed up and cooled down during the day to produce vertical temperature gradients in the system's optical path.

The authors state that "the accuracy with which measurement of ozone concentrations could be made was limited by optical noise related to atmospheric turbulence and thermal gradients. The transmit and receive optics produced spectral attenuation because the diameter of the far field diffraction pattern of the laser beam is proportional to wavelength. The retroreflector is an aperture stop that acts upon these spatial variations to produce spectral attenuation. Hence, when the transmitted beam was focused on the retroreflector, one would expect a spectral return in the presence of atmospheric looming,^{*} which is precisely what we observed. It was shown possible to produce a similar error by deliberately aiming the beam slightly off the edge of the retroreflector. The experiments with defocusing the beam to alleviate this problem, however, resulted in an increase in the observed optical noise and an increase in measurement error. The aggravation of the noise condition with defocusing indicated that spectral non-uniformities were still present in the near field in spite of the spatial filter in the laser transmitter. The signal output of this laser detection system is proportional to the log of the ratio of the signal returned from the retroreflector to the signal on the reference detector. Since it is the relative signal behavior of the two detectors to which the output is sensitive, it is equally possible that drift in the optics preceding the reference detector is also partially responsible for the measured error in the output. However, because the major drift error occurred in the mornings on

^{*} Looming is the refraction of light caused by thermally induced index of refraction gradients in the atmosphere.

clear days following clear nights, the strong change in humidity and ground temperature during the morning hours are considered significant. Water vapor is a fairly well understood spectral interference, but ground fog and liquid water adhering to particulates (haze) is not. In addition, unknown spectral interferences may have entered the beam to offset the system's zero baseline. The effect of looming on the laser beam was noted on many occasions. Reaiming the laser by moving the focusing lens preceding the beam expander to correct for the looming only appeared to compensate for about 50% of the measurement error associated with this time of day phenomenon. The considerable drift in the laser system output signal which has been tentatively attributed to looming was greatest during the mornings on clear days when the wind velocity was low. In these periods, the RMS error between the ILAMS and the point monitor ozone measurements was approximately 28 parts per billion. At other times, the system was relatively stable and the RMS error was about 6 parts per billion. It is expected that the effects of atmospheric looming on the signal are still the dominant source of error even during stable operation and that correcting non-uniformities in the transmitted laser beam will reduce the system error and improve its accuracy."

The other field evaluation of a long-path monitor was conducted by Hinkley and Ku⁽¹⁵⁰⁾. This work was in continuation of an earlier development of a cross stack monitor⁽¹³²⁾ using a pulsed diode laser. The schematic of the field test arrangement is shown in Figure 5. 3. 1-23. The results of the field tests show that the laser beam was approximately rectangular in shape, 40 cm in horizontal extent by 30 cm along the vertical direction. Under the assumption that this represents a diffraction-limited pattern emanating from the collimating lens, then the source image at the lens is calculated to be 1 cm high and 0.76 cm wide — which agrees with the measured laser beam size at this location.

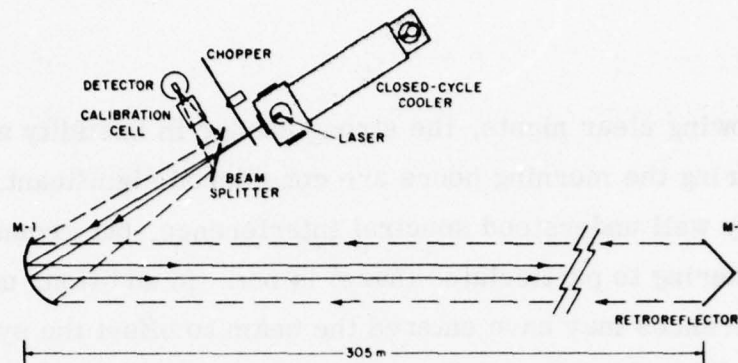


Figure 5. 3. 1-23. Schematic of Long-Path (305-Meter) Diode Laser and Optical System for Monitoring Atmospheric CO

The inherent pulse-to-pulse reproducibility of power from a diode laser is usually better than 1 percent⁽¹³²⁾. Atmospheric turbulence and scattering over long paths can cause much larger variations in the received signal, however. It was found that the signal return is best on a day with high humidity — even in rain — rather than on a dry day. In order to demonstrate the temporal variations in intensity over the 610-meter total path to retroreflector and back, laser pulses were transmitted at different rates, and the pulse-to-pulse variation noted. At times the difference between adjacent pulses was as much as 10 percent. If two such pulses represented the "on" and "off" line pulses for the P(4) line of CO (which has a strength of $3.8 \times 10^{-5} \text{ cm}^{-1}/\text{ppm}$), for example, this would produce an error of 45 ppb. When the time between pulses was reduced to 1.5 msec, the atmospheric turbulence effects could be completely eliminated.

A comparison was made between a remote mirror or retroreflector in terms of return signal and signal-to-noise ratio. The mirror was a high-quality, 15-cm-diameter flat firmly attached to a steel column in

the down-range building. The retroreflector array consisted of four individual retroreflectors, each 5 cm in diameter, tied together in a square configuration. The following results were obtained:

	Signal	Noise	S/N
Flat Mirror	61	7.0	8.7
Retroreflector Array	17	0.6	28.0

In each case, the detector noise was much less than the noise associated with the return signal, and could be neglected. Mechanical vibrations of the mirror, in addition to its inability to return the laser beam in the direction from whence it came (unless the ray is exactly normal), contribute to its much larger noise factor. Moreover, for field applications, the retroreflector is much simpler to position since alignment is noncritical. Authors conclude that the retroreflector is the better choice.

Using 1.5-A laser current pulses, 20 μ sec long and 3.3 msec apart, the influence of artificially produced rain was studied on the return beam from a 4.7- μ m diode laser. It was found that the presence of the rain had no 'dramatic' effect on the laser signal.

The results of monitoring carbon monoxide with the above system were described by Ku, Hinkley and Sample⁽¹⁵¹⁾. The wavelength of radiation from a $\text{PbS}_{0.82}\text{Se}_{0.18}$ semiconductor diode laser was tuned into coincidence with an absorption line of CO in the fundamental band around 4.7 μ m. By employing rapid frequency-modulation of the laser emission to overcome atmospheric turbulence effects it was possible to achieve a minimum detectable concentration of 5 parts per billion over

a 0.61 km path. Continuous around-the-clock monitoring was also performed, and increases in the ambient CO level due to commuter traffic was observed.

The potential of long-path measurement of ethylene generated in a parking lot was demonstrated by Hinkley⁽¹⁵²⁾. The schematic is shown in Figure 5.3.1-24. Using a $\text{Pb}_{0.88}\text{SN}_{0.12}\text{Te}$ diode laser operating at $10.6\text{ }\mu\text{m}$, the emitted laser power was $6\text{ }\mu\text{W}$, and approximately $2\text{ }\mu\text{W}$ was detected after the long beam traverse. The distance from laser to mirror was 0.25 km, so that the total path was 0.5 km long. Figure 5.3.1-25 is a recorder scan of the C_2H_4 concentration between 4:51 and 4:56 p.m., when many automobiles were being driven from the parking area, and between 5:05 and 5:10 p.m., when the number was less. With the laser beam approximately 2 meters above the rooftops, the C_2H_4 averaged over the total path reached a peak of 1.3 ppm, diminishing to near zero during the later time interval due to reduced traffic and atmospheric dispersion. In some cases, C_2H_4 from individual automobiles was detected. The sensitivity of this measurement was 80 ppb, limited primarily by mechanical vibrations of the optical apparatus which altered the beam direction. Turbulence will ultimately limit system sensitivity, and wavelength modulation techniques have been devised to overcome these effects. The laser systems described above have been installed in a van and measurements in St. Louis, Missouri, are taking place⁽¹⁵³⁾. The schematic of the optical arrangement and a photograph of the van are shown in Figure 5.3.1-26 and -27. Note the support of the optical table which is independent of the van.

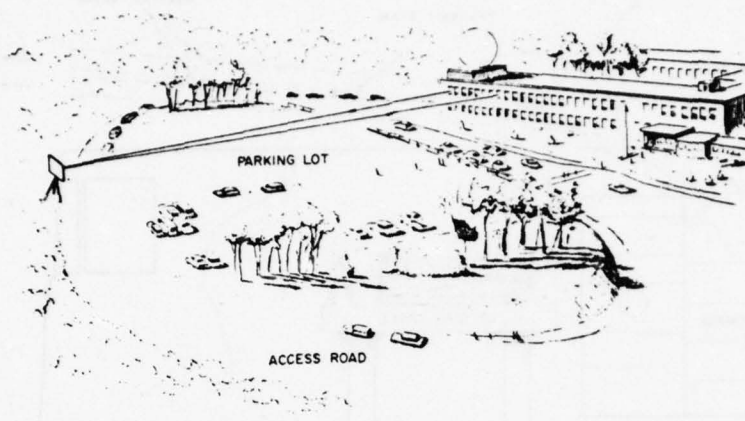


Figure 5. 3. 1-24. Schematic for Parking-Lot Monitoring Experiment

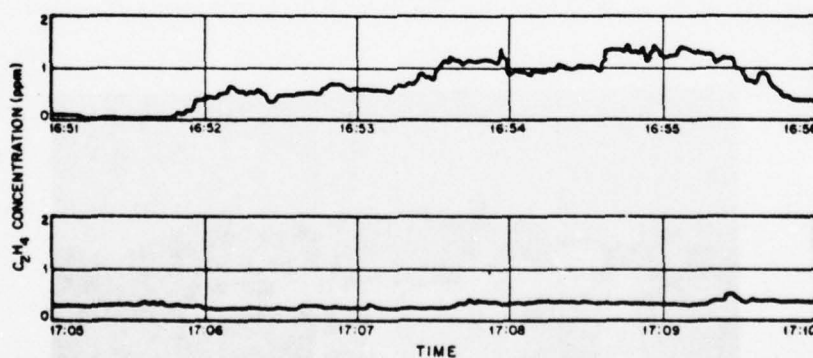


Figure 5. 3. 1-25. Measurement of C_2H_4 Across Parking Lot by Resonance Absorption using a $Pb_{0.88}Sn_{0.12}Te$ Diode Laser at $10.6 \mu m$. Total path was 0.5 km.

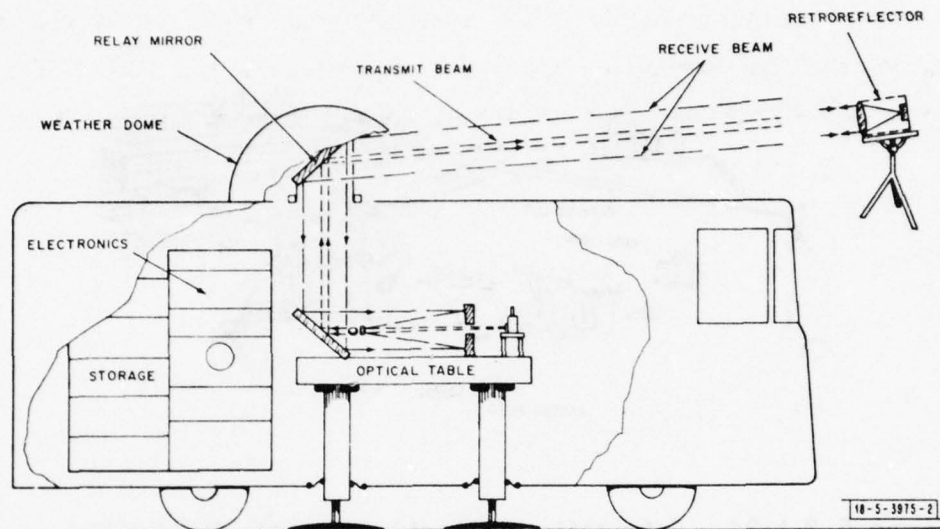


Figure 5. 3. 1-26. Schematic of Laser Monitoring Van, Consisting of Optical Table (Supported on Ground), Electronics, Transmitting Mirrors, Remote Retroreflector, and Infrared Detector



Figure 5. 3. 1-27. Photograph of Van Purchased for Mobile Optical Laboratory

Preliminary results of CO measurements were obtained and comparisons with bag samples show agreement generally to within 10%, except in the cases of higher pollution levels, as indicated in the following table.

<u>Run No.</u>	<u>Laser (ppm)</u>	<u>Bag (ppm)</u>
1	0.55	0.61
2	0.60	0.62
3	0.39	0.56
4	1.65	1.07
5	0.87	1.02
6	3.1	2.3
7	2.13	1.93
8	0.95	0.85

A new field program is planned by Menzies and Schumate⁽¹⁵⁴⁾, in which two CW CO₂ waveguide lasers are mounted in an airplane and the radiation scattered back from the ground surface is received by a telescope on the aircraft. The two lasers emit beams at two neighboring wavelengths in the ozone absorption band and are utilized in the differential absorption mode. Additional sensitivity is obtained by employing the heterodyne scheme. The heterodyne signal is generated by the motion of the laser reflectance point on the ground. Discussions of observing tropospheric pollution from high-flying aircraft or satellites using the ground as diffuse reflector were given by Menzies and Schumate⁽¹⁵⁵⁾, Menzies and Chahine⁽¹⁵⁶⁾, Melfi et al.⁽¹⁵⁷⁾ and Seals and Bair⁽¹⁵⁸⁾.

Murray⁽²⁴⁹⁾ has reported about some long-path measurements with a DF laser, using topographical targets that provide the back-scattered signal. Because these are one of the first reported field data for such a system, we want to compare his results with our calculations of Section 5. 3. 1. 5. A typical trace of raw data is shown in Fig 5. 3. 1-28.

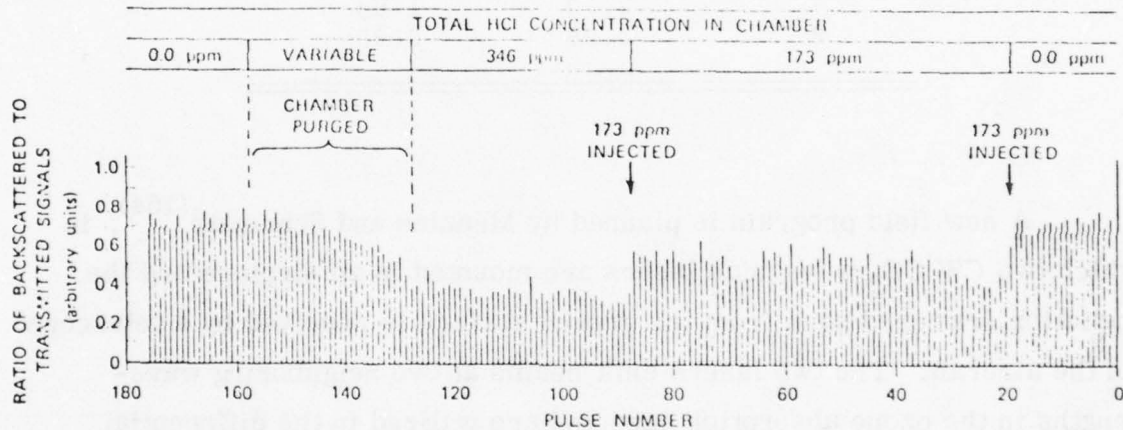


Figure 5. 3. 1-28. Sample of Behavior of the Ratio of Backscattered to Transmitted Signal During System Operation on HCl.

Using a DF laser with an energy of 100 to 150 mJ/pulse and a pulse width of 1 μ sec, a receiver aperture of 792 cm^2 and a D^* of $5 \times 10^9 \text{ cm}\sqrt{\text{Hz}}/\text{W}$, the sensitivity (defined by the concentration for which the standard deviation equals the concentration) was determined for three gases and is given in Table 5. 3. 1-2.

TABLE 5. 3. 1-2. Laser Wavelengths, Absorption Coefficients and Sensitivity

Gas	DF Laser Line	Wavelength (μm)	Absorption Coefficient ($\text{cm}^{-1}\text{atm}^{-1}$)	Sensitivity (ppm-km)
HCl	P ₂ (3)	3.636239	5.64	.05
CH ₄	P ₁ (9)	3.715252	0.047	6.
N ₂ O	P ₃ (7)	3.890259	1.19	.24

The difference in sensitivity is, of course, largely influenced by the difference in absorption coefficients. In a comparison with our results, given in Fig 5. 3. 1-38, we find that the two results qualitatively agree for matching instrument parameters. It is noteworthy that two entirely different targets (plywood board and juniper tree) apparently did not affect the sensitivity, as seen in Figure 5. 3. 1-29.

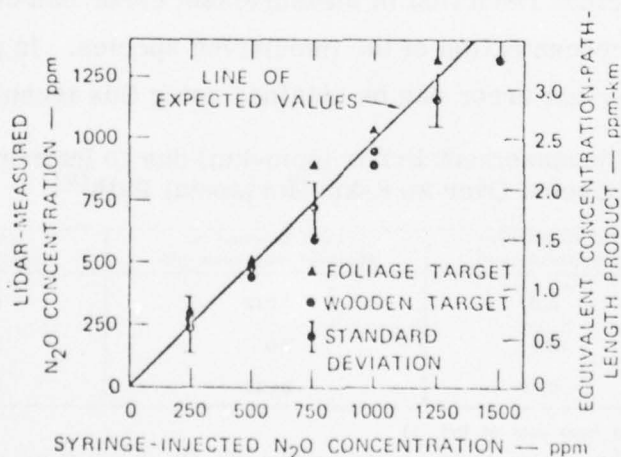


Figure 5. 3. 1-29. Summary of Remote Measurement Tests of N₂O in a Sample Chamber.

Of interest is also Murray's discussion about the influence of interfering species. He states that "in general, gaseous species in the atmosphere, such as water vapor and HDO, can produce errors in the two-wavelength differential-absorption measurements. The error due to interferences is shown in Table 5. 3. 1-3 in ppm-km. These data were calculated using an 8-km horizontal path from the data reported by Spencer et al. ⁽²⁵⁰⁾. The second column represents the measurement error without compensation for interference. The weakly absorbed line was selected as being adjacent to the strongly absorbed line, and this results in the measurement error shown in the second column. By careful selection of the weakly absorbed line so that its transmission by interfering species is matched to that of the strongly absorbed line, obtained by estimating or measuring the effect of the interfering species on the wavelengths selected. By estimating interference effects to within only 30% of their actual value, the measurement errors shown in the fourth column are calculated. The sophistication of the interference compensation for a given problem is dependent on the application and the desired sensitivity. Table 5. 3. 1-3 illustrated the use of just two techniques for interference minimization. Further reduction in measurement error can be obtained by measuring the concentration of the interfering species. In principle, a negligible measurement error can be obtained using this technique."

TABLE 5. 3. 1-3. Measurement Error (ppm-km) due to Interfering Species Over an 8-km Horizontal Path^(a)

Target Gas	No Interference Compensation ^(b)	Line Selection to Minimize Interferences ^(c)	Interference Compensation ^(d)
HCl	0.10	0.012	0.0037
CH ₄	10.6	2.0	0.59
N ₂ O	0.73	0.041	0.012

(a) Errors calculated from data of Ref. 11.

(b) DF laser lines (strongly absorbed/weakly absorbed) for HCl, CH₄, and N₂O are, respectively, P₂(3)/P₁(6), P₁(9)/P₂(5), and P₃(7)/P₁(14).

(c) DF laser lines (strongly absorbed/weakly absorbed) for HCl, CH₄, and N₂O are, respectively, P₂(3)/P₃(6), P₁(9)/P₁(10), and P₃(7)/P₂(10).

(d) Compensation is calculated from an estimate of absorption by interfering species. The ratio between the transmission of the strongly absorbed laser lines and that of the weakly absorbed laser lines is assumed to be accurate to within 30% of the actual value.

AD-A067 242

SCIENCE APPLICATIONS INC LA JOLLA CALIF
DEVELOPMENT OF CRITERIA FOR MONITORING OF AIRPORT GROUND POLLUT--ETC(U)
NOV 78 C B LUDWIG, J R YODER

F/G 1/5

DOT-FA76WA-3725

UNCLASSIFIED

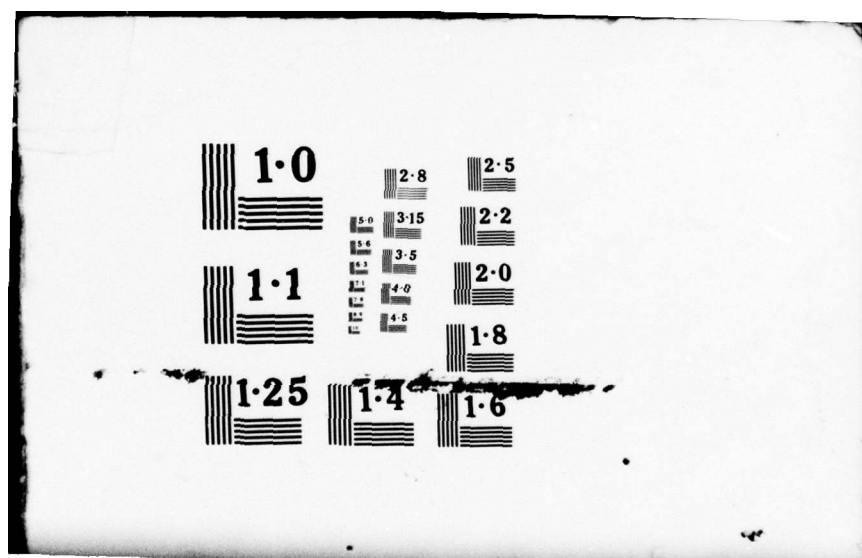
SAI-77-910-LJ-VOL-1-

FAA/RD-77-178-1

NL

4 OF 5
ADA
067242





Another set of field data have recently been reported by Menzies and Shumate⁽²⁵¹⁾. The ambient air pollutants ozone, nitric oxide, and ethylene were monitored in the Pasadena area with a bistatic IR laser apparatus. These pollutants were measured with a differential absorption technique, using selected wavelengths in the 9.5- μm , 5.2- μm , and 10.5- μm regions, respectively. The transmitted laser radiation was detected using both direct and heterodyne detection techniques. In the direct detection case, cube corner retroreflectors provided the return, and the heterodyne detection responded to scattered radiation from various rough surfaces, ranging from 400 m to 1.9 km in distance from the apparatus. Table 5.3.1-4 contains a compilation of various laser wavelengths which were used in this series of measurements. Absorption coefficients of various atmospheric constituents at these wavelengths are also listed.

TABLE 5.3.1-4. Laser Wavelengths Used for Pollutant Monitoring

Laser line	Wavelength (μm)	Absorption coefficient at 300 K (km^{-1})				
		NO (1 ppm)	O ₃ (1 ppm)	C ₂ H ₄ (1 ppm)	H ₂ O (10 Torr)	CO ₂ (330 ppm)
CO:						
6-5, P(19)	5.164				1.86	
6-5, P(20)	5.176	0.275			2.01	
7-6, P(13)	5.166	0.175			1.45	
7-6, P(14)	5.177				1.39	
7-6, P(15)	5.187	0.250			2.16	
9-8, P(9)	5.262	1.04			2.02	
9-8, P(14)	5.317				2.58	
CO ₂ :						
001-II, P(14)	9.504		1.25		0.11	0.123
001-II, P(20)	9.552		0.56		0.11	0.126
001-II, P(24)	9.586		0.08		0.09	0.112
001-I, P(14)	10.529			2.98	0.12	
001-I, P(16)	10.549			0.46	0.12	
001-I, P(20)	10.588			0.15	0.11	

A block diagram of the laser monitoring apparatus is shown in Figure 5. 3. 1-30. The lasers were operated in a cw mode, followed by optical choppers. The chopper electrical pick-offs served as reference inputs to the two synchronous demodulators. When the lasers were tuned to different wavelengths and simultaneously transmitted, the chopper frequencies were offset by a displacement that was larger than the band-pass of the tuned audio amplifiers at the synchronous demodulator inputs. This was done to avoid interaction between the two channels. The authors state that SNR in both the direct and heterodyne detection was very large but that the limiting sources of noise were atmospheric turbulence induced fluctuations or coherent speckle fluctuations.

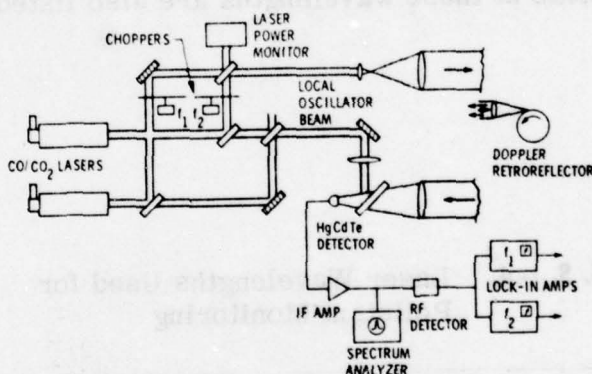


Figure 5. 3. 1-30. Block Diagram of the Laser Differential Absorption Apparatus

The fluctuations induced by the atmospheric turbulence were substantially different for the retroreflection and rough surface scattering cases. When direct detection of the retroreflected signal was used, the power spectrum of the fluctuations fell rapidly above 30 Hz. An example of the fluctuation amplitudes produced in the 10-30-Hz region is shown in

Figure 5. 3. 1-31a for propagation over the 0.8-km path on a calm, sunny day around noon. The signal was chopped at a 400-Hz frequency, producing the regular sawtooth modulation. The turbulence-induced fluctuations correspond to intensity variations of roughly $\pm 15\%$ about the average intensity. Over a longer time scale of several seconds, using a receiver time constant of 3 sec, the peak-to-peak fluctuation amplitudes were about 10-15% of the average reading under the same meteorological conditions. When heterodyne detection of the signal from the scattering plate was observed, large fluctuations at much higher frequencies were found. From a typical signal shown in Figure 5. 3. 1-31b, the authors found significant fluctuations at frequencies as high as 500 Hz.

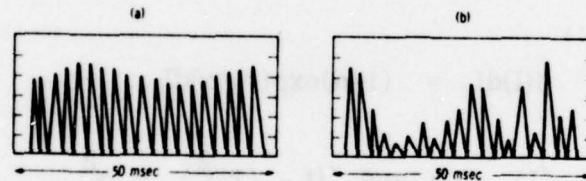


Figure 5. 3. 1-31. High Frequency Fluctuations Observed in the Return Signal due to Atmospheric Turbulence and Coherent Speckle Effects. In (a) the Signal from a Cube Corner Retroreflector is Observed, and in (b) the Signal from a Roughened Scattering Plate is Observed. Speckle in the Scattered Radiation Field is Expected for Case (b). For both cases (a) and (b), the Periodic 100% Modulation at Roughly 400 Hz is due to the Optical Chopper.

The authors explain this effect as follows:

"In the scattering of coherent radiation from rough surfaces, the independent scattering elements of the surface have randomly distributed phases and produce an irregular interference pattern (speckle) in the far field. The speckle lobe widths are given by λ/D_s , where λ is the wavelength of the radiation and D_s is the transmitter spot diameter at the rough surface. (252-255) The speckle is fully developed if the coherence length of the incident radiation is much larger than the rms height distribution of the scattering elements on the rough surface. This was the case in our experiments. Then, for plane polarized incident radiation, the parallel polarized scattered intensity I at various points a given distance from the scattering surface behaves as a random variable that obeys the exponential distribution. (252, 255)

$$p(I)dI = (1/\alpha)\exp(-I/\alpha)dI, \quad (2)$$

where $\langle I \rangle = \alpha$ and $\langle (I - \langle I \rangle)^2 \rangle = \alpha^2$.

In our propagation and monitoring experiments, the receiver aperture subtended one speckle lobe width; thus, it fully resolved the speckle, and a motion of the speckle pattern across the receiver resulted in a fluctuating receiver signal that was distributed according to Eq. (2). The atmospheric turbulence succeeded in changing the speckle pattern near the receiver aperture by moving the transmitted spot on the scattering surface, by slightly changing the angle of arrival of the transmitted beam incident on the surface, and by producing a movement of the speckle lobes in the scattered field across the receiver aperture. It is not clear which of these effects is the predominant cause of the high frequency fluctuations seen in Figure 2(b). However, studies of several photographs such as those depicted in Fig. 2(b)

indicate that the intensity is distributed according to Eq. (2) to a good approximation. Over a time scale of several seconds, using a receiver time constant of 1 sec, the peak-to-peak fluctuation amplitudes in this heterodyne configuration are remarkably similar to those observed when using direct detection. This is not really surprising, for if one assumes that time integration of the exponentially distributed 400-Hz intensity fluctuations, over an integration time of 1 sec, will reduce the standard deviation of the intensity by a factor of $(400)^{1/2}$, these fluctuations will produce rms noise equal to only 5% of the average intensity.

Ratioing the signal returns from two simultaneously transmitted wavelengths proved to be successful in reducing the effects of turbulence-induced fluctuations. When two adjacent CO₂ laser transitions were transmitted, and when care was taken to make sure that the transmitted beams were collinear and had similar cross-sectional patterns (TEM₀₀ mode shapes), their turbulence fluctuations were highly correlated. Peak-to-peak fluctuations in the ratio signal were typically 1-2% of its average value when a 3-sec time constant was used."

Typical results for ozone, ethylene and NO and comparisons with in-situ sensors are shown in Figures 5. 3. 1-32 to -33.

The differences between the in-situ and remote data again show that long-path measurements have a greater information content and are more representative of a given pollution situation.

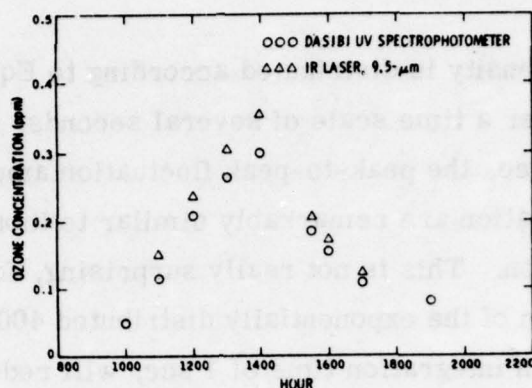


Figure 5. 3. 1-32. Ozone measurements taken when the laser system was operating over the 0.8-km path during a day when photochemical smog was fully developed. Comparison is made with a commercial (Dasibi) point monitor of ozone which was located near one end of the path.

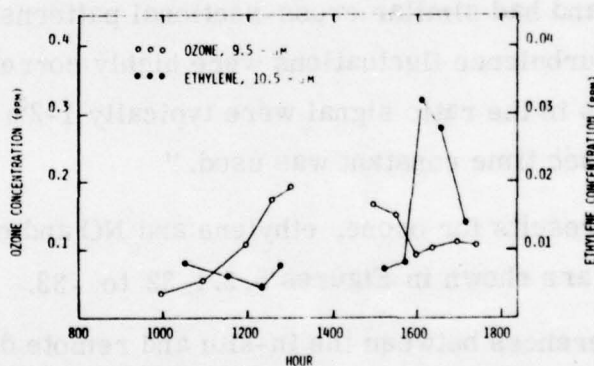


Figure 5. 3. 1-33. Measurements of ozone and ethylene taken when the laser system was operating over the 3.75-km path.

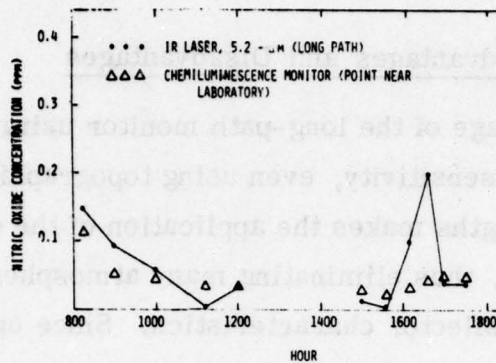


Figure 5. 3. 1-34. Nitric oxide measurements taken when the laser system was operating over the 3. 75-km path.

5. 3. 1. 3 Advantages and Disadvantages

The advantage of the long-path monitor using a tunable laser as a source is the high sensitivity, even using topographic reflectors. The use of two wavelengths makes the application of the differential absorption technique possible, thus eliminating many atmospheric interferences and variations in the reflector characteristics. Since only two measurements are needed for the determination of the line-average pollutant concentration, the resulting errors will be less than the ones for the pulsed system, in which no fixed reflector is used and, thus, four measurements are needed. Because of the high sensitivity of the method, lower power lasers can be used; in addition, measurements will most likely be conducted in the infra-red. Thus, eye safety problems will probably not occur.

The principal disadvantage of the long-path monitor is the inability to obtain profile data; thus, the validation and verification of atmospheric pollution models for airports would be restricted to line-average data. In addition, line-average data depend upon the availability of topographical and artificial reflectors. The use of artificial reflectors entails problems of alignment, diffraction effects and atmospheric effects on the surface areas of the reflectors.

5. 3. 1. 4 System and Operational Requirements

5. 3. 1. 4. 1 System Requirements

As already mentioned, one of the disadvantages is the limited number of fixed lines-of-sight (LOS), given by either reflectors of opportunity or artificially placed ones. Snowman and Gillmeister⁽¹⁵⁹⁾ have considered the application of one centrally located laser system together with a number of permanently installed retroreflectors, which are to be arranged in such a way that their LOS are representative for a given (extended) pollutant source (see Figure 5. 3. 1-35).

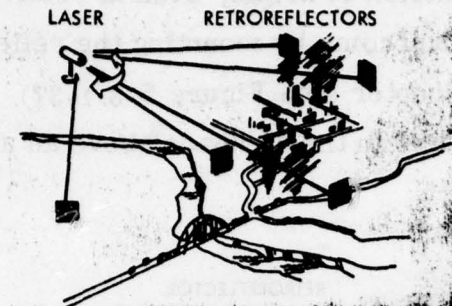


Figure 5. 3. 1-35. Arrangement of One Centrally Located Laser System and Several Retroreflectors

Another arrangement is shown in Figure 5. 3. 1-36 in which the authors consider the case of perimeter monitor, using mirrors at fixed location at several corners of an extended source. Knowing the wind speed and direction, it is possible to monitor the pollution emission generated by the extended source within the perimeter. However, it must be remembered that one LOS at a fixed height above ground may not be quite representative for the air mass entering and leaving the perimeter. It has been found that pollutants may be very much stratified, i. e., showing

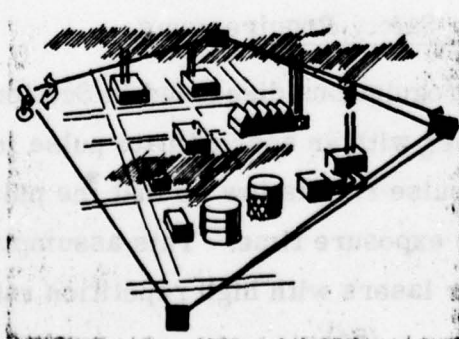


Figure 5. 3. 1-36. Arrangement Useful in Perimeter Monitoring

large variation as a function of height, even at relatively low altitudes⁽¹⁶⁰⁾. This difficulty can be overcome by mounting the reflector on a movable platform such as a helicopter (see Figure 5. 3. 1-37). Of course, stringent requirements must be met in the airspace above an airport.

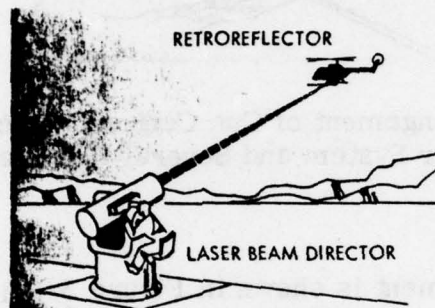


Figure 5. 3. 1-37. Arrangement of Ground Based Laser System and Airborne Retroreflector

5. 3. 1. 4. 2 Eye Safety Requirements

The eye safety regulations discussed in Section 6. 1. 3. 2 are restricted to a pulsed laser with an approximate pulse length of 100 nsec. It is assumed that the pulse rate is low so that the pulse length could be considered equal to the exposure time. This assumption cannot be made for CW operation or for lasers with high repetition rates.

In general, the rules⁽⁵⁴⁾ prescribe the different safety precautions applicable to four classes of laser products. Class I is the lowest power laser product that cannot be considered hazardous even if all

of the laser output were directed into the eye's pupil (8 mm spot size) or focused into a 1 mm spot on the skin for a day⁽¹⁶¹⁾. The maximum permissible exposure (MPE) is based on this rule. The Laser Institute of America (LIA) has issued a "Laser Safety Guide"⁽¹⁶¹⁾ in which the protection standards are listed for intrabeam exposure to many common lasers. These standards are reproduced here as Table 5. 3. 1-5 for single pulsed lasers and as Table 5. 3. 1-6 for CW lasers.

It should be noted that the Class I rule can be applied to enclosed laser products that contain more powerful lasers. However, the emanating radiation must conform to the Class I rule and a warning label must be located at an access panel to alert a user that more hazardous laser radiation is contained in the enclosure.

Laser Type		MPE (J/cm ²)	
Pulsed Lasers	Visible (400-700 nm)	0.1 J/cm ²	0.1 J/cm ²
	UV (100-400 nm)	0.01 J/cm ²	0.01 J/cm ²
	IR (700-1000 nm)	0.1 J/cm ²	0.1 J/cm ²
CW Lasers	Visible (400-700 nm)	0.1 W/cm ²	0.1 W/cm ²
	UV (100-400 nm)	0.01 W/cm ²	0.01 W/cm ²
	IR (700-1000 nm)	0.1 W/cm ²	0.1 W/cm ²

TABLE 5. 3. 1-5. Intrabeam Protection Standards which are Applicable to Many Pulsed Lasers for Eye and Skin Exposure to Laser Radiation

Laser Type	Primary Wavelength(s) (nm)	Pulse Duration	Protection Standard	
			Eye	Skin
Normal-pulsed ruby	694.3	~ 1ms	$10^{-5} \text{ J} \cdot \text{cm}^{-2}$	$0.2 \text{ J} \cdot \text{cm}^{-2}$
Q-switched ruby	694.3	5-100ns	$5 \times 10^{-7} \text{ J} \cdot \text{cm}^{-2}$	$0.02 \text{ J} \cdot \text{cm}^{-2}$
Rhodamine 6G Dye Laser	~ 500-700	0.5-20 μ s	$5 \times 10^{-7} \text{ J} \cdot \text{cm}^{-2}$	$0.03-0.09 \text{ J} \cdot \text{cm}^{-2}$
Normal Pulsed neodymium	1064	~ 1ms	$5 \times 10^{-5} \text{ J} \cdot \text{cm}^{-2}$	$0.2 \text{ J} \cdot \text{cm}^{-2}$
Q-switched neodymium	1064	5-100ns	$5 \times 10^{-6} \text{ J} \cdot \text{cm}^{-2}$	$0.02 \text{ J} \cdot \text{cm}^{-2}$

TABLE 5. 3. 1-6. Intrabeam Protection Standards which are Applicable to Many Common CW Lasers for Eye and Skin Exposure to Laser Radiation

Laser Type	Primary Wavelength(s) (nm)	Protection Standard	
		Eye	Skin
Helium-Cadmium	441.6	a) $2.5 \text{ mW} \cdot \text{cm}^{-2}$ for 0.25s b) $10 \text{ mJ} \cdot \text{cm}^{-2}$ for 10-10,000s c) $1 \mu \text{W} \cdot \text{cm}^{-2}$ for > 10,000s	$0.2 \text{ W} \cdot \text{cm}^{-2}$
Helium-Neon	632.8		
Argon	488.5 14.5		
Krypton	647.1		
Freq. Doubled ND:YAG	532		$0.2 \text{ W} \cdot \text{cm}^{-2}$
Neodymium:YAG	1,064	$0.5 \text{ mW} \cdot \text{cm}^{-2}$ for $t > 100\text{s}$	$0.2 \text{ W} \cdot \text{cm}^{-2}$
Gallium-Arsenide at room temp.	905	$0.25 \text{ mW} \cdot \text{cm}^{-2}$ for $t > 100\text{s}$	$0.2 \text{ W} \cdot \text{cm}^{-2}$
Helium-Cadmium	325	a) $1 \text{ J} \cdot \text{cm}^{-2}$ for < 1000s b) $1 \text{ mW} \cdot \text{cm}^{-2}$ for > 1000s	a) $1 \text{ J} \cdot \text{cm}^{-2}$ for < 1000s
Nitrogen	337.1		b) $1 \text{ mW} \cdot \text{cm}^{-2}$ for > 1000s
Carbon-dioxide (and other lasers 1.4 μ m to 1000 μ m)	10.6 μ m (10,600nm)	$0.1 \text{ W} \cdot \text{cm}^{-2}$ for $t > 10\text{s}$	$0.1 \text{ W} \cdot \text{cm}^{-2}$ for $t > 10\text{s}$

5. 3. 1. 5 Analysis and Critique

As we have done before for the other systems, we will calculate some basic sensitivities for the long-path monitors, using differential absorption techniques with topographic and man-made reflectors. The expression of the signal-to-noise ratio for determining the pollutant concentration by the ratio of two signals can be derived by using the relationship

$$\text{SNR} = \frac{\bar{\xi}}{d\bar{\xi}} \quad (5. 3. 1-6)$$

where $\bar{\xi}$ is the concentration of the pollutant in ppm. According to Equation 5. 3. 1-5

$$\bar{\xi}_1 = \frac{10^6 \ln [P_r(\lambda_2)/P_r(\lambda_1)]}{2 k_1(\lambda_1) R}$$

Thus, from the principle of superposition of errors⁽¹⁶²⁾, we have

$$d\bar{\xi}_1 = \frac{10^6}{2 k_1(\lambda_1) R} \left[\frac{dP_r(\lambda_2)}{P_r(\lambda_2)} - \frac{dP_r(\lambda_1)}{P_r(\lambda_1)} \right]$$

The "most probable error" is the square root of the sum of the squares of the greatest errors due to an error in each measurement:

$$d\bar{\xi}_1 = \frac{10^6}{2k_1(\lambda_1)R} \left[\left(\frac{dP_r(\lambda_2)}{P_r(\lambda_2)} \right)^2 + \left(\frac{dP_r(\lambda_1)}{P_r(\lambda_1)} \right)^2 \right]^{1/2}$$

Assuming a detector-noise limited system (in the infrared), for which the noise is given by the NEP, viz.,

$$dP_r(\lambda_1) = dP_r(\lambda_2) = \text{NEP} = (\Delta f A_d)^{1/2} / D^*$$

we have

$$\text{SNR} = \frac{\ln [P_r(\lambda_2)/P_r(\lambda_1)]}{\text{NEP} \left[(1/P_r(\lambda_1))^2 + (1/P_r(\lambda_2))^2 \right]^{1/2}} \quad (5. 3. 1-7)$$

In the limit of low pollutant concentration, $P_r(\lambda_1) \approx P_r(\lambda_2)$ and

$$\ln (P_r(\lambda_2)/P_r(\lambda_1)) \approx P_r(\lambda_2)/P_r(\lambda_1) - 1$$

Introducing this approximation and re-arranging Eq. (5. 3. 1-7), we get

$$\begin{aligned} \text{SNR} &= \frac{P_r(\lambda_1) - P_r(\lambda_2)}{\text{NEP} \left[1 + (P_r(\lambda_1)/P_r(\lambda_2))^2 \right]^{1/2}} \\ &\approx \frac{P_r(\lambda_1) - P_r(\lambda_2)}{\sqrt{2} \text{NEP}} \end{aligned} \quad (5. 3. 1-8)$$

The signal power $P_r(\lambda)$ is given by Eq. (5. 3. 1-1) for a topographical reflector and by Eq. (5. 3. 1-2) for a retroreflector. The efficiency factor $\Gamma(R)$ in Eq. (5. 3. 1-2) is the ratio of the receiver area A to the beam area at a distance of $2R$ (because of the folded path). It is

$$\Gamma(R) = \frac{A}{\pi (2\alpha \cdot 2R + d_0)^2 / 4} \quad (5. 3. 1-9)$$

where $2\alpha \approx \sqrt{\Omega_L}$ is the divergence (rad) of the laser beam and d_0 is the diameter of the expanded beam at the source. Of course, the maximum value of $\Gamma(R)$ cannot exceed unity.

For $d_0 \ll 4\alpha R$, the expression for $\Gamma(R)$ simplifies to

$$\Gamma(R) \approx \frac{A}{\pi R^2 \Omega_L}$$

Typical infrared lasers have a beam diameter of 1 cm and a divergence of 3×10^{-3} rad, giving $A \Omega_L = 7 \times 10^{-6} \text{ cm}^2 \text{ sr}$. If a beam expansion to a cross sectional area of 10 cm^2 is applied, the divergence becomes $7 \times 10^{-7} \text{ sr}$. However, we have used the more conservative value of $9 \times 10^{-6} \text{ sr}$.

The following instrument parameters have been used, assuming a measurement with a 10% accuracy:

$$\text{SNR} = 10$$

$$\eta = 0.01$$

$$P_t = 1\text{W (expanded into a } 10\text{cm}^2 \text{ beam area, resulting in a value of } 0.1 \text{ W/cm}^2 \text{ which is eye and skin safe in the infrared)}$$

$$\begin{aligned}
 A &= 700 \text{ cm}^2 \text{ (d = 30 cm)} \\
 \Omega_L &= 9 \times 10^{-6} \text{ sr} \\
 \text{NEP} &= 10^{-13} \text{ W}
 \end{aligned}$$

The value for NEP can readily be obtained by state-of-the-art systems, employing a cooled detector with $D^* = 10^{11} \text{ W/cm}^2 \text{ Hz}^{-1/2}$, a detector area of about $.01 \text{ cm}^2$ and a bandpass of 0.01 Hz (i. e., an integration time of 25 sec).

For the background, atmospheric, and pollutant parameters, we have used:

$$\begin{aligned}
 \rho' &= .2 \text{ (representative for walls of buildings)} \\
 k(\lambda_1) &= 1 \text{ cm}^{-1} \text{ atm}^{-1} \\
 p_t &= 1 \text{ atm}
 \end{aligned}$$

and

$$k(\lambda_2)C_2 = .9 k(\lambda_1)C_1$$

which means that we assumed a change in (concentration x absorption) of 10% between "on" and "off" the pollutant line.

Introducing all the parameters into the SNR equation and solving for $\bar{\xi}$ results in

$$\bar{\xi} = 1.6 \times 10^{-5} R(\text{cm})$$

for a topographical reflector. Using a retroreflector, the sensitivity is much increased and the expression for $\bar{\xi}$ becomes

$$\bar{\xi} = 7.1 \times 10^{-4} / (R\Gamma(R))$$

Since $\Gamma(R) = (700/\pi R) R^{-2}$ for $R > 50$ m, and $\Gamma(R) = 1$ for $R < 50$ m, the expression for ξ becomes

$$\begin{aligned}\xi &= 7.1 \times 10^{-4} / R(\text{cm}) && \text{for } R < 50 \text{ m} \\ \xi &= 2.8 \times 10^{-11} R(\text{cm}) && \text{for } R > 50 \text{ m}\end{aligned}$$

It is seen that for distances larger than 50 m, the advantage of the retroreflector over the topographic reflector is about 6 orders of magnitude. Numerical results of pollutant concentration for the two different kinds of reflectors are shown in Figure 5. 3. 1-38 as a function of range. It was assumed that the pollutants are uniformly distributed along the line-of-sights. These results show that, theoretically, all pollution levels of interest can be observed with the man-made retroreflectors. Using topographical reflectors, only relatively high pollution levels (. 1 ppm) can be observed at distances greater than 100 m.

The concentration levels shown here can be improved by using longer integration times, and using pollutant absorption lines whose coefficient is larger than the $1 \text{ cm}^{-1} \text{ atm}^{-1}$ assumed in the present calculations. On the other hand, the favorable results can be degraded by other error sources not considered here. In fact, as already briefly discussed in Section 5. 3. 1. 2, the two field programs conducted under EPA's and NSF's sponsorship^(148, 150) indicated a number of error sources which made the systems background-noise-limited instead of detector-noise limited.

Snowman and Gillmeister⁽¹⁶³⁾ discussed some of the atmospheric and other effects encountered during their field tests of the ILAMS. They state that scintillation was highest at midday during conditions of clear sky. However, scintillation was found to be equally high near midnight also under clear skies; while at dusk the scintillation was minimum both before and

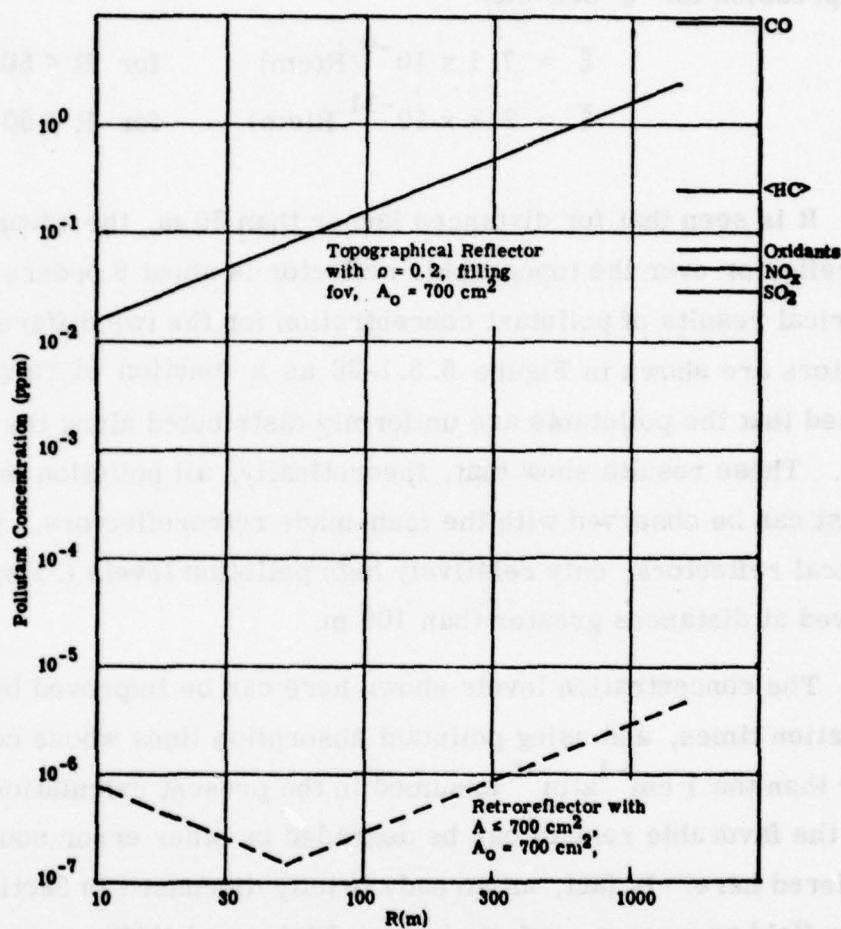


Figure 5. 3. 1-38. Long-Path Measurement (10% Accuracy) for Pollutant Concentration versus Range. Absorption Coefficient of Pollutant is $1 \text{ cm}^{-1} \text{ atm}^{-1}$; Difference between Pollutant Absorption and Background is 10%. The Laser Output is 1 W, Expanded into a Beam Area of 10 cm^2 .

after dark. The correlation between the scintillation magnitude and errors or pseudo-absorption signals on the signal processor output was high. During conditions of maximum scintillation the authors were able to detect five parts per million of ethylene and seven parts per million ammonia in a 27-foot test cell. The measured absorption signals for these concentrations were ten times the RMS error due to scintillation and atmospheric turbulence. To produce the same absorption signal the average concentration over the entire 10-thousand foot range over which the tests were conducted would require 14 parts per billion of ethylene and 19 parts per billion of ammonia. Thus, it is seen that 10-20 ppb of pollutants were detected with an SNR = 10, while the corresponding SNR for a detector-noise limited system would have been about 20,000 (see Figure 5. 3. 1-38). The experimental parameters were roughly the same.

The authors state further that the limit of the detectability of the system, that is, the accuracy with which the average concentration of ethylene and ammonia could be measured reliably over the path, was determined by the optical noise and scintillation produced by atmospheric turbulence and temperature gradients in the path. This noise can be produced by the atmosphere in several ways. The measured intensity distribution of a cross section of the laser beam at the output of the beam expander shows that the pattern is not as symmetrical as one would expect for a TEM₀₀ mode. Contours drawn through areas of constant power density show differences in the beam patterns in the near field. The data that had been accumulated indicate that it is these atmospheric effects (near the beam expander and the retroreflector) that are responsible for the noise and drift recorded.

Two types of retroreflectors have been used with grossly different results. A mosaic of 30 small cube corners with a total capture area of 1-square foot was used initially. This reflector resulted in one hundred percent modulation of the energy returned to the system at each wavelength on a clear but windy day; the modulation at each wavelength was apparently independent. It was found that by shaking the cube corner mosaic back and forth across the beam, the scintillation magnitude could be reduced to approximately 35 percent modulation. A substantial improvement of 20 percent modulation under the same weather conditions, in the magnitude of the scintillation noise was achieved by using a 12-inch aperture Dall-Kirkham telescope with a plane mirror at the image of the laser transmitter as a retroreflector. A similar retroreflector, the two-mirror system described previously as a "cat's eye" retroreflector, has also been used with about the same results as the three-mirror Dall-Kirkham configuration.

The authors report that they also had problems with water condensation on the retroreflector. An attempt was made to reduce the condensation by wrapping heating tape around the primary mirror. The authors state that this had disastrous results on the magnitude of the scintillation noise and had to be discontinued. Temperature and humidity variations did not appear to correlate with scintillation. Wind velocity had only a small effect (that of reducing the scintillation) under clear weather conditions during the day or late at night.

Similar conclusions were reached by Hinkley and Ku⁽¹⁵⁰⁾. They state that thermal fluctuations in the atmosphere were the main causes of noise in the received laser signal; and the problems of beam defocusing and steering have been reported for other laser systems as well⁽¹⁶⁴⁾. The best signal stability was found on cloudy or rainy days when the temperature variation over the outdoor path was small.

As an illustrative example of the signal degradation in the real atmosphere, the authors compare the results of indoor calibration with outdoor long-path measurements (see Figure 5. 3. 1-39).

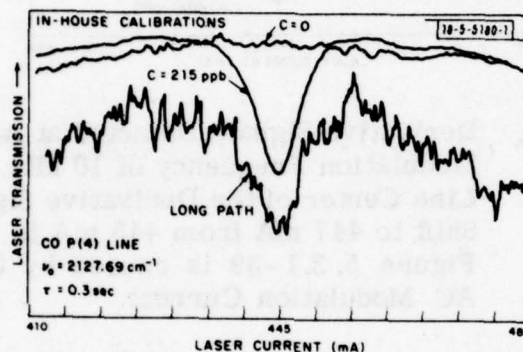


Figure 5. 3. 1-39. Laser Transmitted Signal for In-House Calibration and Outdoor Long-Path Measurement

While the indoor results show a very large SNR (> 100), the outdoor results are apparently degraded to a SNR $\sim 2-3$.

In order to improve the SNR, the authors applied the technique of derivative spectroscopy. The derivative spectroscopy method involves nothing more than modulating the diode current with a 20-mA superimposed sinusoidal current at a high frequency (~ 10 kHz). Since the laser emission frequency was modulated, the derivative of the absorption spectrum was obtained by synchronous detection at 10 kHz. At this high frequency, the effect of turbulence was minimized.

Applying this technique, the derivative of the signals shown in Figure 5. 3. 1. -39 are shown in Figure 5. 3. 1-40.

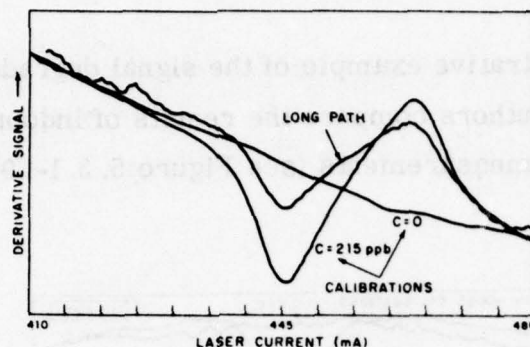


Figure 5.3.1-40. Derivative Signals Detected at AC Modulation Frequency of 10 kHz. Line Center of the Derivative Signal Shift to 447 mA from 445 mA in Figure 5.3.1-39 is caused by the AC Modulation Current.

Long-term effects due to atmospheric turbulence and scattering unrelated to CO content were then eliminated electronically by ratioing the derivative and transmitted signals, since both are usually affected proportionately by such influences. As an example, transmitted signals and the ratio of the derivative to transmitted signals are shown in Figure 5.3.1-41. In the time interval up to 4 minutes, a remarkable improvement in signal-to-background noise is obtained. At the 4-minute mark the fluctuating transmission signal is replaced with a constant voltage—the ratioed signal then becomes noisy.

McClenny⁽¹⁴³⁾ has discussed the methodology for comparison of the long-path monitors with a point sampler. Not surprisingly, they found that in stable meteorological conditions, the data taken by the long-path monitor and by a traversing point sampler agreed well within the statistical errors. However, in cases where the meteorological condition were not

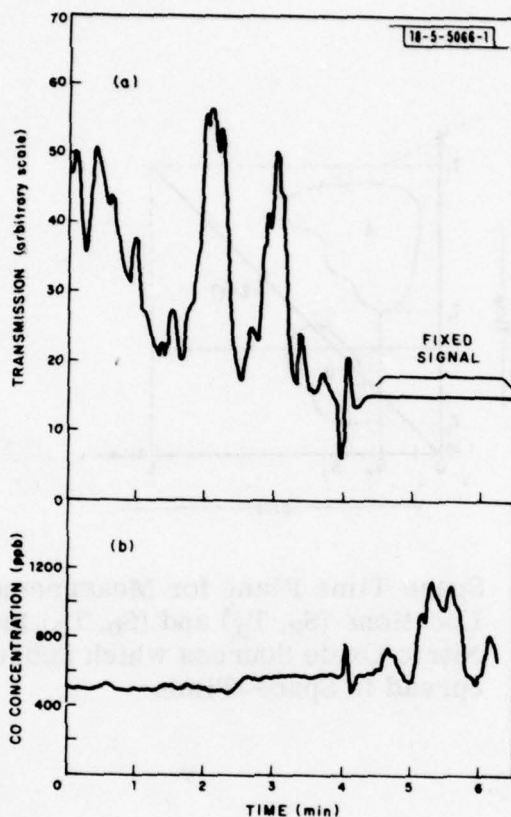


Figure 5. 3. 1-41. Analog Record of CO Monitoring Over 610-m Atmospheric Path. In (a) is the Direct Transmission Corresponding to the 170-Hz Chopped Total Signal; in (b) is the Ratio Between the 10-kHz Derivative Signal and Transmission Signal.

stable and where significant temporal gradients occurred (due to diurnal variations in radiation intensity or to variations in cloud cover), significant nonequivalence was detected. The influence of localized sources of NO on both types of monitors is schematically demonstrated in Figure 5. 3.1 -42.

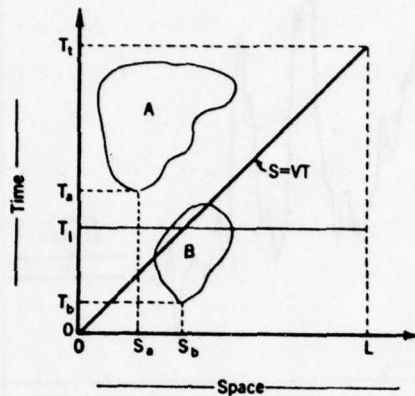


Figure 5. 3. 1-42.

Space Time Plane for Measurement Path; Locations (S_a, T_a) and (S_b, T_b) Indicate Nitric Oxide Sources which Subsequently Spread in Space-Time.

A long-path monitoring system will typically complete a measurement in several seconds, the exact value depending on the signal integration time. At any time, T_i , a value of the average concentration, is obtained which in Figure 5.3.1-42 corresponds to the average of the concentration contour along the line $T = T_i$, between $S = 0$ and $S = L$. Area A represents a region of the space-time plane which has been significantly affected by a source of NO originating at (S_a, T_a) , illustrating a case in which the path monitor reading can be weighted heavily while the source is not even detected by the point monitor. Area B in Figure 5.3.1-42 represents the extent of influence of a source of NO originating at (S_b, T_b) ; in this case the point monitor reading is weighted most heavily.

A comparison based on signal traversal data taken during the afternoon diurnal variation on 23 October 1973 is shown in Figure 5. 3. 1-43. The authors state that the two monitors track reasonably well and a review of the individual chart recordings shows that in those comparisons where significant disparities exist, localized gradients in ozone concentration occur. For ideal comparison conditions the data should agree to within 4 ppb, based on the statistical variations of the traversing point sampler.

A final report about the long-path monitoring of CO was issued by Ku and Hinkley^(242, 243). The system consisted of a tunable diode laser and a retroreflector at various distances. We have judged previously this system approach as the most sensitive one (See Figure 5. 3. 1-38).

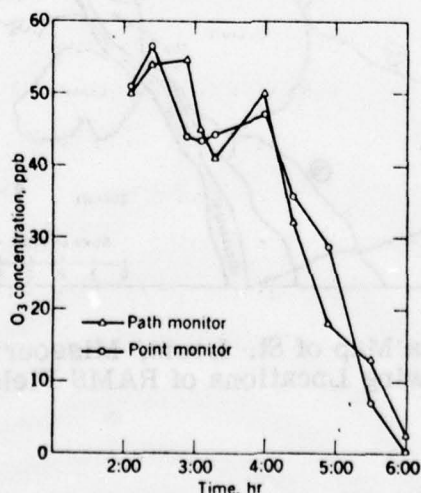


Figure 5. 3. 1-43.

Comparison Sequence Based on Single Point Monitor Traversals

It is thus interesting to compare the predicted results with actual field data, especially since other point samplers were used to provide "ground-truth" data. Two measurement sites were used (#105 and #108 in Figure 5. 3. 1-44. Comparisons were made between the long-path CO results and the RAMS station point readings and/or data from a gas filter correlation instrument (GFC) located in the monitoring van. Meteorological factors such as wind direction and velocity were also considered since the comparison was between a long-path monitor yielding spatially averaged CO data, and point measurements from the RAMS and GFC instruments.

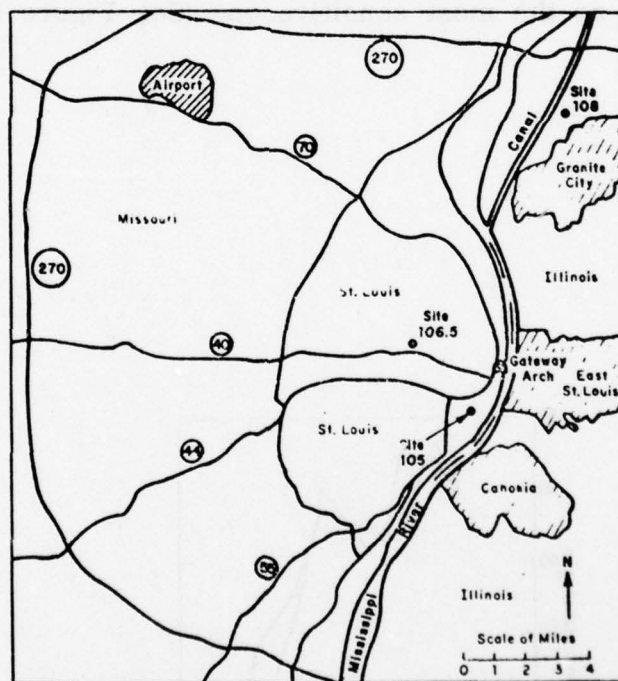


Figure 5. 3. 1-44. Area Map of St. Louis, Missouri, Showing Locations of RAMS Field Sites.

The PbSSe diode laser was tuned to the P(9) or P(10) fundamental absorption lines of CO at 2103 or 2107 cm^{-1} , respectively. At Site 105 an unknown atmospheric pollutant was found to have absorption lines near these particular CO lines, which sometimes interfered with off-line-center measurements during periods of high CO concentration and long-path lengths ($> 1 \text{ km}$), (see Figure 5. 3. 1-45). Further tests will be needed to identify this pollutant. Compared to interference-free CO monitoring with lasers operating on the P(4) line at 2126.69 cm^{-1} during RAPS-74, the frequency region of 2103 - 2107 cm^{-1} is found to be inferior for monitoring CO. Calibration

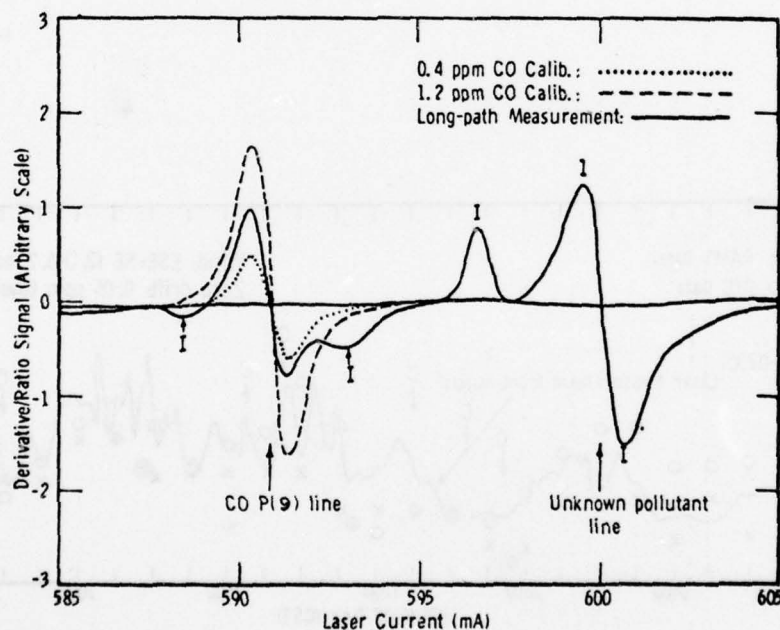


Figure 5. 3. 1-45. Derivative/Ratio Signal (Proportional to CO Concentration). Scans as a Function of Laser Current (or Frequency) through CO P(9) Absorption Line at 591 mA (2107 cm^{-1}), and Absorption Lines from Unknown Interfering Pollutant at 588.7, 592.8, 596.6 and 600 mA.

was found to remain stable to within $\pm 2\%$ over a 25-hour period of continuous monitoring, using an automatic frequency control (AFC). But without such a control, calibration may vary up to $\pm 10\%$. A typical result when the CO concentration was generally low is shown in Figure 5. 3. 1-46 for site 108, together with results of two point samplers, one of which is a gas chromatograph, while the other is a GFC instrument. Calibration times are indicated by a "C". The instability in calibration and zero drift together resulted in an overall uncertainty of $\pm 10\%$. The overall agreement between the long-path monitor and the two-point samplers varied considerably during the 25-hour period. Since the agreement between the

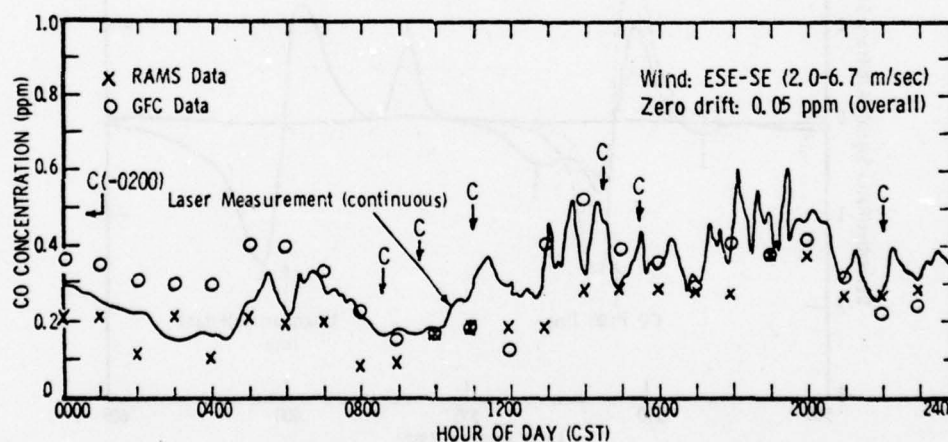


Figure 5. 3. 1-46. Around-the-Clock CO Monitoring on 1 August 1975 at RAMS 108. Distance to Retro = 0.34 km. Monitor Direction: North.

two-point samplers was also not uniformly good, it is difficult to draw conclusions about the compatibility of these data. Some better agreement between the gas chromatograph and the long-path monitor is demonstrated in Figure 5.3.1-47, where two peak concentrations for CO were observed within a 2-hour period, although a small peak at 0630 did show up only on one trace.

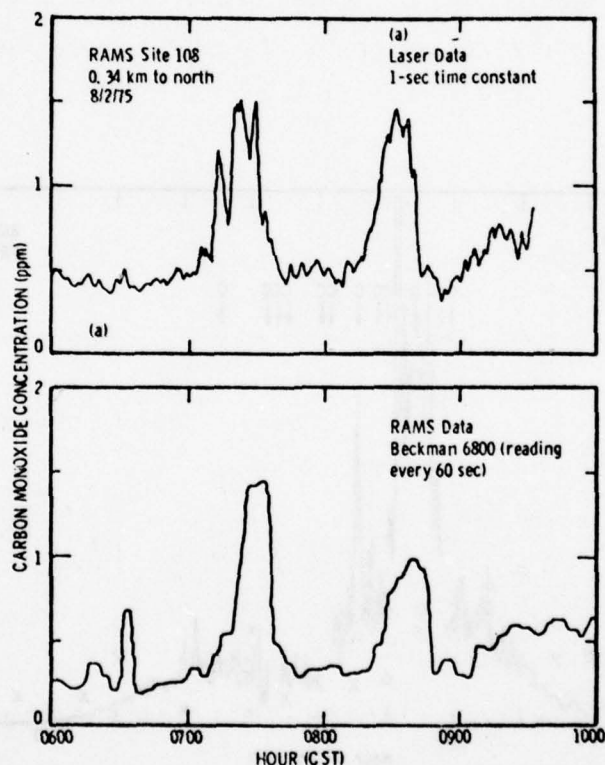


Figure 5.3.1-47. Comparison of CO Monitoring Results, from 0600 to 1000 CST on 2 August 1975 at RAMS 108, between (a) the Long-Path Monitor and (b) RAMS' Beckman 6800 Gas Chromatograph. Time Constant is 1 sec for (a), and 1 min. for (b).

Agreement between long-path data and those of the two point samplers varied also at site 105, where generally higher CO levels were observed during the week. One can see in Figure 5. 3. 1-48 that maximum levels of about 4 ppm were observed in the long-path while the point samplers were below 1 ppm. In this case, non-uniform meteorological conditions probably contributed to the observed difference, indicating again (see p. 5. 3. 1. 5j and Ref. 143) that long-path monitors may observe pockets of polluted air masses that are missed by point samplers.

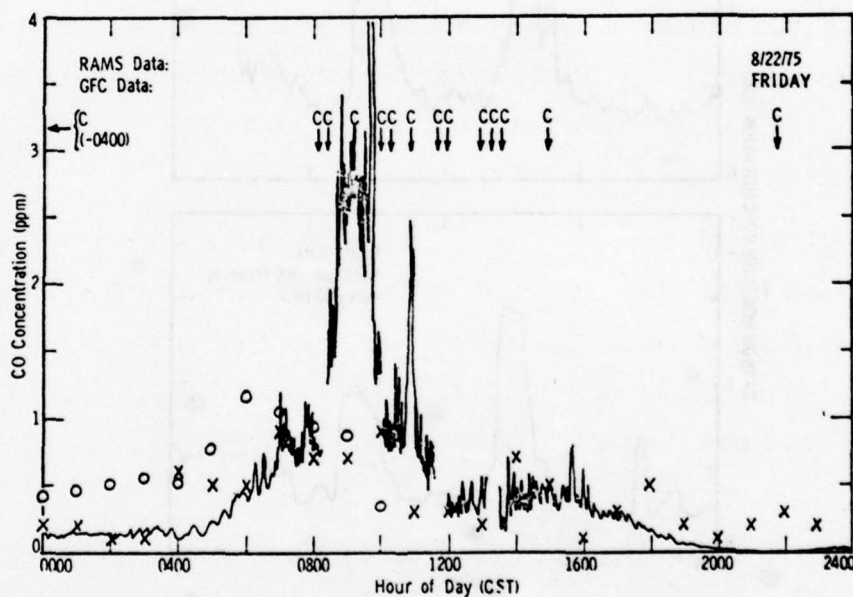


Figure 5. 3. 1-48. Comparison of CO Concentration Measured Over Identical Paths (0.12 km Southerly) on 22 August 1975 (Friday) at RAMS 105.

All the data were taken in the derivative/ratio mode to minimize atmospheric fluctuations. Mathematically, this mode is expressed as

$$\frac{1}{P_r} \frac{d P_r}{d\omega} = \frac{\delta P_r}{\delta k(\omega)} \frac{\delta k(\omega)}{\delta\omega} \frac{1}{P_r} = \frac{2 k_0 l (\omega - \omega_0) c}{\gamma^2 [1 + (\omega - \omega_0)^2 / \gamma^2]^2}$$

where k_0 is the absorption coefficient at the line center, l is the distance, ω is the laser frequency, ω_0 is the frequency at the line center, c is the pollutant concentration, and γ is the half-width at half-height. One can see that the time-dependent scattering parameter in P_r (Eq. 5. 2. 1-1) is eliminated and that for a given laser frequency the signal is directly proportional to the pollutant concentration. Ku and Hinkley state that for maximum sensitivity, the ratioed signal should be evaluated at a laser frequency where the slope of the absorption line is greatest. The only exception is when the pollutant concentration is so high that most of the laser power is absorbed. In such instances a weaker line should be selected.

The signal $[(d P_r/d\omega)/P_r]$ as a function of pollutant concentration can be obtained from laboratory and/or field calibration. The calibration is made by using a gas cell with a known amount of pollutant gas. This can be done during the actual field test by observing the signal change after inserting the gas cell. An example of such a calibration is shown in Figure 5. 3. 1-49.

Summarizing the results by Ku and Hinkley, we draw the following conclusions:

- As predicted theoretically, the long-path laser system with retroreflector provides one of the most sensitive remote monitors. Although the actual SNR is difficult to determine from the presented data, it is certainly adequate to measure CO concentration levels near the "unpolluted" level, i. e., 0. 1 ppm.

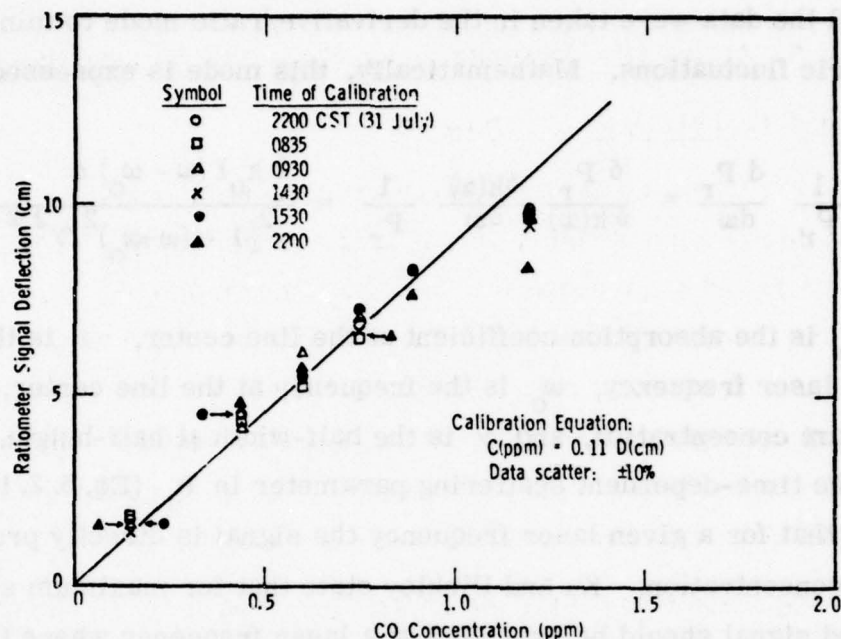


Figure 5. 3. 1-49. CO Calibration Curve for Long-Path Laser Monitoring on 1 August 1975 at RAMS 108. Distance to Retro = 0.34 km.

- However, this result was only obtained after taking the ratio of the derivative to the signal of the return beam. Otherwise, the atmospheric fluctuations would have severely lowered the SNR.
- An absolute uncertainty of at least $\pm 2\%$ must be ascribed to the data due to calibration and zero drift over a period of 24 hours. This degree of stability could only be obtained through the employment of an "automatic frequency control".

5. 3. 2 Active CW System: Long-Path with Broad-Band Source

5. 3. 2. 1 Principle of Operation

In contrast to the systems described in Section 5. 3. 1, the systems of interest in this section utilize a broad-band transmitter that cannot be tuned. They will be called "illuminators". The wavelength discrimination is done at the receiver end, in general. (An exception to this characterization is the gas filter correlation concept, where the spectral filtering can be done at the source by a gas cell). The system is always bistatic. Because of the much lower radiation intensities involved, topographical reflectors cannot be used. A typical arrangement is shown in Figure 5. 3. 2-1.

The equation expressing the energy received from an illuminator is basically the same as given for the system with a laser source and retro-reflector, viz., Eq. (5. 3. 1-2), replacing the transmitted power P_t by

$$P_t = (A \Omega)_t \int_{\lambda_1}^{\lambda_2} \epsilon(\lambda) N^0(\lambda, T) d\lambda \quad (5. 3. 2-1)$$

where $(A \Omega)_t$ is the throughput of the transmitter, $\epsilon(\lambda)$ is the emissivity and $N^0(\lambda, T)$ is the Planck function. The limits in wavelength are given by the system bandpass filter.

Using the expressions for the wavelength-dependent transmission, viz. Eq. (5. 3. 1-4) and for the efficiency of filling the receiver aperture, viz. Eq. (5. 3. 1-9), we have

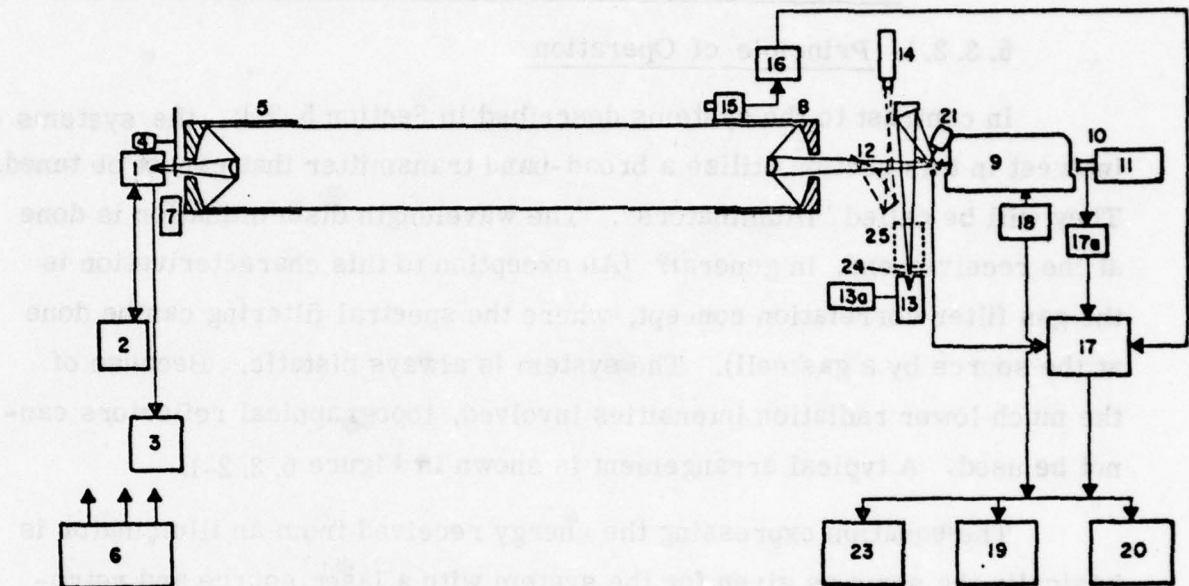


Figure 5. 3. 2-1. Schematic of a Long-Path Monitor⁽¹⁶⁵⁾, using a Blackbody as Illuminator. The Components are:

- | | |
|-----------------------------------|------------------------------|
| 1. Blackbody | 13a. Temperature Controller |
| 2. Temperature Controller | 14. Telescope |
| 3. Continuous Temperature Readout | 15. InAs Detector |
| 4. Chopper | 16. Preamplifier |
| 5. Source Optics | 17. Amplifying System |
| 6. Power Generator | 17a. Preamplifier |
| 7. Boresight Microscope | 18. Wavelength Drive |
| 8. Receiver Optics | 19. DVM-Digital Readout |
| 9. Monochromator | 20. Strip Chart Recorder |
| 10. Ge:Hg Detector | 21. Chopper |
| 11. Mechanical Cooler | 22. Power Supply (not shown) |
| 12. 2 Position Mirror | 23. Magnetic Tape |
| 13. Calibration Blackbody | 24. Precision Aperture |
| | 25. Gas Cell |

$$P_r = \int_{\lambda_1}^{\lambda_2} P_r(\lambda) d\lambda = \frac{(A \Omega)_t A_r}{\pi/4(2\alpha_t R + d_t)^2} \int_{\lambda_1}^{\lambda_2} \epsilon(\lambda') N^0(\lambda', T) \eta(\lambda') \exp \left[-p_t R \sum_{i=1}^n k_i(\lambda') \bar{C}_i \right] d\lambda' \quad (5. 3. 2-2)$$

In the limit of a small spectral interval at λ_1 , Eq. (5. 3. 2-2) may be replaced by

$$P_r = Q'' N^0(\lambda_1, T) \eta(\lambda_1) \exp \left[-p_t R \sum_{i=1}^n k_i(\lambda_1) \bar{C}_i \right] \Delta\lambda_1 \quad (5. 3. 2-3)$$

where $Q'' = (A \Omega)_t A_r \left[\pi/4(2\alpha_t R + d_t)^2 \right]^{-1}$ and $\epsilon(\lambda_1) = 1$, assuming a blackbody source.

In using a spectrally scanning instrument at the receiver end, a transmission spectrum is obtained, whose information content depends upon the spectral resolution of the instrument. This is illustrated in Figure 5. 3. 2-2), where atmospheric transmission spectra are shown taken with three different instrument resolutions between $3.33 \mu\text{m}$ (3000 cm^{-1}) and $5.25 \mu\text{m}$ (1900 cm^{-1}). The spectrum with the highest resolution in this series (2.5 cm^{-1}) shows the greatest amount of individual absorption lines. Of course, even that resolution is not high enough to resolve all the fine structure of atmospheric spectra. Great care has to be exercised to interpret complex spectra and to analyze them in terms of pollutant concentration. In the case of diatomic and light polyatomic molecules and no interference by other molecules, single lines can be observed with a spectral resolution of 0.1 cm^{-1} . In the case of heavier polyatomic molecules and of lower spectral resolution, a number of lines will be observed simultaneously.

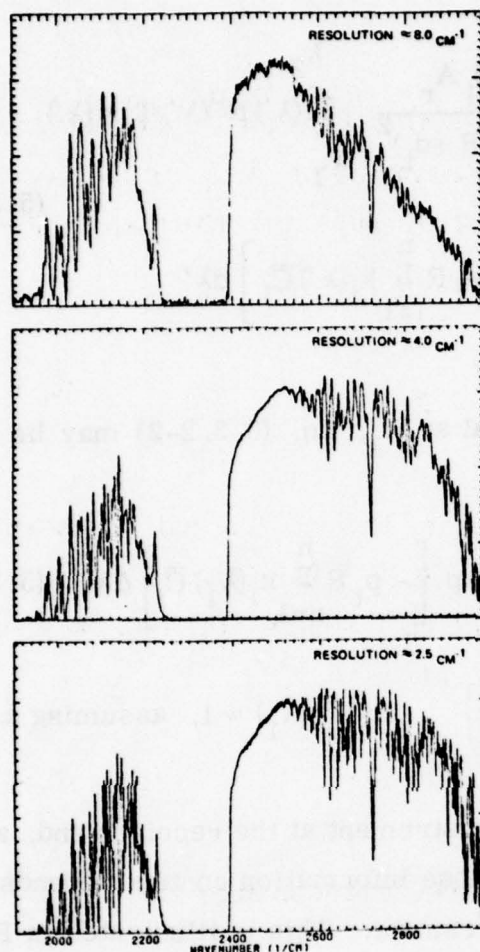


Figure 5. 3. 2-2

Spectra of an 1800°K Blackbody as Seen Through 10,000 Feet of Atmospheric Attenuation, Plotted to Three Different Spectral Resolutions⁽¹⁶⁶⁾.

Thus, for the interpretation of measured spectra in terms of pollutant concentration, spectral parameters have to be known both for the single line and multiple line cases. In the following, we review briefly the interpretation of spectra, composed either of isolated single lines or of multiple lines (band spectra).^(130a, 167)

The absorption of a line is given by

$$\alpha = 1 - \tau = \frac{1}{\Delta\omega} \int [1 - e^{-k(\omega)u}] d\omega \quad (5. 3. 2-4)$$

where $u = C p_t R$ and $\omega(\text{cm}^{-1}) = 1/\lambda(\text{cm}) = 10^4/\lambda(\mu\text{m})$. [For the product $(\alpha \Delta \omega)$, the term "equivalent width" of a single line W_{sl} is frequently used.] At atmospheric pressures, the line shape is Lorentzian and the absorption coefficient $k(\omega)$ is given by

$$k(\omega) = \frac{S\gamma/\pi}{(\omega - \omega_0)^2 + \gamma^2} \quad (5. 3. 2-5)$$

where S is the line strength, γ is the line half width at half height (HWHH) and ω_0 is the line center. Introducing Eq. (5. 3. 2-5) into (5. 3. 2-4) and carrying the integration out from $-\infty$ to $+\infty$, the equivalent width of a single line becomes

$$W_{sl} = 2\pi\gamma x e^{-x} [I_0(x) + I_1(x)] \quad (5. 3. 2-6)$$

where I_0 and I_1 are the modified Bessel functions and

$$x = Su/2\pi\gamma \quad (5. 3. 2-7)$$

The two parameters S and γ are determined in the laboratory by making curve-of-growth measurements. It is convenient to make measurements in the two limits of small and large values of x :

$$W_{sl} = Su \quad \text{for } x < 0.02 p$$

$$W_{sl} = (4S\gamma u)^{1/2} \quad \text{for } x > 12.5 p^{-1}$$

These approximations (called the "linear" and "square root" approximations) are valid within p percent.⁽¹⁶⁷⁾ For instance, the values for W_{sl} are accurate to within 5 percent when $x < 0.1$ and $x > 2.5$, respectively. Experience shows that for a reliable measurement of S three data points in the linear region should be obtained and that for a reliable measurement of the product $(S \gamma)$ three data points should be obtained in the square-root region. Care must be exercised that the assumptions of the validity of these approximations are fulfilled. This is done by plotting the data points (W versus u) on logarithmic scales. In the linear region, the plot is a straight line with a slope of 1, and in the square-root region, it is also a straight line with a slope of $1/2$. Between these two segments lies the "transition" region.

Experimentally, the procedure is as follows: The spectroscopic instrument with a slit function g is scanned over a single spectral line, whose true shape is shown in Figure 5.3.2-3. The true shape of the line is distorted by the slit function $g(\omega - \omega')$, and appears at the output of the instrument in the shape also shown in the figure. One can show that the areas under the undistorted and distorted spectral line profiles remain the same. That means that W is an invariant and does not depend upon the slit function of the instrument. In other words, the W determined in the laboratory with one instrument can be used to interpret the field data taken with another instrument.

If several lines contribute to the absorption in the spectral interval given by the instrument slit function, band models must be used. The most useful band model applicable to atmospheric pollutants is found to be the statistical model. In that case, the mean absorption is given by

$$\alpha = 1 - \bar{\tau} = 1 - \exp(-\bar{W}/d)$$

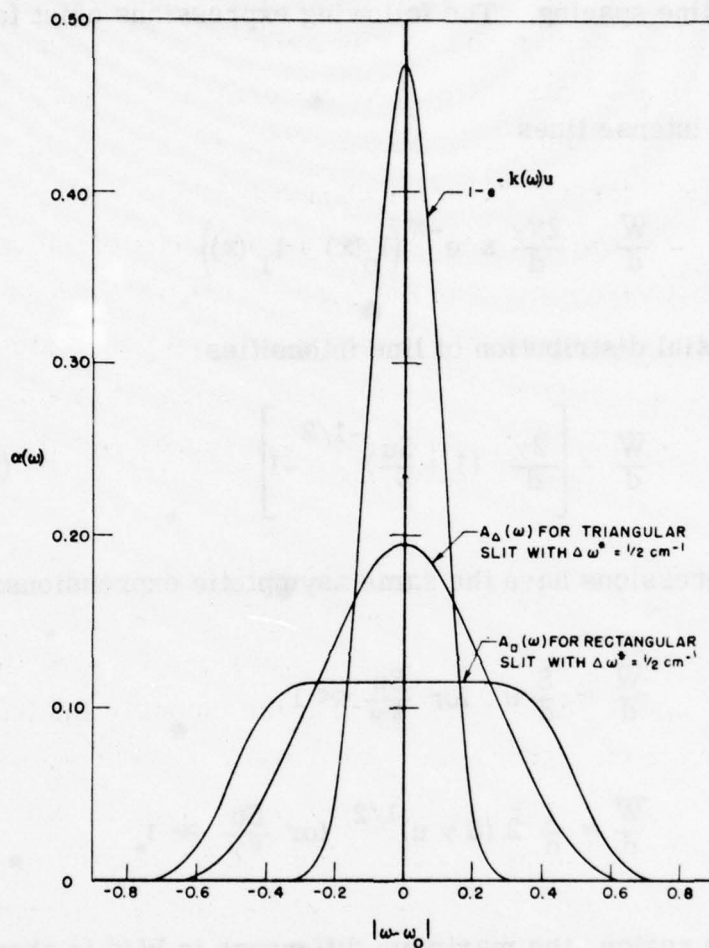


Figure 5. 3. 2-3.

True Line Profile (Doppler) with $\gamma = 0.1 \text{ cm}^{-1}$ and Observed Line Profiles Assuming Triangular and Rectangular Slit Functions ($\Delta\omega = 0.5 \text{ cm}^{-1}$) [Ref. 167a].

where \bar{W} is the mean equivalent width of the lines in this interval and d is the mean line spacing. The following expressions exist for this ratio:

Equally intense lines

$$\frac{\bar{W}}{d} = \frac{2\pi\gamma}{d} \times e^{-x} (I_0(x) + I_1(x))$$

Exponential distribution of line intensities

$$\frac{\bar{W}}{d} = \left[\frac{2\gamma}{d} \left(1 + \frac{Su}{\gamma} \right)^{-1/2} - 1 \right] \quad (5. 3. 2-8)$$

All of these expressions have the same asymptotic expressions:

$$\frac{\bar{W}}{d} \approx \frac{S}{d} u \quad \text{for } \frac{Su}{\pi\gamma} \ll 1$$

$$\frac{\bar{W}}{d} \approx \frac{1}{d} 2 (S \gamma u)^{1/2} \quad \text{for } \frac{Su}{\pi\gamma} \gg 1$$

In the transition region, the maximum difference in W/d is about 25% between the equally intense lines and the $1/S$ distribution (see Figure 5. 3. 2-4).

A standard notation for the parameters S/d and γ/d is

$$\frac{S}{d} = k \quad (\text{cm}^{-1} \text{atm}^{-1})$$

$$\frac{\gamma}{d} = a$$

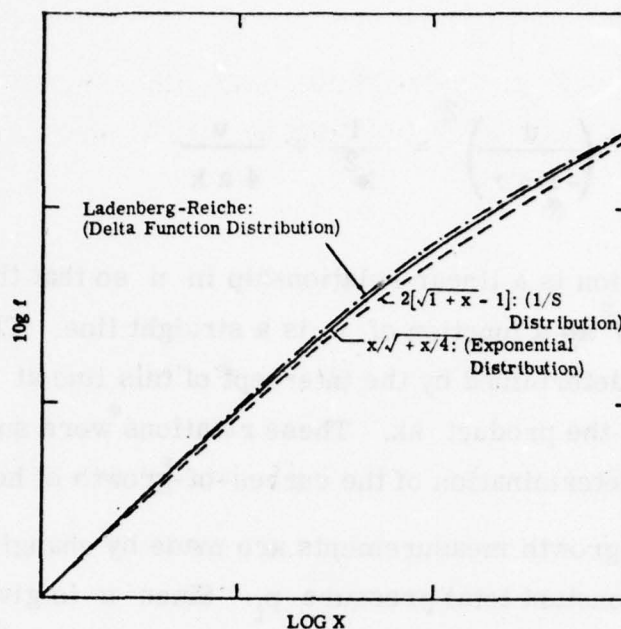


Figure 5. 3. 2-4. Collision-Broadened Curves of Growth for Various Intensity Distributions

where k represents the average absorption coefficient and a is called the fine structure parameter.

The laboratory procedure is the same as previously outlined with one exception. Instead of making measurements only in the linear and square-root regions, measurements in the "transition region" are also required in order to determine which of the three models applies.

If an accuracy of $\pm 12.5\%$ in the transition region is deemed sufficient, the expression given for the statistical model (Eq. 5. 3. 2-8) is recommended. In that case

$$-\ln \tau = ku \left(1 + \frac{ku}{4a} \right)^{-1/2}$$

or

$$\left(\frac{u}{-1 \ln \tau} \right)^2 = \frac{1}{k^2} + \frac{u}{4 a k}$$

This last expression is a linear relationship in u so that the observed quantity $(-u/\ln \tau)^2$ as a function of u is a straight line. The absorption coefficient k is determined by the intercept of this line at $u = 0$ and the shape determines the product ak . These relations were successfully employed in the determination of the curves-of-growth of hot water vapor. (168)

Curve-of-growth measurements are made by changing the optical thickness u at constant total pressure p_t . Since u is given by the product of cell length l and partial pressure $p_p = C p_t$, where C is the fractional concentration and p_t is the total pressure, a change in either l and/or p_p is sufficient. However, it must be remembered that a change in p_p without a simultaneous change in C is not sufficient. In other words, a change in p_t alone does not result in independent values of transmission. This mistake has been made quite often in the past, where researchers prepared a mixture of gases in a mixing tank and added this mixture to the absorption cell at various total pressures, assuming that they had thus measured different points along the curve-of-growth. The fallacy of this procedure is evident if we rewrite Equation (5. 3. 2-8) in the following way, remembering that $a = a_o p_t$:

$$\frac{W/d}{p_t} = \frac{-1 \ln \tau}{p_t} = k C l \left(1 + \frac{k C l}{4 a_o} \right)^{1/2}$$

It is clearly seen that if C and l are kept constant and only p_t is changed, the right-hand side is a constant and neither k nor a_o can be determined separately.

It is usually easier and more accurate to change the cell length l rather than the concentration C . This can be done in cells which have adjustable multiple paths, such as in a White-cell arrangement.

The optical thickness to be measured in the laboratory must cover the range of the optical thickness expected in the field. Thus, for an expected concentration of 10 ppm of a given pollutant to be observed over a pathlength of 4 km, the optical thickness is 4 cm-atm. If it would be possible to use a partial pressure of 1 atm for the pollutant, a cell length of at least 4 cm must be used. However, in this case, the measurements would be made under the condition of self-broadening. The results would thus not be applicable to the atmospheric case, in which air-broadening is dominant. This is especially true for polar molecules, which may have a self-broadening coefficient (ratio of self-broadened half-width to nitrogen-broadened half-width) of the order of 10. Thus to keep the actual half-width within, say, 1% of the self-broadened value, the maximum concentration should not exceed 1000 ppm. At this concentration and 1 atm pressure, a pathlength of 40 m is required to produce an optical thickness of 4 atm-cm.

The above analysis was based on the assumption that the absorption line or lines were not interfered by other species. In cases where that assumption cannot be made, Derr et al.⁽¹⁶⁹⁾ have developed a fitting process, in which all the species concentrations contributing to the measured spectrum are adjusted until a "best-fit" in a least squares sense is produced. However, the authors state that "there are some sets of experimental data which just don't lend themselves properly to the minimization technique of determining atmospheric gas constituents and their corresponding concentrations from their superimposed infrared spectra. This may occur when the data is too noisy, or too imprecise, or when the scales (I/I_0 or ν) must be corrected non-linearly. Without good data, good results cannot be achieved."

We will now briefly describe the principle of the different instruments that can be used as tunable receivers. In Figure 5. 3. 2-5 we show the schematic of six of those.

A filterwheel radiometer (a), consists of a telescope, which collects the radiation from the transmitter, a chopper, a filterwheel, and a relay optics, which refocuses the radiation onto a detector. The advantage of the system is the high throughput ($A\Omega$), because all the received energy per spectral resolution element is utilized. The disadvantage is a poor resolution. For interference filters, the resolution that can be achieved is about 1%, i. e., $0.05 \mu\text{m}$ or 20 cm^{-1} at $\lambda = 5 \mu\text{m}$.

A monochromator (b), consists of a collecting optics (telescope), which focuses the energy of the transmitter onto the entrance slit. A concave mirror collimates the energy, which then gets dispersed by a reflecting grating. Another concave mirror refocuses the energy onto the exit slit. (This is just one of many possible arrangements of focusing mirrors and grating. The one shown here is known under the name Czerny-Turner mounting. Another type is the Ebert mounting, using only one mirror.) An external optics focuses the energy onto a detector. The advantage of the system is the much higher resolution that can be achieved compared with a radiometer. The resolving power ($\lambda/\Delta\lambda$) of a grating is given by the product of nN , where n is the order and N is the number of rulings. A resolving power of 600,000 have been achieved, giving a theoretical spectral resolution of about 0.003 cm^{-1} at $5 \mu\text{m}$. In practice, however, a spectral resolution of 0.1 cm^{-1} is more common. The different overlapping orders must be separated, which can be done by a fore-prism or broadband filter. The disadvantage of a monochromator is that the high resolution can be achieved only by using very narrow widths of the entrance and exit slit, thus limiting the throughput. In addition, time is required to record an extended spectrum.

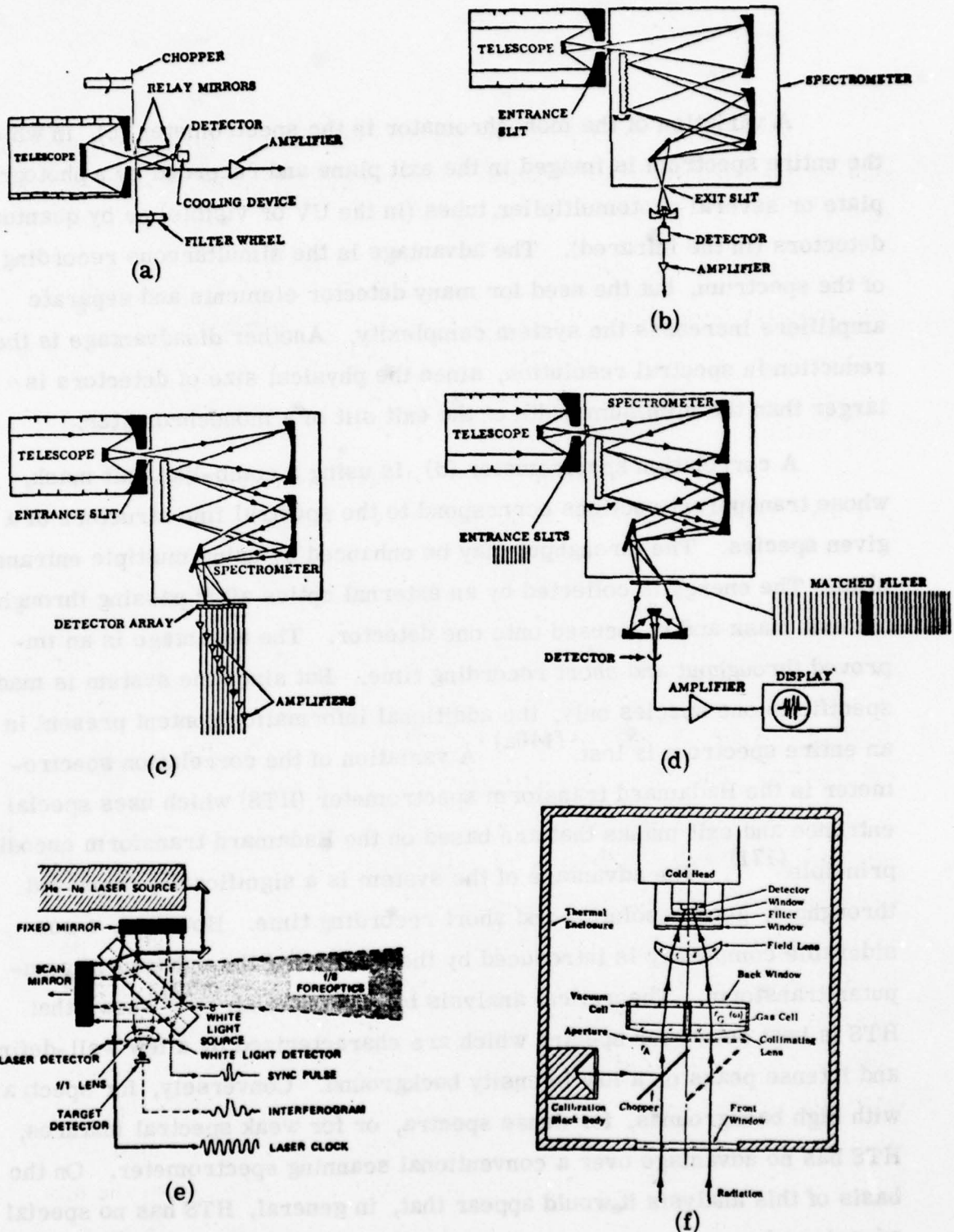


Figure 5.3.2-5. Schematic of Selected Tunable Receivers:
 (a) Filterwheel Radiometer, (b) Monochromator,
 (c) Spectrometer, (d) Dispersive Correlation
 Spectrometer, (e) Interferometer-Spectrometer
 (f) Gas-Filter-Correlation Instrument.

A variation of the monochromator is the spectrometer (c), in which the entire spectrum is imaged in the exit plane and recorded by a photographic plate or several photomultiplier tubes (in the UV or visible) or by quantum detectors (in the infrared). The advantage is the simultaneous recording of the spectrum, but the need for many detector elements and separate amplifiers increases the system complexity. Another disadvantage is the reduction in spectral resolution, since the physical size of detectors is larger than the minimum width of the exit slit of a monochromator.

A correlation spectrometer (d) is using a comb-like exit mask, whose transparent sections correspond to the spectral fine structure of a given species. The throughput may be enhanced by using multiple entrance slits. The energy is collected by an external optics after passing through the exit mask and is focused onto one detector. The advantage is an improved throughput and short recording time. But since the system is made specific to one species only, the additional information content present in an entire spectrum is lost.^(146a) A variation of the correlation spectrometer is the Hadamard transform spectrometer (HTS) which uses special entrance and exit masks that are based on the Hadamard transform encoding principle⁽¹⁷¹⁾. The advantage of the system is a significantly improved throughput, good resolution and short recording time. However, a considerable complexity is introduced by the masks and the subsequent computer transform. Theoretical analysis by Larson et al.⁽¹⁷²⁾ shows that HTS is best suited for spectra which are characterized by a few well-defined and intense peaks on a low intensity background. Conversely, for spectra with high backgrounds, for dense spectra, or for weak spectral features, HTS has no advantage over a conventional scanning spectrometer. On the basis of this analysis it would appear that, in general, HTS has no special advantage for remote sensing of pollutants, since their spectra are generally weak and mixed with interfering spectra.

The next system discussed here is the interferometer-spectrometer (e), which is based upon the Fourier transform. The resolution is given by the maximum mirror travel and, thus, can be made very large. However, the time required would also increase. Using a laser as a fringe reference, the interferometer-spectrometers have found wide-spread use over the last 10 years. Their advantage is the high throughput and high resolution with multiplexing. The disadvantages are the system complexity and computer transform. The theory and practical applications were discussed by Mertz⁽¹⁷³⁾ and Steel⁽¹⁷⁴⁾.

The last system to be described here is the gas filter correlation instrument (f). It is based upon the non-dispersive correlation, using a cell filled with the pollutant species of interest as the reference. The advantage of the system is its simplicity, although great care has to be taken to avoid thermal drifts. Although the approach was first introduced for passive remote sensing^(175, 176), it has found application lately in active remote sensing, using a corner cube reflector array⁽¹⁷⁷⁾.

A qualitative survey of the above systems in terms of sensitivity, specificity, complexity, required observation time and available information content was given by Ludwig et al.^(146a). Their summary table is reproduced here in Table 5. 3. 2-1.

TABLE 5. 3. 2-1. Qualitative Comparison of Spectroscopic Instruments

Instrument	Sensitivity	Specificity	Complexity Of Instrum.	Observ. Time	Information Content	Remarks
Radiometer (filter wheel or many single filters)	Medium	Low	Low	Short	Medium	Limit $\Delta\omega \sim 3 \text{ cm}^{-1}$; many channels required
Radiometer (polychromator)	Low Medium	High Low	Medium	Short Short	Medium	Assuming $\Delta\omega < 1 \text{ cm}^{-1}$ Assuming $\Delta\omega > 1 \text{ cm}^{-1}$; Multiple detectors required
Scanning — Spectrometer	Low Medium	High Low	Medium	Long Medium	High	Assuming $\Delta\omega < \text{cm}^{-1}$ Assuming $\Delta\omega > \text{cm}^{-1}$
Optical Correlation Instrument	High	High	Medium	Short	Medium	Matched filter with multi- ple entrance slits and nondispersive
Interferometer — Spectrometer	High	High	High	Medium	High	Sampling time at least 10 sec; image motion compensation required; large information content for wide spectral interval

5. 3. 2. 2 State-of-the-Art

Although the long-path approach using an illuminator and a tunable receiver appears to be straightforward and relatively easy to assemble, only very few systems have been utilized to monitor the ambient air. One system was specifically designed and fabricated to serve as a prototype that could assist EPA in specifying future systems. This system was built by General Dynamics/Convair for EPA and bears the acronym ROSE (Remote Optical Sensing of Emissions). Originally, it was to perform in the active long-path mode as well as in the smokestack emission mode. However, it has been used much more often in the latter mode^(178, 179). The few field data obtained in the active long-path mode were reported by

Streiff and Ludwig^(130a). The schematic of the system was already shown in Figure 5. 3. 2-1. Both the transmitter and receiver optics consist of Dall-Kirkham telescopes with a 60-cm diameter primary mirror. The tunable receiver consists of a Perkin-Elmer Model 210 linear wave number drive monochromator, that contains two gratings, each being used in first order with long-wave pass filters to cover the spectral ranges 2.8-5.5 and 7.5-14 microns. The spectral resolution is variable, depending on the slit opening, but 1 cm^{-1} at $10\text{ }\mu\text{m}$ and 4 cm^{-1} at $5\text{ }\mu\text{m}$ are achievable in the absorption mode. The Ge:Hg detector is operated at 28°K . The source unit contains a blackbody radiation source, located at the telescope focus. The blackbody is operable over the range $1100\text{-}1800^\circ\text{K}$ and is optically chopped. A photograph of the ROSE receiver telescope, together with the monochromator and the detector housing and cryogenic cooler is shown in Figure 5. 3. 2-6. The black tube at the rim of the telescope housing contains the detector for picking up the chopped signal from the remote transceiver, used in the sync rectification.

Field tests with the ROSE system were conducted in the Pomona area during June/July 1971. Also involved in the tests were the interferometer system provided by General Dynamics/Electro Dynamic Division and a filterwheel radiometer receiver, built by Bendix for EPA. One particular set-up of all those instruments is shown in Figure 5. 3. 2-7. Typical transmission spectra taken by the ROSE system are shown in Figure 5. 3. 2-8. for the spectral region from 4 to $5\text{ }\mu\text{m}$, taken with two different resolutions.

The much enhanced information content in the spectrum with the better resolution is quite apparent. The fine structure between 2100 and 2200 cm^{-1} originates from the CO molecule. The total absorption between 2275 and 2400 cm^{-1} is due to the $4.3\text{ }\mu\text{m}$ band of CO_2 . A spectrum between 8 and $12\text{ }\mu\text{m}$ is shown in Figure 5. 3. 2-9, where the appearance of ozone is

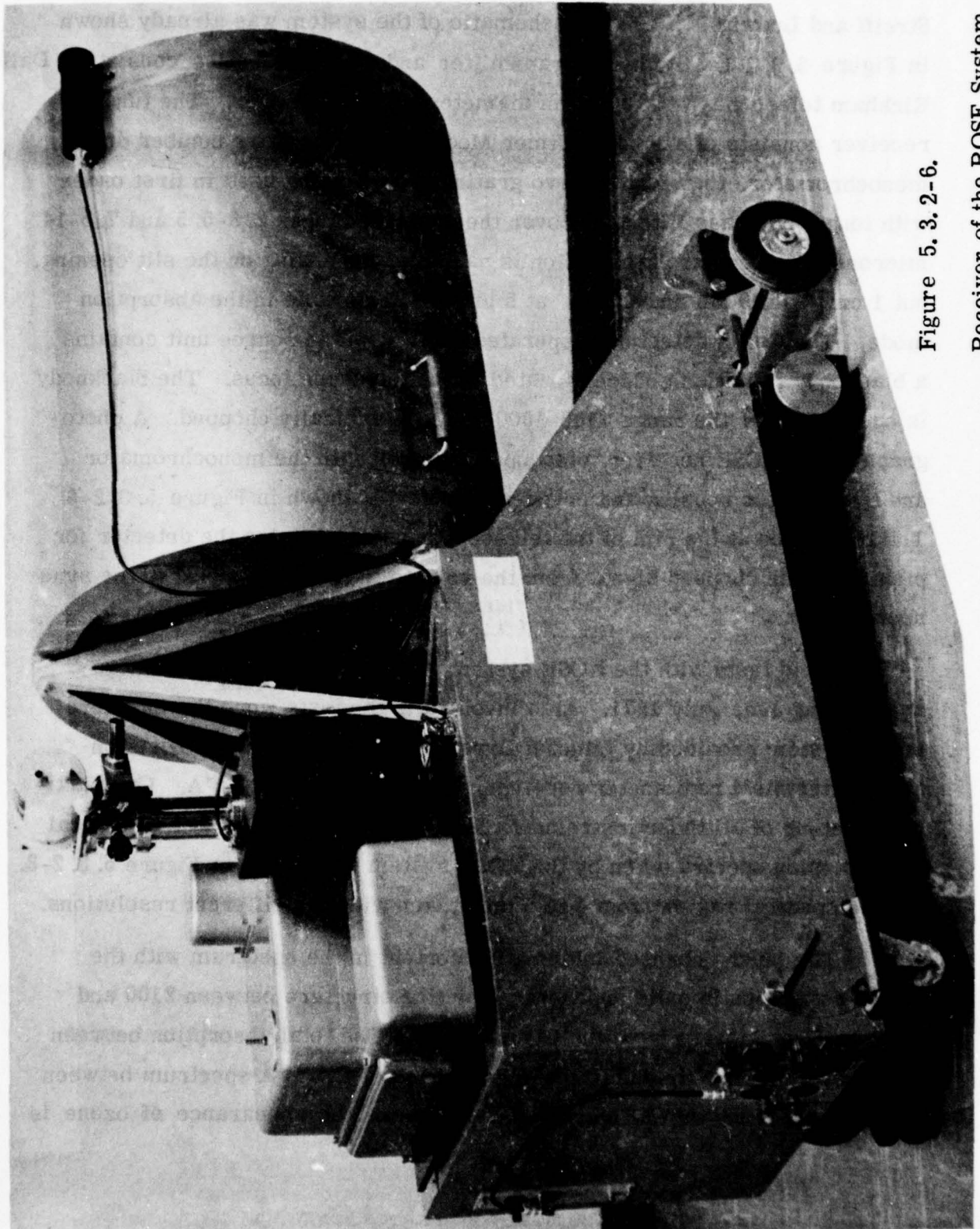


Figure 5. 3. 2-6.
Receiver of the ROSE System

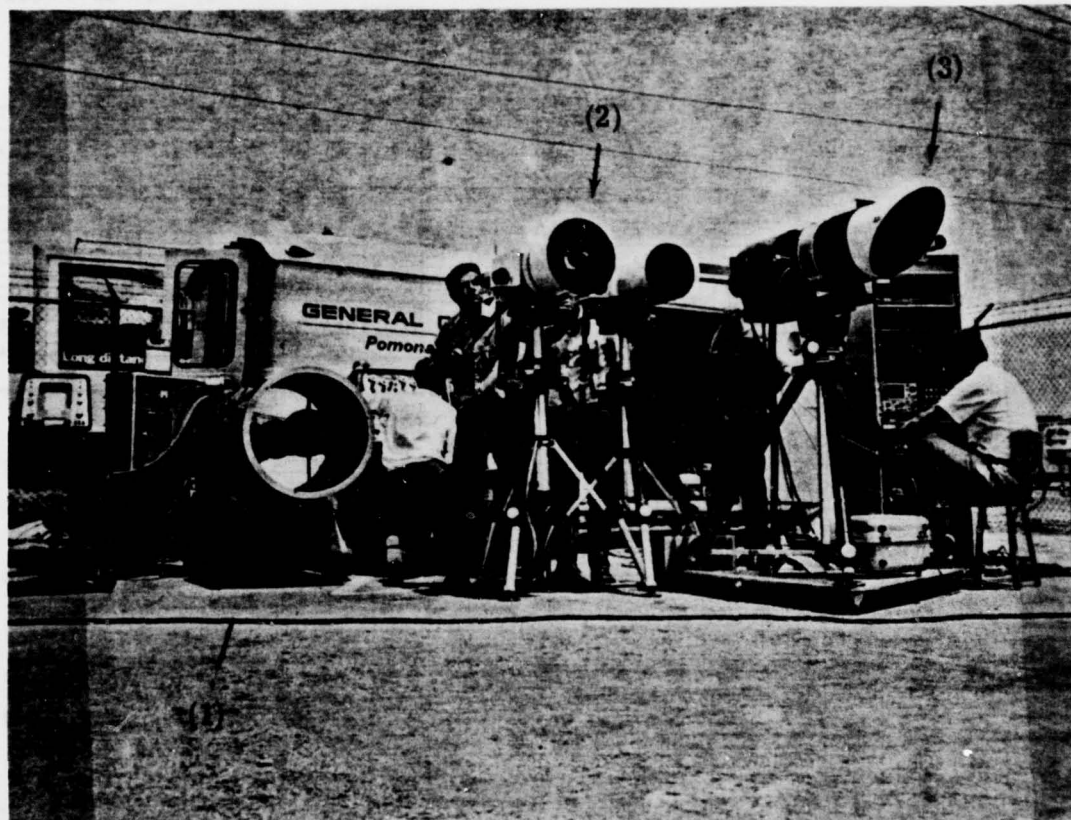


Figure 5. 3. 2-7. The ROSE System (1), the Interferometers (2), and the Filterwheel Radiometer (3) During Field Tests

5. 3. 2. 2e

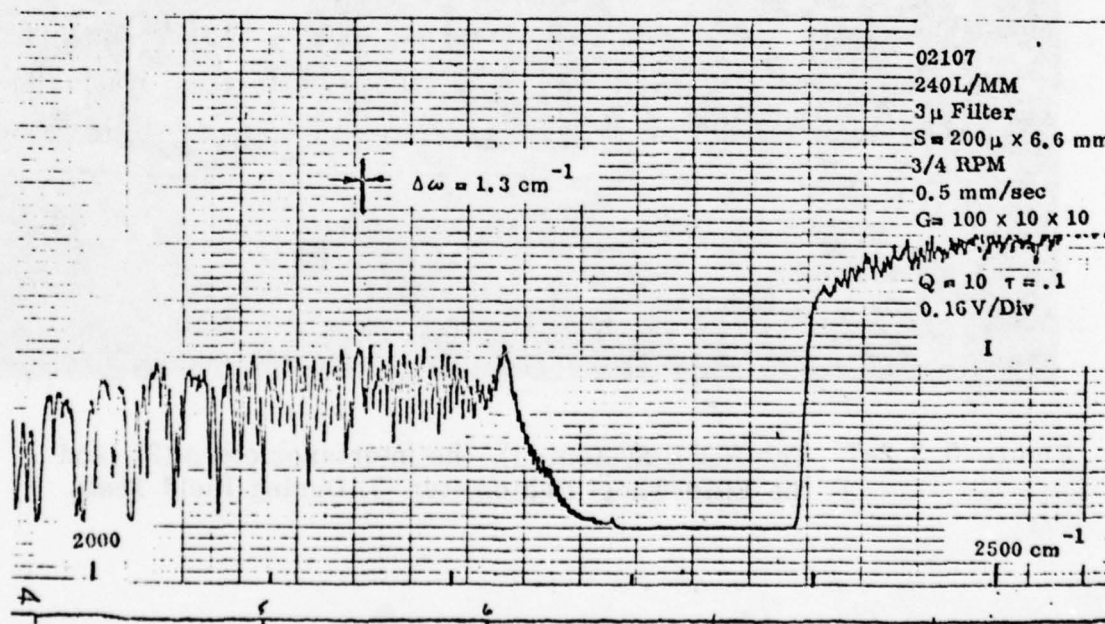
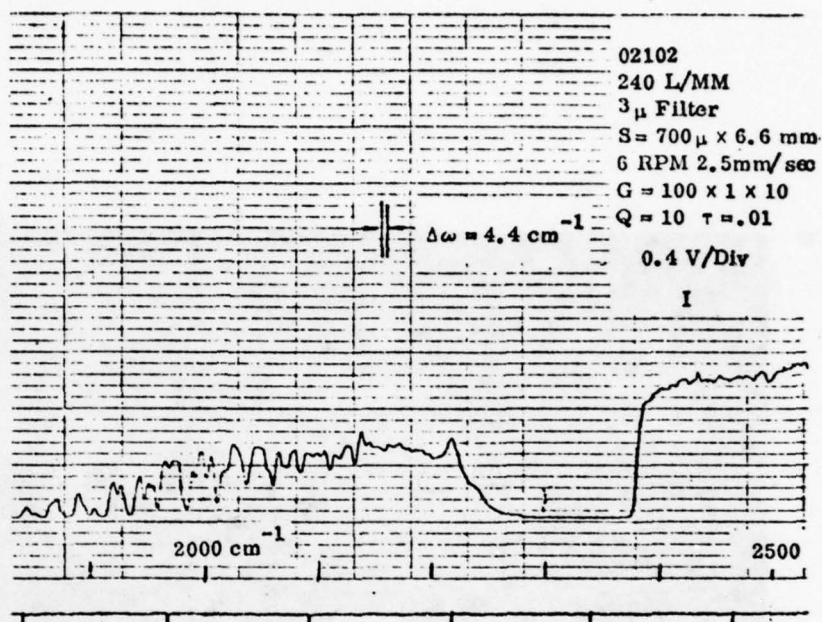


Figure 5. 3. 2- 8. Comparison of CO Spectra with $\Delta\omega = 4.4 \text{ cm}^{-1}$ and 1.3 cm^{-1} .

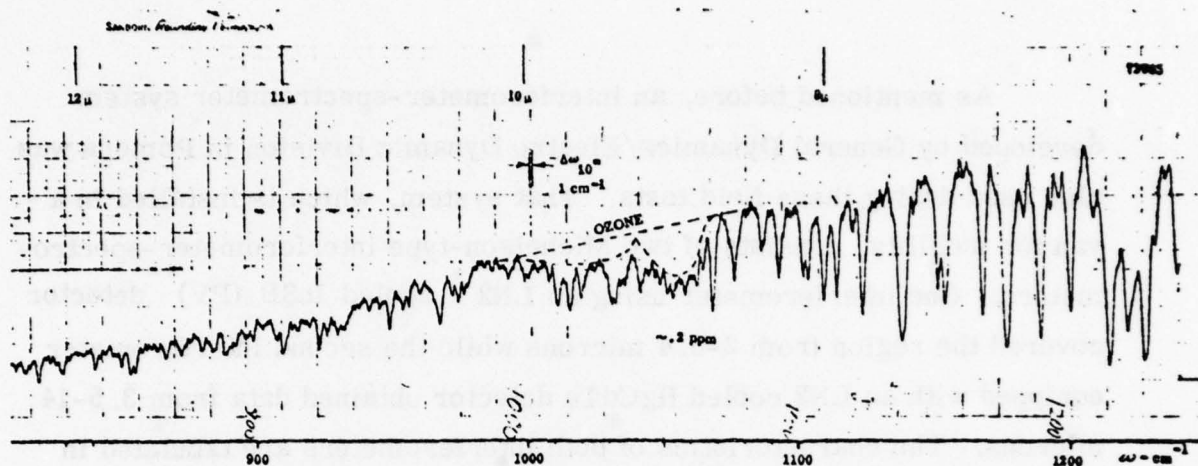


Figure 5. 3. 2-9 . ROSE Spectrum Between 8 and 12 μm , Taken Over a 2 Mile Path with a Slit Width of 1 cm^{-1} .

clearly indicated. The absorption by ozone was used to determine the average concentration over the two mile path. The results are shown in Figure 5. 3. 2-10, together with the data collected by the Pomona Station of the Los Angeles Air Pollution Control District. Considering that the two locations, where the measurements were taken, did not coincide, no better agreement can be expected.

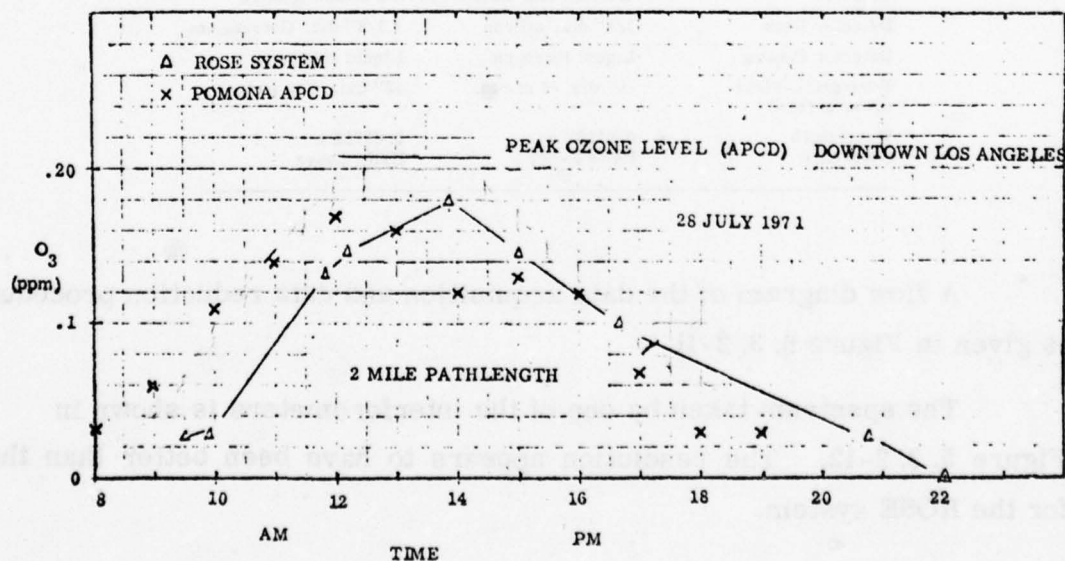


Figure 5. 3. 2-10. Ozone Concentration Versus Time.

As mentioned before, an interferometer-spectrometer system developed by General Dynamics/Electro Dynamic Division in Pomona was also used during these field tests. That system, which is installed in a van for mobility, consists of two Michelson-type interferometer-spectrometers. One interferometer using an LN2^{*} cooled InSB (PV)^{**} detector covered the region from 2-5.4 microns while the second interferometer equipped with an LN2 cooled HgCdTe detector obtained data from 3.5-14 microns. The characteristics of both interferometers are tabulated in Table 5.3.2-2.

TABLE 5.3.2-2. Principal Interferometer Characteristics

Item	Interferometer #1	Interferometer #2
Model Designation (Drive Mechanism)	IF-3	IF-3
Wavenumber Region of Operation	1850 to 5000 cm ⁻¹	716 to 2500 cm ⁻¹
Optical Resolution	~ 2.5 cm ⁻¹	~ 1 cm ⁻¹
Spectrum Recording Rates	1 per 2.5 sec.	1 per 4.5 sec.
Detector	1.0 mm dia. InSb (PV)	2 x 2 mm HgCdTe
Detector Lens	1/4" dia. silicon	1 1/4" dia. Germanium
Detector Cooling	Liquid Nitrogen	Liquid Nitrogen
Foreoptics/Field-of-View (50%)	10" dia. /2 m rad.	12" dia. /6 m rad.
Wavelength Reference	0.63282 μ HeNe Laser	0.63282 μ HeNe Laser

A flow diagram of the data acquisition and data reduction procedures is given in Figure 5.3.2-11.

The spectrum taken by one of the interferometers is shown in Figure 5.3.2-12. The resolution appears to have been better than the one for the ROSE system.

* LN - Liquid Nitrogen

**PV - Photo Voltaic

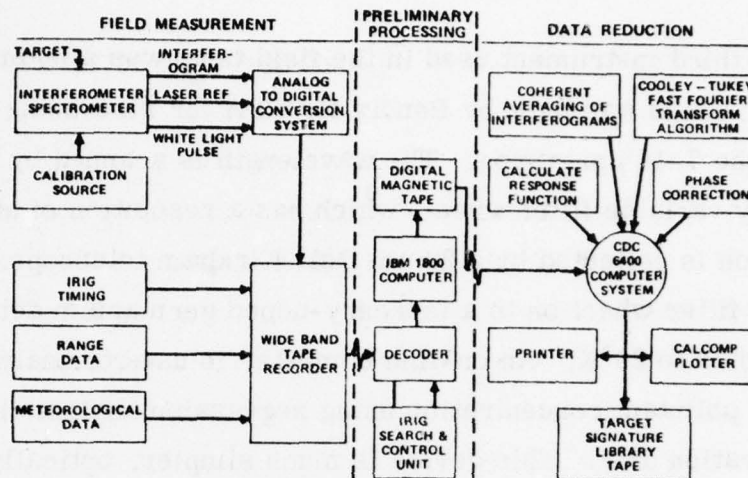


Figure 5. 3. 2-11.

Data Acquisition and Reduction Procedures
Block Diagram of the General Dynamics
Interferometer System [Ref. 166].

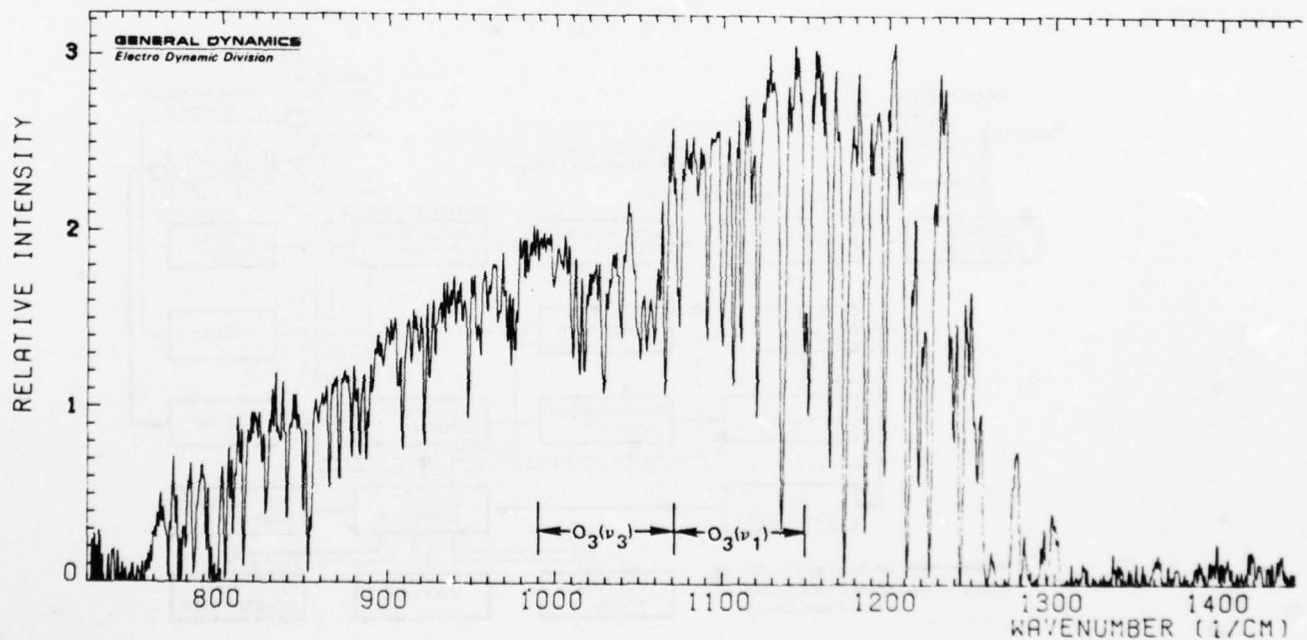


Figure 5. 3. 2-12. Interferometer Spectrum Between 7 and 12 μm ,
Taken Over a 2 Mile Path.

The third instrument used in the field tests was a filterwheel radiometer⁽¹⁸⁰⁾, which was built by Bendix for EPA for measuring pollutant spectra in the 7-14 μm region. The wavelength is scanned by rotating a continuously variable filter wheel, which has a resolution of about 1 percent. The radiation is collected by a 28 cm Dall-Kirkham telescope, and passed through the filter wheel on to a mercury-doped germanium detector mechanically cooled to 28°K. An on-line computer is used to analyze the spectra in terms of pollutant concentration using regression analysis based on previous calibration data. This device is much simpler, optically (see schematic in Figure 5.3.2-13, than the scanning spectrometer or interferometer, but due to the poor spectral resolution, the data interpretation is difficult even with help of the on-line computer. No results were reported and the technique does not seem to have been pursued since the field tests in 1971.

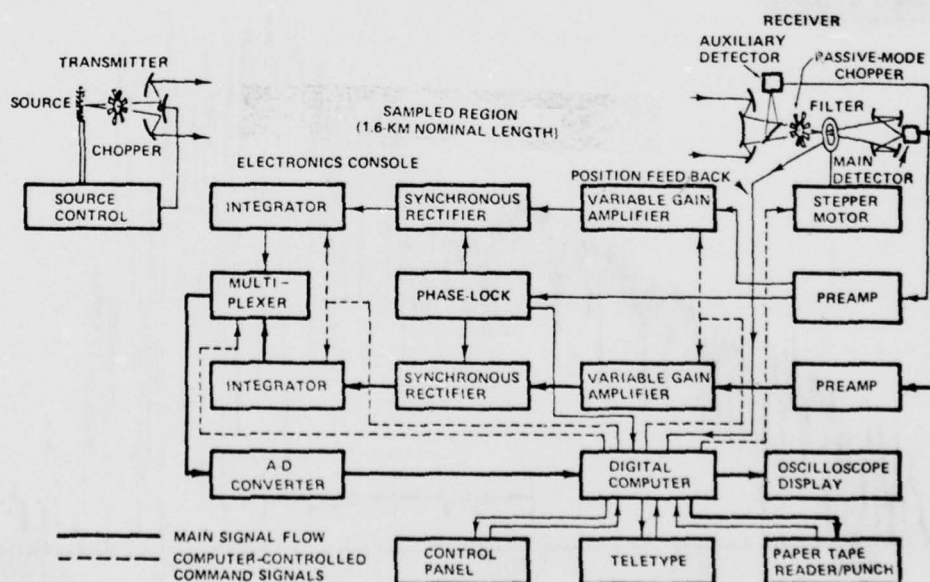


Figure 5.3.2-13. Block Diagram of the Bendix Filter-wheel Radiometer [Ref. 180].

In Section 1. 3 we have mentioned a joint program between the Air Force and EPA that is conducted for the purpose "to evaluate mathematical models of pollution dispersion from airports". Herget⁽²⁴⁶⁾ has reported on some results with the ROSE system⁽¹⁷⁸⁾. He states that "the long-path measurements, which give a path-averaged value of the CO concentration, were included as a part of the program because of the inherent difficulty of comparing the average value predictions of dispersion models with the point values obtained from conventional sampling stations". Unfortunately, Herget had to take data when the point sampling stations were not in operation, thus depriving one of the comparisons between the different methods. One typical data plot is shown in Figure 5. 3. 2 -14, where we have connected the data points presented by Herget by straight lines. In that way the trend of the pollution levels showing apparently three maxima is more clearly visible. Two maxima reach levels over 3 ppm at 0645 and at 1030) and one over 2 ppm (at about 1500). To fully utilize these data it is necessary to relate that graph with the aircraft traffic and meteorology.

Of interest is the description of the calibration procedure by Herget. Instead of using the method of equivalent width as discussed in Section 5. 3. 2. 1, he relates the signals obtained from the absorption of the pollutant in an absorption cell directly to the signals obtained in the field. This procedure is acceptable as long as the calibration mixture is similar to the actual atmosphere being probed and no "unknown" pollutants interfere. In addition, the zero level from which I and I_0 are measured must be well known and should frequently be checked. In general, calibration runs should be conducted during the field test (as was done by Ku and Hinkley⁽²⁴²⁾) in order to avoid instrument drifts, although the simultaneous measurement of I/I_0 eliminates most of them. Herget states that the experimental error

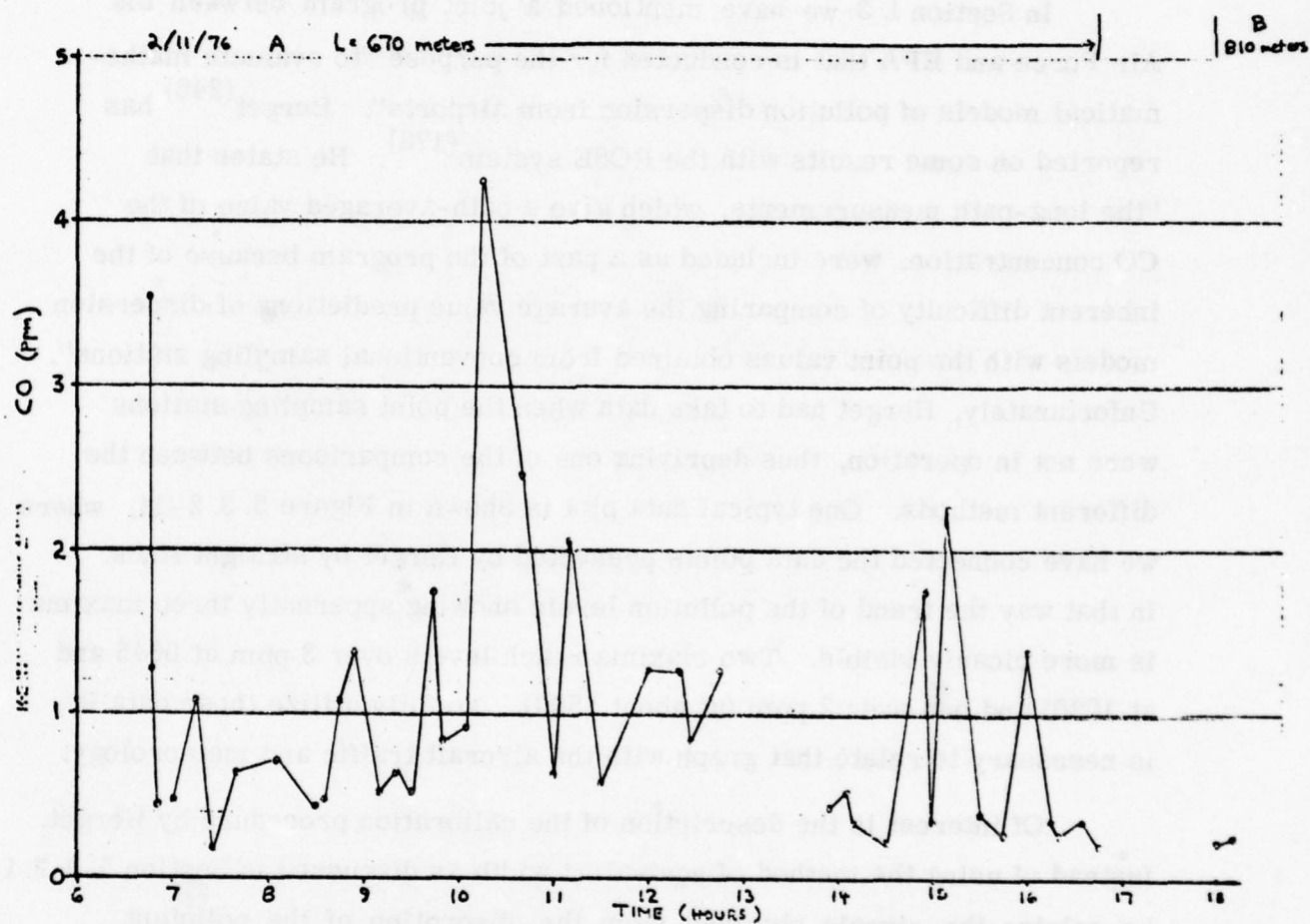


Figure 5. 3. 2-14. Measurements in the Vicinity of Jet Warmup, Taxi and Shutdown.

is dictated by the scatter of data in the calibration curve, which was about $\pm 15\%$ (see Figure 5. 3. 2-15). The SNR of the CO data in the field appear to be 30:1 for measuring the engine exhaust and about 15:1 for measuring the atmosphere. This latter result is in qualitative agreement with our theoretical predictions (Figure 5. 3. 2-16) which shows a limiting concentration of about .02 for a 600 m path length and a SNR = 10.

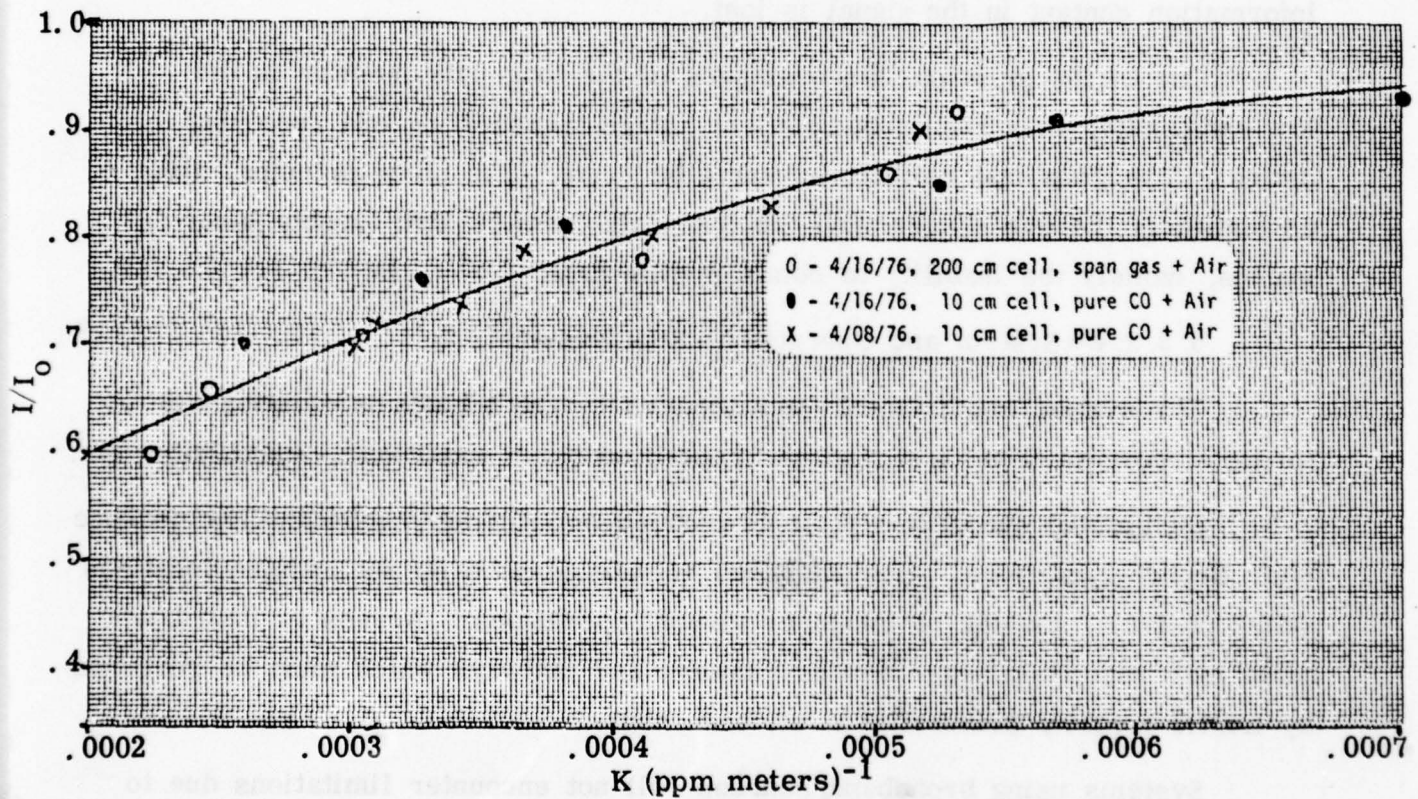


Figure 5. 3. 2-15.

Calibration Curve for CO of the
ROSE System (Herget⁽²⁴⁶⁾).

5. 3. 2. 3 Advantages and Disadvantages

The advantage of the long-path monitor using a tunable receiver is the high information content embodied in one spectrum, i.e., more than one pollutant species can be detected and measured in one spectrum and interfering species and continuum radiation can be accounted for. By replacing the tunable receiver by a fixed one, such as a radiometer or correlation device, the instrument complexity can be reduced, but the high information content in the signal is lost.

One of the principal disadvantages of the long-path monitor is the low sensitivity, thus requiring relatively large transmitting and receiving optics. Topographical reflectors cannot be used. The other principal disadvantage is the one shared with the long-path monitor with tunable laser source, namely the inability to obtain profile data.

5. 3. 2. 4 System and Operational Requirements

The system requirements are dictated by the NAAQS in relationship to the airport environ, i.e., range, repetition rate, sensitivity, specificity, etc.

Monitoring operations must be carried out without significant interference with airport operations. Ground-based remote sensors do not require locations which obstruct, impede or endanger airport operations. Access to instrument sites may require passage across runways and taxiways which must be governed by traffic control, preferably at off-peak hours.

Systems using broadband sources will not encounter limitations due to eye safety requirements. If the source emits visible energy it must be located and directed so as not to interfere with vision or visual cues of pilots.

Broadband sources are not likely to emit significant RF interference.

5. 3. 2. 5 Analysis and Critique

The basic signal-to-noise ratio equation applicable to the differential absorption mode in a long-path monitoring system was developed in Section 5. 3. 1. 5 and was given by Eq. (5. 3. 1-8). The signal power was given by Eq. (5. 3. 2-2) and, in the limit of a small spectral interval, by Eq. (5. 3. 2-3). The great loss in sensitivity (compared with a laser system) is apparent when one compares the transmitted power. While in the previous analysis, the transmitted laser power was assumed to be 1 W (expanded into a beam with a cross-sectional area of 10 cm^2 for safety reasons), the transmitted power of a blackbody illuminator is orders of magnitude less in a small spectral interval. For example, consider the ROSE system in which the temperature of the source was 1800°K and the transmitter throughput was $0.04 \text{ cm}^2 \text{sr}$ (max). From Eq. (5. 3. 2-1) with $\epsilon = 1$ and $\Delta\lambda = 0.0025 \text{ } \mu\text{m}$ at $5 \text{ } \mu\text{m}$ (i. e., a resolution of 1 cm^{-1}), the transmitted power becomes

$$P_t = 0.04 \times 0.97 \times 0.0025 = 9.7 \times 10^{-5} \text{ W}$$

This power is further reduced at the receiver because $\Gamma(R) < 1$.

For the conditions selected in Section 5. 3. 1. 5 and for the instrument parameters pertaining to the ROSE system, we have

SNR	=	10
η	=	0.01
$P_t / (A\Omega)_t$	=	$2.43 \times 10^{-3} \text{ W/cm}^2 \text{sr}$
A_t	=	2412 cm^2 (net)
A_r	=	2412 cm^2 (net)
NEP	=	$6.7 \times 10^{-13} \text{ W}$
$k(\lambda_1)$	=	$1 \text{ cm}^{-1} \text{atm}^{-1}$
p_t	=	1 atm
$k(\lambda_2)C_2$	=	$.9 k(\lambda_1)C_1$

Introducing these values into Eq. (5. 3. 1-8) and solving for ξ , we obtain

$$\xi = 2.62 \times 10^{-7} R \text{ (cm)} .$$

Comparing this result with the ones obtained for the long-path monitor using a tunable laser (Section 5. 3. 1. 5), we find that the ROSE system is more sensitive by about 2 orders of magnitude than the laser system using a topographical reflector, but that it is less sensitive by about 4 orders of magnitude than the laser system using a retroreflector. Numerical results are shown in Figure 5. 3. 2-16.

Of course, it must be remembered that the telescopes of the ROSE system are larger by about a factor of three in area than the ones assumed for the laser systems and that the spectral resolution is much lower. Thus, the comparison is not quite on an equal basis.

In comparison with the ROSE system, an interferometer-spectrometer system would have a higher sensitivity due to its higher throughput and multiplex advantage. A theoretical improvement in throughput is due to the increased solid angle of acceptance, and the increased power on the detector per unit radiance for equal resolution, area, and transmission is in the order of 40 to 300 times that of a grating spectrometer. The multiplex advantage is proportional to \sqrt{m} , where m is the number of spectral elements contained within one spectrogram. Thus, a total maximum theoretical improvement of over 3 orders of magnitude may be predicted. However, due to atmospheric fluctuations, we found that the practical improvement is about 10 to 100.

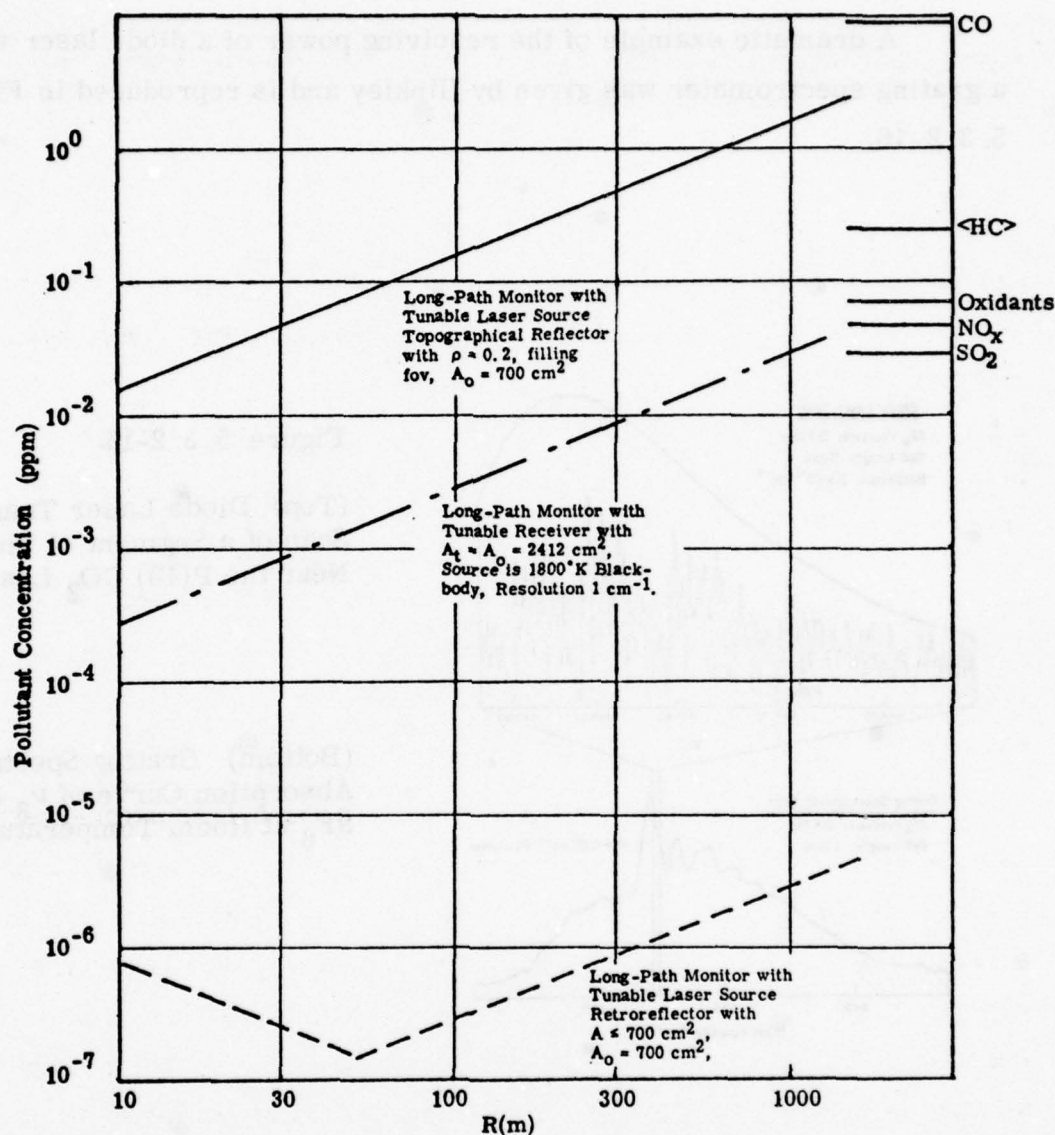


Figure 5. 3. 2- 16. Long-Path Measurement (10% Accuracy) for Pollutant Concentration versus Range. Absorption Coefficient of Pollutant is $1 \text{ cm}^{-1}\text{atm}^{-1}$. Difference Between Pollutant Absorption and Background is 10%. The Dot-Dash Line is for Tunable Receiver System. The Solid and Dashed Lines are for the Tunable Laser Systems, Repeated from Figure

A dramatic example of the resolving power of a diode laser versus a grating spectrometer was given by Hinkley and is reproduced in Figure 5. 3. 2-16.

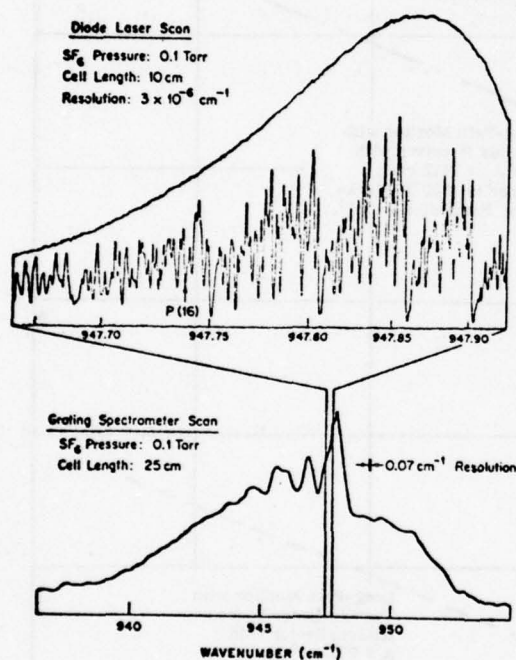


Figure 5. 3. 2-16.

(Top) Diode Laser Transmission Scan of a Segment of This Band Near the P(16) CO_2 Laser Line;

(Bottom) Grating Spectrometer Absorption Curve of ν_3 Band of SF_6 at Room Temperature.

5. 3. 3 Passive Systems

5. 3. 3. 1 Principle of Operation

In general, these systems can provide both "line averaged" data, when looking at a boundary, and "line integral" data, when looking along a line-of-sight (LOS) with no end point. The source energy is provided by the atmospheric species and the solid boundary, if there is one. This source energy is a function of both the species concentration along the LOS and their temperature. Thus, the data interpretation is more complex than in the case of a pure transmission measurement.

In the following analysis we distinguish two cases that are of practical interest. The first is the uplooking case, having no defined end point (see Figure 5. 3. 3-1a). However, knowing the mixing height and making the assumption that all pollutants are trapped within the mixing depth, an end point may be defined and a "line averaged" concentration may be obtained. The second case is the downlooking case, where the sensor is placed on board a helicopter or airplane (see Figure 5. 3. 3-1b).

In perimeter monitoring the mass flow of pollutant across a line is given by

$$M = \bar{L}_m \bar{v} s \sin \theta$$

where M is the mass flow in g/sec, s is the line length in meters, L is the mean vertical loading of pollutant in grams per square meter, v is the mean wind velocity across the line in meters per sec., and θ is the angle between the wind direction and the perimeter line.

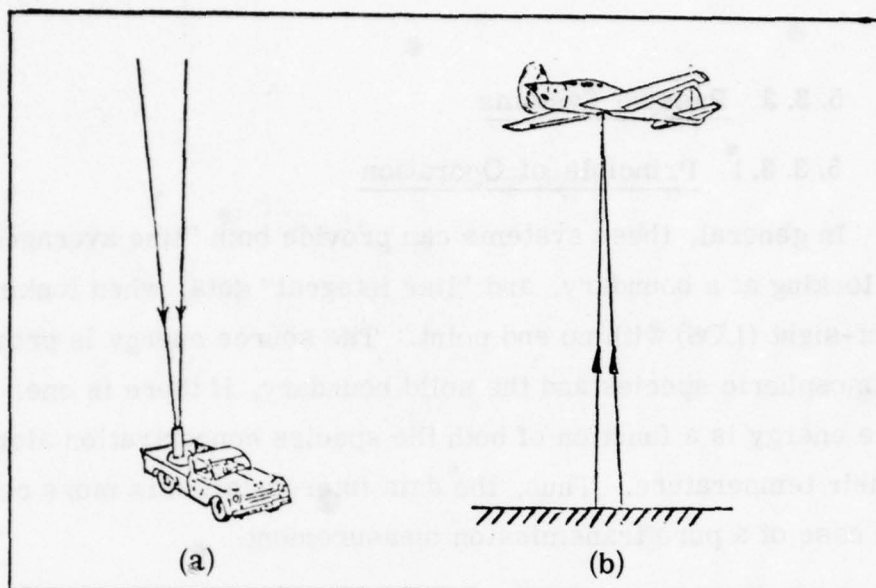


Figure 5. 3. 3-1. Ground Based and Airborne Passive Monitoring

If this vertical burden is measured continuously along a closed path around a source or a complex of sources, the net mass flow out of this closed path gives the source emission rate (M_s), viz.

$$M_s = v \oint L(s) \sin \theta(s) ds.$$

The equations describing the uplooking and downlooking cases are given in the following. The available radiant power from an extended source (filling the field-of-view) is proportional to the throughput of the system and the spectral radiance seen by the detector:

$$P_r = \int_{\Delta\lambda} P_r(\lambda) d\lambda = \int_{\Delta\lambda} \eta_\lambda A_o \Omega_o \int_x N_\lambda^o(T, x) d\tau_\lambda(x) d\lambda \quad (5. 3. 3-1)$$

where η_λ is the efficiency of the instrument, A_o is the entrance area, Ω_o is the solid angle, $N_\lambda^o(T, x)$ is the blackbody radiance ($W/cm^2 sr-\mu m$) at the temperature $T(K)$, $\tau_\lambda(x)$ is the transmission, and x is the position along the line-of-sight.

For the first case, the integration limits go from $x = 0$ to $x = h$, where h is either ∞ or the mixing height if known.

For the second case, Eq. (5. 3. 3-1) may be written as

$$P = \int_{\Delta\lambda} P_\lambda d\lambda = \int_{\Delta\lambda} (\eta_\lambda A_o \Omega_o) \left[\epsilon_\lambda^G N_\lambda^o(T_G) \tau_\lambda + \int_{x=0}^{x=h} N_\lambda^o(T_A(x)) d\tau(x) \right] d\lambda \quad (5. 3. 3-2)$$

where h is the altitude of the aircraft [with $\tau(h) = 1$], ϵ_λ^G is the spectral emissivity of the ground, which has the temperature T_G and τ_λ is the integrated atmospheric transmissivity. At the shorter wavelengths ($\lambda < 5 \mu m$), the sun reflection must be accounted for, which is given by

$$P = \int_{\Delta\lambda} P_\lambda d\lambda = \int_{\Delta\lambda} \rho_\lambda^G \frac{\cos \theta}{\pi} H_\lambda^S \tau_\lambda(h) [\tau_\lambda(\infty)]^{\sec \theta} d\lambda \quad (5. 3. 3-3)$$

where ρ_λ^G is the ground diffuse reflectivity, θ is the sun zenith angle, H_λ^S is the sun irradiance at the top of the atmosphere, $\tau_\lambda(h)$ is the vertical atmospheric transmission from the ground to the height of the aircraft and $\tau_\lambda(\infty)$ is the atmospheric transmission to the entire atmosphere traversed by the sun rays.

If the atmosphere can be approximated by a single slab of uniform temperature and uniform species concentration, Eq. (5. 3. 3-2) can be simplified, viz.

$$\begin{aligned}
 P_{\lambda_1} &= \eta(A_o \Omega_o) \Delta\lambda \left[\epsilon^G N^o(\lambda_1, T_G) \tau + (1-\tau) N^o(\lambda_1, T_A) \right] \\
 &= \eta(A_o \Omega_o) \Delta\lambda \left\{ \tau [\epsilon^G N^o(\lambda_1, T_G) - N^o(\lambda_1, T_A)] + N^o(\lambda_1, T_A) \right\}
 \end{aligned}
 \tag{5. 3. 3-4}$$

where the integration over λ has also been executed, assuming a small spectral interval at λ_1 . From that equation it is seen that when the ground brightness temperature* and the mean atmospheric temperature of the single slab are equal, the received power becomes independent of the species transmission τ , viz.

$$\begin{aligned}
 P_{\lambda_1} &= \eta(A_o \Omega_o) \Delta\lambda N^o(\lambda_1, T_A) \\
 &= \eta(A_o \Omega_o) \Delta\lambda \epsilon^G N^o(\lambda_1, T_G)
 \end{aligned}
 \tag{5. 3. 3-5}$$

Therefore, the difference in signal between "on" and "off" the pollutant line is a critical function of the difference in ground brightness and atmospheric temperature for a given pollutant concentration.

From the above discussion it is clear that the data interpretation poses particular problems in passive monitoring. Several ideas have been developed to overcome those problems, either by additional measurements and/or by special data processing. A ratio technique using a gas filter correlation (GFC) instrument has been used by Bartle⁽¹⁸¹⁾ to minimize the temperature dependency of measuring the SO_2 concentration in smokestack plumes. Hinkley⁽¹⁸²⁾ has suggested the laser heterodyne radiometer for measuring pollutants in smokestacks, while Menzies⁽¹⁸³⁾, Menzies and Shumate⁽¹⁸⁴⁾, and Seals⁽¹⁸⁵⁾ have discussed that method for

* The ground brightness temperature T_B is defined by the relation

$$N(\lambda, T_B) = \epsilon_\lambda N^o(\lambda, T_G)$$

measuring pollutants in the ambient air. More details will be given in the next section. Here we wish to give the basic formulation of the concepts of the GFC instrument and the laser heterodyne radiometer.

In the GFC instrument (see Figure 5. 3. 2-5f), the incoming signal is alternately viewed through a cell containing the pollutant species having a transmission $\tau_G(\lambda)$ and through a cell containing nitrogen, having a transmission of 1. To balance the transmission through the two cells, an aperture is introduced, having an effective transmission τ_A , which is not a function of λ . Thus, the signal obtained through one half of the cycle is given by

$$V_1 = \int_{\Delta\lambda} \phi_1(\lambda) P_r(\lambda) \tau_G(\lambda) d\lambda$$

and through the other half of the cycle by

$$V_2 = \tau_A \int_{\Delta\lambda} \phi_2(\lambda) P_r(\lambda) d\lambda$$

where $\phi_1(\lambda)$ and $\phi_2(\lambda)$ are functions of the instrument parameters. In an ideal instrument the two functions are equal. Thus, the signal difference $\Delta V = V_1 - V_2$ is given by

$$\Delta V = \int_{\Delta\lambda} \phi(\lambda) [\tau_G(\lambda) P_r(\lambda) - \tau_A P_r(\lambda)] d\lambda \quad (5. 3. 3-6)$$

The aperture is adjusted to achieve a balanced condition with no pollutant gas in the outside beam. Experimentally, the balanced condition is established through an external calibration source at temperature T_C , having a radiance $N(\lambda, T_C)$:

$$\tau_A = \frac{\int \phi(\lambda) N(\lambda, T_C) \tau_G(\lambda) d\lambda}{\int \phi(\lambda) N(\lambda, T_C) d\lambda} \quad (5. 3. 3-7)$$

After that adjustment, the GFC instrument is then very sensitive to any particular pollutant which is contained in the gas cell, and insensitive to other interfering species.

In the laser heterodyne radiometer (see Figure 5. 3. 3-2), the laser beam is used as a local oscillator. After mixing, a beat frequency is produced whenever the difference frequency is within the bandpass of the electronics. It has been shown that the noise-equivalent-power (NEP) for a Dicke-type heterodyne infrared radiometer is⁽¹⁸⁶⁾

$$NEP = \frac{2 h \nu}{\eta} \sqrt{\frac{B_{IF}}{t}} \quad (5. 3. 3-8)$$

where ν is the laser frequency, η is the quantum efficiency of the mixer, B_{IF} is the bandwidth and t is the post-detection integration time. It has further been shown⁽¹⁸⁷⁾ that for any heterodyne configuration the integrated

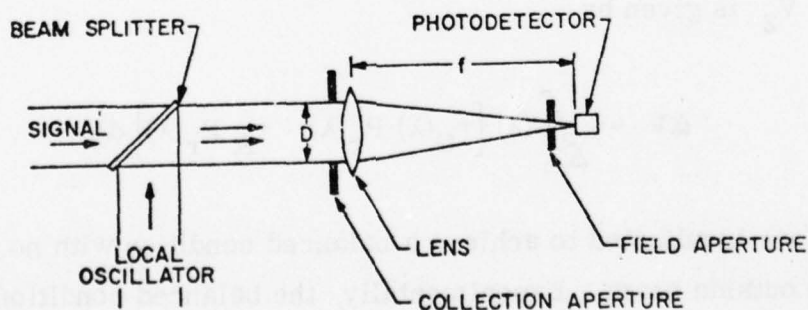


Figure
5. 3. 3-2.

Schematic of the Laser
Heterodyne Radiometer [Ref. 188].

effective aperture is proportional to the square of the laser wavelength. The solid angular field-of-view becomes

$$\Omega \approx \lambda^2/D^2 \quad (5. 3. 3-9)$$

where D is the diameter of the entrance pupil. The significance of these two relationships will be analyzed in Section 5, 3, 3, 5.

Finally, we want to mention a special data processing procedure, developed by Walter and Flanigan⁽¹⁸⁹⁾ for passive remote sensing of pollutants with a spectrally scanning instrument, using the sky (5-15° above the horizon) as the background. A correlation function for a particular target pollutant is calculated by the simplex optimization method⁽¹⁹⁰⁾, which constrains the response of the monitor to background changes while optimizing it to the target pollutant. The authors state that the response to a target pollutant was 2 to 3 times greater than any background induced change over a period of 2 weeks.

5. 3. 3. 2 State-of-the-Art

Edgewood Arsenal has been involved in the passive remote detection of trace gases in the atmosphere for some time. The spectral region from 8 to 12 μm was found to be most useful since many hydrocarbons and organophosphorous compounds have a spectral signature and the atmosphere has a transmission window in this region. Also, the blackbody function is near its maximum at temperatures of interest, thus providing near the maximum of radiant energy available. In addition, the most troublesome interfering atmospheric species, H_2O and CO_2 , have very weak spectral signatures in this region. The most significant interferences originate from the ozone band at 9.6 μm and common dust⁽¹⁹¹⁾.

The passive remote monitor, used by Edgewood Arsenal, was designed and constructed by Block Engineering, Inc.⁽¹⁸⁹⁾. It is composed of two subsystems: a spectroradiometer and a discriminator (correlator). The spectroradiometer uses a circular variable filter (CVF) and a nitrogen cooled Hg:Cd:Te detector. The CVF covers half of a wheel that rotates at 1 Hz. The chopper, which is mechanically connected to the rotating filter wheel, rotates at 1000 Hz with the detector alternately viewing the scene and an internal reference blackbody. The field stop of the CVF is set so that the spectroradiometer has about 1% spectral bandwidth, but the actual spectral resolution is about 2%.

The discriminator is a small, special purpose, hybrid computer, which computes the absolute value of

$$\sum_{i=1}^{16} C_i V_i ,$$

where V_i is the signal from the i th channel, C_i is the coefficient associated with the i th channel.

Walter and Flanigan⁽¹⁸⁹⁾ have described the field tests as follows: "The target gas was dimethylmethylphosphonate (DMMP). A small DMMP cloud was generated by spraying at a distance of 25 m from the detection instrument. Figure 5. 3. 3-3 shows the sky background spectrum and the background spectrum plus DMMP. There are only minor apparent differences between the two spectra, but signal averaging and background subtraction clearly show the DMMP as seen in Figure 5. 3. 3-4. The concentration (mg/m^3) times pathlength (m), CL, of the DMMP was estimated to be $175 \text{ mg}/\text{m}^2$.

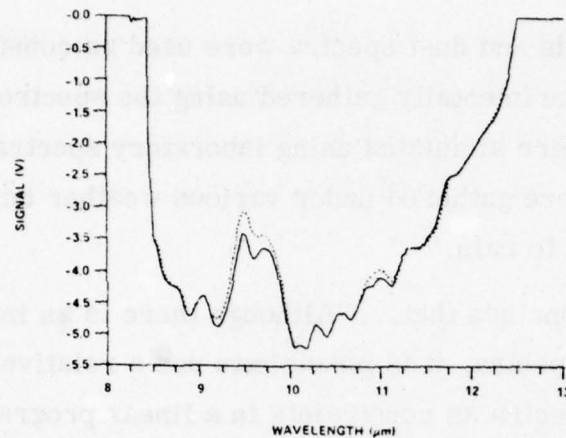


Figure
5. 3. 3-3.

Target and Background Spectra. The Solid Line is Background Only, and the Dotted Line is Background Plus DMMP. Each Spectrum is the Result of Averaging Approximately 50 Scans.

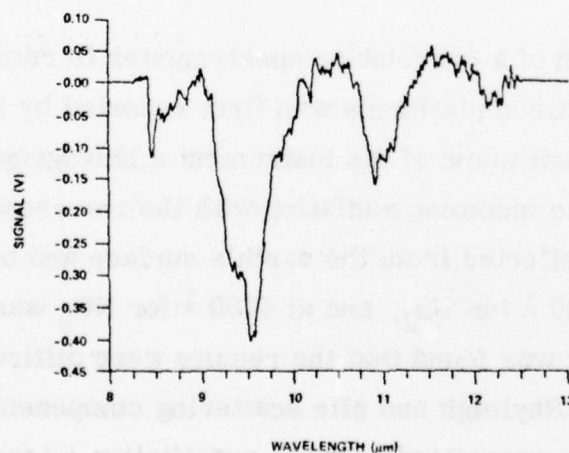


Figure
5. 3. 3-4.

Difference Between the Background Spectrum and Background Plus DMMP.

Sky backgrounds and dust spectra were used as constraints. The backgrounds were experimentally gathered using the spectroradiometer, but the dust spectra were simulated using laboratory spectral data. The background spectra were gathered under various weather conditions ranging from blue sky to rain. "

The authors conclude that... "Although there is an infinite range of possible background spectra, it is possible to use a relatively small number of carefully chosen spectra as constraints in a linear programming problem and achieve a solution that discriminates between background changes and a target compound. This is true even though the target and the background both exhibit strong spectral bands at the same wavelength. The method may be extended to other interferences having strong bands at approximately the same location as the target. It is well recognized that the number of useful channels is limited by the resolution of the spectroradiometer. As the number of channels are increased to this limit, they must be located with increasing accuracy. "

The application of a correlation spectrometer to remote sensing of air pollutants from balloon platforms was first reported by Barringer et al. in 1965⁽¹⁹²⁾. In the exit plane of the instrument a photographic plate was used to "correlate" the incoming radiation with the one recorded on the plate. The solar radiation reflected from the earth's surface and backscattered by the atmosphere at 3100 Å for SO₂, and at 4400 Å for NO₂ was used in this mode of operation. It was found that the results were difficult to interpret⁽¹⁹⁴⁾ because of the strong Rayleigh and Mie scattering components. A general treatment of problems associated with the quantitative interpretation of data from correlation-mask instruments has been given by McGreight and Tien⁽¹⁹⁵⁾.

In a later development, the photographic plates were replaced by slits photoetched in a thin foil⁽¹⁹³⁾. This instrument, called COSPEC, is shown schematically in Figure 5. 3. 3-5. The incoming radiation is focused onto the entrance slit of an Ebert-Fastie spectrometer with a focal length of 25 cm. The incoming beam is collimated by the parabolic mirror, dispersed by the grating and focused onto the multi-slitted exit mask and photomultiplier tube. In the remote sensing mode the spatial modulation is achieved through two fork-driven refractor plates behind the entrance slit.

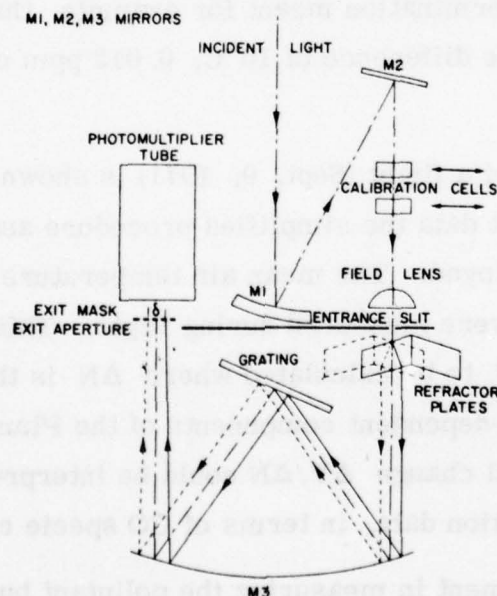


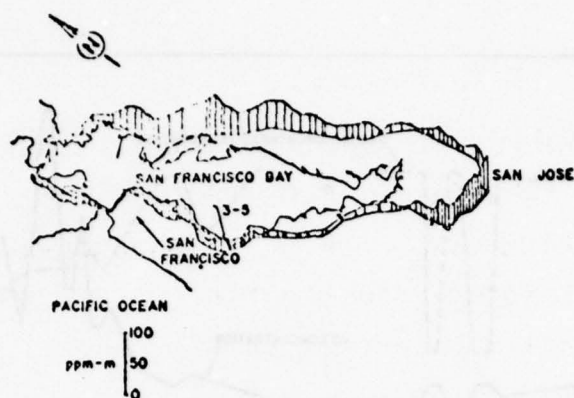
Figure 5. 3. 3-5. Schematic Layout of the Remote Sensor COSPEC [Ref. 193].

Newcomb and Millan⁽¹⁹³⁾ describe the application of the COSPEC in the uplooking mode, using the scattered sunlight as light source. The instrument was installed in a van which was driven in a loop around the bay area to measure the vertical burden of NO_2 . Typical results for three different measurements are shown in Figure 5. 3. 3-6.

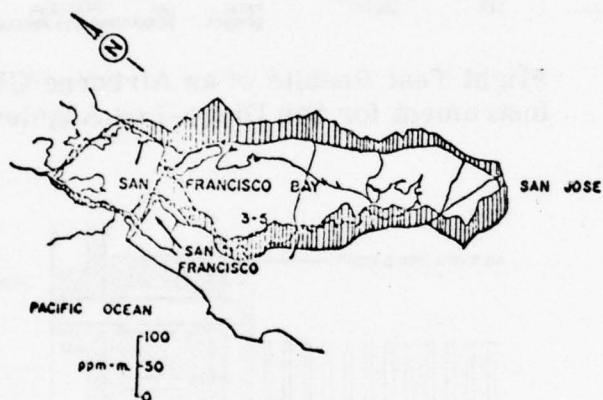
Acton et al.⁽¹⁷⁵⁾ have described the remote measurements of CO taken by an airborne GFC instrument. The instrument, which operates in the $4.6 \mu\text{m}$ band of carbon monoxide, looks down and provides an output signal related to the amount of carbon monoxide in the atmosphere. This output, together with measurements of the surface temperature and the atmospheric temperature profile, allows the mean carbon monoxide concentration between the aircraft and the ground to be determined. Calibration data of the modulation function indicated that the threshold sensitivity was $130 \text{ ppm-m}/^\circ\text{C}$. This determination meant for example, that in a column of 1 km with a temperature difference of 10°C , 0.013 ppm could be observed with an $\text{S/N} = 1$.

The reduced data of a flight (Sept. 9, 1971) is shown in Figure 5. 3. 3-7. In the analysis of the flight data the simplified procedure assuming a one-slab atmosphere was employed. The mean air temperature and the ground brightness temperatures were measured during flight. This temperature data allowed values of ΔN to be calculated where ΔN is the difference between the temperatures-dependent components of the Planck function. Thus the normalized signal change $\Delta V/\Delta N$ could be interpreted directly, using the one-slab calibration data, in terms of CO specie concentration.

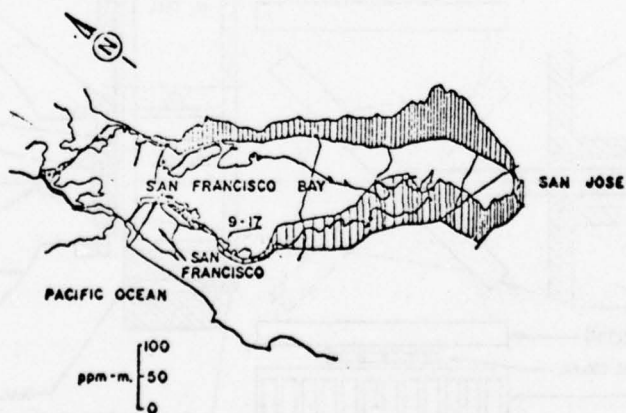
The latest development in measuring the pollutant burden in the up-looking mode is being pursued by SAI under EPA sponsorship⁽¹⁷⁷⁾. The design is based on the GFC principle and the pollutant of interest is SO_2 . The schematic of the instrument is shown in Figure 5. 3. 3-8. The 45° mirror



Measurements of the NO₂ burden in the San Francisco basin on November 11, time: 1030-1330.



Measurements of the NO₂ burden in the San Francisco basin on November 13, time: 1030-1315.



Measurements of the NO₂ burden in the San Francisco basin on November 14, time: 1100-1400.

Figure
5. 3. 3-6.

Uplinking Measurements of NO₂ with
the COSPEC [Ref. 193].

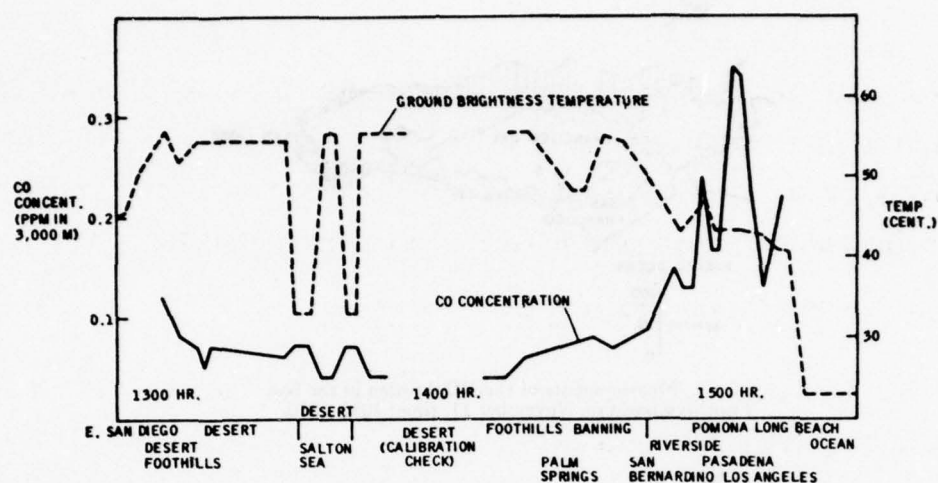


Figure 5. 3. 3-7. Flight Test Results of an Airborne GFC Instrument for San Diego-Los Angeles Area.

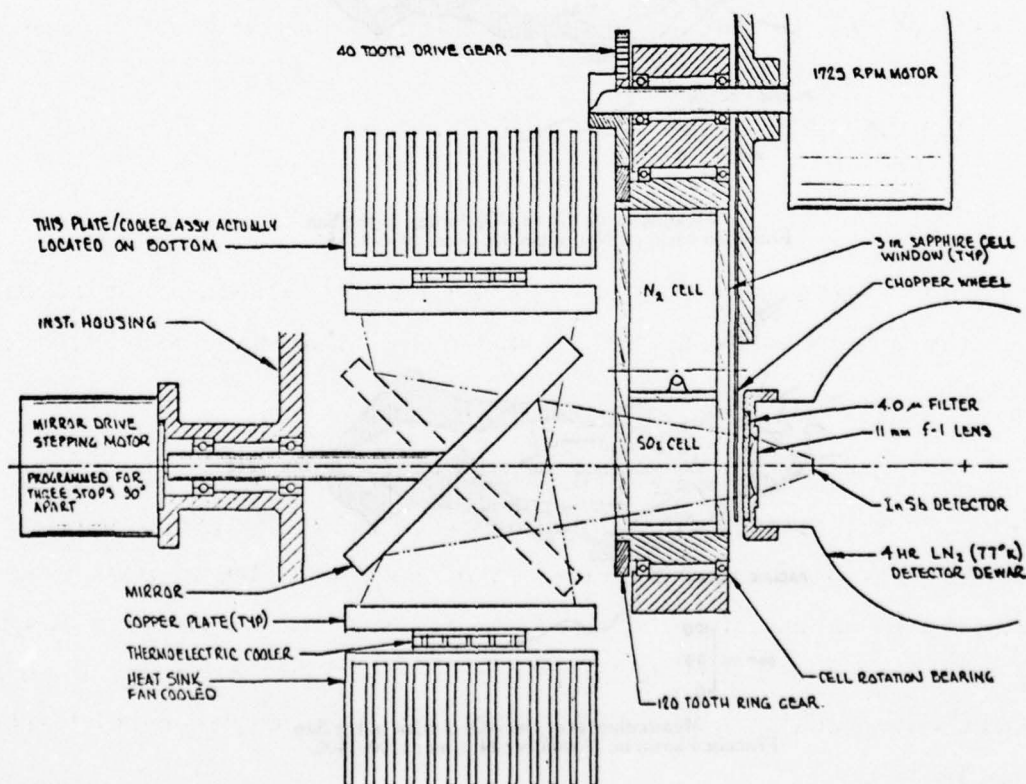


Figure 5. 3. 3-8. Schematic of the Uplooking SO_2 Monitor [Ref. 177].

has three positions, one for looking up and two for looking at a hot and a cold calibration source respectively. Two cells filled with SO_2 and N_2 , respectively, are rotated alternately into the beam of light. Field tests with this instrument were conducted in the summer of 1976.

5. 3. 3. 3 Advantages and Disadvantages

The fundamental advantage of a passive system is its low system complexity and mobility. By using a tunable receiver, more than one species may be detected, similar to the active systems described in Section 5.3.2. By replacing the tunable receiver by a fixed one, such as a correlation device, the instrument complexity can be further reduced, but the high information content embodied in a resolved spectrum is lost. In contrast to the two long-path monitors that are operated in the transmission mode (described in Sections 5.3.1 and 5.3.2), the passive sensor has the theoretical potential of obtaining profile data.

5. 3. 3. 4 System and Operational Requirements

The system requirements are dictated by the NAAQS in relationship to the airport environ, i.e., range, repetition rate, sensitivity, specificity, etc.

Monitoring operations must be carried out without significant interference with airport operations. Ground-based remote sensors do not require locations which obstruct, impede or endanger airport operations. Access to instrument sites may require passage across runways and taxiways which must be governed by traffic control, preferably at off-peak hours. Airborne down-looking sensors (Fig 5.3.3-1a) will require careful scheduling and traffic control.

Passive systems, since they do not include lasers or illuminators, are free of high power or energetic pulsed circuits. They therefore are not likely to emit RF interference. Since no lasers are employed in passive monitors, there are no limitations due to eye safety requirements.

5. 3. 3. 5 Analysis and Critique

In this section we discuss and derive the radiance seen by a passive instrument in both the uplooking and downlooking modes. The signal-to-noise ratio (SNR) is derived for a tunable receiver, a gas filter correlation (GFC) instrument and a heterodyne radiometer.

Throughout this section reference is made to the basic derivation of SNR and discussion of errors presented in Appendix VII, and to the numbered equations of that Appendix.

5. 3. 3. 5. 1 Radiances in the Uplooking and Downlooking Modes

The downwelling radiance depends on the atmospheric temperature profile and on the vertical distribution of the pollutant and others species. The upwelling radiance depends in addition on the ground brightness temperature. The radiative transfer through a non-homogeneous atmosphere is a complex problem. Both line-by-line and band model calculations have been made by us^(59, 196) and many other workers⁽¹⁹⁷⁻¹⁹⁹⁾ to obtain the up- and down-welling spectral radiances under a variety of conditions.

In the case when the pollutant is confined to the lowest layers of the atmosphere, say below 500 m, the mean temperature of this layer is only 1.5°C different from the values at the top and bottom since the temperature lapse rate is typically about 6°C km⁻¹. Hence, assuming the pollutant temperature has equilibrated with that of the atmosphere, the radiance from the layer may be approximated closely by a single slab model, i. e.,

$$N_{\lambda} = N^0(\lambda, T) (1 - \tau_{\lambda}) \quad (5. 3. 3-10)$$

Of course, the lapse rate will vary with the meteorological conditions, but we believe that the mean temperature of the 500 m layer can be estimated within $\pm 2^{\circ}\text{C}$ by measuring the surface temperature, and by knowing the typical diurnal meteorological variations for the location. Of course, a measured temperature at altitude may be available by other means, such as a radiosonde, a tower or tethered balloon, in which case the mean layer temperature would be known more accurately.

In using the perimeter monitoring technique, the pollutant may be dispersed uniformly (or non-uniformly) through the lowest layers, or it may be confined to a relatively thin layer, depending on the meteorological

conditions. These variations in distribution mean that the pollutant average temperature and pressure varies, so that the signal is expected to vary. However, since the vertical variation of temperature and pressure is small within the anticipated vertical extent of the pollutant, the effect of the pollutant vertical distribution is small.

In a computer simulation at the long wavelength region ($10\ \mu\text{m}$), we found that the results of the single slab model in the range 100 ppm-m to 10,000 ppm-m varies from a model using a profile by less than 1%, and that the maximum effect of the variations in the vertical distribution is an additional 1%. These single slab effects are approximately twice as great at the shorter wavelengths ($\leq 4\ \mu\text{m}$) due to the greater change of blackbody radiance with temperature.

As an illustration of the spectral sky radiance, the results of an observation looking vertically up (zenith angle = 0°) are shown in Figure 5.3.3-9⁽²⁰⁰⁾. The radiance in the windows is about $1\ \text{watt}/\text{cm}^2\text{sr-cm} = 10^{-6}\ \text{watt}/\text{cm}^2\text{sr-cm}^{-1}$, which corresponds to a blackbody temperature of about 205 K.

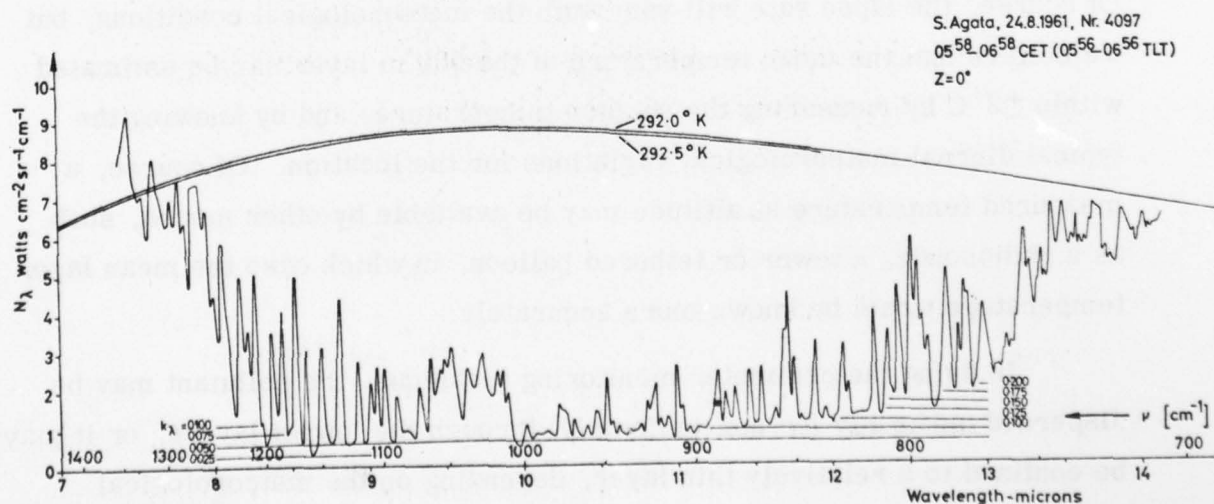


Figure
5.3.3-9.

Spectral Sky Radiance of the Zenith (7.5-14 μ)

Assuming that the radiance in these windows represent the radiance of the clean air, an effective "clean air emissivity" of an air mass having a temperature of 300 K may be obtained from Eq. (5. 3. 3-10), viz.

$$\begin{aligned}\epsilon(10 \mu\text{m}) &= 1 - \tau(10 \mu\text{m}) = N^\circ(205 \text{ K}, 10 \mu\text{m}) / N^\circ(300 \text{ K}, 10 \mu\text{m}) \\ &= 10^{-6} / 9.93 \times 10^{-6} \approx 0.1\end{aligned}$$

Assuming that a pollutant line exists in the clean air window, the emissivity of the polluted air mass, having a vertical mixing depth of 500 m, may then be calculated from

$$\epsilon_p = 1 - 0.1 e^{-k_p C p_T \ell} \quad (5. 3. 3-11)$$

where k_p is the absorption coefficient of the pollutant in $\text{cm}^{-1} \text{atm}^{-1}$, C is the concentration, p_T the total pressure and ℓ the path length (500 m in the present example).

Combining Eqs. (5. 3. 3-10) and (5. 3. 3-11), one can calculate the radiance emitted by a pollutant. The results in terms of the radiance integrated over a spectral bandpass of 1 cm^{-1} at $10 \mu\text{m}$ as a function of different pollutant levels and strength of pollutant lines are given in Figure 5. 3. 3-10. It is seen that the radiance for weak lines ($k = 0.1 \text{ cm-atm}^{-1}$) does not change significantly with pollutant levels. (Between 10 and 100 ppm-m, the change is only 0.8 percent).

Similar calculations have been made for the shorter wavelengths and the results at $\lambda = 4 \mu\text{m}$ are shown in Figure 5. 3. 3-11. In comparison with

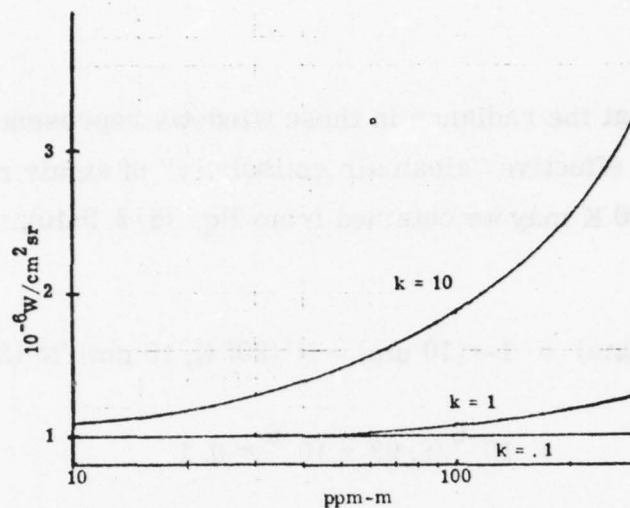


Figure
5. 3. 3-10.

Radiance Integrated Over a Spectral Bandpass of 1 cm^{-1} Versus Pollutant Level Within a Mixing Depth of 500 m for 3 Different Line Strengths (. 1, 1 and $10 \text{ cm}^{-1} \text{ atm}^{-1}$) at $\lambda = 10 \mu\text{m}$.

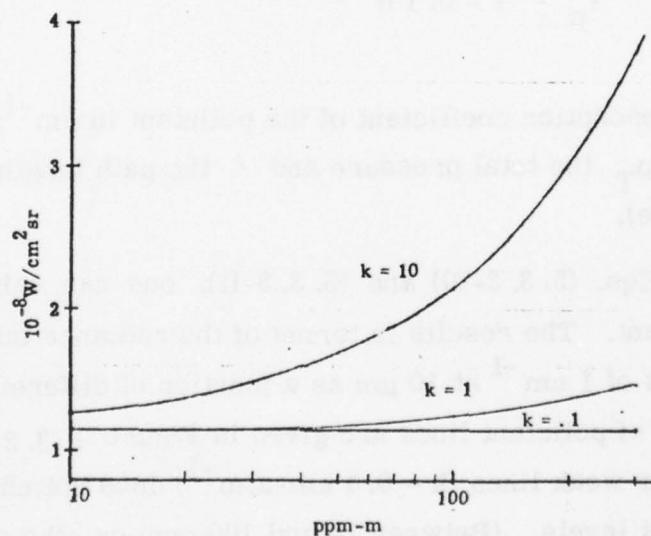


Figure
5. 3. 3-11.

Radiance Integrated Over a Spectral Bandpass of 1 cm^{-1} Versus Pollutant Level Within a Mixing Depth of 500 m for 3 Different Line Strengths (. 1, 1 and $10 \text{ cm}^{-1} \text{ atm}^{-1}$) at $\lambda = 4 \mu\text{m}$.

the results at $\lambda = 10 \mu\text{m}$, the radiances are less by about 2 orders of magnitude. The functional relationship between the rate of change is, of course, the same for both wavelength regions since we have used the same Eq. (5. 3. 3-11) for both cases.

In the downlooking mode, Eq. (5. 3. 3-10) must be modified to include the emitted radiance from the ground surface, i. e.,

$$\begin{aligned} N_{\lambda} &= \epsilon_G(\lambda) N^{\circ}(\lambda, T_G) \tau_{\lambda} + (1 - \tau_{\lambda}) N^{\circ}(\lambda, T_A) \\ &= \tau_{\lambda} [\epsilon_G(\lambda) N^{\circ}(\lambda, T_G) - N^{\circ}(\lambda, T_A)] + N^{\circ}(\lambda, T_A) \end{aligned} \quad (5. 3. 3-12)$$

where the subscripts G and A refer to the "ground" and "atmosphere", respectively. Eq. (5. 3. 3-12) was already derived in Section 5. 3. 3. 1 and is directly comparable with Eq. (5. 3. 3-4) by setting

$$P_{\lambda_1} = \eta (A_o \Omega_o) \Delta\lambda N_{\lambda} \quad (5. 3. 3-13)$$

As was already pointed out, for $\epsilon_G(\lambda) N^{\circ}(\lambda, T_G) \approx N^{\circ}(\lambda, T_A)$ the observed radiance N_{λ} at the entrance of the instrument (or the observed radiant power P_{λ} at the detector) becomes independent of τ_{λ} and, thus, of the pollutant concentration.

These results are shown in Fig 5. 3. 3-12 at $\lambda = 10 \mu\text{m}$ with $\epsilon_G(\lambda) = 1$, $T_G = 300 \text{ K}$ and different air temperatures, assumed to be constant throughout the mixing layer of 500 m depth.

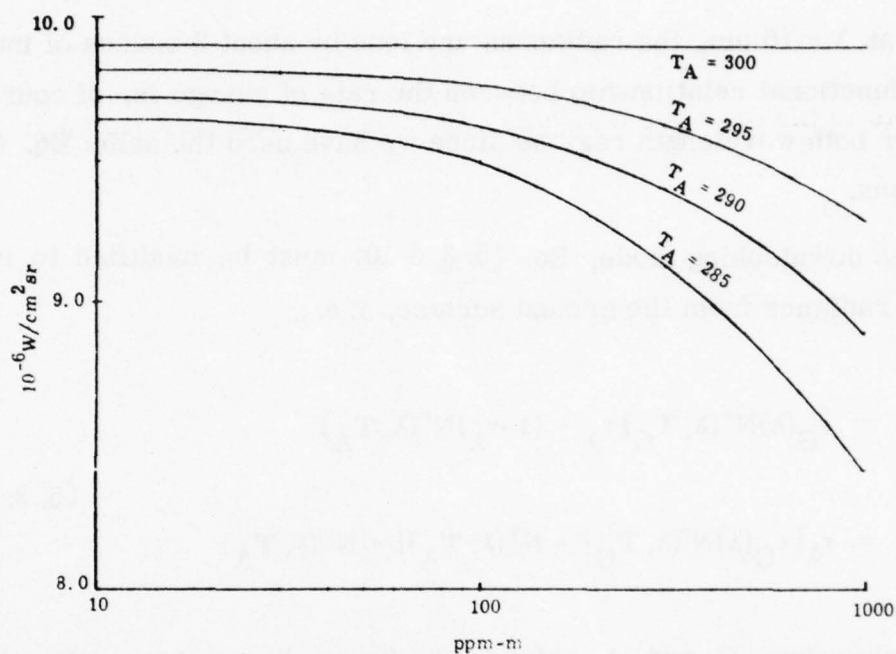


Figure
5. 3. 3-12.

Radiance Integrated Over a Spectral Bandpass of 1 cm^{-1} Versus Pollutant Level Within a Mixing Depth of 500 m for 4 Different Air Temperatures at $\lambda = 10 \mu\text{m}$, Using a Line Strength of $k = 10 \text{ cm}^{-1} \text{ atm}^{-1}$.

Since the air mass was assumed to be colder than the surface (as is usually the case), the radiance decreases with increasing pollutant concentration.

5. 3. 3. 5. 2 SNR of a Tunable Receiver

As in the previous analyses, the pollutant concentration will be determined by taking the natural log \ln of the ratio of two observations, one on the pollutant line, the other one "off" the line. Thus, either Eq. (VII-8) or (VII-9) is applicable. We use the latter one because the approximation $\ln P_1/P_2 \approx P_2/P_1 - 1$ is valid. With $dP = \text{NEP}$ and Eq. (5. 3. 3-13), the signal-to-noise ratio becomes

$$\begin{aligned} \text{SNR} &= \frac{\eta A_o \Omega_o \Delta\lambda [N_{\lambda_1} - N_{\lambda_2}]}{\sqrt{2} \text{NEP}} \\ &= \eta \sqrt{\frac{A_o \Omega_o}{2 \Delta f}} \frac{D_{\lambda}^* \Delta\lambda [N_{\lambda_1} - N_{\lambda_2}]}{f/\text{no}} \end{aligned}$$

where $f/\text{no} \approx (\Omega_d)^{-1/2}$ and $\Omega_o \approx 0.17 \Delta\lambda/\lambda$ for spectrometers, and N_{λ_1} is the radiance at the wavelength where a pollutant line is located and N_{λ_2} is the radiance between absorption lines. Using Eqs. (5. 3. 3-10) and (5. 3. 3-11) and solving for the pollutant level ($C p_t$), we obtain

$$(C p_t) = - \frac{1}{k} \ln \left[1 - \sqrt{\frac{2 \Delta f}{A_o \Omega_o}} \frac{f/\text{no} \times \text{SNR}}{\eta D_{\lambda}^* \times 0.9 \times N^{\circ}(\lambda, T)} \right]$$

The following instrument parameters were used:

$$\begin{aligned} \eta &= 0.01 \\ A_o &= 78.5 \text{ cm}^2 \\ f/\text{no} &= 5 \end{aligned}$$

$$\begin{aligned}
 \Delta f &= 4.17 \times 10^{-3} \text{ Hz (60 sec time constant)} \\
 \Omega_o &= 6.8 \times 10^{-5} \text{ sr (at } 4 \mu\text{m)} \\
 \Omega_o &= 1.7 \times 10^{-4} \text{ sr (at } 10 \mu\text{m)} \\
 A_d &= .13 \text{ cm}^2 \text{ (at } 4 \mu\text{m)} \\
 A_d &= .33 \text{ cm}^2 \text{ (at } 10 \mu\text{m)} \\
 D^* &= 3 \times 10^{11} \text{ W}^{-1} \text{ Hz}^{1/2} \text{ cm (at } 4 \mu\text{m)} \\
 D^* &= 10^{10} \text{ W}^{-1} \text{ Hz}^{1/2} \text{ cm (at } 10 \mu\text{m)}
 \end{aligned}$$

Introducing these values in the above equation results in

k	ppm-m at 4 μm	ppm-m at 10 μm
.1	21370	4580
1	2137	458
10	214	46

These results indicate that the pollutant concentration in a mixing layer of 500 m depth must at least be 0.43 ppm at $\lambda = 4 \mu\text{m}$ and 0.09 ppm at $\lambda = 10 \mu\text{m}$ (for $k = 10 \text{ cm}^{-1} \text{ atm}^{-1}$) in order to be observed with a $\text{SNR} = 10$. A plot extending these results to mixing depth from 1 to 1000 m and pollutant concentrations from .01 to 100 ppm is presented in Figure 5.3.3-13. It is seen that the long wavelength region is more sensitive, and that pollutants with relatively strong lines ($k > 1 \text{ cm}^{-1} \text{ atm}^{-1}$) can be measured at NAAQS levels. Carbon monoxide whose fundamental band is at $4.6 \mu\text{m}$ and whose spectral lines have absorption coefficients in the order of $1 \text{ cm}^{-1} \text{ atm}^{-1}$, can be measured in pollution layers of greater than 200 m thickness at NAAQS levels.

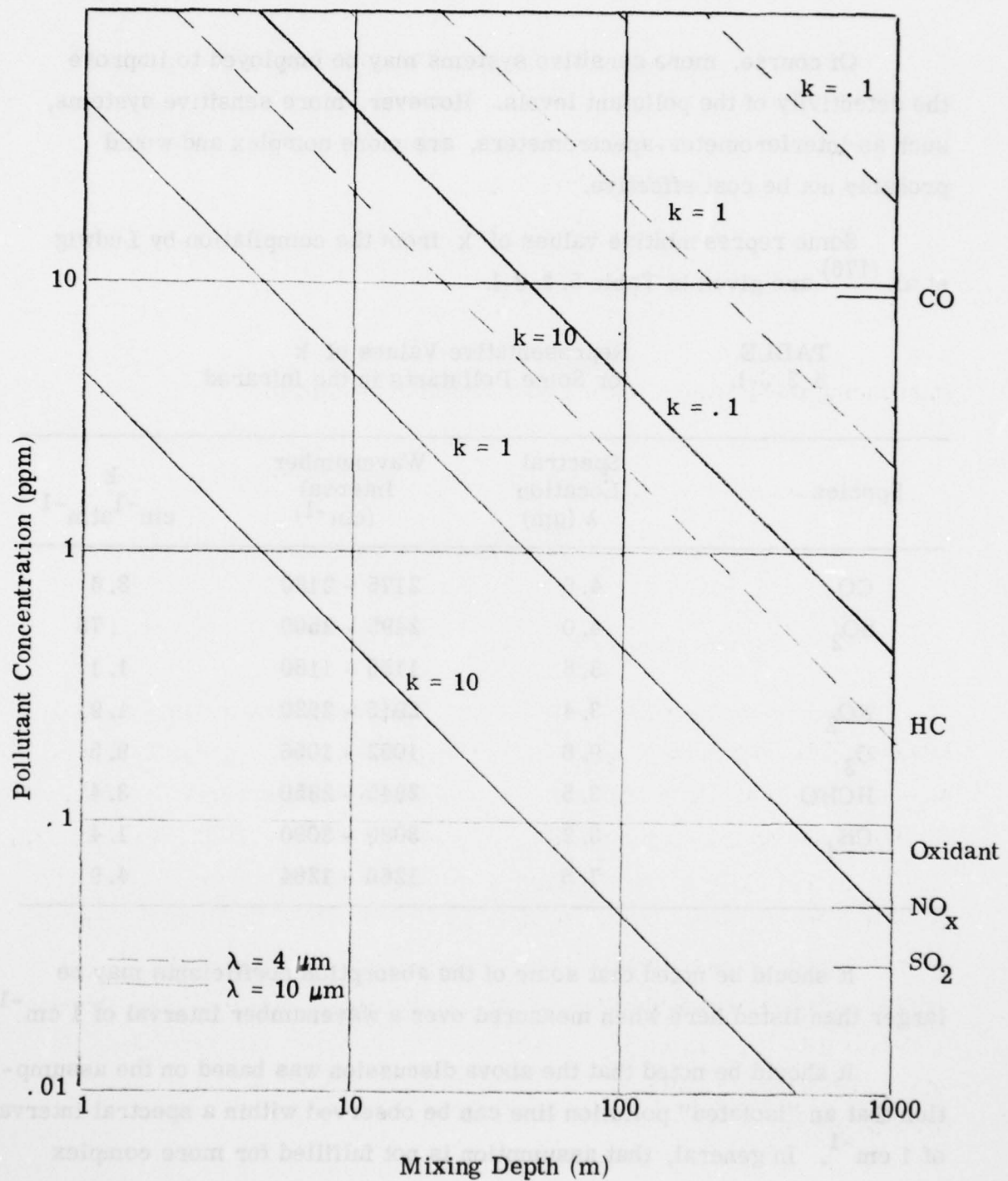


Figure
5. 3. 3-13.

Pollutant Concentrations Observed with SNR = 10
Versus Mixing Depth for Three Different Line
Absorption Coefficients

Of course, more sensitive systems may be employed to improve the detectivity of the pollutant levels. However, more sensitive systems, such as interferometer-spectrometers, are more complex and would probably not be cost effective.

Some representative values of k from the compilation by Ludwig et al. (176) are given in Table 5. 3. 3-1.

TABLE
5. 3. 3-1. Representative Values of k
for Some Pollutants in the Infrared

Species	Spectral Location λ (μm)	Wavenumber Interval (cm^{-1})	k $\text{cm}^{-1}\text{atm}^{-1}$
CO	4.6	2175 - 2180	3.6
SO ₂	4.0	2495 - 2500	.76
	8.6	1155 - 1160	1.1
NO ₂	3.4	2915 - 2920	1.9
O ₃	9.6	1052 - 1056	9.5
HCHO	3.5	2845 - 2850	3.4
CH ₄	3.2	3080 - 3090	1.4
	7.5	1260 - 1264	4.9

It should be noted that some of the absorption coefficients may be larger than listed here when measured over a wavenumber interval of 1 cm^{-1} .

It should be noted that the above discussion was based on the assumption that an "isolated" pollution line can be observed within a spectral interval of 1 cm^{-1} . In general, that assumption is not fulfilled for more complex molecules.

Similar results to those shown in Figure 5. 3. 3-13 for the up-looking mode are found also for the down-looking mode. However, the actual performance of the airborne instrument will, in addition, be heavily influenced by the varying ground emissivity, which will introduce fluctuations that must be accounted for.

5. 3. 3. 5. 3 SNR of a GFC Instrument

The simplified calculations using radiances and emissivities integrated over spectral bandpass of 1 cm^{-1} as was done in the previous two sections cannot be utilized here because the GFC instrument is based on correlating the rotational fine structure within a rotation-vibration band. Thus, the calculations have to be performed on a line-by-line basis instead of on a line averaging basis. This difference in spectral appearance was clearly demonstrated in Figure 5. 3. 3-14, in which a resolution element of 0.07 cm^{-1} was shown that included over 100 lines. Calculations involving that many lines have to be performed on a larger computer. This has been done for the up-looking mode and one specific pollutant, namely SO_2 .⁽⁵⁹⁾

The GFC signal as given by Eq. (5. 3. 3-6) has been programmed by us for the CDC 7600, and the computer code POLAYER has been developed.⁽¹⁷⁶⁾ This code is a necessary tool in the understanding of the nature of the problem and in the data interpretation.

We have calculated the correlation term ΔV for several atmospheric conditions with different SO_2 vertical loadings in the two infrared rotation-vibration bands at $4 \mu\text{m}$ and $8.6 \mu\text{m}$. The $4 \mu\text{m}$ band is essentially free of interfering species, whereas the $8.6 \mu\text{m}$ band has many interfering water vapor lines. It is apparent from the following analysis that although the signal in the $8.6 \mu\text{m}$ is stronger, its uncertainty, due to water vapor interference, is significantly greater than in the $4 \mu\text{m}$ band.

The GFC signal in the $4 \mu\text{m}$ band for SO_2 levels from about 10 ppm-m to 5000 ppm-m for the effective atmospheric temperatures of 275, 286 and 300 K is shown in Fig 5. 3. 3-14. The ordinate is $[(\Delta V/A_0 \Omega_0)]$, which has the units $\text{W/cm}^2 \text{sr}$. In the calculations, the values of the filter function (unnormalized) are given in Table 5. 3. 3-2.

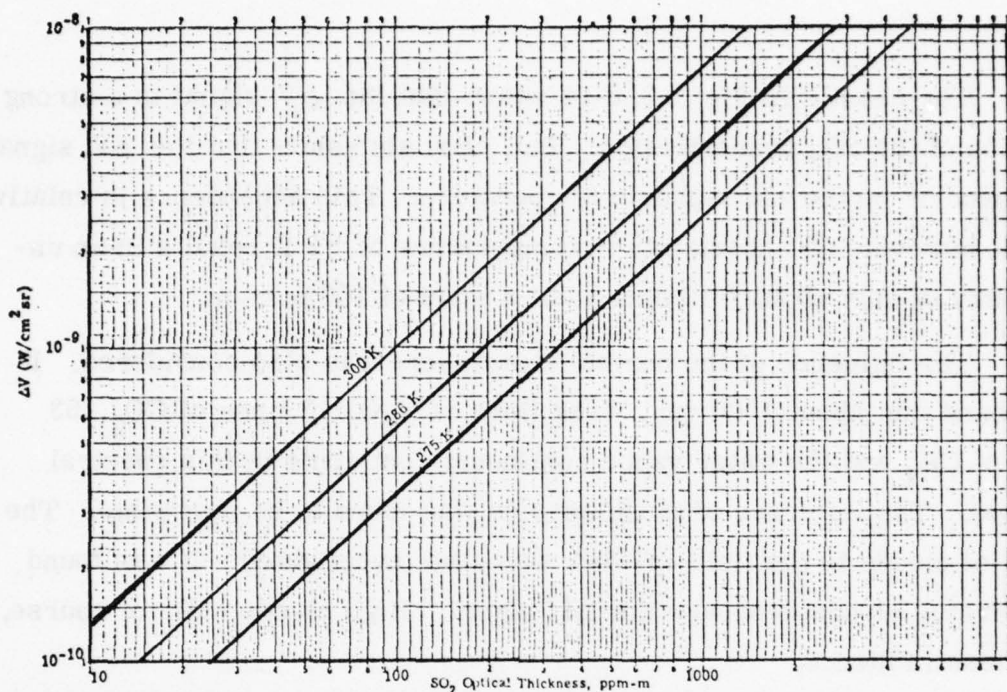


Figure
5. 3. 3-14.

GFC Signal as a Function of SO_2 Loading
at $4 \mu\text{m}$ for Three Temperatures

TABLE
5. 3. 3-2.

Filter Function for the GFC
Instrument at $\lambda = 4 \mu\text{m}$

$\lambda(\mu\text{m})$	$\omega(\text{cm}^{-1})$	τ
4.1300	2421.308	0.0000
4.1150	2430.134	.0150
4.1000	2439.024	.0350
4.0850	2447.980	.0780
4.0700	2457.002	.1550
4.0550	2466.091	.2680
4.0400	2475.248	.3670
4.0250	2484.472	.4250
4.0100	2493.766	.4760
3.9950	2503.129	.5050
3.9800	2512.563	.4800
3.9650	2522.068	.2700
3.9500	2531.646	.0870
3.9350	2541.296	.0210
3.9200	2551.020	0.0000

The results in Fig 5. 3. 3-14 show that the ΔV signal is a strong function of the SO_2 concentration. But, they also show that the ΔV signal is dependent on the atmospheric temperature. This dependence is relatively small, however; an uncertainty in temperature of ± 2 K results in an uncertainty of only about ± 10 ppm-m at a level of 100 ppm-m.

The influence of the normal atmosphere was also considered. It was found that about 1000 very weak lines of N_2O , 10 lines of CO_2 , 53 lines of CH_4 and the water vapor continuum contribute in this spectral interval. The influence of these species was found to be negligible. The effect of clouds in the field-of-view was also investigated. It was found that stratus clouds decrease the ΔV signal. High clouds will, of course, have less influence.

In Fig 5. 3. 3-15 we show the results for the case of SO_2 at $8.6 \mu\text{m}$. The values of the filter function (unnormalized) are given in Table 5. 3. 3-3.

Because the slope of the Planck function is much less in this spectral region than in the $4 \mu\text{m}$ region, the error due to ± 2 C in atmospheric temperature is only ± 2 ppm-m at 100 ppm-m. However, the influence of the other atmospheric species, especially that of water vapor, is considerably greater than in the $4 \mu\text{m}$ region. There are 262 lines of CO_2 , 2518 lines of O_3 , 1978 lines of N_2O , 89 lines of CH_4 and 497 lines of water vapor plus its continuum radiation in this spectral region. A change in concentration of any of these species will influence the determination of SO_2 vertical loading.

The influence of water vapor variation was investigated in greater detail. The effect manifests itself both in terms of a "correlation signal" (water lines on SO_2 lines) as well as an "uncorrelated emission signal".

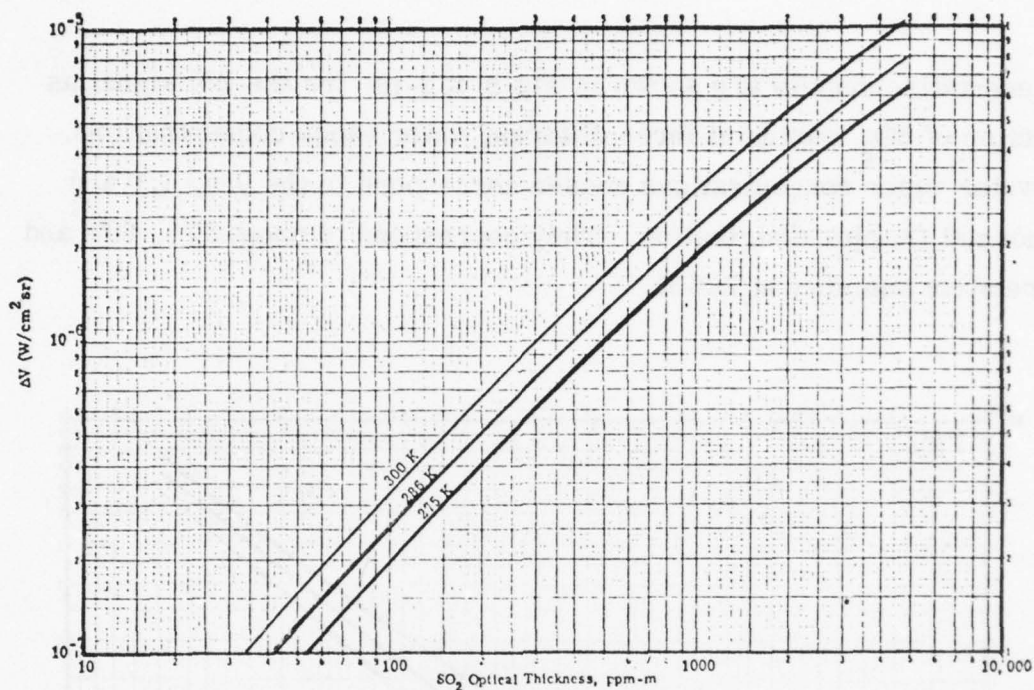


Figure 5. 3. 3-15. GFC Signal as a Function of SO_2 Loading at $8.6 \mu\text{m}$ for Three Temperatures Without Interfering Atmosphere

TABLE 5. 3. 3-3. Filter Function for the GFC Instrument at $\lambda = 8 \mu\text{m}$

$\lambda(\mu\text{m})$	$\omega(\text{cm}^{-1})$	τ
1057.000	0.0000	0.0000
1087.000	.0500	.0500
1104.000	.2000	.2000
1122.000	.5200	.5200
1136.000	.6200	.6200
1156.000	.6500	.6500
1176.000	.6200	.6200
1190.000	.5200	.5200
1208.000	.2000	.2000
1225.000	.0500	.0500
1255.000	0.0000	0.0000

Representative results are shown in Fig 5. 3. 3-16 for the ΔV signal as a function of SO_2 loading at three different water vapor concentrations. The water vapor concentrations chosen correspond to the 0.5, 1.0 and 1.5 normal Gutnick distribution. They correspond to about 30%, 60% and 90% relative humidity at 286 K.

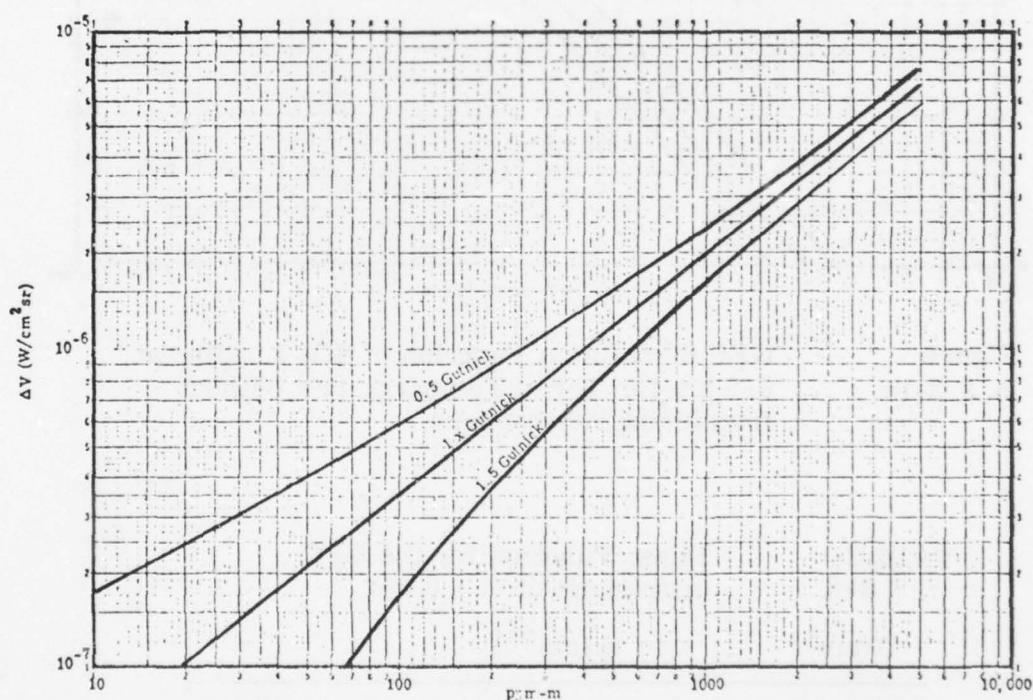


Figure 5. 3. 3-16. GFC Signal as a Function of SO_2 Loading for Three Water Vapor Concentrations ($8.6 \mu\text{m}$)

The data presented in Figures 5. 3. 3-14 and -15 have been used to estimate the SO_2 concentrations that may be detected in a given mixing layer with a $\text{SNR} = 10$ by a GFC instrument having the following parameters:

AD-A067 242

SCIENCE APPLICATIONS INC LA JOLLA CALIF
DEVELOPMENT OF CRITERIA FOR MONITORING OF AIRPORT GROUND POLLUT--ETC(U)
NOV 78 C B LUDWIG, J R YODER

F/G 1/5

DOT-FA76WA-3725

UNCLASSIFIED

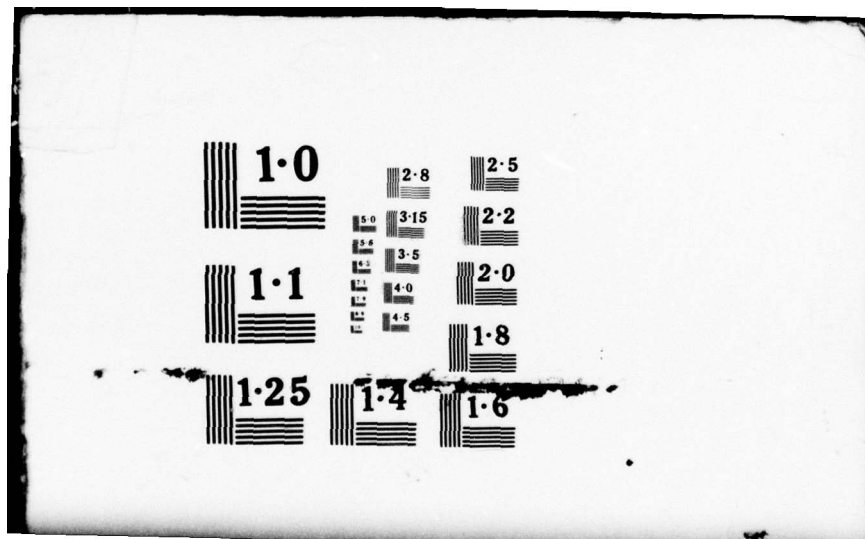
SAI-77-910-LJ-VOL-1-

FAA/RD-77-178-1

NL

5 OF 5
ADA
067242





$$\begin{aligned}
 \eta &= 0.01 \\
 A_d &= 0.23 \\
 \Delta f &= 4.17 \times 10^{-3} \text{ Hz (60 sec time constant)} \\
 D^* (4\mu\text{m}) &= 3 \times 10^{11} \text{ W}^{-1} \text{ Hz}^{1/2} \text{ cm} \\
 D^* (8\mu\text{m}) &= 10^{10} \text{ W}^{-1} \text{ Hz}^{1/2} \text{ cm} \\
 A_o \Omega_o &= 0.143 \text{ cm}^2 \text{ sr}
 \end{aligned}$$

The values for $(\Delta N \Delta \lambda)$ become $1.03 \times 10^{-9} \text{ W/cm}^2 \text{ sr}$ and $3.1 \times 10^{-8} \text{ W/cm}^2 \text{ sr}$ for the SO_2 bands at $\lambda = 4 \mu\text{m}$ and $8.6 \mu\text{m}$ respectively. From Figures 5.5.3-14 and -15, we find the basic sensitivities which are listed in the following:

T(K)	ppm-m at $\lambda = 4 \mu\text{m}$	ppm-m at $\lambda = 8.6 \mu\text{m}$
300	100	9
286	200	12
275	350	15

Note that the results for $\lambda = 8.6 \mu\text{m}$ have been linearly extrapolated. A plot extending the above listed sensitivities to mixing depths from 1 to 1000 m and pollutant concentrations from 0.01 to 100 ppm is presented in Fig 5.3.3-17. It is seen that the long wavelength region is more sensitive than the short wavelength region, and is also less influenced by the atmospheric temperature. However, the humidity and its distribution through the mixing layer introduce a large uncertainty at the long wavelength region.

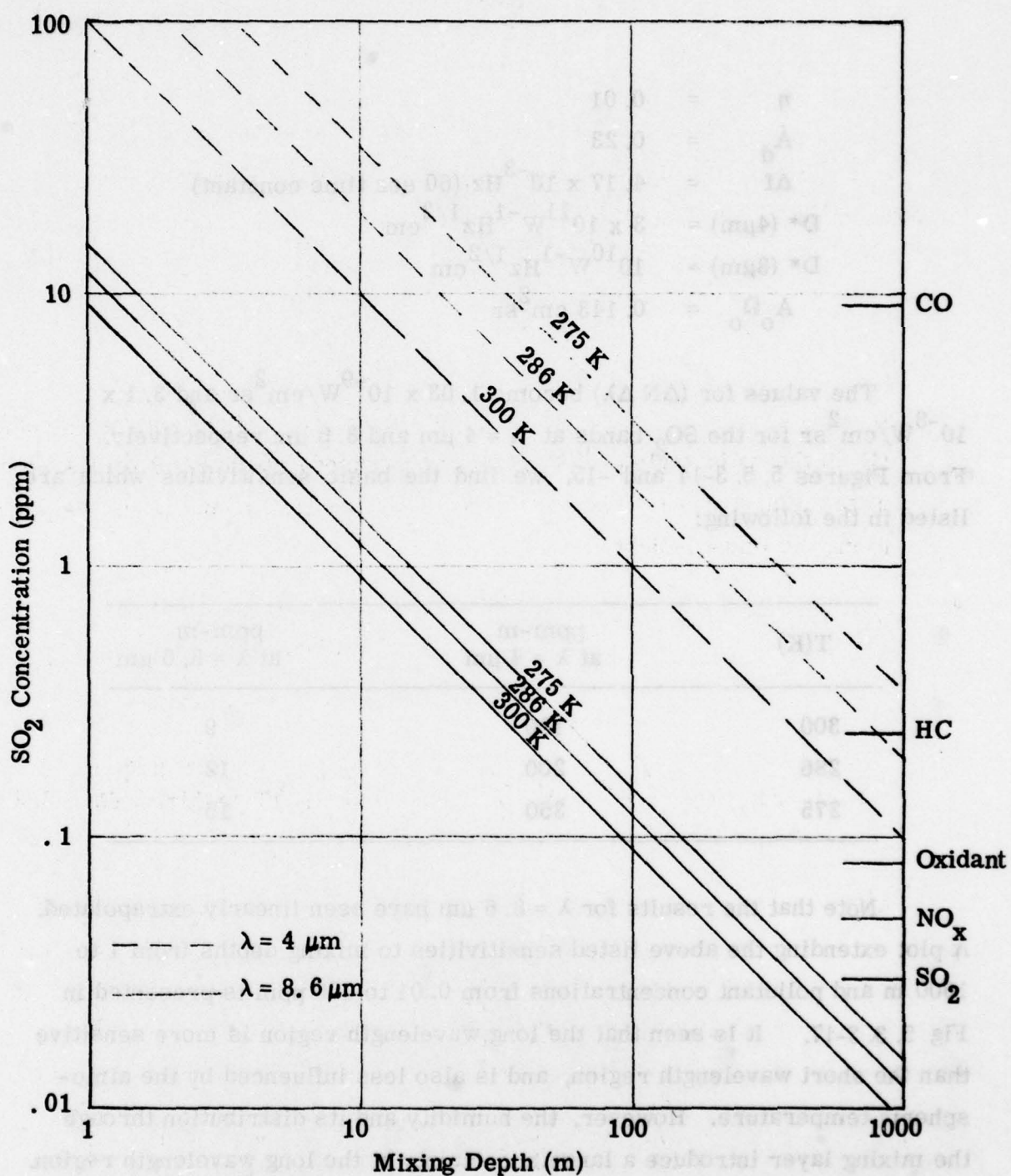


Figure
5. 3. 3-17.

SO₂ Concentration Versus Mixing Depth for a
GFC Instrument with SNR - 10 at Two
Different Wavelength Regions

5. 3. 3. 5. 4 SNR of a Heterodyne Radiometer

As already briefly discussed, the incoming radiation and the radiation from a local oscillator are combined by a beam splitter and focused onto a detector. The intermodulation frequency (IF) is passed through an IF amplifier with bandwidth B_{IF} . The advantage of a heterodyne radiometer is its low noise-equivalent-power, given by Eq. (5. 3. 3-8), which permits the use of a very narrow spectral resolution, thus increasing the specificity. For a local oscillator line-width of about 0.05 cm^{-1} , the IF bandwidth becomes about 10^9 Hz . With an integration time of 60 sec and a mixer quantum efficiency η_Q of 50%, the NEP as a function of wave-number becomes

$$\text{NEP} = \frac{2 \text{ hc} \omega}{\eta_Q} \sqrt{\frac{B_{IF}}{t}} = 8 \times 10^{-20} \omega(\text{cm}^{-1}) [\text{watt}] \quad (5. 3. 3-14)$$

Eq. (5. 3. 3-14) is plotted in Figure (5. 3. 3-18), together with typical NEP values of ordinary, non-heterodyne radiometers, that have a detector area of 0.1 cm^2 , the same integration time and theoretical achievable D^* . One can see that the heterodyne radiometer is more sensitive by over three orders of magnitude at the long wavelengths than the ordinary one.

However, since the heterodyne radiometer is utilizing only a small portion of an emitting pollutant line, the signal-to-noise ratio that can be achieved is limited.

In the following, the pollutant concentration detectable in the ambient air with a SNR = 10 are calculated using Eq. (VII-8). With Eq. (5. 3. 3-14) and

$$P_1 = \eta \lambda^2 \Delta \omega N^\circ(\omega, T) (1 - \tau_p \tau_A)$$

$$P_2 = \eta \lambda^2 \Delta \omega N^\circ(\omega, T) (1 - \tau_A)$$

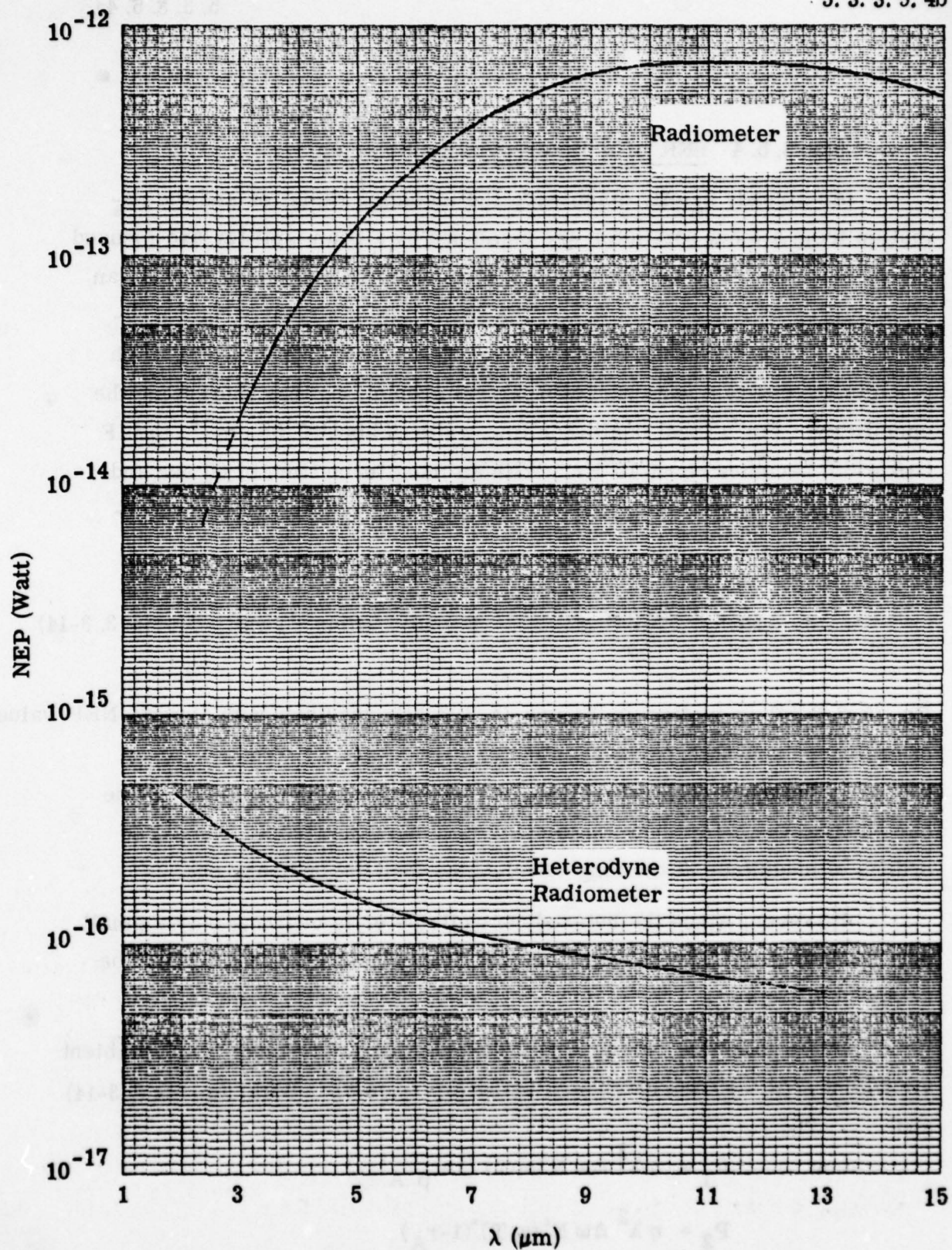


Figure
5. 3. 3-18.

NEP Versus Wavelength for Ordinary and
Heterodyne Radiometers

we have

$$\text{SNR} = \frac{\eta \lambda^2 \Delta\omega N^*(\omega, T)(1 - \tau_p \tau_A)(1 - \tau_A) \ln \frac{1 - \tau_p \tau_A}{1 - \tau_A}}{\text{NEP} \sqrt{(1 - \tau_p \tau_A)^2 + (1 - \tau_A)^2}}$$

The substitution $A_o \Omega_o \approx \lambda^2$ has been made because Siegman⁽²⁰²⁾ and Teich⁽²⁰³⁾ have shown that in a heterodyne laser radiometer the entrance pupil is limited by the coherence area $A_o \leq A_c \approx \lambda^2 / \Omega_o$.

This equation was implicitly calculated for the product of (concentration) x (mixing depth) using the following parameters:

SNR	=	10
η	=	0.02
λ	=	10 μm
$\Delta\omega$	=	0.05 cm^{-1}
T	=	300 K
NEP	=	8 x 10 ⁻¹⁷ Watt
τ_A	=	0.9

The results in terms of pollutant concentration as a function of mixing depth are given in Figure 5. 3. 3-19 for three different absorption coefficients. The range of these coefficients was extended to 100 $\text{cm}^{-1}\text{atm}^{-1}$ since the high resolution allows one to utilize the emission in the line center, which can have rather large absorption coefficients.

The results presented in Fig 5. 3. 3-19 show that the detection of pollutant levels of interest to NAAQS is marginal with the passive heterodyne system, a result confirmed by other workers in the field^(111, 155). It is

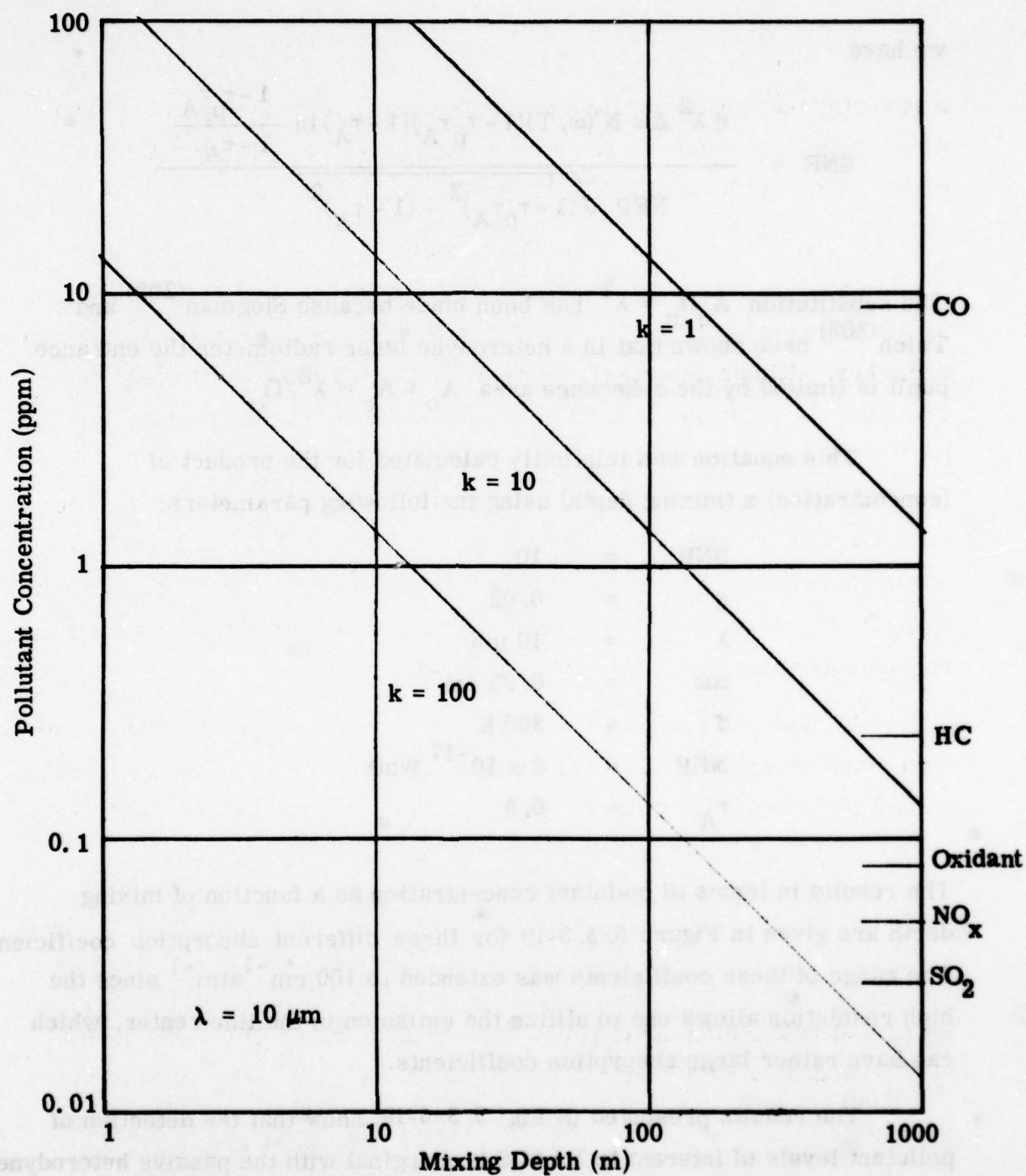


Figure
5. 3. 3-19.

Pollutant Concentrations Observed with SNR = 10
Versus Mising Depth for Three Different Line
Absorption Coefficients (Passive Heterodyne).

noteworthy that the measurement capabilities are restricted to the longer wavelengths. The signals received at the shorter wavelengths are so weak that the limiting SNR (for black lines) is only 0.25.

Seals⁽¹⁸⁵⁾ has analyzed theoretically the possibility of utilizing heterodyne radiometry to obtain pollutant profiles through the atmospheres by scanning over the line profiles. The line profiles are pressure dependent and, thus, altitude dependent. Retrieval of an altitude profile requires inverting the equation of radiative transfer. Seals has utilized the iterative procedure described by Smith⁽²⁰⁴⁾. The calculated results show that the vertical distribution of H_2O and CH_4 can be accomplished from satellite altitudes by a tunable laser having a resolution of 10^8 Hz. Calculations are presently being performed to simulate measurements of other gases such as N_2O , O_3 , SO_2 , NH_3 , and C_2H_4 . No experimental results have been reported as yet.

It should be noted that Siegman⁽²⁰²⁾ gave an expression for the minimum temperature a thermal radiator must have in order to be observed by a heterodyne receiver with $SNR = 1$. However, he did not include the effect of post detection integration. The proper expression becomes

$$T \geq \frac{hc}{k} \omega \ln(1 + \eta \sqrt{Bt})^{-1}$$

Using that expression the temperature T is below 300 K for $B = 10^9$ Hz, $t = 60$ sec and $\omega = 1000 \text{ cm}^{-1}$. Practical results have been obtained by Betz⁽²⁰⁶⁾ in astronomical observations.

5. 3. 3. 5. 5 Pollutant Profile Measurements by Ground-Based Passive Sensors

An analysis of measuring the low altitude water vapor profiles from ground-based infrared measurements was performed by Wang⁽²⁰⁵⁾. The method involves the measurement of several radiances at preselected wavelengths in the $6.3 \mu\text{m}$ water band and the solution of the radiative transfer equation by iteration. The method is being successfully employed for retrieving temperature and water profiles from satellite measurements. An example of Wang's theoretical results is shown in Figure 5. 3. 3-20. It can be seen that the fine-scale detailed structure of the profile cannot be reconstructed. The mixing ratio assumed in this example for the lowest kilometer corresponds to a species concentration of about 7000 ppm. For applying the method to an actual pollution situation, more than four orders of increased sensitivity are required. Since this is not feasible the possibility of measuring pollutant profiles from the ground by passive sensors must be discounted.

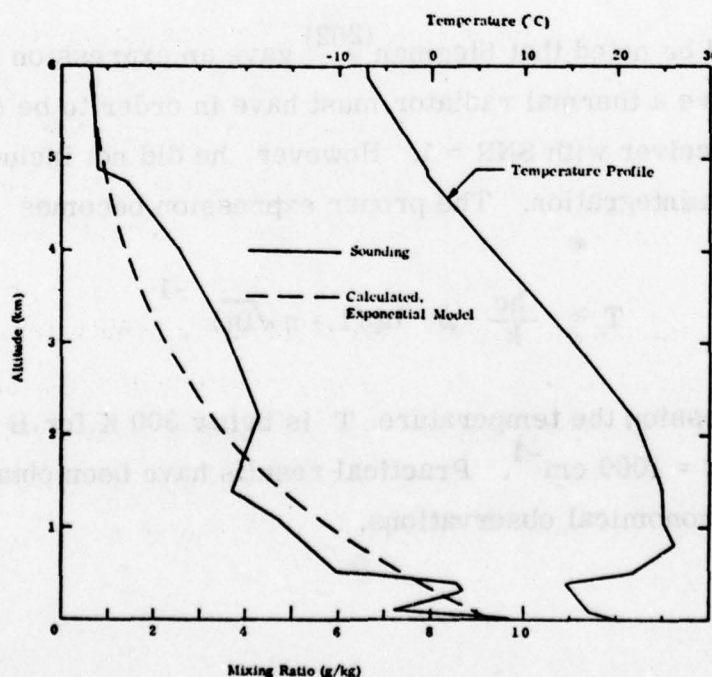


Figure 5. 3. 3-20. Retrieved Mixing Ratio Profile Using the Linear Inversion Technique

6.0 SELECTION AND RANKING OF REMOTE MONITORS

In this section we develop first the selection criteria for remote monitors and, second, select and rank the remote monitors discussed in Section 5 according to the selection criteria and ranking guidelines. The selection criteria for the two applications of R&D monitoring and air enforcement monitoring are based upon (1) the concept of "equivalent method", (2) instrument capability to meet NAAQS requirements, and (3) special requirements for airport operations.

6.1 Development of Criteria

6.1.1 The Equivalency of Remote Monitors

6.1.1.1 General

As was stated previously in this report (Section 4.0), the present regulations for ambient air monitoring distinguish between "manual methods" and "automated methods". Only the specific manual methods for measuring the total suspended particles (TSP) and sulfur dioxide (SO_2) are designated as "reference methods", for the other primary air pollutants "measurement principles and calibration procedures" are specified instead. Any analyzer that is based on the specific "measurement principle and calibration procedure" can be designated as "reference method" (see Section 4.2). However, any other measurement principle (both manual and automated) can be designated as an "equivalent method", if it can be determined to have a "consistent relationship with the reference method", according to 40CFR53 (Subpart C). Several methods have been so designated by EPA (see Section 4.2.3). None of these, however, utilized the measurement principle of remote sensing.

The question arises whether or not any of the remote sensors can ever be designated as a "reference method" or "equivalent method". Let us deal with the question of "reference method" first. EPA has codified the "supersession of reference methods" (41FR11252, March 17, 1976), by which it is intended to encourage and take advantage of advances in the art of monitoring pollutants in ambient air. Accordingly, procedures and criteria have been established to specify a new manual reference method, or a new measurement principle and calibration procedure for automated reference methods. EPA will ordinarily take action only if it is determined that a candidate method (or some variation thereof) is substantially superior to the existing reference method(s). In exercising its discretion, EPA will consider not only the benefits that would result from such action, but also State and local air pollution control agencies and any disruption of the programs that might result from the necessity of replacing existing air monitoring equipment within a reasonable period. As a result, it is expected that supersession of reference methods will occur relatively infrequently, and only when the advantages of such action clearly outweigh potential disadvantages.

Based on the foregoing and the fact that the present National Air Quality Standards (NAAQS) were developed on the basis of the measurement methodology of point samplers, it is clear that remote monitors cannot be designated as a new reference method. However, it is conceivable that a new (parallel) set of NAAQS could be developed which would be based upon the measurement methodology of remote monitors. Then, procedures could be developed to establish certain measurement principles that qualify remote monitors as reference methods. It is clearly beyond the scope of the present program to develop this new set

of NAAQS because this will probably take years, involving a great number of field measurements and cooperative efforts between different Federal and State agencies that are concerned with ambient air programs.

After having dealt with the questions of "reference method", let us now turn to the question of "equivalent method". Since, as stated above, the NAAQS are based upon the measurement methodology of point samplers, a relationship between the data sampled by point and by remote monitors must be established. Remote monitors provide data based upon optical principles in the form of a

line profile

line average

line integral

The line profile data taken by the pulsed DAS systems come closest to the point sampled data. However, the volume samples by the remote sensor is somewhat larger (by at least a factor of 10) than the volume sampled by the point samplers. The line averaged data taken by the long-path monitors are different in nature than the ones taken by the point samplers. The two data can be related to each other by comparing one remote measurement taken at a given time with several point sampled data taken at the same time along the LOS of the remote sensor. A unique relationship of the data taken by a single point sampler traveling along the LOS of the remote sensor exists only in calm and stable meteorological conditions. Regardless of these considerations it may be argued that the line average data provided by a long-path remote monitor are more representative of a polluted air mass than single point samplers. Thus, line average data to monitor the NAAQS will probably become acceptable eventually.

At present, a direct and unique relationship between point sampled data and line integral data does not exist. It may be possible to establish a relationship through mathematical models, requiring additional input data. Another approach would be to establish standards that are based upon line integral data.

Based on the foregoing discussion, it is concluded that "equivalency" between existing "reference methods (point samplers)" and remote monitors providing line profile and line average data can conceivably be established. Thus, in the next section, we outline the procedures to establish this consistent relationship between candidate remote monitors and reference methods.

6. 1. 1. 2 Procedures for Determining a Consistent Relationship
Between Candidate Remote Monitors and Reference Methods

As stated previously, the principal difference between manual or automatic samplers and remote monitors is the character of data (point versus line average or line profile) and the potentially significant influence of the atmosphere on the remote data. It is evident that these different characteristics and atmospheric influences must be dealt with in the procedures to establish equivalency. In addition, a distinction is made here between remote instruments that are used for continuous monitoring and those that are used on a short time basis only. The reasons for this is that the requirements for continuous remote monitors are much more difficult to fulfill than for non-continuous monitors.

EPA in 40CFR53 does not provide equivalency for measuring hydrocarbons and TSP. These are included here, although the remote monitor will not, in general, measure the total hydrocarbons but a specific one, and the lidar will measure a backscattered signal, whose relationship to TSP has not been established yet.

We note that the test procedures for establishing a consistent relationship between candidate manual or automated methods and reference methods demand a certain number of measurements. For oxidants and carbon monoxide, a total of 14 measurements are required in sets of no more than six 1-hour measurements per day. If one or two failures are encountered, a total of 18 additional measurements are required. For sulfur dioxide, a total of seven 1-hour measurements and seven 24-hour measurements are required. If one or two failures are encountered, 8 additional measurements are required for 1-hour as well as 24-hour measurements. The reason for setting the procedures applying to CO and oxidants apart from the ones applying to SO₂ have to do with the different NAAQS requirements. For CO and oxidants the low concentration levels are specified for less than 24-hour averages, while for SO₂ the high level is specified. The low concentration level for SO₂ is specified only as an annual arithmetic mean (see Table 6-1).

TABLE 6-1. Summary of NAAQS

Pollutant	Max. 1-hour Conc. not to exceed once a year	Max. () Hour Average (once a year)	Annual Mean
CO	35 ppm	9 ppm (8 hr)	
Oxidant	.08 ppm		
SO ₂		.12 ppm (24 hr)	.03 ppm (arith)
secondary		.5 ppm (3 hr)	
NO ₂			.05 ppm (arith)
<HC>		.24 ppm (3 hr)	
TSP		260µg/m ³ (24 hr)	75µg/m ³ (geom)
secondary		150µg/m ³ (24 hr)	60µg/m ³ (geom)

In order to specify requirements for remote monitors, one approach is to adopt the existing specifications as given in Table C -1 of 40CFR 53, Subpart C (see Appendix II) and extend them to the other pollutants (HC and TSP). Another approach is to tailor the specifications to the particular needs of monitoring the pollution in the vicinity of airports during periods of alert stages only.

We have adopted here the first approach because it embodies the specifications for the second one; in addition, it covers the requirements for R&D projects, such as the validation and verification of mathematical modeling.

In the following we give a suggested outline of the required provisions, i. e., general provisions, test conditions, test procedures, and test facilities. Further work is needed to provide the details necessary for promulgation, which is within the jurisdiction of the Environmental Protection Agency.

General Provisions

(a) Description of Candidate Remote Monitor

The description should include: A clear identification of the candidate method which will distinguish it from all other methods and by which it may be referred to unambiguously. A detailed description of the candidate method: The measurement principle, manufacturer, name, model number, and other forms of identification; a listing of the significant components; schematic diagrams; and a detailed description of the apparatus and measurement procedures. A copy of a comprehensive operation or instruction manual providing a complete and detailed description of the operational and calibration procedures prescribed for field use of the candidate method and all instruments utilized as part of that method. The manual shall include adequate warning of potential

safety hazards that may result from normal use, or malfunction, and a description of necessary safety precautions. The manual should include a clear description of installation and operation procedures and of necessary periodic maintenance, as well as comprehensive troubleshooting and corrective maintenance procedures. (213, 214)

(b) Determination of Consistent Relationship for Continuous Remote Monitors

In general this is shown when the differences between measurements made by a candidate remote monitor and measurements made simultaneously by one or more reference methods are less than or equal to the value specified in the appropriate column of Table 6-2.

TABLE 6-2. Test Concentration Ranges and Maximum Discrepancy Specifications

Concentration Range (ppm)			1-Hour		24-Hour		Maximum Discrepancy Specification (ppm)
			First Set	Second Set	First Set	Second Set	
Oxidants	Lo	.06 - .1	5	6			.02
	Med	.15 - .25	5	6			.03
	Hi	.35 - .45	4	6			.04
CO	Lo	7 - 11	5	6			1.5
	Med	20 - 30	5	6			2.0
	Hi	35 - 45	4	6			3.0
SO ₂	Lo	.02 - .05			3	3	.02
	Med	.10 - .15			2	3	.03
	Hi	.40 - .50	7	8	2	2	.04
NO ₂	Lo	.02 - .08			3	3	.02
	Med	.10 - .20			2	3	.02
	Hi	.25 - .35			2	2	.03
HC *	Lo	.2 - .28	5	6			.06
	Med	.5 - .6	5	6			.08
	Hi	1 - 2	4	6			.10
$\mu\text{g}/\text{m}^3$							$\mu\text{g}/\text{m}^3$
TSP *	Lo	60 - 90			3	3	20
	Med	150 - 200			2	3	30
	Hi	250 - 350			2	2	40

* Data for HC and TSP are not given in 40CFR53. They constitute suggested values.

(c) **Determination of Consistent Relationship for
Non-Continuous Remote Monitors**

In general this is shown when the differences between measurements made by a candidate remote monitor and measurements made simultaneously by one or more reference methods are less than or equal to the value specified in the appropriate column of Table 6-3.

**TABLE 6-3. Test Concentration Ranges and
Maximum Discrepancy Specifications**

		Concentration Range (ppm)	First Set	Second Set	Maximum Discrepancy Specification (ppm)
Oxidants	Lo	.06 - .1	5	6	.02
	Med	.15 - .25	5	6	.03
	Hi	.35 - .45	4	6	.04
CO	Lo	7 - 11	5	6	1.5
	Med	20 - 30	5	6	2.0
	Hi	35 - 45	4	6	3.0
SO ₂	Lo	.02 - .05	5	6	.02
	Med	.10 - .15	5	6	.03
	Hi	.40 - .50	4	6	.04
NO ₂	Lo	.02 - .08	5	6	.02
	Med	.10 - .20	5	6	.02
	Hi	.25 - .35	4	6	.03
HC	Lo	.2 - .28	5	6	.06
	Med	.5 - .6	5	6	.08
	Hi	1 - 2	4	6	.10
		$\mu\text{g}/\text{m}^3$			$\mu\text{g}/\text{m}^3$
TSP	Lo	60 - 90	4	5	20
	Med	150 - 200	4	5	30
	Hi	250 - 350	4	5	40

Although the National Standards do not have provisions for a 1 or 3 hour standard for the pollutants NO₂ and SO₂, they are nevertheless included here because of their importance in photochemical smog situations and because they may be included in State Standards (see Section 2.2).

(d) **Selection of Test Sites**

The specification of test sites will be quite different from those for the manual and automatic samplers and must be considered carefully for the remote monitors. The placement of the reference instruments will depend upon the data obtained (line average and line profile). Additional instruments that measure the interfering atmosphere must be specified. For certain methods and pollutants, the utilization of test chambers may be considered.

(e) **Test Atmosphere**

When the tests are conducted in the ambient air, the air sampled at the test sites shall be used. If necessary, the concentration of pollutant in the sampled ambient air may be augmented with artificially generated pollutants to facilitate measurements in these specified ranges. When the tests are conducted by means of test chambers, the air sampled from the chamber during the tests shall be used.

(f) **Submission of Test Data and Other Information**

All recorder charts, calibration data, records, test data, procedural descriptions and details, and other documentation obtained from (or pertinent to) these tests shall be identified, dated, signed by the analyst performing the test, and submitted. Also included are the data generated by the computer data reduction procedure, where applicable.

(g) **Sample Manifold**

A significant difference exists between remote monitoring and measurements by sampling. Remote measurements do not alter the ambient air, but the intake of a manual or automatic sampler may. For this reason, Subpart C of 40CFR53 emphasizes that "precautions shall be taken in the design and construction of the manifold (for the manual or automatic reference method) to minimize the removal of particulates and trace gases, and to insure that identical samples reach the two methods."

Test Conditions

(a) All Methods

All test measurements made and test samples collected shall be in a range of ambient conditions that may be encountered in the measurements at airports. All instruments involved in the tests shall be calibrated as specified in paragraph (c) of this section prior to initiation of the tests.

Since §53.31 (a) specifies a temperature range from 20° to 30° C only, special provisions must be made when tests are required outside that temperature range.

(b) Remote Monitor and Automated Reference Method

Set-up and start-up of the remote monitor and the automated analyzer (if the reference method is automated) shall be in strict accordance with the applicable operation manual(s). Allow adequate warm-up or stabilization time as indicated in the applicable operation manual(s) before beginning the tests.

The corresponding paragraphs in §53.31 (b) asks for the use of an integral strip chart recorder of the servo-null balance type in order to facilitate evaluation of data submitted. The practicality of such a device for a remote monitor must yet be established.

(c) Calibration

The reference method shall be calibrated according to the applicable operation manual. A candidate remote monitor shall be calibrated according to procedures specified by the manufacturer in a test facility and/or in the field.

Test Procedures

(a) Conduct a set of simultaneous measurements with the candidate remote monitor and the reference method(s), according to specifications for the three different types of data to be obtained (line integral, line average and line profile).

(b) For each pair of measurements, determine the discrepancy between the candidate method measurement and reference method measurement. A discrepancy which exceeds the discrepancy specified in Tables 6-2 and 6-3 constitutes a failure.

(c) The results of this set of measurements shall be interpreted as follows [following verbatim the specifications as given in § 53.32 (c)]:

"(1) Zero (0) failures: The candidate method passes the test for consistent relationship.

(2) Three (3) or more failures: The candidate method fails the test for consistent relationship.

(3) One (1) or two (2) failures: Conduct a second set of simultaneous measurements as specified in Tables 6-2 and 6-3. The results of the combined total of first-set and second-set measurements shall be interpreted as follows:

(i) One (1) or two (2) failures: The candidate method passes the test for consistent relationship.

(ii) Three (3) or more failures: The candidate method fails the test for consistent relationship."

Test Facilities

We suggest that one or more National Test Facilities for remote monitors be established. It would be desirable that these test facilities could simulate a variety of meteorological conditions, such as occur in stable (stagnant) and unstable situations. In the following we list a number of desirable characteristics and capabilities for such a test facility:

- Range (at least up to 1 km);
- Generation and control of different atmospheres to test background and polluted airmasses;
- Generation and control of different visibility situations due to
 - aerosols
 - rain
 - fog
- Line-of-sight well instrumented with manual and/or automated analyzer that have been designated as reference of equivalent method;
- Line-of-sight well instrumented with calibrated analyzers that provide supporting data, such as interfering gases;
- Meteorological conditions of ambient air, such as wind speed and direction, temperature and lapse rate, and humidity (a number of instruments are described in Appendix VIII).

Ideally, the test facility should be located in a large enclosure, in which the different pollutant conditions could be simulated. In a somewhat less ambitious approach, an open range could be utilized, in which the line-of-sight passes through a test chamber. The atmosphere in the test chamber must then be the controlled variable.

6. 1. 2 Required Instrument Capabilities

In the previous section, we have established that only remote sensors which provide line profile and line average data are potentially suitable to be designated as "equivalent methods". In this section, we specify the required instrument capabilities. It is necessary to specify only general parameters; viz. ,

Sensitivity

Range

Type of Data

Maximum permissible transmitter (laser) energy

At this time we introduce the distinction between two applications of remote monitors:

R&D projects

Air Enforcement Programs

Although many of the instrument capabilities must be similar for both applications, differences can exist. These are summarized in Table 6-4 for the parameters. The particular sensitivities for the different primary gaseous pollutants are listed in Table 6-5.

**TABLE 6-4. Generalized Selection Criteria
for Remote Monitors**

	R&D Application	Air Enforcement
Sensitivity	Desirable range: ~0.1 x NAAQS to 10 x NAAQS	Required range: ~0.8 x NAAQS to 10 x NAAQS
Range	Desirable range: 100 m to several km	Required range: > 100 m
Type of Data	Line profile Line average Line integral	Must be relatable to standards viz., line profile and line average
Maximum Laser Energy	With proper precautions, could be higher than eye safety regulations	Must abide by eye safety regulations

TABLE 6-5. Required Sensitivities (Air Enforcement)

	Minimum Sensitivity (ppm)	Maximum Sensitivity (ppm)	Dynamic Range
CO	7	350	50
O ₃	.06	.8	13
SO ₂	.02	1.2	60
NO ₂	.04	.5	13
THC	.2	2.4	12

6.1.3 Special Requirements for Airport Operations

6.1.3.1 Limitations Due to Airport Operations

The basic philosophy of the FAA regarding electronic instrumentation installed at airports is that nothing will be arbitrarily excluded until it has been demonstrated that the equipment does in fact interfere with aircraft safety.⁽²⁹³⁾ No regulations exist to specify, for example, the maximum spurious radiated power at specified frequencies from such equipment; rather, each airport is considered to be a unique installation and is evaluated individually on the basis of empirical data. This is because of the differing physical layouts and instrument landing systems (ILS) among airports.

Guidelines can be given concerning those radio frequencies and other parameters which are most likely to be a source of interference so that the design/installation can be made with the greatest chance of success. The frequency bands in use for ILS are 108 - 135 MHz and 200 - 400 MHz, plus 1000 - 1500 MHz for air surveillance radar (ASR) systems. The actual frequencies in use vary among airports; Los Angeles International, for example, operates eight separate ILS systems plus Air Surveillance Radar (ASR).

Also, reflection of radio waves from pollution monitoring equipment may cause interference, in this case it would be of a passive nature since the interference does not originate within the instrument but simply because of its presence. This was indicated to be a possible serious problem.⁽²⁹³⁾ To avoid this, large (e.g., automobile-sized) installations should not be adjacent to the sides of an active runway.

The intensity and directivity of visible light sources must be controlled, but there are no landing systems presently in use or known to be in planning which utilize either the IR or UV spectral regions.

Acoustic detectors are or have been in use for the detection of air turbulence, but this would not seem to affect any pollution monitoring equipment now conceived.

Access to monitoring equipment for service or data retrieval is under the control of the local airport authorities and is not the responsibility of the FAA.

6. 1. 3. 2 Operational Limitation due to Eye Safety Requirements

The most obvious hazard with the laser beam is direct axial viewing, but specular reflections are also a risk, and considerable care must be exercised in the use of laser systems. The skin can be burned by some laser beams, but the main hazard is damage to the eye. The danger varies with wavelength of the laser radiation due to the wavelength dependent optical properties of the eye.

The most sensitive region is the visible region, 400 to 7000 Å, since the cornea, aqueous humor and the lens readily transmit this radiation. Thus, the full laser beam energy is focused on the retina in an image 10-20 μm in diameter resulting in high power densities of kilowatts/cm² on the retina even for milliwatt powers incident on the pupil of the eye. These high power densities can cause severe damage to the retina, and the fovea, resulting in loss of visual acuity.

In the UV region, the radiation below about 4000 Å is absorbed by the lens, and below about 3150 Å it is absorbed by the cornea, so that UV hazards are mostly limited to these parts of the eye. The radiation is absorbed over a larger area than is the focused visible light on the retina, so the power densities are not so high. Exposure to excessive UV results in inflammation of the cornea and conjunctiva at the shorter wavelengths, and cataract formation at the longer wavelengths.

In the IR region, up to 1.4 μm, the ocular transmission is less than that of the visible, and varies with wavelength. From 1.4 to 1.9 μm, essentially all radiation is absorbed by the cornea and the aqueous humor. Beyond 1.9 μm all the radiation is absorbed by the cornea alone. The absorbed energy can be conducted to the interior of the eye, raising the temperature of the lens, and resulting in the formation of cataracts.

The Department of Health, Education, and Welfare⁽⁵⁴⁾ has proposed Performance Standards for Laser Products to minimize the hazards of laser systems. The proposed standards are somewhat complex, but may be summarized in terms of a Maximum Permissible Exposure (MPE)

which varies with the laser emission duration. The following values are for pulse lengths of about 0.1 μsec . In the visible band from 4010 to 7000 \AA the MPE is $4 \times 10^{-7} \text{ J/cm}^2$. In the IR, this value increases to $2 \times 10^{-6} \text{ J/cm}^2$ at 1.06 μm and remains constant out to 1.4 μm . From 1.4 to 13.0 μm the MPE is $1.58 \times 10^{-4} \text{ J/cm}^2$. In the UV, the MPE at 4000 \AA is $1.6 \times 10^{-2} \text{ J/cm}^2$ decreasing to $4.8 \times 10^{-5} \text{ J/cm}^2$ at 3020 \AA , and remaining constant to 2500 \AA . These values are plotted in Figure 6-1. There are discontinuities (or, at least, a very rapid change in MPE with wavelength) in the MPE values near 4000 \AA and near 1.5 μm .

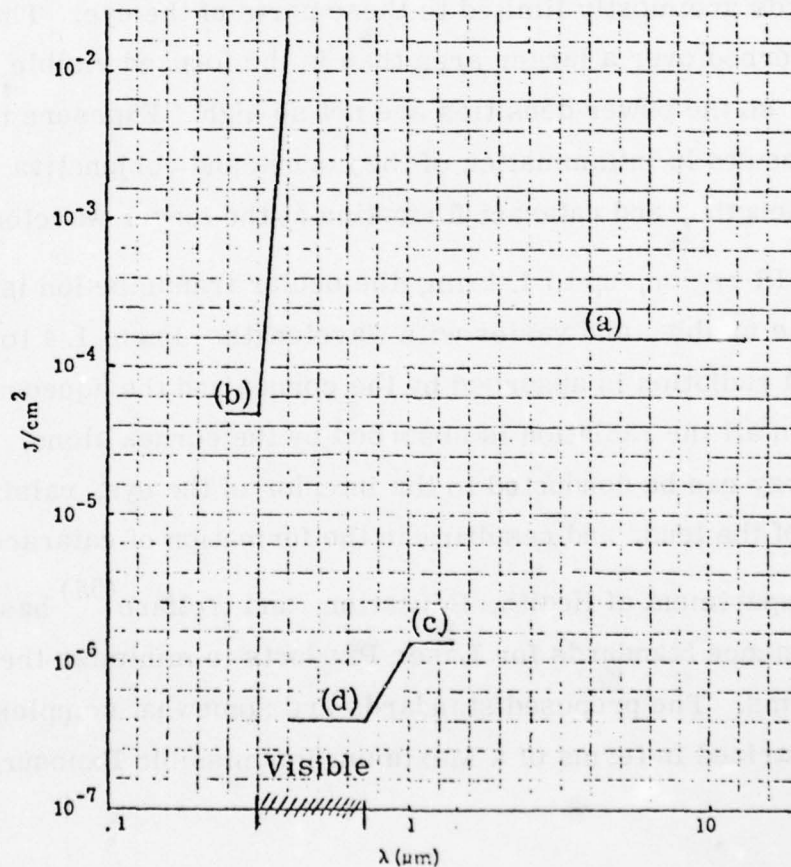


Figure 6-1. Maximum Permissible Exposure versus Wavelength

The implication of this requirement is plotted in Figure 6-2 for the different regions in the spectrum in terms of maximum permissible laser energy P (Joules) and "minimum permissible beam diameter". One

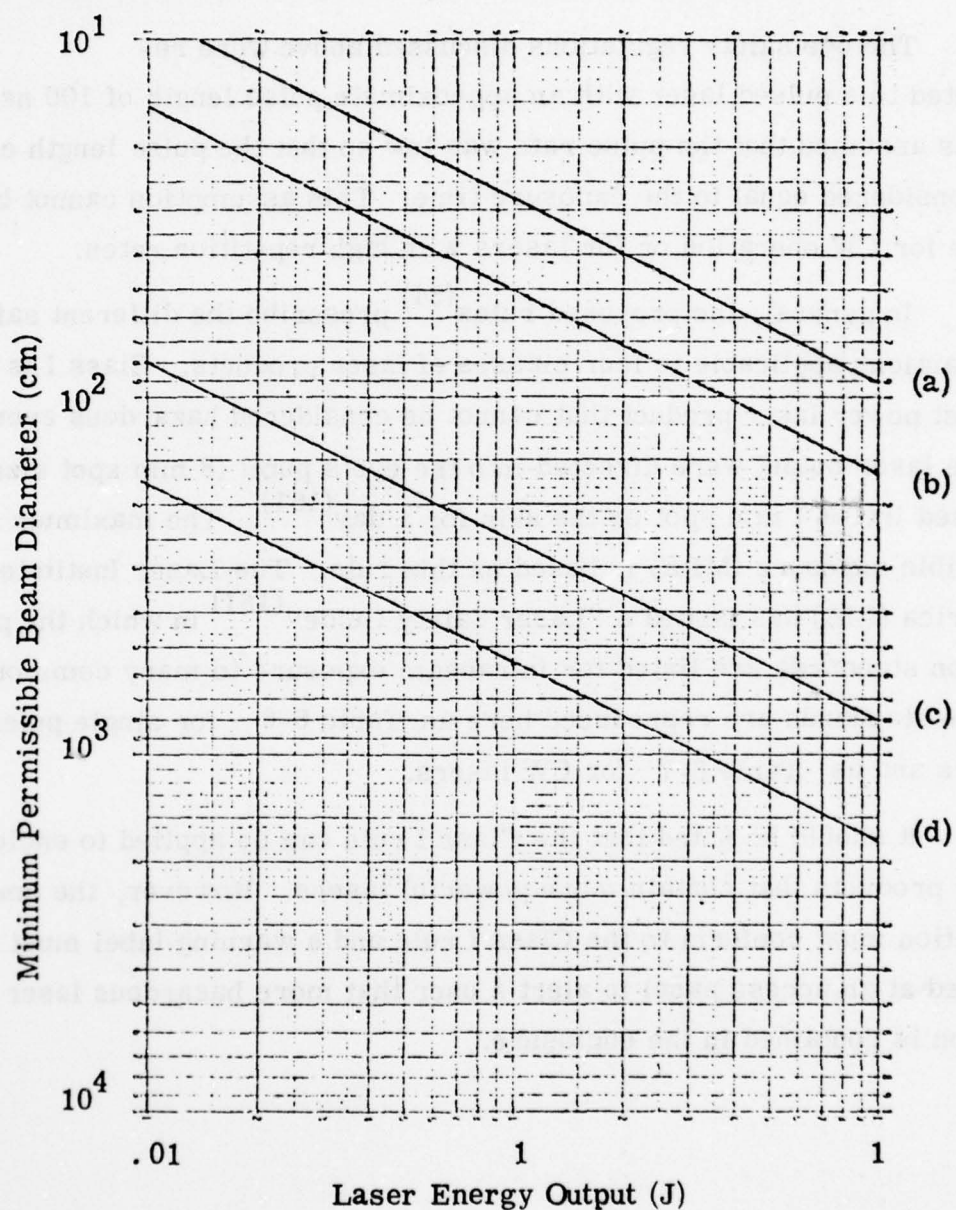


Figure 6-2. Minimum Permissible Beam Diameter as a Function of Laser Pulses with a Duration of $0.1 \mu\text{sec}$ for the Four Spectral Regions as Indicated in Figure 6-1.

can see that a beam diameter of over 5 m is required for a laser pulse of 100 mJ with a pulse length of 0.1 μ sec in the visible spectrum. This value is reduced to 50 cm for a laser operating in the ultraviolet.

The eye safety regulations discussed above were restricted to a pulsed laser with an approximate pulse length of 100 nsec. It was assumed that the pulse rate was low so that the pulse length could be considered equal to the exposure time. This assumption cannot be made for CW operation or for lasers with high repetition rates.

In general, the proposed rules⁽⁵⁴⁾ prescribe the different safety precautions applicable to four classes of laser products. Class I is the lowest power laser product that cannot be considered hazardous even if all of the laser output were directed into the eye's pupil (8 mm spot size) or focused into a 1 mm spot on the skin for a day⁽¹⁶¹⁾. The maximum permissible exposure (MPE) is based on this rule. The Laser Institute of America (LIA) has issued a "Laser Safety Guide"⁽¹⁶¹⁾ in which the protection standards are listed for intrabeam exposure to many common lasers. These standards are reproduced here as Table 6-6 for single pulsed lasers and as Table 6-7 for CW lasers.

It should be noted that the Class I rule can be applied to enclosed laser products that contain more powerful lasers. However, the emanating radiation must conform to the Class I rule and a warning label must be located at an access panel to alert a user that more hazardous laser radiation is contained in the enclosure.

TABLE 6-6. Intrabeam Protection Standards which are Applicable to Many Pulsed Lasers for Eye and Skin Exposure to Laser Radiation

Laser Type	Primary Wavelength(s) (nm)	Pulse Duration	Protection Standard	
			Eye	Skin
Normal-pulsed ruby	694.3	~ 1ms	$10^{-5} \text{ J} \cdot \text{cm}^{-2}$	$0.2 \text{ J} \cdot \text{cm}^{-2}$
Q-switched ruby	694.3	5-100ns	$5 \times 10^{-7} \text{ J} \cdot \text{cm}^{-2}$	$0.02 \text{ J} \cdot \text{cm}^{-2}$
Rhodamine 6G Dye Laser	~ 500-700	0.5-20 μ s	$5 \times 10^{-7} \text{ J} \cdot \text{cm}^{-2}$	$0.03-0.09 \text{ J} \cdot \text{cm}^{-2}$
Normal Pulsed neodymium	1064	~ 1ms	$5 \times 10^{-5} \text{ J} \cdot \text{cm}^{-2}$	$0.2 \text{ J} \cdot \text{cm}^{-2}$
Q-switched neodymium	1064	5-100ns	$5 \times 10^{-6} \text{ J} \cdot \text{cm}^{-2}$	$0.02 \text{ J} \cdot \text{cm}^{-2}$

TABLE 6-7. Intrabeam Protection Standards which are Applicable to Many Common CW Lasers for Eye and Skin Exposure to Laser Radiation

Laser Type	Primary Wavelength(s) (nm)	Protection Standard	
		Eye	Skin
Helium-Cadmium	441.6	a) $2.5 \text{ mW} \cdot \text{cm}^{-2}$ for 0.25s b) $10 \text{ mJ} \cdot \text{cm}^{-2}$ for 10-10,000s c) $1 \mu \text{W} \cdot \text{cm}^{-2}$ for > 10,000s	$0.2 \text{ W} \cdot \text{cm}^{-2}$
Helium-Neon	632.8		
Argon	488.514.5		
Krypton	647.1		
Freq. Doubled ND:YAG	532		
Neodymium:YAG	1,064	$0.5 \text{ mW} \cdot \text{cm}^{-2}$ for $t > 100\text{s}$	$0.2 \text{ W} \cdot \text{cm}^{-2}$
Gallium-Arsenide at room temp.	905	$0.25 \text{ mW} \cdot \text{cm}^{-2}$ for $t > 100\text{s}$	$0.2 \text{ W} \cdot \text{cm}^{-2}$
Helium-Cadmium	325	a) $1 \text{ J} \cdot \text{cm}^{-2}$ for < 1000s b) $1 \text{ mW} \cdot \text{cm}^{-2}$ for > 1000s	a) $1 \text{ J} \cdot \text{cm}^{-2}$ for < 1000s b) $1 \text{ mW} \cdot \text{cm}^{-2}$ for > 1000s
Nitrogen	337.1		
Carbon-dioxide (and other lasers 1.4 μ m to 1000 μ m)	10.6 μ m (10,600nm)	$0.1 \text{ W} \cdot \text{cm}^{-2}$ for $t > 10\text{s}$	$0.1 \text{ W} \cdot \text{cm}^{-2}$ for $t > 10\text{s}$

The Z-136 Committee on the Safe Use of Lasers (American National Standards Institute) has also issued eye safety regulations. That committee has defined the control aperture in the infrared to have a diameter of 1 mm rather than 7 mm as given in the HEW performance standards for laser products. Thus, the infrared lasers (1.4-13 μm) of Class I can have 50 times more energy/power, which is a significant difference. However, we are still using the more conservative HEW performance standards, since it will be those standards that will govern the use of lasers in the vicinity of airports. In case HEW eventually relaxes the performance standards in the infrared, our performance predictions must then be revised. However, these revisions would not basically change our selection of remote monitoring systems.

6. 1. 3. 3 Electromagnetic Interference Characteristics Requirements for Equipment

Since air pollution monitoring equipment generates electric signals, especially the pulsed active systems, it is necessary that they conform with the interference characteristics requirements given in MIL-STD 461A. This standard describes the test requirements for different equipment categories. Air pollution monitors would fall into Class II. Equipment in this class may generate rf energy intentionally for other than communication purposes or may consist of motors, pumps, regulators, generators and/or processing equipment.

Excerpts from MIL-STD 461A are given in Appendix IX.

6. 1. 4 Conclusions

It is concluded that the solution criteria can be based upon

- the EPA procedures to establish equivalency between remote monitors and reference methods
- instrument capabilities that meet NAAQS requirements
- the MIL-STD-461A standards that regulate rf interference, and
- the HEW performance standards for laser products that regulate the maximum permissible exposure to the skin and eye.

It is further concluded that a difference be made between remote monitors that are used in air enforcement and those that are involved in R&D. The more stringent criteria apply to the monitors used in air enforcement.

6. 2 Selection and Ranking of Remote Monitors

6. 2. 1 Summary of Selection Criteria

6. 2. 1. 1 Air Enforcement Programs

Monitors to be used in air enforcement programs, i. e. , those programs that can lead to the curtailment or shut-down of air traffic in airports, must fulfill the following requirements.

- Monitors must have the potential of being designated as an "equivalent method"; as a consequence, only monitors that provide either line profile or line average data can be selected;
- Monitors must have a sensitivity and a dynamic range that span the "National Ambient Air Quality Standards (NAAQS)"; i. e. , 7-350 ppm for CO, 0.06 to .8 ppm for O₃, 0.02-1.2 ppm for SO₂, 0-04-0.5 ppm for NO₂ and 0.2-2.4 ppm THC;
- Monitors should have a range capability of greater than 100 m;
- Monitors using lasers as the transmitter must not emit more than the maximum permissible exposure (MPE);
- Monitors (transmitter and receiver stations) must not interfere with normal airport operations;
 - (a) electromagnetic emission must not interfere with any instrument landing systems (ILS) or air surveillance radar (ASR), as determined by the FAA, and
 - (b) the access to monitoring equipment for services or data retrieval must not interfere with air traffic on the ground as determined by the local airport authority.

It should be noted that items such as zero and span drift, lag time, rise and fall time, accuracy, and precision are not included as selection criteria. This is because we based the selection and ranking upon measurement principles rather than existing instruments (there do not exist off-the-shelf instruments). However, those parameters not used in the selection play an important role in the definition of the operational procedures, as will be outlined in Section 7. 0.

6. 2. 1. 2 R&D Programs

The criteria for monitors to be used in R&D programs are somewhat more relaxed than those to be used in air enforcement programs. In general, they should not interfere with airport operations and should not emit more energy than the MPE. However, if special arrangements are made with the FAA and local airport authority, these restrictions may be somewhat relaxed provided adequate safety precautions are monitored. On the other hand, it would be desirable that the monitors have a greater sensitivity in order to be useful in answering research questions.

6. 2. 2 Selection and Ranking

6. 2. 2. 1 Selection of Measurement Principle for Air Enforcement Programs

(a) Remote Monitors Providing Line Profile Data

At the present time and in the near future only pulsed laser systems can provide line profile data practically and reliably. Of these systems, only lidar and differential absorption by scattering have the necessary performance characteristics to measure pollutants covered by the NAAQS at distances of interest, i. e., greater than 100 m and up to 1 km. In Table 6-8, we list all the measurement principles and their useful applicability to certain pollutants.

TABLE 6-8. REMOTE MONITORS PROVIDING LINE PROFILE DATA

Measurement Principle	TSP	CO	HC	O ₃	NO _x	SO ₂
Lidar	(Yes) *					
DAS (infrared)		Yes	Yes	Yes	Yes	Yes
DAS (ultraviolet)					Yes	Yes
Raman	_____	Not acceptable			_____	_____
Resonance Raman	_____	Not acceptable			_____	_____
Fluorescence	_____	Not acceptable			_____	_____

*Requires establishment of relationship between scattering and mass density

(b) Remote Monitors Providing Line Average Data

Two types belong to this category: monostatic and bistatic systems. The monostatic systems utilize natural reflectors such as hillsides and walls, while the bistatic systems utilize man-made retro-reflectors. Another distinction is the utilization of a narrow band (typically a laser) or broadband light source. In Table 6-9, we list all the measurement principles and their useful applicability to certain pollutants.

(c) Remote Monitors Providing Line Integral Data

These monitors employ a source at an indefinite distance (the sky) to yield data interpretable as the total integrated burden in the line of sight. None of these systems are far enough developed to be selected at this time for Air Enforcement Programs. One system, the upward-looking monitor using gas filter correlations shows adequate sensitivity and specificity to be very promising for future selection.

TABLE 6-9. REMOTE MONITORS PROVIDING LINE AVERAGE DATA

Measurement Principle	TSP	CO	HC	O ₃	NO _x	SO ₂
Long-path laser system in the IR		Yes	Yes	Yes	Yes	Yes
Long-path laser system in the UV/Visible	(Yes)*				Yes	Yes
Long-path system in the IR:						
Dispersive type		Yes		Yes		
Gas Filter Correlation		Yes	Yes		Yes	Yes
Interferometer		Yes	Yes	Yes	Yes	Yes
Filterwheel		Yes		Yes		
Long-path system in the UV/Visible:						
Matched Filter					Yes	Yes
Passive Downward Looking	-----Not Acceptable-----					

*Requires establishment of relationship between scattering and mass density

6. 2. 2. 2 Summary of Performance Characteristics of All Monitors

In this section, we present the performance characteristics in summary form of all remote monitors discussed in Section 5.0. The summaries are given for

a) Monitors that provide line profile data*

Lidar
 LWIR DAS
 MWIR DAS
 SWIR DAS
 UV/Vis DAS
 Raman Scattering
 Resonant Raman/Fluorescence Scattering

b) Monitors that provide line average data

LWIR Long-Path with Laser Source (Mono- and Bi-static)
 MWIR Long-Path with Laser Source (Mono- and Bi-static)
 SWIR Long-Path with Laser Source (Mono- and Bi-static)
 UV/Vis Long-Path with Laser Source (Mono- and Bi-static)
 IR Long-Path with Broad Band Source (Bi-static)
 Using Dispersive Receiver
 IR Long-Path with Broad Band Source (Bi-static)
 Using Fourier Transform Spectrometer Receiver
 IR Long-Path with Broad Band Source (Bi-static)
 Using Gas Filter Correlation Receiver
 IR Long-Path with Broad Band Source (Bi-static)
 Using Filterwheel Receiver
 UV/Vis Long-Path with Broad Band Source (Bi-static)
 Using Matched Filter and Gas Filter Correlation Receiver
 Passive Downward Looking

c) Monitors that provide line integral data

Passive Upward Looking using Gas Filter Correlation Receiver
 Passive Upward Looking using Matched Filter Receiver

* LWIR - Long Wavelength Infrared (8-12 μm)
 MWIR - Medium Wavelength Infrared (4-6 μm)
 SWIR - Short Wavelength Infrared (2-4 μm)

TECHNOLOGY: REMOTE MONITORING - LINE PROFILE
SYSTEM: LIDAR
PRINCIPLE OF OPERATION: DIFFERENCING THE ELASTIC BACKSCATTERING SIGNAL
OF SEQUENTIAL LASER PULSES

PERFORMANCE PARAMETER	VALUE/COMMENT
POLLUTANT SPECIES:	Particles in the size range from 0.1 to 100 μm
WAVELENGTH REGION:	Visible
LASER:	Pulsed Ar, Nd-YAG, Ruby, Dye
MAXIMUM PERMISSIBLE ENERGY:	$4 \times 10^{-7} \text{ J/cm}^2$
RANGE:	100 m to several km
SENSITIVITY:	Not established (see below)
MAJOR INTERFERENCE:	Fog, rain
ADVANTAGES:	Monostatic
DISADVANTAGES:	No standards for opacity; NAAQS requirements are for $<60 \mu\text{g/m}^3$; no direct measurement by lidar, since lidar measures transmissivity (opacity); relationship needs yet to be established or standards be developed for opacity as was done for stationary sources.
STATUS:	Extensive field tests of prototypes for R&D by NASA, NOAA, GE, SRI, EPA.

TECHNOLOGY: REMOTE MONITORING - LINE PROFILE

SYSTEM: LWIR DIFFERENTIAL ABSORPTION

PRINCIPLE OF OPERATION: DIFFERENCING AND RATIOING THE BACKSCATTERED SIGNAL OF SEQUENTIAL LASER PULSES EMITTED AT TWO WAVELENGTHS

PERFORMANCE PARAMETER	VALUE/COMMENT
POLLUTANT SPECIES:	O ₃ , HC
WAVELENGTH REGION:	8 - 12 μm
LASER:	Pulsed gas lasers (N ₂ O and CO ₂) and semi-conductor - diode lasers ²
MAXIMUM PERMISSIBLE ENERGY:	2 x 10 ⁻⁴ J/cm ² for 1-100 ns pulses 1.1 x 10 ⁻² J/cm ² for 100 ns-10 s pulses Maybe 50x larger if defining aperture is 1 mm instead of 7 mm
RANGE:	.1-1 km
SENSITIVITY:	.01 ppm
MAJOR INTERFERENCE:	Fog, rain, water vapor, high particulate concentration
ADVANTAGES:	Monostatic
DISADVANTAGES:	Complex, only two pollutants
STATUS:	Fieldable prototype being tested by SRI
SPECIAL REQUIREMENT:	Heterodyne detection

TECHNOLOGY: REMOTE MONITORING - LINE PROFILE

SYSTEM: MWIR DIFFERENTIAL ABSORPTION

PRINCIPLE OF OPERATION: DIFFERENCING AND RATIOING THE BACKSCATTERED SIGNALS OF SEQUENTIAL LASER PULSES EMITTED AT TWO WAVELENGTHS

PERFORMANCE PARAMETER	VALUE/COMMENT
POLLUTANT SPECIES:	CO, NO
WAVELENGTH REGION:	4.8- 5.2 μm
LASER:	Pulsed CO gas laser; Diode (solid state) laser
MAXIMUM PERMISSIBLE ENERGY:	$2 \times 10^{-4} \text{ J/cm}^2$ for 1- 100 ns pulses $1.1 \times 10^{-2} \text{ J/cm}^2$ for 100 ns to 10 s pulses Maybe 50x larger if defining aperture is 1 mm instead of 7 mm
RANGE:	100- 500 m
SENSITIVITY:	.1 ppm
MAJOR INTERFERENCE:	Fog, rain, water vapor, high particulate concentration
ADVANTAGES:	Monostatic
DISADVANTAGES:	Usefulness reduced because of restricted range capability, can be improved with higher energy lasers if permitted (see above)
STATUS:	Theoretical only
SPECIAL REQUIREMENT:	Heterodyne detection, although gain over direct detection is only a factor 5

TECHNOLOGY: REMOTE MONITORING - LINE PROFILE

SYSTEM: SWIR DIFFERENTIAL ABSORPTION

PRINCIPLE OF OPERATION: DIFFERENCING AND RATIOING THE BACKSCATTERED SIGNALS OF SEQUENTIAL LASER PULSES EMITTED AT TWO WAVELENGTHS

PERFORMANCE PARAMETER	VALUE/COMMENT
POLLUTANT SPECIES:	NO ₂ (3.3 μ m), HC(3.5 μ m), SO ₂ (4 μ m), CO(4.6 μ m)
WAVELENGTH REGION:	2.6- 5.0 μ m
LASER:	HF(2.6-3.6 μ m), DF(3.6-5 μ m), HCl(3.5-5.1 μ m); Diode; Parametric oscillator
MAXIMUM PERMISSIBLE ENERGY:	2 x 10 ⁻⁴ J/cm ² for 1- 100 ns pulses 1.1 x 10 ⁻² J/cm ² for 100 ns to 10 s pulses Maybe 50x larger if defining aperture is 1 mm instead of 7 mm
RANGE:	100- 250 m
SENSITIVITY:	.1 ppm
MAJOR INTERFERENCE:	Fog, rain, water vapor, high particulate concentration
ADVANTAGES:	Monostatic
DISADVANTAGES:	Only two pollutants covered by any of the lasers; range limited, but can be improved with higher energy lasers if permitted (see above)
STATUS:	Theoretical only

TECHNOLOGY: REMOTE MONITORING - LINE PROFILE

SYSTEM: UV/VIS DIFFERENTIAL ABSORPTION

PRINCIPLE OF OPERATION: DIFFERENCING AND RATIOING THE BACKSCATTERED SIGNALS OF SEQUENTIAL LASER PULSES EMITTED AT TWO WAVELENGTHS

PERFORMANCE PARAMETER	VALUE/COMMENT
POLLUTANT SPECIES:	Particles, NO ₂ , SO ₂
WAVELENGTH REGION:	3000—5000 Å
LASER:	Ruby, N ₂
MAXIMUM PERMISSIBLE ENERGY:	4 x 10 ⁻⁷ J/cm ² from 4010 to 7000 Å 4.8 x 10 ⁻⁵ J/cm ² at 3020 Å
RANGE:	Not established yet
SENSITIVITY:	Not established yet
MAJOR INTERFERENCE:	Rain, fog, excitation of other species (fluorescence), high particulate concentration
ADVANTAGES:	Monostatic
DISADVANTAGES:	Appears impractical because of interference by other fluorescing species
STATUS:	Theoretical only

6. 2. 2. 2h

TECHNOLOGY: REMOTE MONITORING - LINE PROFILE

SYSTEM: RAMAN SCATTERING

PRINCIPLE OF OPERATION: OBSERVING MAGNITUDE OF FREQUENCY SHIFTED
BACKSCATTERED SIGNAL

PERFORMANCE PARAMETER	VALUE/COMMENT
POLLUTANT SPECIES:	CO, SO ₂ , NO _x , HC, O ₃
WAVELENGTH REGION:	UV/Visible
LASER:	Ruby, Ar, Nd-YAG
MAXIMUM PERMISSIBLE ENERGY:	$4 \times 10^{-7} \text{ J/cm}^2$
RANGE:	<25 m
SENSITIVITY:	1 ppm
MAJOR INTERFERENCE:	Excitation of other species, especially of NO ₂
ADVANTAGES:	Monostatic, all species
DISADVANTAGES:	Not suitable because of short range
STATUS:	Laboratory tests only

TECHNOLOGY: REMOTE MONITORING - LINE PROFILE

SYSTEM: RAMAN RESONANCE/FLUORESCENCE SCATTERING

PRINCIPLE OF OPERATION: OBSERVING MAGNITUDE OF FREQUENCY SHIFTED BACKSCATTERED SIGNAL

PERFORMANCE PARAMETER	VALUE/COMMENT
POLLUTANT SPECIES:	CO, SO, NO _x , HC, O ₃
WAVELENGTH REGION:	Visible
LASER:	Ruby, Ar, Nd-YAG
MAXIMUM PERMISSIBLE ENERGY:	$4 \times 10^{-7} \text{ J/cm}^2$
RANGE:	100-1000 m
SENSITIVITY:	10^{-2} - 10^2 at 500 m 1 - 10^3 at 1000 m
MAJOR INTERFERENCE:	Excitation of other species, especially of NO ₂
ADVANTAGES:	Greatly improved over non-resonant Raman scattering
DISADVANTAGES:	Sensitivity not sufficient for monitoring NAAQS; both scattering phenomena may take place simultaneously and results are difficult if not impossible to separate
STATUS:	Laboratory tests and limited field

TECHNOLOGY: REMOTE MONITORING - LINE AVERAGE

SYSTEM: LWIR LONG-PATH WITH LASER SOURCE (BISTATIC OR MONOSTATIC)

PRINCIPLE OF OPERATION: TRANSMISSIONS AT TWO DIFFERENT WAVELENGTHS ARE DIFFERENCED TO OBTAIN ABSORPTION OF POLLUTANT

PERFORMANCE PARAMETER	VALUE/COMMENT
POLLUTANT SPECIES:	O ₃ , HC
WAVELENGTH REGION:	9.1- 11.3 μ m
LASER:	CW or pulsed CO ₂ laser
MAXIMUM PERMISSIBLE ENERGY:	2 x 10 ⁻⁴ J/cm ² for 1- 100 ns 1 x 10 ⁻² t ^{1/4} J/cm ² for 100 ns- 10 s pulses 2 mW/cm ² for CW
RANGE:	10- 1000 m
SENSITIVITY:	10 ⁻⁶ ppm (retroreflector) 10 ⁻¹ ppm (topographical reflector, heterodyne detection)
MAJOR INTERFERENCE:	Fog, rain, atmospheric turbulence
ADVANTAGES:	Bistatic, using retroreflector, is one of the most sensitive methods; monostatic, using topographical reflector, is convenient to set up.
DISADVANTAGES:	Bistatic system needs optical alignment; monostatic system has low sensitivity, may be improved with higher laser power, if permitted.
STATUS:	Field tests by GE and Jet Propulsion Laboratory

TECHNOLOGY: REMOTE MONITORING - LINE AVERAGE

SYSTEM: MWIR LONG-PATH WITH LASER SOURCE (BISTATIC OR MONOSTATIC)

PRINCIPLE OF OPERATION: TRANSMISSIONS AT TWO DIFFERENT WAVELENGTHS ARE DIFFERENCED TO OBTAIN ABSORPTION OF POLLUTANT

PERFORMANCE PARAMETER	VALUE/COMMENT
POLLUTANT SPECIES:	CO, NO
WAVELENGTH REGION:	4.8- 5.2 μm
LASER:	CO gas laser; Diode (solid state) laser
MAXIMUM PERMISSIBLE ENERGY:	$2 \times 10^{-4} \text{ J/cm}^2$ for 1- 100 ns $1 \times 10^{-2} \text{ t}^{\frac{1}{2}} \text{ J/cm}^2$ for 100 ns- 10 s pulses 2 mW/cm^2 for CW
RANGE:	10- 1000 m
SENSITIVITY:	10^{-6} ppm (retroreflector) 10^{-1} ppm (topographical reflector, heterodyne detection)
MAJOR INTERFERENCE:	Fog, rain, atmospheric turbulence
ADVANTAGES:	Bistatic, using retroreflector, is one of the most sensitive methods; monostatic, using topographical reflector, is convenient to set up.
DISADVANTAGES:	Bistatic system needs optical alignment; monostatic system has low sensitivity, may be improved with higher laser power, if permitted.
STATUS:	Field tests by MIT and JPL

TECHNOLOGY: REMOTE MONITORING - LINE AVERAGE

SYSTEM: SWIR LONG-PATH WITH LASER SOURCE (BISTATIC)

PRINCIPLE OF OPERATION: TRANSMISSIONS AT TWO DIFFERENT WAVELENGTHS ARE DIFFERENCED TO OBTAIN ABSORPTION OF POLLUTANT

PERFORMANCE PARAMETER	VALUE/COMMENT
POLLUTANT SPECIES:	NO ₂ (3.3 μm), HC(3.5 μm), SO ₂ (4 μm), CO(4.6 μm)
WAVELENGTH REGION:	2.6—5 μm
LASER:	HF, DF, HCl, gas lasers; Diode (solid state) laser
MAXIMUM PERMISSIBLE ENERGY:	2 x 10 ⁻⁴ J/cm ² for 1—100 ns 1 x 10 ⁻² t ^{1/2} J/cm ² for 100 ns—10 s pulses 2 mW/cm ² for CW
RANGE:	10—1000 m
SENSITIVITY:	10 ⁻⁶ ppm (retroreflector) 10 ⁻¹ ppm (topographical reflector, heterodyne detection)
MAJOR INTERFERENCE:	Fog, rain, atmospheric turbulence
ADVANTAGES:	Bistatic, using retroreflector, is one of the most sensitive methods; monostatic, using topographical reflector, is convenient to set up.
DISADVANTAGES:	Bistatic system needs optical alignment; monostatic system has low sensitivity, may be improved with higher laser power, if permitted.
STATUS:	Some field tests by SRI using low-reflecting surface

TECHNOLOGY: REMOTE MONITORING - LINE AVERAGE

SYSTEM: UV/VISIBLE LONG-PATH WITH LASER SOURCE (BISTATIC)

PRINCIPLE OF OPERATION: TRANSMISSIONS AT TWO DIFFERENT WAVELENGTHS ARE DIFFERENCED TO OBTAIN ABSORPTION OF POLLUTANT

PERFORMANCE PARAMETER	VALUE/COMMENT
POLLUTANT SPECIES:	(Particles), NO ₂ , SO ₂
WAVELENGTH REGION:	3000- 5000 Å
LASER:	Ruby, N ₂
MAXIMUM PERMISSIBLE ENERGY:	.39 μw (CW in visible)
RANGE:	Not established yet
SENSITIVITY:	Not established yet
MAJOR INTERFERENCE:	Rain, fog, high particulate concentration
ADVANTAGES:	High specificity
DISADVANTAGES:	Sensitivity limited by low permissible power output
STATUS:	No laboratory or field tests

TECHNOLOGY: REMOTE MONITORING - LINE AVERAGE

SYSTEM: LONG-PATH WITH BROAD BAND (BLACKBODY) SOURCE (BISTATIC)
& DISPERSIVE RECEIVER

PRINCIPLE OF OPERATION: DIFFERENCING TRANSMISSION ON AND OFF
LINES GIVES POLLUTANT ABSORPTION

PERFORMANCE PARAMETER	VALUE/COMMENT
POLLUTANT SPECIES:	CO, O ₃ , HC(?)
WAVELENGTH REGION:	2.5—12 μ m
RECEIVER:	Dispersive (medium resolution)
RANGE:	10—1000 m
SENSITIVITY:	10 ⁻² ppm (~1 cm ⁻¹ resolution)
MAJOR INTERFERENCE:	Rain, fog, atmospheric species, other pollutants
ADVANTAGES:	Relatively simple receiver
DISADVANTAGES:	Resolution not high enough to separate overlapping spectra of different pollutants
STATUS:	In use by EPA (ROSE system) for R&D

TECHNOLOGY: REMOTE MONITORING - LINE AVERAGE

SYSTEM: LONG-PATH WITH BROAD BAND (BLACKBODY) SOURCE (BISTATIC)
& FTS RECEIVER

PRINCIPLE OF OPERATION: DIFFERENCING TRANSMISSION ON AND OFF
LINES GIVES POLLUTANT ABSORPTION

PERFORMANCE PARAMETER	VALUE/COMMENT
POLLUTANT SPECIES:	CO, SO ₂ , NO _x , O ₃ , HC
WAVELENGTH REGION:	2.5- 12 μ m
RECEIVER:	Fourier transform spectrometer
RANGE:	10- 1000 m
SENSITIVITY:	10 ⁻³ ppm (\sim .1 cm ⁻¹ resolution)
MAJOR INTERFERENCE:	Rain, fog
ADVANTAGES:	Spectral resolution higher than dispersive spectrometer, thus easier separation between different pollutants
DISADVANTAGES:	More complex than dispersive spectrometer; needs computerized data reduction
STATUS:	Several systems have been tested in the field; ROSE system is scheduled to be outfitted with a FTS system

TECHNOLOGY: REMOTE MONITORING - LINE AVERAGE
 SYSTEM: LONG-PATH WITH BROAD BAND (BLACKBODY) SOURCE (BISTATIC)
 & GFC RECEIVER
 PRINCIPLE OF OPERATION: POLLUTANT AMOUNT INDICATED BY DIFFERENCE
 IN RECEIVED RADIANCE THROUGH SPECIFIER
 AND REFERENCE CELLS

PERFORMANCE PARAMETER	VALUE/COMMENT
POLLUTANT SPECIES:	CO, light HC, NO ₂ , SO ₂
WAVELENGTH REGION:	2-12 μ m
RECEIVER:	Gas filter correlation
RANGE:	10-300 m
SENSITIVITY:	10 ⁻³ ppm
MAJOR INTERFERENCE:	Fog, rain
ADVANTAGES:	Very simple device
DISADVANTAGES:	Not suitable for O ₃
STATUS:	Several instruments built by SAI under field evaluation by EPA

TECHNOLOGY: REMOTE MONITORING - LINE AVERAGE

SYSTEM: LONG-PATH WITH BROAD BAND (BLACKBODY) SOURCE (BISTATIC)
& FILTER WHEEL RECEIVER

PRINCIPLE OF OPERATION: POLLUTANT AMOUNT INDICATED BY DIFFERENCE
IN RECEIVED RADIANCE THROUGH IN-BAND AND
OFF-BAND

PERFORMANCE PARAMETER	VALUE/COMMENT
POLLUTANT SPECIES:	O ₃ , CO
WAVELENGTH REGION:	4.5- 10 μ m
RECEIVER:	Filter wheel
RANGE:	10- 1000 m
SENSITIVITY:	10 ⁻² ppm (5 cm ⁻¹ resolution)
MAJOR INTERFERENCE:	Rain, fog, other species
ADVANTAGES:	Simple device
DISADVANTAGES:	Limited application because of low resolution
STATUS:	Limited field evaluation of O ₃ radiometer built by Bendix for EPA; was not successful and has not been pursued

TECHNOLOGY: REMOTE MONITORING - LINE AVERAGE
SYSTEM: LONG-PATH WITH ULTRAVIOLET/VISIBLE SOURCE (BISTATIC)
WITH MFC/GFC RECEIVER
PRINCIPLE OF OPERATION: POLLUTANT AMOUNT INDICATED BY MODULATION
PRODUCED BY CORRELATOR

PERFORMANCE PARAMETER	VALUE/COMMENT
POLLUTANT SPECIES:	NO ₂ , SO ₂
WAVELENGTH REGION:	3000-5000 Å
RECEIVER:	Matched filter; Gas filter correlation
RANGE:	Not established
SENSITIVITY:	Not established
MAJOR INTERFERENCE:	Fog, rain, high particulate concentration
ADVANTAGES:	High specificity for NO ₂ and XO ₂
DISADVANTAGES:	Atmospheric scattering has significant effect
STATUS:	COSPEC was used in field demonstration using UV/Vis light source; has not been pursued

TECHNOLOGY: REMOTE MONITORING - LINE AVERAGE

SYSTEM: PASSIVE DOWNWARD LOOKING WITH GFC RECEIVER

PRINCIPLE OF OPERATION: NATURALLY EMITTED RADIANCE FROM
POLLUTANT AND BACKGROUND ARE CORRE-
LATED BY GAS FILTER

PERFORMANCE PARAMETER	VALUE/COMMENT
POLLUTANT SPECIES:	CO, Light HC
WAVELENGTH REGION:	4-10 μ m
RECEIVER:	Gas filter correlation
RANGE:	1000 m
SENSITIVITY:	.1 ppm
MAJOR INTERFERENCE:	Fog, rain
ADVANTAGES:	Wide coverage
DISADVANTAGES:	Interference with air traffic near airports
STATUS:	Extensive field tests by NASA using instrument built by SAI and TRW/Barringer

TECHNOLOGY: Remote Monitoring - Line Integral
 SYSTEM: Passive Upward Looking (Infrared-Atmospheric Emission)
 PRINCIPLE OF OPERATION: NATURALLY EMITTED RADIANCE FROM POLLUTANT
 AND BACKGROUND ARE SEPARATED BY GAS FILTER
 CORRELATION

PERFORMANCE PARAMETER	VALUE/COMMENT
POLLUTANT SPECIES:	SO ₂ , CO, CH ₄
WAVELENGTH REGION:	4.0 μ m, 4.6 μ m, 4.3 μ m
RECEIVER:	Gas filter correlation
RANGE:	Undetermined
SENSITIVITY:	Not established yet
MAJOR INTERFERENCE:	Fog, rain
ADVANTAGES:	Knowledge of wind velocity gives net source flux of pollutant. Can be used at night.
DISADVANTAGES:	Some contribution from scattered sunlight in daytime operation
STATUS:	CO-SO ₂ instrument built and field tested by SAI for EPA. Apparently no recent work by Barringer Corporation on CO and CH ₄ measurements.

TECHNOLOGY: Remote Monitoring - Line Integral

SYSTEM: Passive Upward Looking (Ultraviolet/Visible-Scattered Sunlight) Using MFC

PRINCIPLE OF OPERATION: NATURALLY EMITTED RADIANCE FROM POLLUTANT AND BACKGROUND ARE CORRELATED BY MATCHED FILTER

PERFORMANCE PARAMETER	VALUE/COMMENT
POLLUTANT SPECIES:	NO ₂ , SO ₂
WAVELENGTH REGION:	3000 - 5000 Å
RECEIVER:	Matched Filter Correlation
RANGE:	Undetermined
SENSITIVITY:	Not established yet
MAJOR INTERFERENCE:	Fog, rain, high particulate concentration
ADVANTAGES:	Knowledge of wind velocity gives net source flux of pollutant
DISADVANTAGES:	Cannot be used at night
STATUS:	COSPEC has been used in field operation.

6. 2. 2. 3 Ranking of Selected Monitors

Since no commercial systems are available, ranking of systems is not possible; it is only possible to rank measurement principles. Thus, the ranking guidelines are concerned only with parameters that are part of the measurement principles. These are:

- Number of pollutants measurable with any given measurement principle;
- Line profile versus line average;
- Sensitivity and range as determined by theoretical analysis;
- Bistatic versus monostatic;
- Complexity in data analysis.

Under these guidelines, we have ranked those instruments that were selected in Section 6. 2. 2. 1. The ranking was applied to only those measurement principles that have the potential of monitoring all of the pollutants. All other measurement principles, even if they were selected, have not been ranked because their relative advantages and disadvantages are about even.

- (1) SWIR Long-Path with Laser Source (bistatic) - Only line average values can be obtained. All pollutants can be measured, possibly including TSP. It is one of the most sensitive methods, far exceeding the required sensitivities. Range can exceed several km. Although the measurement principle has been field tested for the MWIR and LWIR, no operational system exists in the SWIR.
- (2) Long-Path with Blackbody Source and FTS Receiver - Only line average values can be obtained. All pollutants can be measured, possibly including TSP. Sensitivity sufficient for NAAQS. An

instrument is operational (EPA-Research Triangle Park) at ranges up to several km. However, the FTS system is expensive and the transmitter needs to be lined up with the receiver. The interpretation of the raw data is very involved.

- (3) SWIR DAS/DIAL - Line profile can be obtained. All pollutants can be measured, including TSP. It is monostatic and easy to set-up. However, the system is complex and requires skilled operators. No operational system is in existence. Theoretical predictions indicate a limited range (~100 m), which may be increased if and when the eye safety rules are relaxed. Heterodyne techniques are not useful for SWIR.
- (4) Long-Path with Blackbody Source and GFC Receiver - Only line average values can be obtained. All gaseous pollutants can be obtained; special provisions would have to be made for O_3 . Sensitivity sufficient for NAAQS. Range of over 1 km can be achieved. Transmitter has to be lined up with receiver. Instruments using this measurement principle have been used in the field. However, an operational system for all pollutants is not in existence.

